

# Leviathan of the Sky Hybrid Rocket Project Technical Report

## Team 145 Project Technical Report to the 2023 Spaceport America Cup

Mabel Aung, Zhenbo Bian, Cristian Bicheru, Robert Cai, Joey Chen, Jack Christensen, Joe Dolina, Delaney Dyment, Lydia Susanne Griffith, Joel Godard, Matthew Gordon, Domenic Hampson, Roman Kobets, Elias Kountouris, Ryan Lau, Aaron Leszkowiat, Jennifer Li, Davis Liu, Rio Liu, Tessa Pugh, Dharmik Ramlingam, Kavin Satheeskumar, Artem Sotnikov, Kyle Tam, Jason Xu, Francis Yao, Michael Zhou, and Nahvid Zolfaghari

*University of Waterloo, Waterloo, Ontario, N2L 3G1, Canada*

**Leviathan of the Sky (LotS) is a hybrid rocket developed by Waterloo Rocketry for the 30,000 ft apogee, Student Research & Developed (SRAD) hybrid/liquid propulsion system category at the 2023 Intercollegiate Rocket Engineering Competition (IREC). The primary objective of the LotS launch campaign is to attain an apogee of 30,000 ft and achieve a non-hazardous descent using a reefed parachute system. The secondary objective is to collect state estimation data through the payload module during flight. The LotS launch vehicle is powered by the Kismet engine, a nitrous oxide/hydroxyl-terminated polybutadiene SRAD hybrid engine. Engine control is managed by RocketCAN, a modular and extensible avionics system which also includes subsystems for radio communication, GPS tracking and remote recovery arming. All launch operations are conducted using the Remote Launch Control System (RLCS), which provides launch control capabilities from a range of over 3,000 ft.**

### Nomenclature

$A_e$	=	exit area
$A^*$	=	throat area
$c_g$	=	center of gravity
$c_p$	=	center of pressure
$D_a$	=	Damköhler number
$\gamma$	=	heat ratio
$g_0$	=	acceleration due to gravity, $9.81 \text{ m/s}^2$
$G_{ox}$	=	oxidizer mass flux
$I_{sp}$	=	Specific impulse
$M$	=	molecular weight

$M_e$	= nozzle exit mach number
$OF$	= oxidizer to fuel ratio
$P_{cc}$	= combustion chamber pressure
$P_e$	= nozzle exit pressure
$P_a$	= ambient pressure
$\tau$	= thrust
$T_{cc}$	= combustion chamber temperature
$R$	= ideal gas constant, 8.314 J / K mol

#### Acronyms

AGL	= Above Ground Level
COTS	= Consumer Off The Shelf
DAQ	= Data Acquisition
DTEG	= Design, Test, and Evaluation Guide
EGSE	= Electrical Ground Support Equipment
FOS	= Factor of Safety
GSE	= Ground Support Equipment
GSPD	= Ground Side Power Distribution
ID	= Inner Diameter
IMU	= Inertial Measurement Unit
IREC	= Intercollegiate Rocketry Engineering Competition
KotS	= Kraken of the Sky
LotS	= Leviathan of the Sky
MEOP	= Maximum Expected Operating Pressure
OD	= Outer Diameter
P&ID	= Piping & Instrumentation Diagram
RLCS	= Remote Launch Control System
RPN	= Risk Priority Number
SAC	= Spaceport America Cup
SF	= Static Fire
SotS	= Shark of the Sky
SRAD	= Student Researched and Designed

## I. Introduction

WATERLOO Rocketry is a student engineering design team representing the University of Waterloo from Waterloo, Ontario, Canada. The team will be competing in the 2023 Intercollegiate Rocketry Engineering Competition (IREC) at the Spaceport America Cup (SAC) with the Leviathan of the Sky (LotS) rocket, which is entered in the 30,000 ft apogee Student Researched and Developed (SRAD) hybrid/liquid propulsion category.

### A. Project Background and Scope

Leviathan of the Sky is the fourth iteration rocket in the Kismet series, following Unexploded Ordnance (UXO) in 2018, Shark of the Sky (SotS) in 2019, and Kraken of the Sky (KotS) in 2022. The primary mission goal of LotS is to achieve an apogee of  $30,000 \text{ ft} \pm 2,000 \text{ ft}$  and complete a non-hazardous descent. Both parts of the primary goal are mission critical outcomes of equal importance. The secondary mission goal is to collect data for the scientific payload housed in the rocket, which aims to gather state estimation data in addition to hosting an experiment testing the effects of microgravity on alcohol dehydrogenase activity in sourdough yeast cultures. Above all else, the foremost objective of the team is to provide students with opportunities to engage in hands-on learning through practical engineering and science challenges. The research, design, manufacturing, and testing involved with the creation of LotS is some of the most involved and complex work the team has ever taken on.

In order to achieve the above goals, there have been projects to redesign many of the components from KotS and optimize them for LotS. Most notably this includes an almost fully redesigned hybrid engine, a strong focus on weight optimization, and an improved suite of ground support equipment. A more focused approach to system design and integration was Development this year has also introduced the formation of a new flight dynamics team, who have investigated and implemented numerous methods to predict and optimize the LotS flight profile throughout the design cycle. As always, Waterloo Rocketry continues to pride itself on making as many components as possible in-house.

### B. Team Structure and Operations

Waterloo Rocketry comprises approximately 60 students studying engineering, science, and mathematics at the University of Waterloo. All currently active team members are undergraduate students. The rocketry team is one of many design teams at the University of Waterloo who operate under the Sedra Student Design Centre. Team Leads are responsible for overall project management and team direction, including overseeing all technical, administrative, and operational activities necessary to achieve the team's objectives and goals. Subsystem Leads are responsible for managing the main modules of the rocket and ground support equipment (GSE), including avionics, aerostructures, recovery, propulsion, flight dynamics, infrastructure, and payload. They supervise the overall timelines, integration, and development of each project in their subsystem. Technical projects are led by Project Leads, who are chosen based on experience, skill set, and interest. Project Leads are responsible for coordinating and managing all aspects related to

their projects, leading the design, manufacturing, and testing of their projects, and ensuring the successful integration of their project with other launch vehicle and ground systems. Despite this hierarchy the team maintains a somewhat loose structure; team members are welcome to work on any projects that interest them, not being restricted to work on a given subsystem, and project subteams often have significant overlap and collaboration. The Operations Director oversees all launch and propulsion testing logistics and procedures. The Safety Captain is responsible for the development and maintenance of safety documentation and procedures; however, safety is the responsibility of every team member and is always the highest priority.

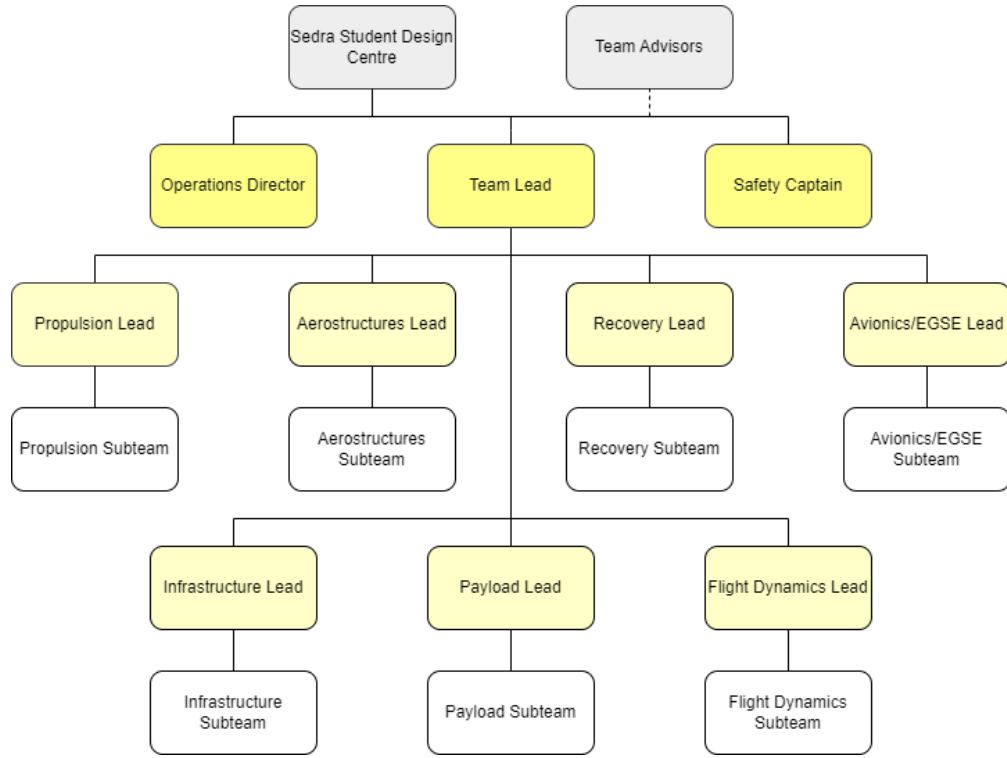


**Fig. 1 Waterloo Rocketry Organizational Chart**

Waterloo Rocketry's stakeholders include its academic partners, advisors, sponsors, and team members. The team represents the University of Waterloo and owes much to the institutions and resources that the University makes available to student teams. Sponsors are additional stakeholders, as they have provided significant material and financial support essential for the team's operation. Advisors from within the University and from industry share knowledge and provide insight as Waterloo Rocketry continues to develop more complex and sophisticated systems. Finally, the team's most important stakeholders are its members. Waterloo Rocketry's growth and continuity is contingent on its ability to maintain this atmosphere of learning and collaboration while remaining competitive and improving year-to-year. Past and present members dedicate significant time, energy, and resources to achieve the team's objectives, and Waterloo Rocketry owes its continued success to the commitment of its team.

### **C. Design Goals and Success Criteria**

Table 1 details the overall design requirements for Leviathan of the Sky, as well as additional requirements for each subsystem.

**Table 1 Leviathan of the Sky System Requirements**

<b>1.0 Vehicle Requirements</b>	
1.1	The rocket shall reach an apogee of 30,000 ft with an uncertainty of 2,000 ft
1.2	The rocket shall safely descend from apogee and land without significant damage
1.3	The rocket shall maintain a static stability margin between 1.5 and 6.0 cal throughout ascent
1.4	The rocket shall be capable of launching in wind speeds up to 20 mph
1.5	All systems shall comply with the rules listed in the SAC Rules & Regulations, and the Design, Test, & Evaluation Guide (DTEG)
<b>2.0 Engine Requirements</b>	
2.1	The total impulse of the engine shall not exceed 40,960 Ns
2.2	All feedsystem components shall be chemically compatible with nitrous oxide and able to hold pressure
2.3	There shall be a method employed by which the mass of oxidizer in the tank can be reliably determined
2.4	The aluminium shell of the combustion chamber shall not exceed 300 °C
<b>3.0 Recovery System Requirements</b>	
3.1	Deployment events shall not produce undue shock loads on the rocket
3.2	The parachute shall deploy in a reefed state at apogee and shall slow the rocket to a predetermined reefed descent speed
3.3	The parachute shall disreef at 1,500 ft Above Ground Level (AGL) and shall slow the rocket to a predetermined disreefed descent speed
3.4	The recovery system shall be capable of being armed remotely
3.5	A communication failure with the remote arming system shall not prevent the recovery system from being disarmed
<b>4.0 Avionics System Requirements</b>	
4.1	The rocket shall transmit telemetry regarding altitude, velocity, and attitude throughout the flight from ignition to touchdown
4.2	The rocket shall log all system commands and sensor data gathered during flight for post-flight analysis and troubleshooting
4.3	It shall be possible to replace any avionics board at competition with an identical copy without compromising or negatively affecting system function
<b>5.0 Aerostructures Requirements</b>	
5.1	The rocket fins shall have an aeroelastic flutter threshold velocity higher than the maximum rocket airspeed.
5.2	The airframe shall withstand all bending, compression, and impact loads encountered throughout flight
5.3	Airframe manufacturing processes shall reduce surface roughness in the interest of drag reduction wherever possible.
<b>6.0 Payload Requirements</b>	
6.1	The payload shall conform to the CubeSat standard with a form factor of 3U
6.2	The payload shall be unnecessary for nominal rocket performance
6.3	It shall be possible to compare flown samples to a control on the ground
<b>7.0 GSE Requirements</b>	
7.1	The fill and ignition process shall be operable remotely from a range of at least 3,000 ft.
7.2	An electrical or software failure in the launch control system shall not cause the rocket to enter an unsafe state when personnel are nearby.
7.3	There shall be a method of remotely disconnecting the fill system plumbing from the rocket prior to launch.
7.4	Fill and pressurization procedures shall take no more than 15 minutes

## D. Design Process

The backbone of good engineering is iterative progress. To ensure the rocket was designed with high-level integration and performance goals in mind, this year the team implemented a cycle based project management system. The goals of this system were to:

- 1) Force closer attention to integration and catch issues earlier in the design cycle
- 2) Determine which projects have the most impact on flight performance while major changes can still be implemented
- 3) Increase confidence in stability
- 4) Ensure project timeline requirements are tracked and met, decreasing stress on team members closer to competition

The primary implementation of this project management system came in the form of changing the flow of the design cycle. Previously the team followed a relatively linear design methodology, from subsystem conceptual design to competition as shown in figure 2.

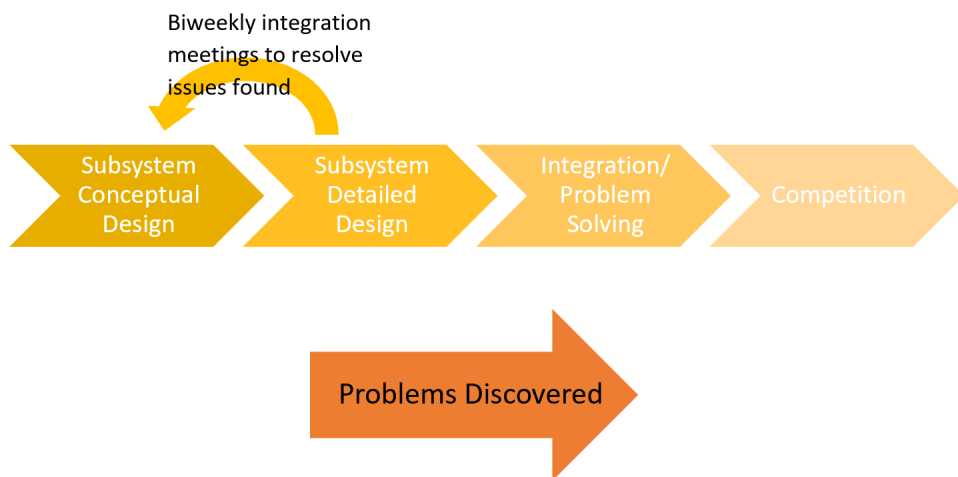


**Fig. 2 2022 Design Cycle Management**

While this design and integration methodology served the team well in the past, the more complexly integrated design of the last few years has lead to discovering problems and potential optimization improvements late in the design cycle while time may not exist to properly troubleshoot and implement proper solutions.

In order to address these issues, this year the team has changed its design process style to a more cyclic one, as shown in figures 3 and 4.

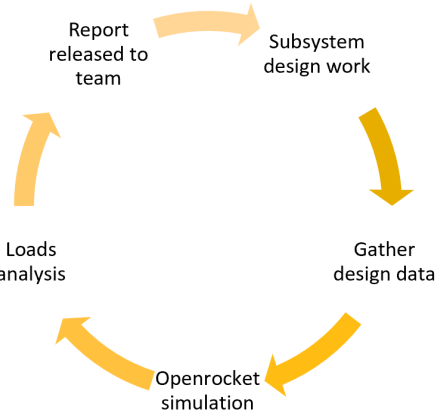


**Fig. 3 2023 Design Cycle Management**

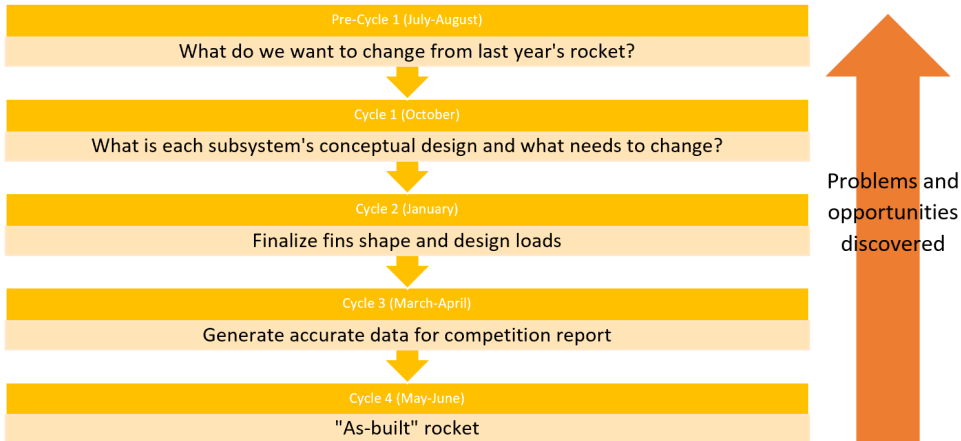


**Fig. 4 2023 Design Cycle Stages**

Gathering of design data was accomplished through mass, length, and CG tracking, where a spreadsheet was sent out to system and project leads to update at the beginning of each of the 4 cycles. In addition, engine RSE files were generated after each static fire. More information on flight dynamic simulations is available in section III.B. OpenRocket simulations and loads analysis covering a variety of scenarios were generated during each cycle, used both to predict the expected flight profile of the rocket and to determine the impact of given design changes or environmental conditions. A report containing the most important results and suggested action items was distributed to team members at the end of each cycle, who would then use this information to update their designs.

Overall this system proved to be a great success, driving improvements that added several thousand feet of apogee and helping to catch potential integration issues long before they were critical. The team plans to continue use of this design process style in the future.

## II. System Architecture Overview

Leviathan of the Sky is a hybrid rocket designed to fly to an apogee of 30,000 ft and make a safe descent. The rocket has an outer diameter of 6 inches and is 175 inches in length. The rocket system architecture consists of a hybrid engine to propel the rocket, an electronics system to communicate with and provide control to the rocket, a payload to collect sensor data through flight, a recovery system to return the rocket to the ground safely, and an airframe to structurally and aerodynamically support the other 4 systems.

These broad systems are broken into 10 distinct subsystems which are further broken into 35 different subassemblies. The subsystems are categorized by function within the rocket. They are: The recovery system, the cubesat payload, the upper airframe, the tank vent system, the oxidizer tank, the Ox-Tank-Aft-Skirt structure, the injector feed system, the combustion chamber, the fin body, and the electrical harnesses. By breaking up the whole rocket into systems, subsystems, and subassemblies, interfaces are easily identified within the rocket. These can be one or more of mechanical, fluid, electrical, and informational interfaces. The system architecture map below illustrates the relationship between all of the systems in the rocket. Conducting this exercise early in the design cycle was a key part of ensuring that the vehicle would integrate together to fulfill the mission goal.

The physical architecture of LotS consists of 5 main modules: the engine bay, the feedsystem, the payload bay, the recovery system, and the nosecone. Information and commands are relayed through the custom CANbus, RocketCAN, which also connects the on-board avionics to mission control.

LotS has also been decomposed into a physical architecture, which is a representation of the mechanical assembly of the system. This architecture is used as the structure for the CAD assembly of the vehicle and was instrumental in planning assembly order and procedures. The physical architecture breaks the vehicle into the 5 major components that it will be transported in: The nosecone, the recovery system, the payload bay, the feed system (including the oxidizer tank and Ox-Tank-Aft-Skirt section), and the combustion chamber and fin body. A detailed breakdown of the physical architecture can be seen below and a cross-section of Leviathan of the Sky is shown in Figure 5.



**Fig. 5 Sectional View of Leviathan of the Sky**

The work breakdown structure (WBS) in figure 6 details further the overall physical architecture of Leviathan of the Sky.

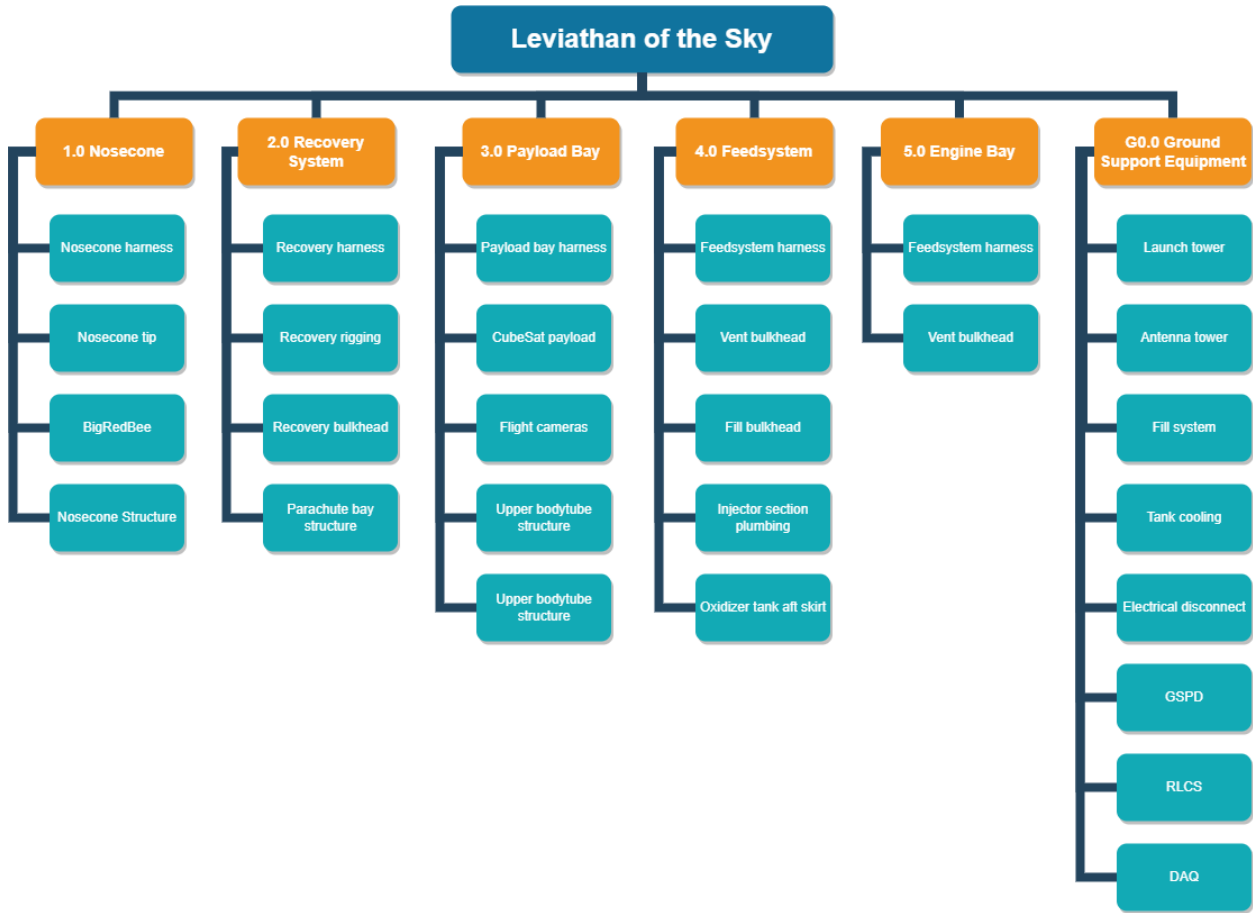


**Fig. 6 Leviathan of the Sky Work Breakdown Structure**

## A. Propulsion

### 1. Overview

Leviathan of the Sky is powered by the fourth iteration of the Kismet engine, which was originally developed for the 2018 IREC. In order to support the primary mission goal of a 30,000 ft apogee, engine modifications over the 2022-2023 design cycle focused heavily on improvements to combustion stability, and efficiency, as well as decreasing the inert mass of the feedsystem and combustion chamber. Kismet is an SRAD hybrid engine using a propellant combination of nitrous oxide ( $N_2O$ ) and hydroxyl-terminated polybutadiene (HTPB) with 5%  $3\mu m$  ultra-fine Al powder. Figure 7 shows the piping and instrumentation diagram (P&ID). Engine key parameters are summarized in Table 2.

### 2. Combustion Chamber: Mechanical Design

The combustion chamber comprises a structural pressure vessel containing the fuel grain and several combustion devices which are described subsequently. O-rings are used for the main seals at the forward and aft ends of the chamber. To prevent hot combustion gases from reaching the casing and/or o-rings, most interfaces between internal components

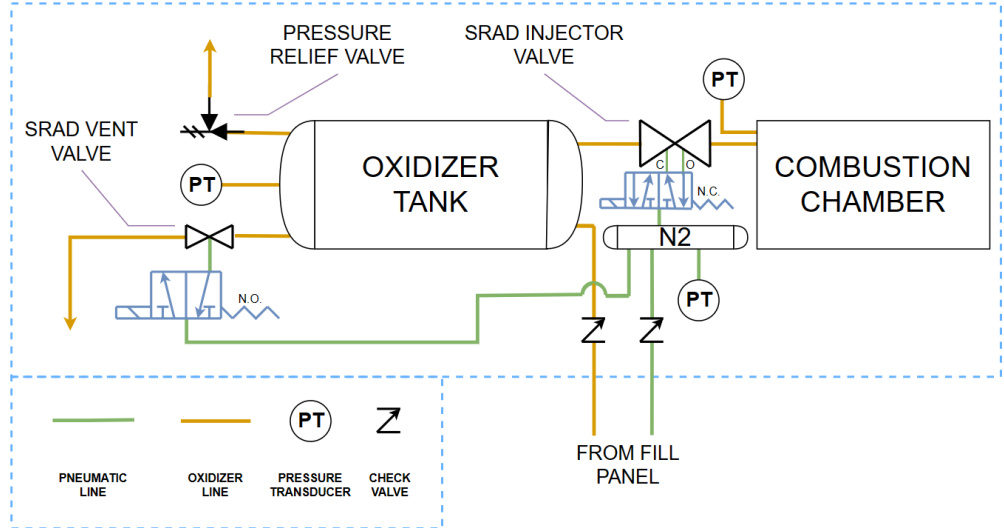


**Fig. 7 Rocket P&ID**

of the combustion chamber are sealed with high-temperature RTV gasket maker (Permatex 26BR). A high-temperature synthetic grease (Super Lube 41160) is applied liberally to the exterior surface of the stack of internal components to fill the gap between the liner and the casing, which facilitates disassembly of the combustion chamber assembly after the burn, as well as helping to transmit radial pressure forces into the casing. A sectional view of the combustion chamber is shown in figure 8.

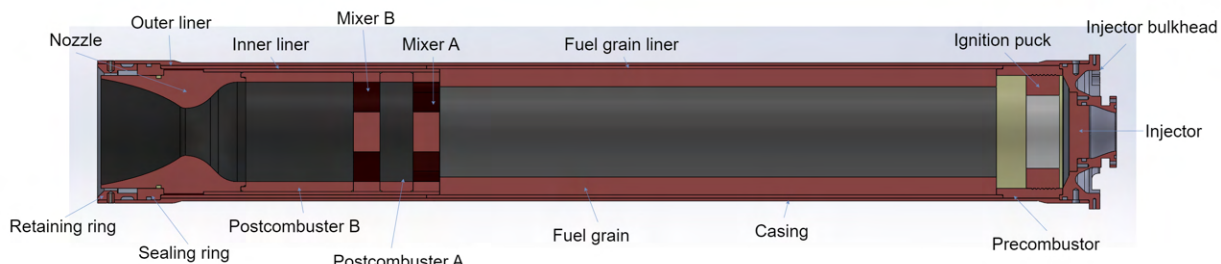


**Fig. 8 Cross-section of the combustion chamber**

## Casing

The combustion chamber casing is made of 6061-T6 aluminum and consists of a main section in the middle containing the fuel grain and other internal components, and two enlarged end sections which are bored out to accommodate the o-ring seals for the injector bulkhead and sealing ring. It is 37.4" in length. The outer diameter is 5.25" in the main section and 5.365" at the forward and aft ends. The wall thickness is 0.1" in the main section and 0.12" in the end sections. These dimensions were chosen to minimize mass while still maintaining adequate strength against the pressure load produced by the burn.

**Table 2 Key Engine Parameters**

Parameter	Value
Oxidizer	16 kg N <sub>2</sub> O
Fuel	2.1 kg HTPB+5%Al
Impulse	36.1 kNs
Burn Averaged $I_{sp}$	203 s
Liquid Phase Averaged $I_{sp}$	216 s
Thrust (peak)	10.9 kN
Thrust (sustained)	4.9 kN
Burn duration	5 s (liquid), 12 s (overall)
Mean O/F ratio	7.8 (liquid phase), 7.0 (overall)
Oxidizer tank pressure	850 psi
Chamber pressure	450 psi (peak)
Chamber length	37.4"
Chamber OD	5.25"
Chamber wall	0.1"
Nozzle geometry	80% Parabolic
Throat diameter	1.779"
Expansion ratio	5.05

### Injector bulkhead

The injector bulkhead forms the forward seal of the combustion chamber pressure vessel. It is CNC-machined from 6061-T6 aluminum and contains an instrumentation port to facilitate measurement of the combustion chamber pressure in flight. CNC machining allowed the mating interfaces with the aerostructures (i.e., the longerons and the fin can) to be incorporated into the bulkhead as a single part, where in the previous design cycle a separate interface ring was required. The bulkhead is retained into the combustion chamber by a radial bolt circle of 24 1/4"-28 button head cap screws. Finite element analysis was used to optimize the geometry of the bulkhead considering the pressure loads as well as the structural loads imparted by the vehicle in flight.

The injector bulkhead contains two feedsystem interface seals in addition to its combustion gas seals. The first is a radial o-ring gland to the injector. In the previous design cycle, this seal was an o-ring face seal gland, but using a radial seal allows the injector to be retained with a smaller number of bolts as there is no preload required to keep the injector and the bulkhead from separating. A small amount of bolt preload is still required to keep the bolts from vibrating loose during flight. The second feedsystem seal is a face seal o-ring gland, which interfaces with the feed line downstream of the injector valve. A face seal is used here to increase the ease of assembly (since this type of joint requires zero insertion depth), as the analogous seal in the previous design cycle was difficult to assemble.

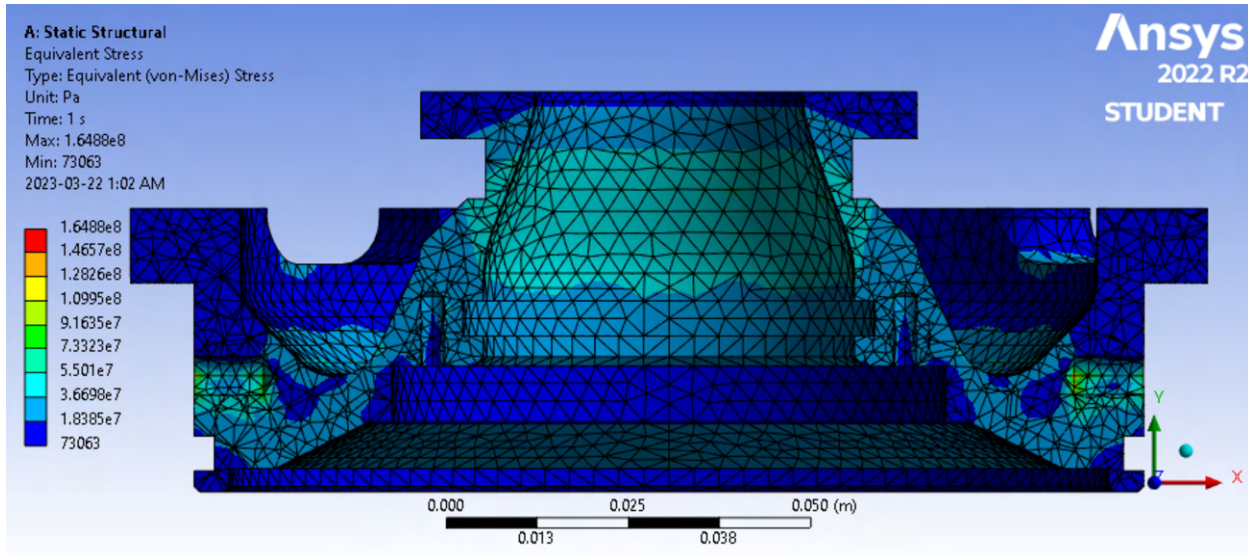


**Fig. 9 Injector Bulkhead FEA**

### Sealing Ring

The sealing ring forms the rear seal of the combustion chamber pressure vessel, which is its primary purpose. One radial o-ring seal is used between the sealing ring and the combustion chamber casing, and another is used between the nozzle and the sealing ring. The secondary purpose of the sealing ring is to transmit the force generated by pressure loads from the nozzle into the casing. To do so, it sits in direct contact with the nozzle on its forward side, and with the retaining ring on its aft. As it sits in direct contact with the nozzle, it is machined from G3 phenolic-fiberglass composite, giving it a good combination of mechanical strength and insulative performance.

### Retaining Ring

At the very bottom of the stack of combustion chamber internal components is the retaining ring. It is made from 6061-T6 aluminum and is secured in place by 20 custom-machined dowel pins, which transmit the pressure forces from the sealing ring into the casing. Dowel pins are used here instead of machine screws, as the lack of protruding bolt heads allows the boattail to be smoother to reduce aerodynamic drag on the vehicle. The pins are inserted into the retaining ring and the boattail is slid onto the combustion chamber assembly to hold the pins in place. The boattail itself is secured to the combustion chamber by 4 1/4"-28 machine screws, which substitute 4 of the holes in the radial dowel pin pattern to form an equally-spaced pattern of 24 fasteners (20 pins and 4 screws).

### 3. Combustion Chamber: Combustion Design

In terms of combustion design, the single most important feature of Kismet v4 compared to its predecessors is its much higher thrust and much shorter burn duration. The peak thrust of 10.9 kN is approximately 260% larger than that of Kismet v3, while the burn duration of 12 s is less than 50% that of Kismet v3. This allows Kismet v4 achieves a

similar total impulse to Kismet v3 while running at a higher average chamber pressure. This fact, coupled with the other aspects of the combustion design, increased the specific impulse of Kismet v4 by around 50% compared to its predecessors. The much larger injector mass flow rates required by this design necessitated the use of a custom coaxial injector valve (described subsequently) in order to meet mass and size requirements for integration into the vehicle. In addition, increasing the size of the injector valve decreased the pressure drop in the feedsystem, which allowed the chamber to be run at an even higher pressure than otherwise possible, while also reducing combustion instabilities hypothesized to have been caused by excessive vapour formation in the feed line.

## **Ignition**

Engine ignition relies on two separate events: heat application via ignition of a puck of solid rocket fuel, and oxidizer flow initiation through opening of the injector valve. The ignition puck is a toroidal disc composed of 70% potassium nitrate ( $\text{KNO}_3$ ) and 30% epoxy, and sits above the fuel grain at the top of the combustion chamber. The puck is cast with two embedded coils of nichrome wire, which connect to wires that exit the chamber through the nozzle. The puck is ignited when current passes through the nichrome coils, causing them to heat up. Once the puck successfully ignites, the nichrome coils break, and the change in current is displayed over RLCS. The operator then sends the signal to open the injector valve, which is performed via RocketCAN. Once the valve opens and oxidizer flow begins, thrust ramp of the engine is immediate.

## **Injector**

After passing through the injector valve, the nitrous oxide is injected into the combustion chamber through the injector. The injector is made of 6061-T6 aluminum and uses 53x 1.61 mm orifices to finely atomize the oxidizer as it enters the chamber.

When designing nitrous oxide injectors, it is advantageous to design the injector such that the mass flow rate is "choked" due to the phase change effects which occur as the oxidizer pressure drops through the injector orifices. This can help stabilize the engine as it decouples downstream pressure oscillations from the flow rate. Thus, the orifices are 3/4" long and a pressure drop of 250 psi at a minimum is maintained across the injector. Further tuning of the engine in the future could reduce the minimum acceptable pressure drop, allowing higher combustion pressures and thus efficiencies to be achieved.

All of the orifices in the injector are also tilted 10 degrees tangentially to create a swirling effect in the combustion chamber. This significantly improves regression rates and mixing and has also been shown to eliminate low frequency instabilities [1].



**Fig. 10** Injector (Valve Side Up)



**Fig. 11** Injector (CC Side Up)

## **Precombustor**

During this design cycle, a precombustor was added at the forward end of the fuel grain. The precombustor improves stability and efficiency by allowing the nitrous oxide to fully dissociate and heat up before it comes into contact with the fuel grain. This is aided by the ignition puck, which is located at the forward end of the precombustor to maximize the heating time of nitrous oxide in the precombustor. The precombustor is made of G11 fiberglass to withstand the thermal loads in this section of the engine.

## **Postcombustors and Mixers**

In order to improve propellant mixing and increase overall engine efficiency, a two-stage mixer and postcombustor design is employed in Kismet v4. The mixers are CNC machined from a 1" thick G3 phenolic fibreglass sheet, and have three  $\frac{3}{4}$ " thick spokes placed radially with a 120 degree offset from each other. Their purpose is to increase turbulence and improve the mixing of the propellants in the post-combustor before they leave the chamber. The post-combustor is divided into two sections which surrounds the mixers and improves efficiency by giving propellants more time to fully mix and combust before reaching the nozzle, resulting in higher thrust and specific impulse. Both postcombustors are made of graphite to withstand the extremely high temperatures in this section of the engine, which are the highest overall since the combustion products are most fully reacted in this region of the flow, but have not yet entered the nozzle.

## **Fuel Grain**

The solid fuel grain is composed primarily of HTPB, with 5% of ultra-fine graphite-coated aluminum powder (Eckart Pyro 5413 H Super) added by mass. The aluminum serves as a regression rate dopant, used to keep the O/F ratio closer to stoichiometric throughout the burn. The grain contains a circular port geometry achieved through investment casting. Updated from the previous six-slot pseudo-finocyl geometry, this port shape allows for better mixing of propellants while still maintaining a more consistent O/F ratio for the duration of the burn. The previous pseudo-finocyl geometry produced much higher fuel regression rates than necessary (resulting in inefficient, fuel-rich combustion), and also would have disrupted the swirl pattern formed by the injector, so for these reasons the circular port geometry was selected.

## **Nozzle**

The nozzle is CNC machined from graphite, and has a thrust-optimized parabola (TOP) profile geometry of 80% equivalent length. While the increase in efficiency afforded by this geometry is small compared to that of a conical nozzle, it allows for the same area ratio to be fit into a shorter length, reducing the dry mass of the engine.

#### *4. Combustion Chamber: Thermal Design*

In previous iterations of the Kismet engine, unmanageably high temperatures in the combustion chamber casing necessitated the use of a large, solid-walled aluminum boattail, which acted as a heat sink to keep the temperatures low enough to prevent annealing. Kismet v4 has a much shorter burn duration (12 s compared to 25-30 s) than its predecessors, which substantially reduces the total heat load on the combustion chamber. Since Kismet v4 has a relatively large area of very hot internal components in proximity to the chamber wall (i.e., the postcombustors), the heat loads on the combustion chamber casing are still relatively large but still acceptable.

#### **Thermal Liners**

The fuel grain is cast into a G3 phenolic-fiberglass composite liner, which has a low thermal conductivity and delays heat transfer in order to protect the chamber casing from the hot combustion temperatures.

As the nozzle area sees the hottest temperatures during the burn, two thermal liners are put in place to keep temperatures on the casing and fin can within an acceptable range. The inner aft liner is made of 0.125" thick G11 fibreglass, perforated with 667 holes arranged radially in 46 rows, which create trapped air pockets to further reduce thermal conduction. The outer aft liner is also made of G3 phenolic composite, which further impedes heat transfer to the casing. During Static Fire 8, casing temperatures in the nozzle region were observed to be between 280°C and 290°C. Although this value is on the upper bound of the acceptable range (making annealing a potential concern) post-firing hydrostatic testing showed that the structural integrity of the casing was preserved.

#### *5. Coaxial Injector Valve*

The main propellant valve used by LotS is an SRAD valve at an 1" nominal size with flow path that is coaxial with its actuator. The valve is actuated using compressed nitrogen gas from the rocket's pneumatic supply. Previous iterations of the Kismet engine have used a 1/2" nominal size valve, but the need for greater oxidizer mass flow rates to support engine upgrades necessitated a larger valve. The assembled valve is shown in Figure 12.

The flow of oxidizer enters from the left side in Figure 13, and through the hollow cylindrical piston in the middle, referred to as the sleeve. When the valve is actuated closed, the fluid is stopped by the seal formed by the interface between the sleeve and the conical surface of the valve seat, colored white. When the valve is actuated open, the flow diverts around the valve seat, through an annular passage in the valve seat holder, and exits to the right. Figure 14 shows the valve in an open state, with fluid flow highlighted in red.

The main valve seat is a machined plastic seal made of 25% glass-filled PTFE. The sleeve incorporates a dynamic piston seal, which allows it to be actuated pneumatically. A spring loads the valve to a normally-closed state for safety during propellant loading. The spring was sized to provide adequate force to overcome o-ring friction and to make the sleeve seal against the valve seat, should pneumatic pressure holding the valve closed be lost. The position of the sleeve



Fig. 12 Injector valve, assembled

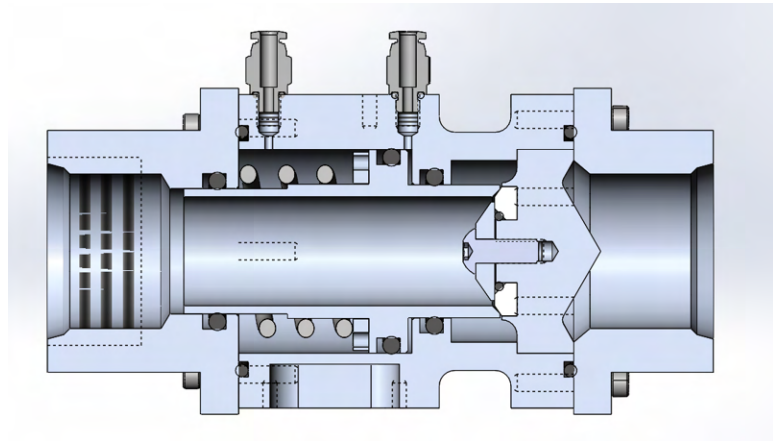


Fig. 13 Injector valve cross section, closed

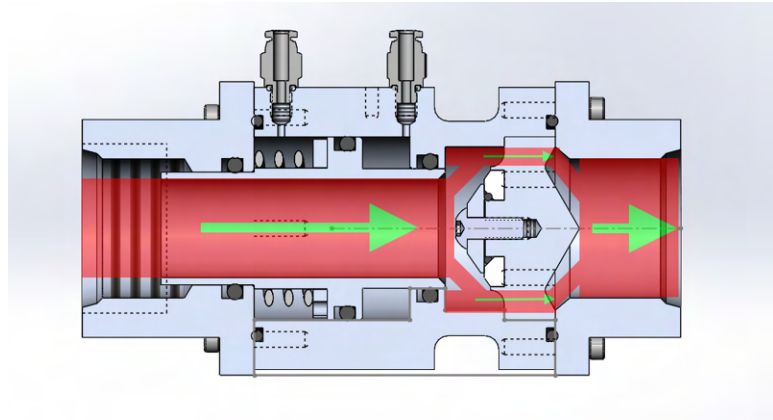


Fig. 14 Injector valve cross section, open, flow path highlighted

is sensed through the use of a hall-effect sensor, which detects a ring of neodymium magnets that travel along with the sleeve.

Two main valve types were considered during the development of the injector valve: a coaxial valve design versus a ball valve plus actuator. Criteria including mass and volume, cost, development risk, and learning opportunities were considered and are summarized in Table 3.

**Table 3 Analysis of candidate injector valve designs**

Factor	Ball valve	Coaxial valve
Mass	<ul style="list-style-type: none"> <li>COTS 1" ball valves are very heavy. Custom bodies or end plates would be needed to reduce the mass of the assembly</li> <li>Large ball valves require high torque, necessitating a heavy and bulky actuator</li> </ul>	<ul style="list-style-type: none"> <li>Actuator is integrated into main valve body, low mass and volume</li> </ul>
Cost	<ul style="list-style-type: none"> <li>Likely to be high since large COTS components (ball valve, actuator, solenoid, or motor) need to be purchased</li> </ul>	<ul style="list-style-type: none"> <li>Cost of raw stock, hardware, seals, fittings may be lower</li> <li>Fewer highly engineered COTS components needed</li> </ul>
Development risk	<ul style="list-style-type: none"> <li>Lighter housing for the ball valve would need to be designed and qualified</li> <li>Appropriate actuators and auxiliary hardware needs to be sourced or designed</li> <li>Pneumatic actuators need higher pneumatic pressures to reduce the volume to fit inside the rocket, necessitating a redesign of rocket pneumatics</li> <li>Electric actuators require new rocket power systems to be developed</li> </ul>	<ul style="list-style-type: none"> <li>The team has no prior experience with PTFE valve seat designs.</li> <li>The team does have prior experience with designing pneumatic devices</li> <li>Existing rocket pneumatic system (&lt;145psi) does not need extensive redesign to support this valve</li> </ul>
Learning opportunities	<ul style="list-style-type: none"> <li>Selection and integration of COTS components for a fluid systems assembly</li> </ul>	<ul style="list-style-type: none"> <li>Clean sheet design of new valve</li> </ul>

Based on these factors, the coaxial sleeve valve design was chosen because of its lower development risk, which required less modification to other vehicle systems, and for its learning opportunity to design a valve from a clean sheet.

As of the writing of this report, the valve has been validated through component testing, including hydrostatic testing to 1500 psi (1.5x MEOP), testing of actuation under fluid pressure, and as part of integrated tests with the rest of the propulsion system in two engine static fires.

Through the development of this valve, we encountered issues during testing that included:

- Valve Sticking in Cold Conditions:** During the SF7 engine test campaign, a cold flow using CO<sub>2</sub> was used for a test of the injector element without the rest of the combustion chamber attached. The valve failed to actuate open

when commanded. Probable root cause of this failure was determined to likely be very cold temperatures (less than -10°C) causing the o-ring material to become stiffer, increasing the friction such that the pneumatic force was no longer sufficient to overcome the break out force of the dynamic o-ring seals. An additional cause may have been moisture in the pneumatic systems getting into the dynamic seals of the sleeve and freezing. The pneumatic pressure was increased to 130psi, which successfully actuated the valve for the engine firing. This issue was determined to not need hardware changes since climate conditions at SAC are expected to be significantly warmer, making the possibility of valve sticking by cold and stiff o-rings remote.

- **Valve Seat Radial Extrusion:** Initial iterations of the valve seat holder had a flat surface which the valve seat rested on. It was found that hydrostatic pressure would cause the valve seat to gradually deform radially when closed at pressures of 1000psi (MEOP) for prolonged periods of time ( 5min) and rapidly when at the hydrostatic test pressure of 1500psi. This particular failure mode was resolved by adding a lip feature on the valve seat holder, which prevented the valve seat from extruding radially. Figure 15 shows the design change in the seat holder geometry. Photos of the extruded seat can be found in the Appendix.

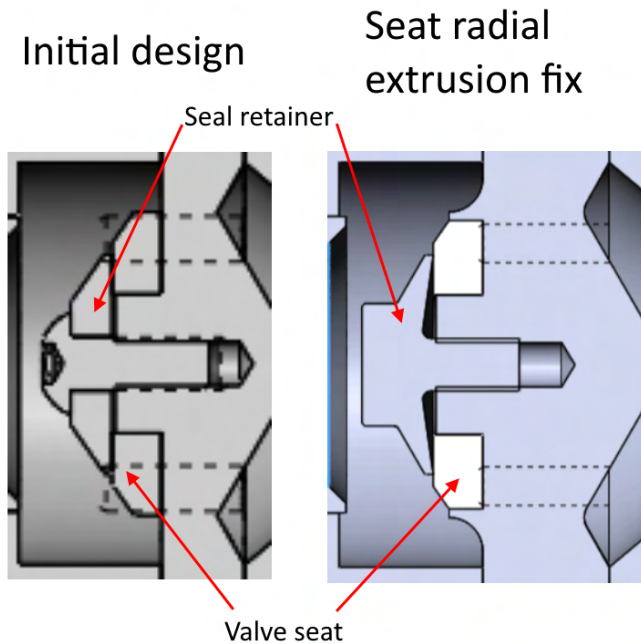


**Fig. 15 Revision of seat holder geometry to fix radial extrusion issue.**

- **Valve Seat Axial Extrusion:** After the radial seat extrusion issue was resolved, the valve seat was found to have extruded out of the recess of the seat holder, bulging upwards around the seat retainer screw after prolonged period of time under pressure ( 1.5h @ up to about 800psi). The probable cause was determined to be pressurized fluid leaking through the interface between the seat retainer and the valve seat into the back side of the valve seat,

forcing it out of the seat recess. This leak path was sealed using an o-ring after modifying the valve seat geometry to accommodate a triangular o-ring gland. Figure 15 shows the addition of the secondary seal. Photos of the extruded seat can be found in the Appendix.

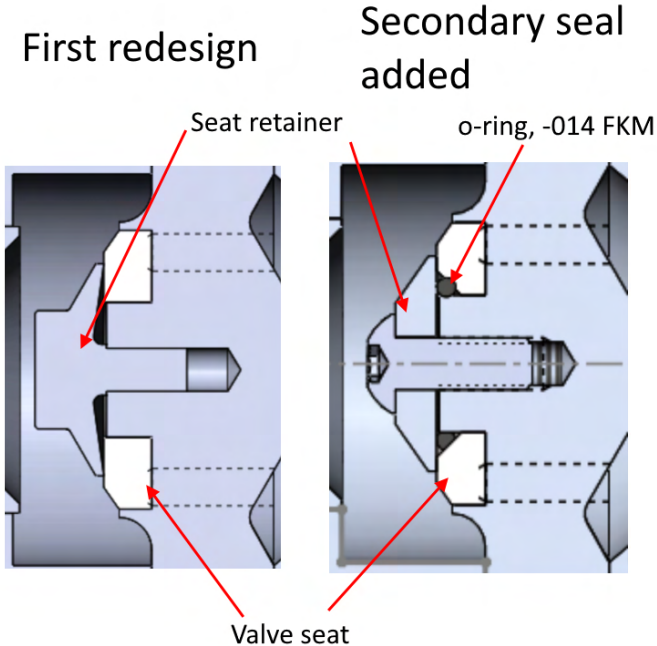


**Fig. 16 Revision of seat holder geometry to fix axial extrusion issue.**

Seat deformation  
Seat deformation, again.

#### 6. Vent Valve 2

The vent valve is the main valve responsible for controlled venting of the oxidizer tank during fill and launch. It is an SRAD, normally open valve that is pneumatically actuated by a COTS solenoid valve at 145psi pneumatic pressure provided by the rocket's pneumatic system. The valve houses a piston that is pushed by pneumatic air to seal the oxidizer at the valve inlet (the specific sealing mechanisms are described under the design goals), and a spring biases the piston to a normally-open position in the absence of pneumatic pressure. This ensures the oxidizer tank is in the venting state in case of any system failures.

The team's 2022 competition cycle rocket, KotS, featured the first iteration of the SRAD vent valve. Since it has already been proven to be highly reliable through various integrated tests and launch attempts with the rocket, the design goals for the second iteration, vent valve 2, of the 2023 competition cycle, are only further optimizations:

- 1) Reduce the size of the vent valve for easier integration of the valve in the rocket's vent section
- 2) Reduce the mass of the vent valve as part of the weight-reduction and flight dynamics-improvement campaign for LotS

To achieve these goals while exploring different valve technologies for the sake of experimentation, a new sealing mechanism is employed. The previous vent valve sealed against oxidizer pressure with an O-ring seal on the stem at the inlet port. To open the valve, the stem needs to slide up along the valve body by enough distance such that the sealing O-ring slides above the outlet port. Vent valve 2 seals against oxidizer pressure by pressing a PTFE-tipped stem into the internal edge of the inlet port, forming a soft seal. A to-scale comparison of the two iterations of the vent valve is shown in the figure below.

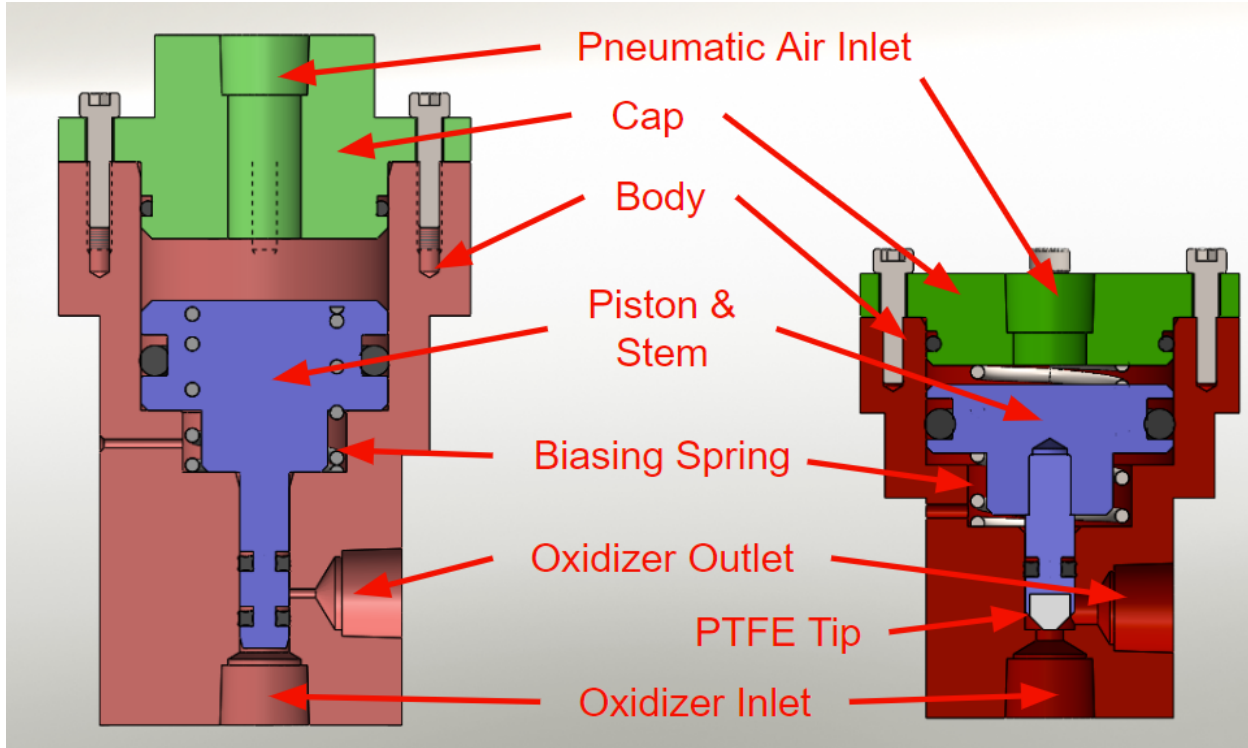


**Fig. 17 Cross-section geometries of the two iterations of the vent valve**

Since vent valve 2's seal is directly formed at the stem and the inlet port interface, the piston requires a much shorter travel length in order to fully open the valve, thus reducing the valve's overall height and mass. This new sealing mechanism also avoids the first iteration vent valve's issue of having an O-ring slide over the outlet port, which could increase wear on the O-ring and/or damage it if the port is not properly de-burred. Based on this main design change and removal of unnecessary material for mass optimization, vent valve 2 has a height of 2in and a mass of 0.31lb, down from the first generation vent valve's 3.14in and 0.49lb.

The figure below shows the various machined parts of vent valve 2. The body, cap, and piston are machined from aluminum 6061. The narrow stem of vent valve 2 is a separate part so that it can be machined from stainless steel, which is harder to bend than aluminum. This separation of the piston and stem allows for an easier and less error-prone machining process of both parts on the lathe.



**Fig. 18 Machined vent valve 2 parts**

The valve has been validated through hydrostatic testing to 1500psi (1.5x MEOP), testing of actuation under fluid pressure, and integrating testing with the entire propulsion system in Kismet engine static fire 8.

### 7. Oxidizer Tank

The oxidizer tank is a 6" OD, 62" long tank sealed on both ends with removable bulkheads. The system is blow-down, utilizing the self pressurizing properties of nitrous oxide to feed oxidizer into the injector. The oxidizer tank is made of 6061-T6 aluminium. Due to increases in engine efficiency, the length of the oxidizer tank was reduced from previous iterations of the Kismet engine, allowing for significant mass savings.

### 3D Printed Fill Bulkhead

The fill bulkhead caps the lower end of the oxidizer tank, and connects to the injector valve and fill system. This year, a significantly more complex bulkhead was 3D printed from AlSi10Mg alloy using Laser Powder Bed Fusion (LPBF). This bulkhead incorporates a multitude of different features including:

- 1) A reservoir for pressurized nitrogen gas used in the pneumatic systems
- 2) A mass and strength optimized internal honeycomb structure
- 3) Connection points for pneumatic tubing
- 4) Inlets for Nitrous oxide fill plumbing
- 5) Optimized internal flowpaths for pneumatics and propellants
- 6) Mounting points for PCBs
- 7) Mounting points for the longerons which connect to the Combustion Chamber
- 8) Mounting points to interface directly with the injector valve

The bulkhead, as shown in Figure 19 has two radially-sealing o-rings, with one acting as a backup ring to ensure no nitrous oxide will leak out in the event of the first seal failing, and is connected to the oxidizer tank using 24 1/4"-28 button head cap screws. This bulkhead has significantly decreased the complexity of assembling the injector section, and has provided significant mass savings over previous iterations.



**Fig. 19 3D printed aluminium fill bulkhead**

### Multi-Port Vent Bulkhead

The vent bulkhead caps the top end of the oxidizer tank, and connects to the vent section plumbing. Previous iterations of this bulkhead featured a single central hole, which required a significant amount of plumbing and adapters to connect the pressure transducer, pressure relief valve, and vent valve. This year, a multi-port vent bulkhead was designed that incorporates three separate ports that connect to the oxidizer tank, one each for the pressure transducer, pressure relief valve, and vent valve, as shown in Figure 20. This has reduced the number of fittings present in the vent section as each of the 3 ports was sized to interface directly with one of the vent section components.



**Fig. 20 Multi-Port Vent Bulkhead**

## 8. Test Results

### Static Fire 7

On January 29th, 2023, the Waterloo Rocketry team held its' first static fire of the year (SF7) in which the new Kismet V4 engine and feed system were put to the test in a full duration burn. The engine performed spectacularly, achieving a peak thrust of 11 kN and a specific impulse of 195s, with extremely smooth combustion. To improve combustion efficiency, a single G7 phenolic mixer was placed in the combustion chamber, leading to improved propellant mixing and more complete combustion. The setup for the test can be seen in the plumbing and instrumentation in Figure 21. Additionally, a suite of thermocouples was placed along the combustion chamber in order to monitor the temperature distribution. An image of this can be seen in figure ???. The aim of the thermocouples was to monitor the efficiency of the thermal protection in the engine. Based on analysis of the data, no annealing took place.

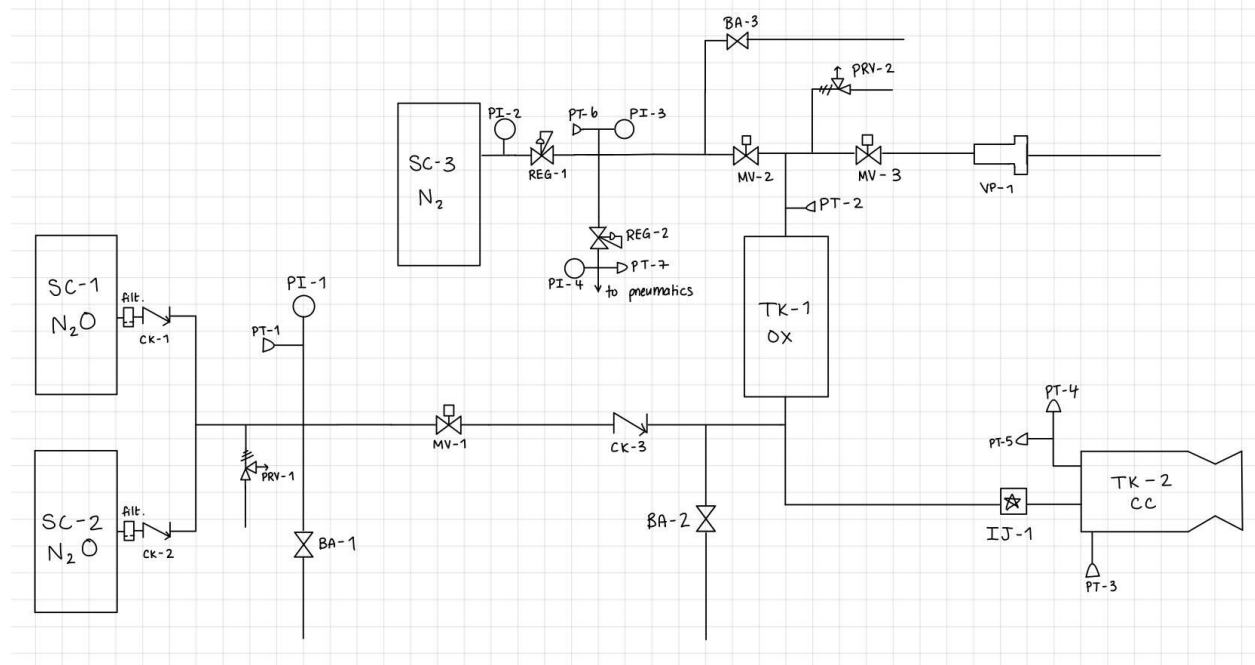


**Fig. 21 SF7 P&ID Diagram**

### Static Fire 8

On April 27th, 2023, a second full duration static fire (SF8) of Kismet V4 was successfully carried out. This full duration burn validated several new systems including containerized GSE, upgraded versions of the coaxial injector and SRAD vent valves, and the new combustion chamber housing and bulkhead that will be used in the flight engine. A new nozzle was created with a more optimized profile, and a second mixer was added as previously described resulting in a peak thrust of 10.9 kN and a burn-averaged specific impulse of 203s. SF8 also incorporated lessons learned from SF7, most notably packing the tubes connecting the combustion chamber to the suite of attached pressure transducers with

grease to prevent combustion gases from reaching the sensors and clogging the lines with soot in the process. This tactic was successful and resulted in a significant improvement in combustion chamber pressure readings during the burn. This test also validated the Hall effect sensor on the coaxial injector valve, allowing for the injector valve state to be determined remotely. Further plots and analysis relating to Static Fire 8 are available in the appendices.

### **Wet Dress Rehearsal**

On May 14th, 2023, a Wet Dress Rehearsal (WDR) was conducted using the full suite of ground support equipment. This test was successful in validating the function of all of these systems (described in the infrastructure section of the report) as well as testing the procedures for launch operations and abort scenarios.

### *9. Simulation*

This year, a number of numerical tools were created to aid with engine development. One tool that was used to make preliminary estimates on engine performance and to sanity check other calculations was the Python Propulsion Analysis Library (ProPAL). This tool implemented the approach described in [2], which is a complete coupled numerical model of the tank blowdown, propellant combustion, fuel grain regression, and nozzle gas dynamics. The code was for this was written and subsequently optimized in performance through the creation of thermochemical lookup tables. However, this tool could not accurately predict some of the more complex dynamics or the thrust spike observed. As such, more sophisticated techniques such as CFD were subsequently employed for the remainder of engine development.

### **B. Aerostructures**

Aerostructures on Leviathan of the Sky can be subdivided into composite components and metallic components. The former include the majority of the outer airframe; details can be found in Tables 4 and 5. The latter includes the oxidizer tank, couplers between bodytubes, and various internal components. The LotS aerostructure breakdown can be found in figure 22.

**Table 4 Composite Components Overview**

Component	Stacking Sequence	Fabric Used
Nosecone	[45] <sub>4</sub>	Composites Canada Plain Weave Fibreglass
Parachute Bay	[45] <sub>2</sub>	A & P 6" OD Braided Fibreglass Biaxial Sleeving
Upper Bodytube	N/A	MadCow Rocketry COTS G12 Fibreglass
Oxidizer Tank Aft Skirt Fairings	[45, 0, 45, 0]	4HS Fibreglass Cloth, Textreme 80 Spread Tow Carbon Fiber, A & P 6" OD Braided Carbon Fiber Biaxial Sleeving
Fin Can/Combustion Chamber Bodytube	[45 <sub>3</sub> , 0]	Composites Canada 4HS Fibreglass Cloth, A & P 6" OD Braided Carbon Fiber Biaxial Sleeving, Textreme 80 Spread Tow Carbon Fiber
Fins	[0, 45 <sub>4</sub> , 0]	2x2 Twill Double Bias A & P Carbon Fiber, Textreme 80 Spread Tow Carbon Fiber laid up on COTS 3/16" Thick [0,90] Carbon Fibre Plate Stock

**Table 5 Resin System and Method Used to Make Composite Parts**

Component	Epoxy System	Manufacturing Method
Nosecone	Aeropoxy PR 2032 resin and PH 3663 hardener	Vacuum Bag Hand Layup
Parachute Bay	Airstone 780E resin and 786H hardener	Resin Infusion
Upper Bodytube	N/A	COTS
Oxidizer Tank Aft Skirt Fairings	Airstone 780E resin and 786H hardener	Resin Infusion
Fin Can/Combustion Chamber Bodytube	Airstone 780E resin and 786H hardener	Resin Infusion
Fins	Airstone 780E resin and 786H hardener	Wet Tip-to-Tip Layup

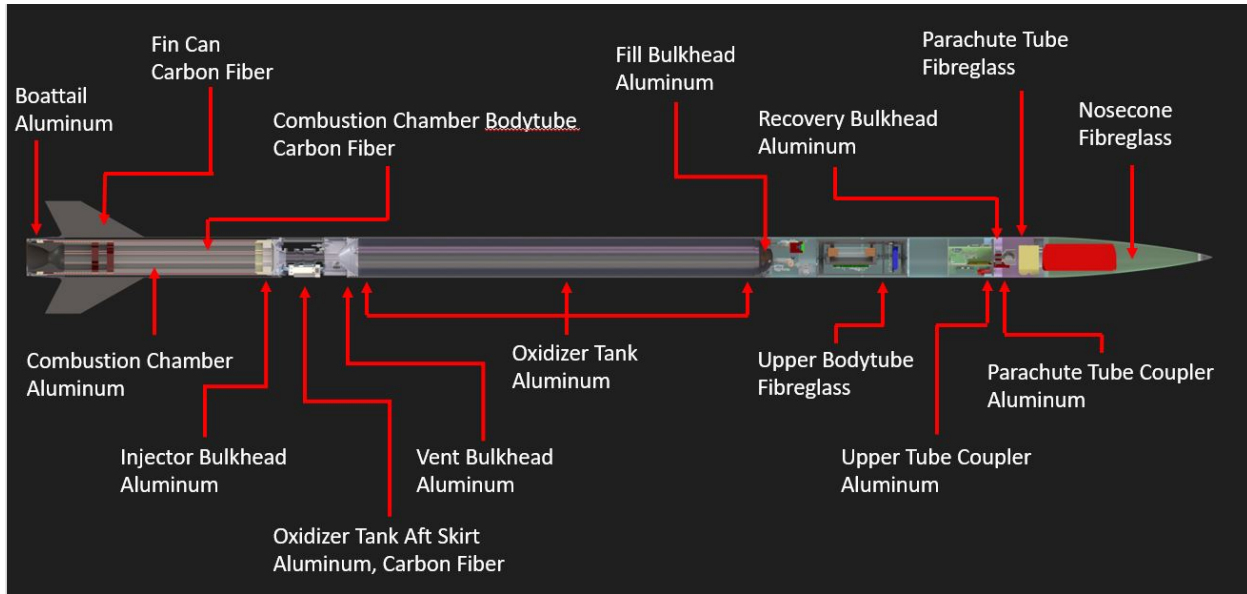


**Fig. 22 Aerostructures Layout**

The oxidizer tank, boattail, couplers, and various internal structural components are machined out of aluminum. The entire structure is monocoque, with the oxidizer tank aft skirt supported by longerons meant to resist compression.

### 1. Load Analysis

The publicly available BENDIT7 spreadsheet was used to estimate axial, shear and bending moments experienced by the rocket at maximum acceleration (takeoff) and maximum aerodynamic pressure (Max Q). The flight conditions used were taken from OpenRocket simulation data. Thus, stress analysis of components on the rocket during the boost phase considers both bending and axial forces due to acceleration. Due to the uncertainty in the input values and assumptions made in the calculation process, adequately high FOS have been applied to any components that were designed based off the results of the loads analysis. The plots of these results are shown in Figure 23, Figure 24, Figure 25, and Figure 26. See Appendix B, section IV.C for the loads analysis inputs.

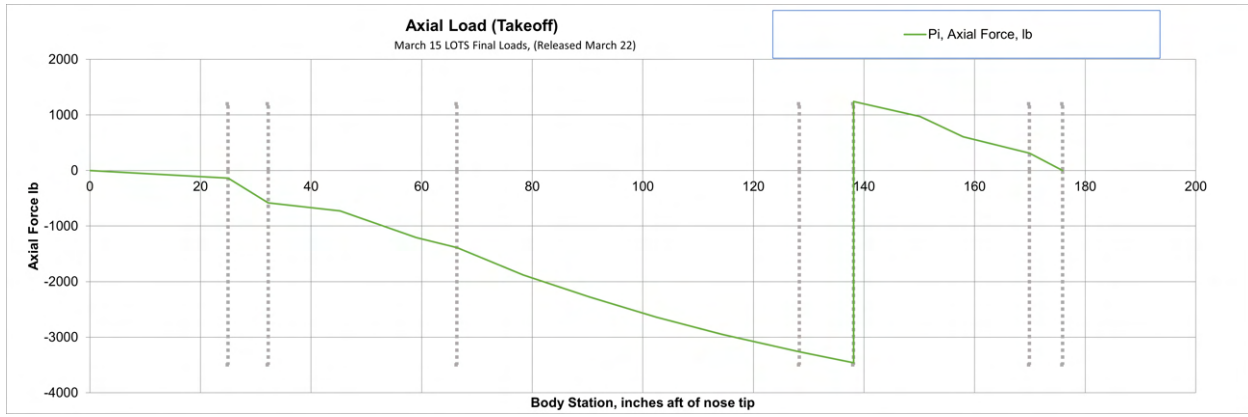


**Fig. 23 Takeoff Axial Loads**

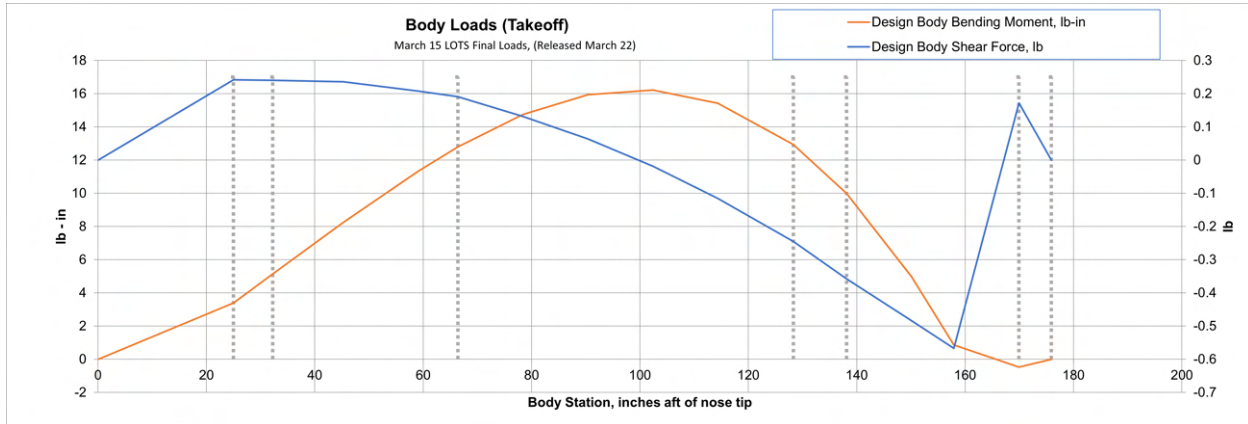


**Fig. 24 Takeoff Body Loads**

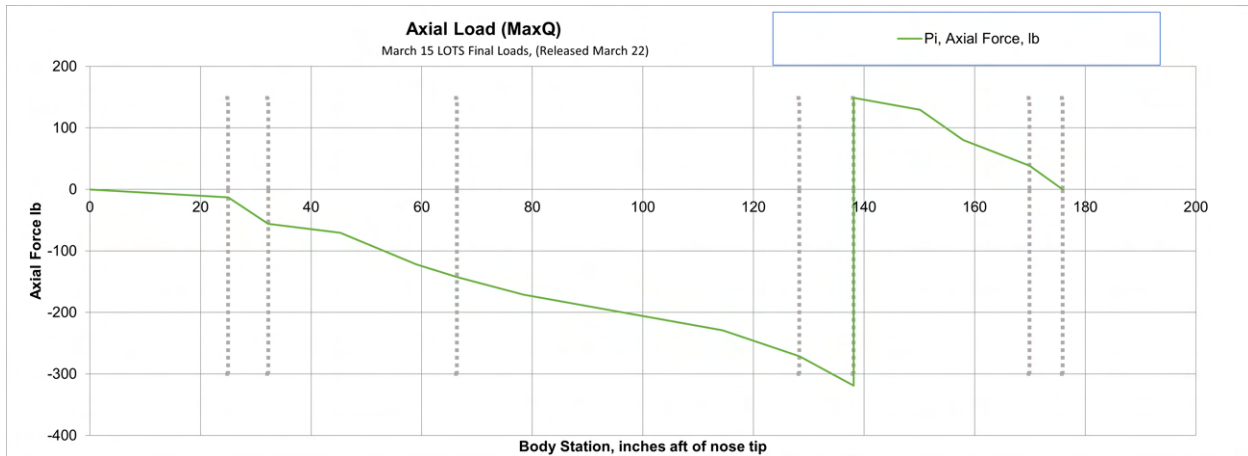


**Fig. 25 MaxQ Axial Loads**

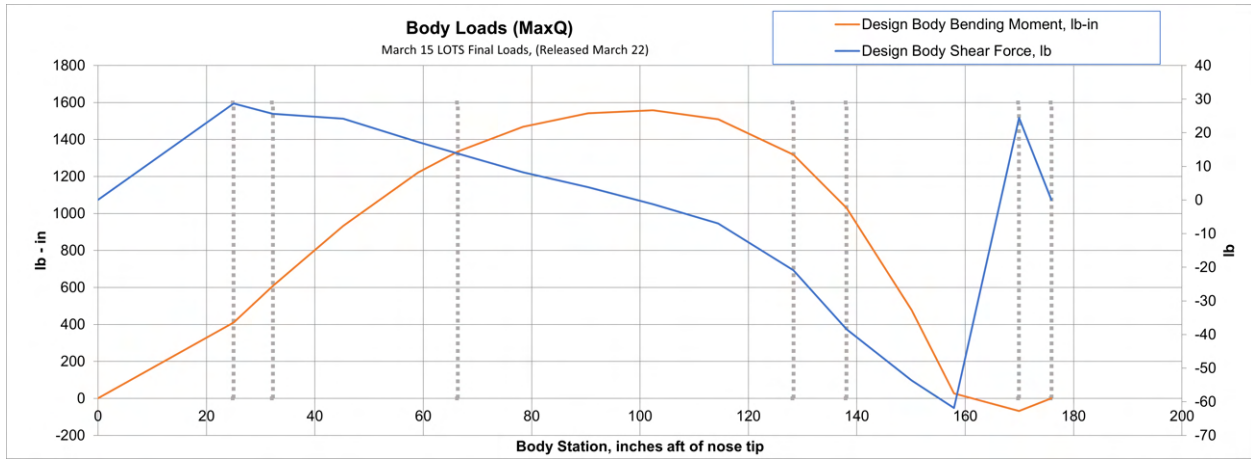


**Fig. 26 MaxQ Body Loads**

## 2. Nosecone

The fibreglass nosecone is built in a Von Karman shape with a 4:1 fineness ratio optimized for transonic and supersonic flight. It was manufactured in a vacuum bag layup process using a female mold as shown in figure 27. Each of the 2 halves used 4 fibreglass plies arranged in a scarf joint, shown in figure 28. The entire mold was left in vacuum as shown in figure 29 to evenly distribute the epoxy, remove excess epoxy and help the nosecone maintain its shape while curing.

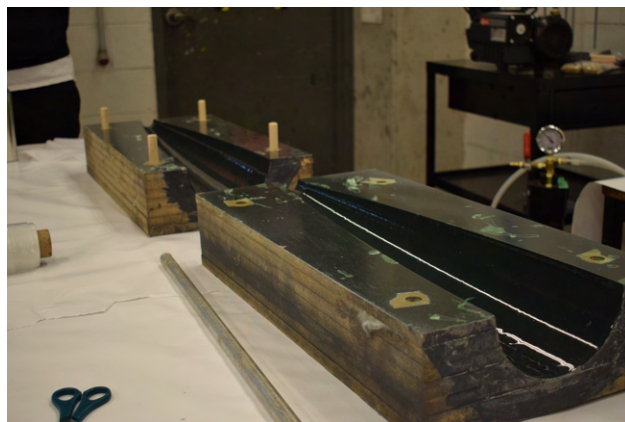


**Fig. 27 Nosecone Mold Halves**

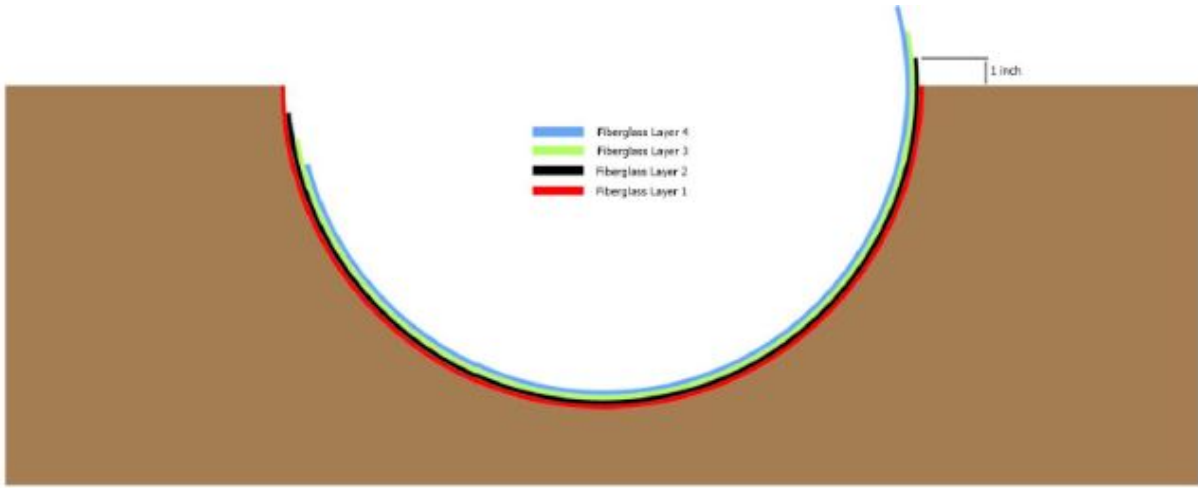


**Fig. 28 Scarf Joint**

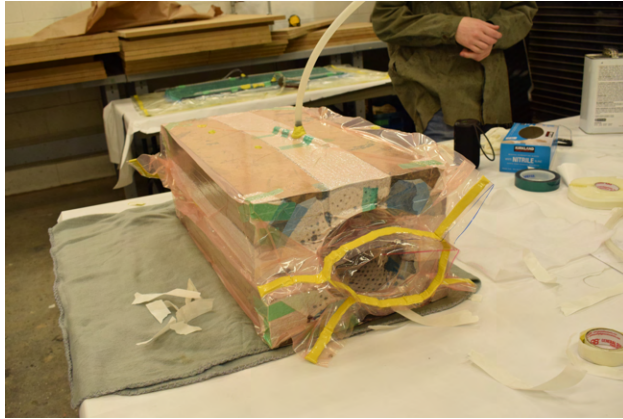


**Fig. 29 Nosecone Curing Under Vacuum**

The shape of the nosecone was verified through research and simulation in OpenRocket. It remains unchanged since Shark of the Sky, the team's 2019 rocket, which had a successful launch at SAC. Shark of the Sky (2019), Kraken of the Sky (2020-2022) and this year's Leviathan of the Sky all fly in the transsonic and supersonic regimes which allowed for the continued use of the 4:1 fineness, Von Karman nosecone shape. The nosecone tip is machined stainless steel and aluminum bonded together with epoxy. The stainless steel provides wear resistance as well as thermal protection from aerodynamic heating, and the aluminum provides a more lightweight medium in which threads for an eyebolt can be tapped. A line from the parachute connects to this eyebolt which keeps the nosecone attached to the rocket after parachute deployment. the parachute itself is also partially located inside the nosecone along with a 3D printed BigRedBee GPS enclosure. A shear pin coupler is epoxied to the underside of the nosecone to allow it to come off during parachute deployment. The nosecone is made from plain weave fibreglass in a stacking sequence of  $[\pm 45]_4$ , which is the number of plies used to create the scarf joint as shown in figure 28. With the number of plies, the nosecone

is thicker than the SRAD bodytubes (detailed in section II.B.3). The strength calculations for the SRAD composite bodytubes are based on the thickness of the part. The thicker the part, the lower the stress on the part. By having the nosecone be thicker than the SRAD bodytubes, it is reasonable to assume that the nosecone would be able to resist higher loads. This, coupled with the loads analysis (section II.B.1) showing lower loads on the nosecone than the bodytubes and the lowest safety factor on the bodytubes being at least 3, it can be confidently assumed the nosecone will not fail in flight.

### *3. Composite Bodytubes*

LotS features a combination of COTS and SRAD composite bodytubes that make up the airframe. The SRAD composite bodytubes were designed to be superior to COTS bodytubes in a number of specific ways. First, the SRAD bodytubes can be made to variable length, increasing material uniformity and reducing manufacturing complications. As well, in-house bodytube fabrication removes the need to deal with external vendors who may have long or inconsistent lead times, which allowed for greater flexibility and better project planning. Next, the stacking sequence of the bodytubes can be tailored to the load case experienced by each specific tube which creates greater weight savings while still maintaining the required strength. Finally, it provides an opportunity for team members to get hands on experience at composites manufacturing, which further develops the team's composite knowledge and manufacturing capabilities. For these reasons, almost all LotS bodytubes are SRAD, with the exception of the upper bodytube. This part is COTS due to various defects in the manufacturing process of the SRAD bodytube which made the part unfit for flight. Due to timeline constraints, it was decided to use a COTS bodytube instead of attempting to manufacture another tube.

### **Layup Schedule Calculations**

Calculations were performed to determine the required number of plies and type of fabric needed to create the bodytubes based on the predicted loads. It was known that the upper sections of the rocket, including the nosecone, parachute bay and upper bodytube, needed to be made of fibreglass. This was due to a requirement for RF transparency in order to ensure proper function of the avionics components located in those sections, including the GPS. The lower sections of the rocket, including the oxidizer tank aft skirt fairings and the fin can/combustion chamber bodytube, were made of carbon fibre due to it having a higher strength-to-weight ratio than fibreglass and having no requirement for RF transparency. The oxidizer tank aft skirt fairings in particular did not have a strength requirement, because load in the oxidizer tank aft skirt is entirely supported by the longerons (see section II.B.6). The bodytubes that did have a strength requirement were the parachute bay, upper bodytube and fin can/combustion chamber bodytube (both sections are fabricated as one tube). The lowest safety factor for each is shown in Table 6. The calculations for these are detailed in Appendix B, section IV.D.1.

**Table 6 Bodytube Lowest Safety Factors**

Bodytube	Lowest Safety Factor
Parachute Bay	8.1
Upper Bodytube	3.0
Fin Can/Combustion Chamber Bodytube	3.0

The safety factor was dependent on the thickness of the bodytube, which itself was dependent on the specific fiber and number of plies used. Using the thickness of the composite at 50% fibre volume given by the manufacturer, the layup schedule was iteratively refined by adding/removing material until the desired safety factor was reached. The upper bodytube was intended to be an SRAD bodytube, however as mentioned earlier, the part had defects when it was manufactured and therefore was deemed not fit for flight. Due to time constraints, the decision was made to use a COTS fibreglass bodytube for the upper bodytube instead.

### **Manufacturing Process**

The composite bodytubes were manufactured using a Vacuum Assisted Resin Transfer Molding (VARTM) process, also known as resin infusion. First, a surface preparation process was done through cleaning, waxing, and applying Polyvinyl Alcohol (PVA) to ensure that no contaminants were cured onto the part, and that the bodytubes were released from the mold without damage. Next, plies of fibreglass and/or carbon fiber were laid out in a female mold using Super 77 spray adhesive. Then, the part was placed under vacuum through poly-tubing attached on one end, with resin allowed to enter from the other via vinyl-tubing. As a result, the resin was pulled through the fibreglass by the vacuum, which ensures an optimal surface finish and low void content. The infusion setup is displayed in figure 30, along with an image of the combustion chamber-fin can bodytube manufactured using the VARTM process displayed in figure 31.

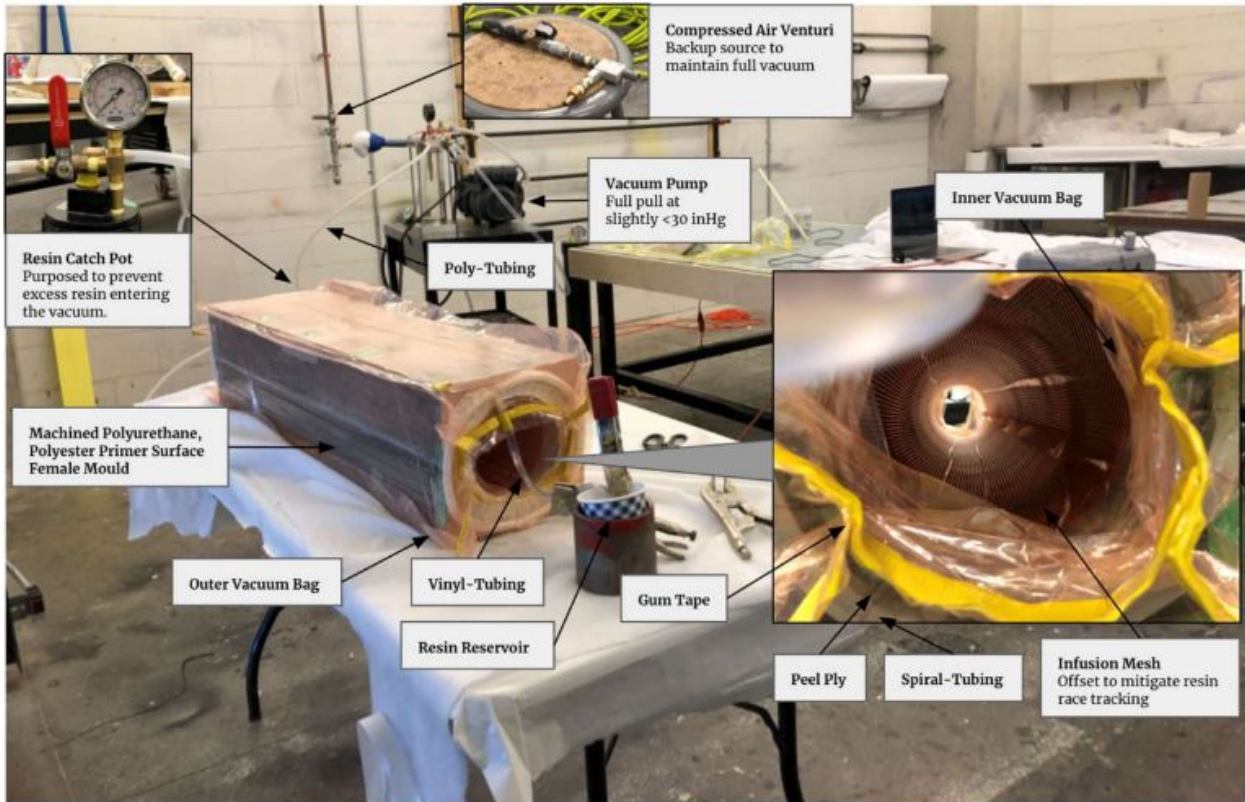


**Fig. 30 Infusion Setup**



**Fig. 31 Fin Can and Combustion Chamber Bodytube**

Material property characterization of these bodytubes is a work-in-progress, but so far, a compression test has been completed of a fibreglass bodytube with a stacking sequence of  $[\pm 45]_3$ . The stress-strain chart derived from that test can be found in figure 32. In the absence of a larger data set, high FOS and non-destructive testing have also been employed to ensure all components are unlikely to undergo structural failure. All composite components including bodytubes will be post-cured in the team's SRAD PID controlled curing oven to raise the components' glass transition temperatures

above the temperatures expected in the New Mexico desert and fully establish their desired physical properties.

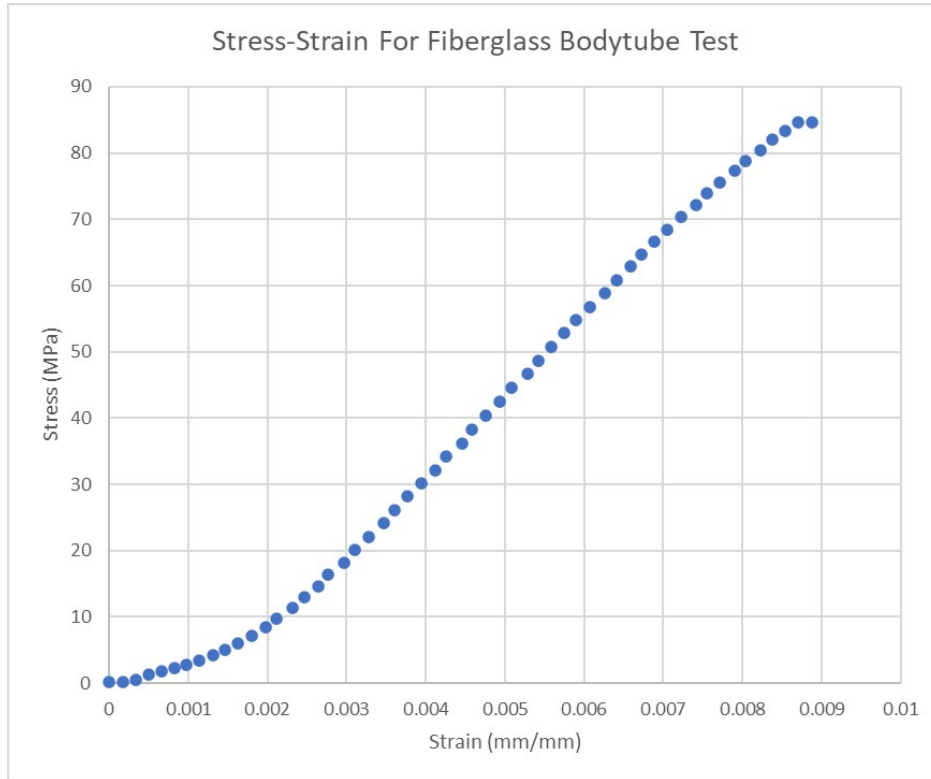


**Fig. 32 Stress-Strain Curve for Fibreglass Bodytube Test**

#### 4. Couplers

There are two styles of couplers in use on the rocket to fasten sections together: 2-piece metallic lap shear couplers with radial bolts, and longerons with axial bolts.

Longerons are only used in the Oxidizer tank aft skirt section to allow access to the inside of the rocket while on the launch rail. Everywhere else, unique aluminum lap shear couplers are used for their simplicity and low weight. Each of these joints

Each of these joints requires 2 couplers with mating features each extending 1" into their respective bodytubes. At joints where the bodytubes can be joined permanently, the adhesive extends across the entire surface of the coupler such that once cured, the two bodytubes are effectively joined as one component. When assembled, the couplers will be fastened using 6 radial screws.

#### 5. Upper Bodytube

An infusion was completed to create the upper body tube. However, due to some manufacturing defects, it was deemed not suitable for flight. Instead, a COTS upper body tube was purchased, cut, sanded, and squared to the desired length. The COTS upper body tube is much heavier and thicker than the SRAD body tubes, which affected the results of

previous simulations. This change also affected some parts which are to be bonded into the upper body tube, changing their outer diameters or fit constraints.

### **Recovery Bulkhead**

The recovery electronics and bulkhead assembly were designed to rigidly and efficiently provide mounting to the recovery and telemetry components. The bulkhead was designed to be as lightweight and easy to manufacture as possible, while providing mounting to the CO<sub>2</sub> Ejectors, main eyebolt, and panel mount pyrotechnic circular connectors. It is secured to two overlapping couplers via eight 1/4"-20 socket head cap screws, such that one coupler can be removed without needing to remove the other. This isolation of the parachute bay and recovery electronics eliminates the time spent unnecessarily unpacking and repacking the parachutes, an improvement from last year. However, the single row of radial bolts were maintained such that the bulkhead is kept as thin as possible. Since this design is statically indeterminate, dynamic analysis was conducted in SolidWorks FEA to verify that the bulkhead could withstand the maximum shock loading as discussed above. In a modal-time history simulation, dynamic load was applied in a curve resembling the expected shock loading curve as covered by Knacke. As an upper limit, a load of maximum 464 lbf was applied to the central eyebolt thread, as calculated and described above in the shock Loading section. The bolt holes were placed in a fixed condition. The deployment time was taken from similar 2019 flight altimeter data. This analysis showed that the bulkhead experiences a maximum stress of 13 MPa thus has a factor of safety over 20. Furthermore, stresses on the bolted holes were calculated, with a minimum factor of safety of 11 under shear stress for the steel bolts.

### **Payload Bay**

#### *Payload Bay Design*

The payload bay is the module that prevents the payload from moving around inside the rocket while in flight. The payload bay on LotS is shown in figure 33 and consists primarily of 2 centering plates, a bottom plate, a clamping plate and a shear ring.

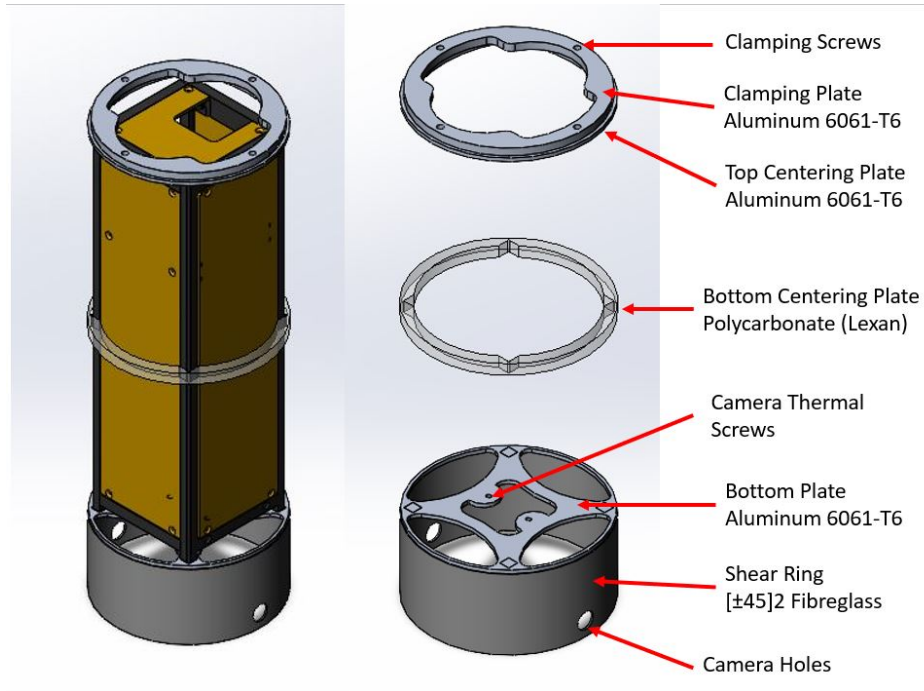


**Fig. 33 Payload Bay Layout**

The clamping plate prevents the payload from moving upward through the bodytube during descent. It has a smaller OD than the other plates because it is meant to bolt on after the payload is placed into the payload bay during competition. This would require it to fit through the recovery coupler at the top of the upper bodytube whereas the other plates are bonded into the bodytube before the recovery coupler. The bottom plate prevents the payload from moving downward during ascent. This plate also has 2 x 8-32 tapped holes. The bolts that go into those holes are part of a thermal bridge between the cameras and the bottom plate. The bottom plate will act as a heat sink for the cameras since the cameras can produce excessive heat during operation. The centering plates prevent any rotation of the payload. Finally, the shear ring provides added support to the bottom plate and provides reinforcement to the bodytube around the camera holes. The strange geometry and cutouts are meant to allow the CANBus wire and other electrical harnesses to pass through the payload bay to reach the payload itself and recovery sections above.

This design is an improvement over the design used in 2022 in that it uses 4 x 6-32 clamping bolts that are loaded in tension to prevent upward movement of the payload during flight. Last year, a single 4-40 bolt screwed into the side of the CubeSat and prevented upwards translation. At the time, that bolt was assumed to only be loaded in simple shear. Calculations performed last year showed that the single 4-40 would be sufficient to constrain the payload with a safety factor of 1.6. However, bending was not accounted for. With the addition of bending, the calculations showed that the safety factor was 0.07 and the design was deemed not viable. On KotS, the side screw was installed into the CubeSat through a polycarbonate plate which is far less stiff than the aluminum plate used on LotS. With the axial clamping

screws, it is assumed there is no bending in the bolts. The distribution of the 4 clamping bolts also limits any bending in the plate. The safety factors for various failure modes of the clamping bolts are shown in table 7. To clarify, shear ring failure is when the epoxy between the shear ring and bodytube fails so the shear ring becomes detached from the bodytube. The shear ring must be able to support the entire payload and payload bay, if necessary, without failing. Internal thread shear is that failure of the threads in the tapped hole. Detailed calculations on these failure modes can be found in Appendix B, section IV.D.2.

**Table 7 Payload Bay Safety Factors**

Failure Mode	Safety Factor
Bolt Failure	7.8
Shear Ring Failure	137.6
Internal Thread Shear	4.5
Bolt Tear Out	30.9

In addition to these failure modes, the minimum thread engagement length was calculated at 0.418 inches in Appendix B, section IV.D.2, Table 22. This is how deep the tapped hole, and thus the plate itself, needs to be. However, this number is based on the notion that the bolt must fail before the thread shears. [3] The bolt has a tensile strength of 170,000 psi while the plate only has 40,000 psi.[4][5]. In reality, it was calculated that the bolt would still not fail even if it had a tensile strength of 40,000 psi. Since this is the case, the difference in tensile strengths between the materials can be ignored and the minimum thread engagement length drops to around 0.098 in. This determines the minimum thickness that the top centering plate, with the tapped holes for the clamping bolts, can be.

With the bolts and shear ring having high safety factors, the plates themselves needed to be analyzed. For that, a static FEA was conducted using SolidWorks on the clamping plate and the bottom plate since these are the plates that the payload rests on directly and transmits force to. Figure 34 shows the load application and meshing for the clamping plate.

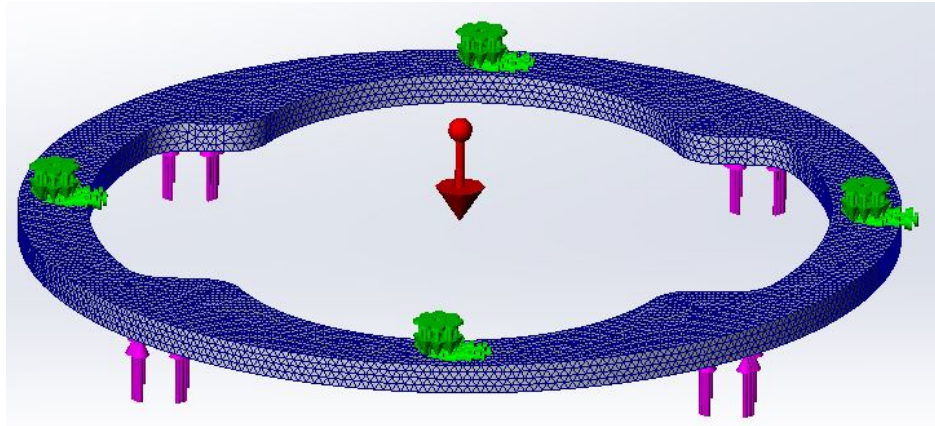


**Fig. 34 Clamping Plate Meshing**

The purple arrows denote the applied load from the CubeSat feet onto the plate. The applied load is 176 lbf which comes from multiplying the mass of the CubeSat (8.8 lbm) by the maximum predicted rocket acceleration of 20 g's. This load is distributed amongst the 4 CubeSat feet. The large red arrow in the middle denotes a gravitational acceleration of  $643.7 \text{ ft/s}^2$  which corresponds to 20 g's. In reality, these loads are caused by the acceleration of the rocket upwards which means the force from the payload would be acting on the bottom plate and not the clamping plate. However, using 20 g's for all load cases gives a more conservative estimate. The green arrows denote the constraints from the bolts. A fixed constraint is applied on a circular imprint of the bolt head on the surface of the plate. The finest mesh size is used for greater accuracy. The results of the simulation can be seen in figure 35.

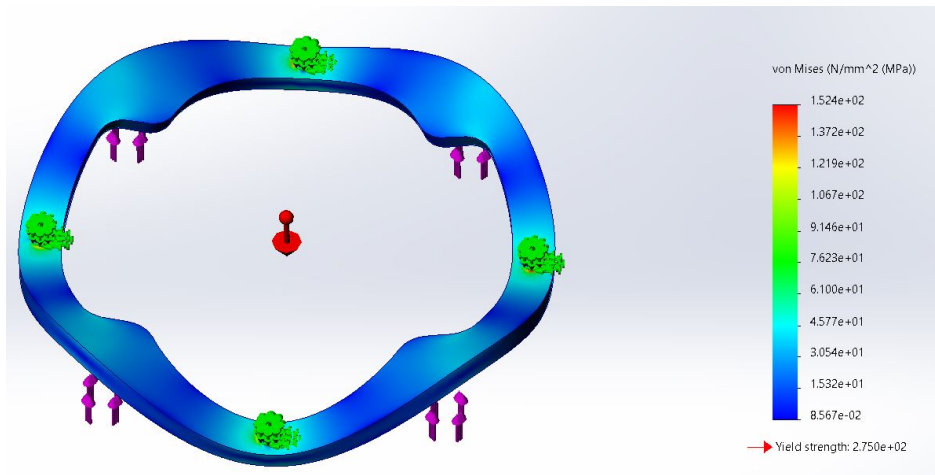
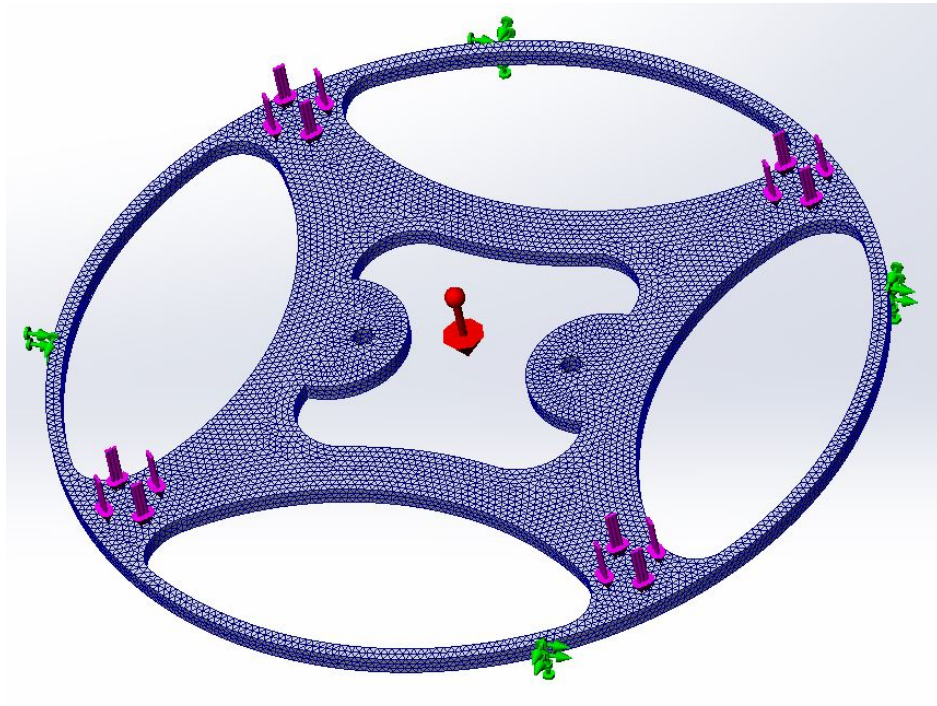


**Fig. 35 Clamping Plate Simulation Result**

The bar on the right of the figure indicates that the maximum stress in the plate is 22.1 ksi (152.4 MPa) whereas the yield strength of the plate, made of 6061-T6 aluminum, is 39.9 ksi (275 MPa). This gives a safety factor of 1.8. This

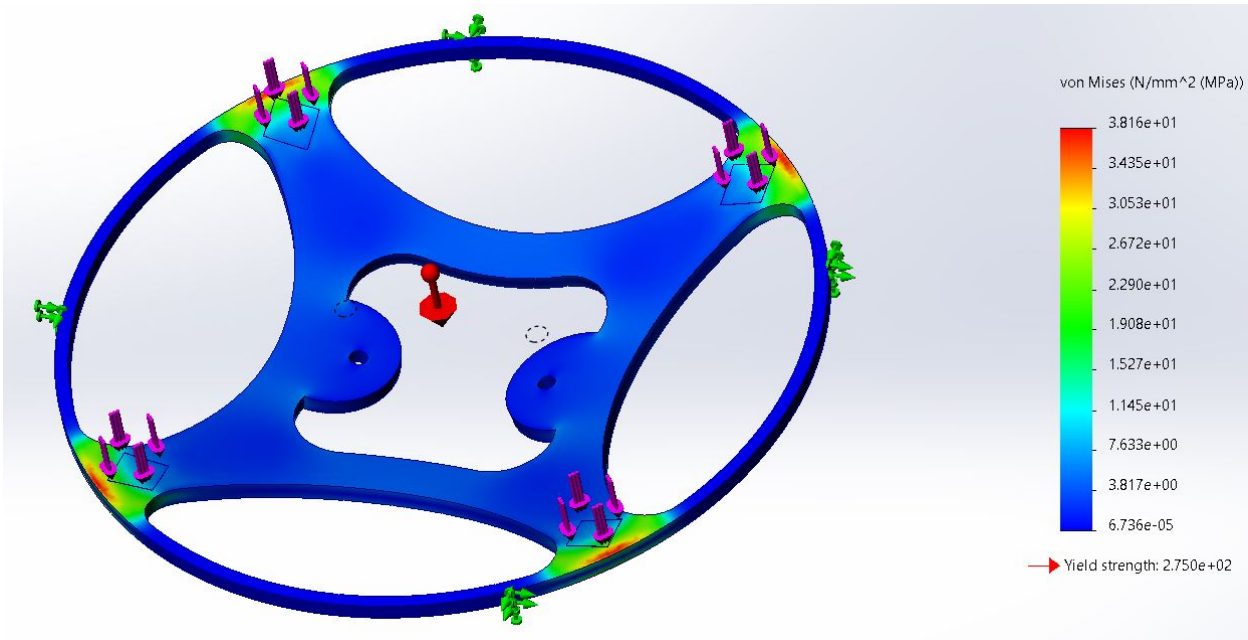
was deemed acceptable due to the conservative nature of the applied loads.

Figure 36 shows the meshing and applied loads for the bottom plate. The loads have the same magnitude and point of application as the clamping plate with the only difference being that the forces on the bottom plate act in the same direction. The mesh size is also set to the smallest for greater accuracy. The fixed constraint is all around the outside face. This represents the epoxy bond between the plate and the bodytube.



**Fig. 36 Bottom Plate Meshing**

The stress results from the simulation shown in figure 37 show that the highest stress on the plate is 5.5 ksi (38.16 MPa) which gives a safety factor of 7.2.



**Fig. 37 Bottom Plate Simulation Result**

The results from the simulations were used to size the thickness of the clamping plate at 1/4 inches and the bottom plate at 1/8 inches. The bottom centering plate, made of 3/8 inch polycarbonate, was not analyzed because it only experiences shear loads which are negligibly small.

#### *Payload Bay Manufacturing Process*

To manufacture the payload bay, plate stock was purchased from a material supplier. Then, the clamping plate, both centering plates and the bottom plate were cut using a waterjet to achieve their unconventional geometry. The 8-32 holes in the bottom plate and the 6-32 holes in the top centering plate were tapped. The shear ring was cut from a spare piece of SRAD bodytube. Next, all components, except the clamping plate, were bonded into the bodytube in a multi-step process. First, bonding surfaces were prepared by sanding with a low grit sandpaper, washing the surface using Simple Green household degreaser, and then wiping with acetone. Then, West Systems 105 epoxy resin and 206 hardener were mixed and the batch was split in half. One half of the epoxy was mixed with cabosil to thicken it. The unthickened epoxy was used to wet out the bonding surfaces after they had been prepared. Next, the thickened epoxy was slathered onto the bonding surfaces before the component was inserted into the bodytube and left to cure. This process happened over multiple days with the shear ring and bottom plate being bonded first. Then, the centering plates were bonded by resting the payload structure on the bottom plate and using it to align the centering plates. Finally, once the epoxy had cured, the camera holes were created in the bodytube and shear ring using a Dremel.

## 6. Oxidizer Tank Aft Skirt

The oxidizer tank aft skirt consists of an assembly of 3 longerons which are used to transmit the rocket loads between the injector bulkhead below and the fill bulkhead above. This differs from the monocoque bodytube structure used throughout the rest of the rocket. The reason for the longerons are to make the pneumatics, battery, fill plumbing, and injector valve in the oxidizer tank aft skirt accessible for maintenance while the rocket is on the launch tower. The section was covered by three SRAD carbon fibre fairings which each cover a third of the section and serve no structural purpose, but are easy to remove and provide the outer surface for aerodynamics of the section. A picture of the CAD for this section is provided in Figure 38

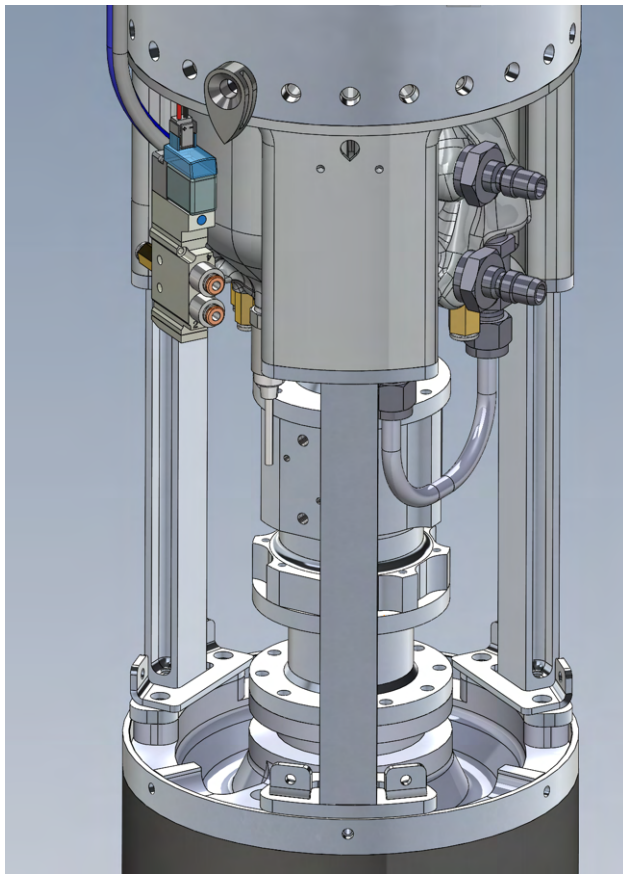


**Fig. 38 The oxidizer tank aft skirt section structure**

### Longerons

The longerons are 5.9 inch columns which take all of the load for the oxidizer tank aft skirt. They are pictured in Figure 39. They are bolted to longeron mounting brackets at the top and bottom with countersunk 10-32 bolts which are then bolted to the injector bulkhead and fill bulkhead with 1/4-28 bolts. An I beam shape with capped ends manufactured of 7075-T6 aluminum was chosen since it provided the highest eccentrically loaded buckling resistance, the limiting method of failure, at the lowest overall mass. Various other cross-sectional areas were investigated, but I-beams provided

the highest moment of inertia while also being relatively simple to manufacture. Aluminum 7075-T6 was chosen since its yield strength is almost double that of 6061-T6 aluminum, which means the eccentric buckling resistance increases significantly.



**Fig. 39 A longeron**

Various computer simulations were also conducted to support the paper calculations summarized in the appendices. This includes a thermal simulation to validate the thermal effects of the feedsystem cooling causing additional compressive stress on the longerons. A simple stress FEA and buckling analysis were completed as demonstrated in Figure 40. The FOS according to the buckling simulation is 1.72. This is slightly lower than the FOS provided by the hand calculations, but is within the same order of magnitude. A summary of the calculations and FOS for the oxidizer tank aft skirt section are shown in Appendix IV.D.3.

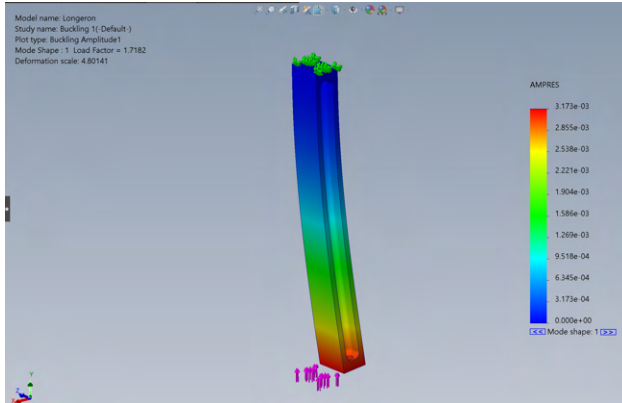


**Fig. 40 Buckling simulation on a longeron**

Initially, the idea was proposed to directly drill and tap the longerons to mount the fairings. However, the stress concentrations as a result of these holes would have required section mass to increase by 0.3 lb to maintain a FOS > 2. Instead, light sheet metal brackets attached to the longeron mounting brackets are used to secure the fairings. These allowed for a net 0.25 lb mass savings in the longerons. The sheet metal brackets were waterjet and bent to shape, with the addition of press fit nuts for the fairing mounting screws to thread into.

## Fairings

The  $\frac{1}{3}$  fairings make the oxidizer tank aft skirt section easy to access by removing the 6-32 bolts which hold each one in place. They are manufactured using the same resin infusion process used to manufacture the rocket's structural bodytubes. Once trimmed and sanded to size, they provide smooth and flush transitions from the oxidizer tank above to the injector bulkhead and combustion chamber bodytube below. The fairings are also the mounting position for the fill disconnect hatch and electrical disconnect systems. These are bonded into the fairings using West Systems 105 epoxy resin and 206 hardener, securing them in place.

## Fill Disconnect Hatch

The fill disconnect hatch provides an opening in the body tube covering the fill section for the pneumatic and oxidizer fill system to interface with the rocket. The hatch is mounted to a cutout in the body tube, must accommodate the fill disconnect mechanism, and must automatically close under its own means when the fill system is disconnected from the rocket following filling. This year's hatch consists of a 3D printed PETG frame and hatch with torsion spring sprung pins and magnets for a secure closure.

This year's iteration of the fill disconnect hatch was focused on three things:

- 1) the compact packaging of the fill section, due to the printed fill bulkhead
- 2) aerodynamic impact, due to the predicted hypersonic system velocity

- 3) the closure soundness, due to vibration

The design architecture was selected to ensure closure of the hatch by aerodynamic loading in case the hatch bounces open during flight or fails to close under its own means. The hatch is set to be flush with the body tube to minimize parasitic drag.

The size of the hatch was determined based on the profile of the fill disconnect system. Small torsion springs were chosen for compactness, with the understanding that they would be relied upon for keeping the hatch shut during flight. Two 270 degree bent torsion springs were implemented such that they were preloaded to the 180 degree position in the latch closed position.

Magnets were attached to the inside face of the hatch and carbon steel attach plates were attached to the frame for secure latching. This was desired and necessary due to the low torque of the small torsion springs, and high expected acceleration of the new rocket. The magnets and steel were attached with adhesive, and the frame is attached to the inside surface of the body tube with epoxy.

## *7. Fin Can*

### **Fin Can Design**

The fin can consists of a bodytube, fins, top coupler, and boattail. These components interface at the top and bottom of the combustion chamber to the engine. Some of the important considerations are: stability, flutter, drag, and composite ply/manufacturing design.

For stability, the team determined that a lowest stability of 2.5 cal in the expected condition was a good design target. 1.5 cal is considered the lowest launchable condition, however a safety margin is desired due to wind speed variation, manufacturing error, and design changes which can change the rocket center of gravity (CG). Having a stability higher than 2.5 is also undesirable, as it significantly increases drag. Due to manufacturing timelines, the fin can shape was finalized before the majority of the rocket design. This was possible due to the iterative cycle based design process discussed previously.

To determine the wind speed to design for, the team analyzed historical wind data from the launch site to determine what launch conditions are likely. This resulted in the data shown in the table below and an expected wind case of 9mph.

**Table 8 Historical Wind Data**

Wind Speed Range (MPH)	Number of Occurrences	Percentage
<=5	75	22.7%
>5 and <=10	145	43.9%
10 and <15	95	28.8%
15 and <=20	12	3.6%

From the table above, if the rocket is designed to launch in 15mph winds, it is clear that the rocket will be able to launch in over 96% of wind conditions. Any speed above 20mph will cause the range to close. Analysis was also done on temperature and pressure, and it was not determined to impact stability significantly enough to be a concern.

Fin flutter is the main failure mode to prevent on the fin can, and careful steps were taken to prevent it. Using an article from Peak of Flight [6] the flutter velocity of a given set of fins can be calculated using the formula below.

$$V_f = a \sqrt{\frac{G}{\frac{1.337 AR^3 P(\lambda+1)}{2(AR+2)(t/c)^3}}} \quad (1)$$

As various fin shapes were simulated the data was input into a spreadsheet to calculate fin flutter FOS and the results were used to dial in the fin shape.

A requirement to launch from the DTEG is a FOS on fin flutter of 1.5 . with the LotS FOS being 1.8. This means a flutter velocity of 2831ft/s. It is important to note that these calculations are using a 4.12GPa sheer modulus for carbon fiber. This is a conservative estimate for shear modulus, but due to unavailability of university lab equipment, this data could not be acquired experimentally.

Another large consideration while designing the fins is the reduction of drag. While this can be approached from a few ways, the approach used for LotS was to design various fin shapes using first principles and best practices, then simulate in OpenRocket to determine the apogee difference between different designs. From research done prior to fin sizing and previous team rockets it was known that clipped delta and trapezoid fins are commonly used for transonic and supersonic rockets due to low drag to lift ratios. Thus the team started with clipped delta and trapezoidal fins and iterated from there.

Manufacturing must also be considered while designing the fin can. The key to consider is that historically the fin can layup has resulted in fins around 10% thinner than theoretically predicted. As the layup is a time intensive procedure (100+ human hours) it is important to avoid a too thin condition which would result in flutter. In order to prevent this, historical manufacturing data was used to create a better estimation of thickness, with some additionally error margin. A spreadsheet was used to determine what layup schedule and plate stock would result in practical thicknesses and this

was used iteratively alongside the fin sizing.

Bringing all of those considerations together the process for fin design was started by creating an accurate OpenRocket file using rocket data gathered from each subsystem. Then fins were iteratively designed to achieve the stability, flutter, drag and manufacturing targets. Typically this was done by creating 3-5 shapes and simulating various weather conditions and rocket conditions (min/max mass etc.) to compare the shapes. This data was collected and used to create more potential shapes to consider. After running >100 OpenRocket simulations with collected data a swept delta shape was chosen. It is theorized that the sweep increases the moment arm of each square unit of area on the fin (as it is farther from the CG) which improves stability without increasing drag by increasing fin size. It was also found that increasing the fin number from three to four (compared to last year) increased performance. A picture of the fin can shape chosen can be seen in figure 41 below.

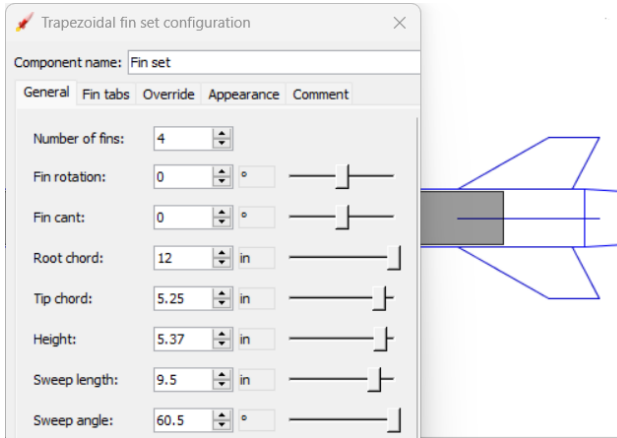


**Fig. 41 Fin Shape**

The upper coupler was designed using hand calculations to ensure coupler tear out, bearing and sheer all had greater than 2.4 FOS considering loading at liftoff, Max Q and deployment. There is also a stress concentration on this part which was analyzed in a similar manner.

### Fin Can Manufacturing

The bodytube is an SRAD carbon fiber tube made using two layers of braided sleeving, one layer of 4HS fiberglass and 1 layer of Textreme as discussed in the bodytube section.

The fins were made using 3/16in carbon fiber plate stock. This was cut on a CNC router into the fin shape chosen. Then the plate stock was bonded using Aeropoxy ES6228 to the fin can. A two part laser cut jig was used to ensure alignment and only two fins were bonded at a time. The jig can be seen in figure 42 below

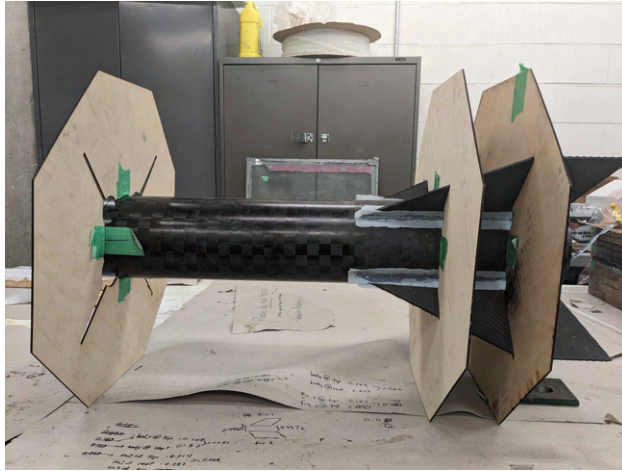


**Fig. 42 Fin Bonding Jig**

To ensure alignment a dial gauge and blocks were used to measure how square the bodytube was to the jig and to measure how square the fins were to the jig. After taking these measurements it was concluded that the error in the fin alignment was not measurable with the precision of the setup. This can be seen in figure 43 below.

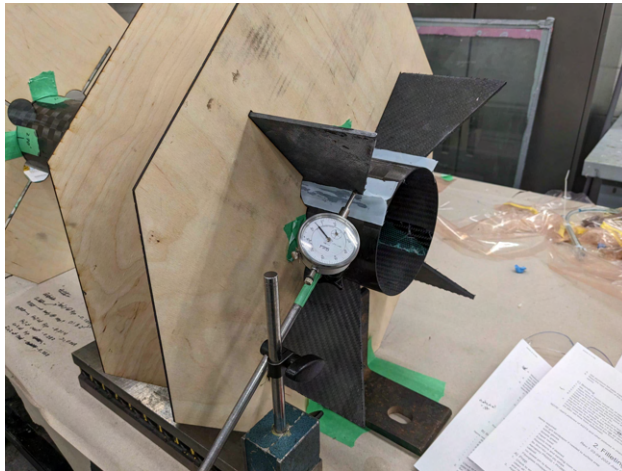


**Fig. 43 Fabric on Fin Can Prior to Vacuum**

Then a fillet was created between the fin and the bodytube using Aeropoxy PR2032 + PH3663 and Cabosil. A 1in diameter dowel pin and peel ply were used to form a consistent shape. This can be seen in figure 44 below.



**Fig. 44 Fin Fillet Forming**

After filleting, the shape was sanded by hand to remove excess epoxy and create the profile desired. This is the last step prior to the tip to tip layup. The results of this can be seen in figure 45 below



**Fig. 45 Fin Fillet Post Sanding**

In the tip to tip layup 5 layers of carbon fiber were used. 4 layers of 194gsm 2x2 twill and 1 layer of Textreme 80gsm. This was chosen to achieve the required thickness and to get a good surface finish out of the bag. The fabric was wet out between plastic sheeting and then put onto the fin can layer by layer. All 20 large pieces of fabric were done in one large layup. Then the entire setup was vacuum bagged and vacuum was pulled to draw out excess epoxy. Pictures of this process can be seen below.



**Fig. 46 Fabric Wetting Process**



**Fig. 47 Fabric on Fin Can Prior to Vacuum**



**Fig. 48 Vacuum Pulling Excess Epoxy Out**

After the tip to tip layup, the fin can was demoulded and will be repeatedly epoxy coated and sanded to improve the

surface finish. Sanding jigs were 3d printed to achieve the desired leading and trailing edge tapers.

The upper coupler will be machined out of 6061 T6 Aluminum and bonded to the fin can bodytube.

#### 8. *Boattail*

The conical boattail the aft end of the engine, producing a more streamlined vehicle shape and thereby reducing pressure drag. The geometry of the boattail and the position of the boattail on the rocket are shown in figures 49 and 50 below. Retaining pins are used instead of machine screws to seal the aft end of the combustion chamber, so that only 4 screw heads are protruding, giving a smoother profile to reduce drag.

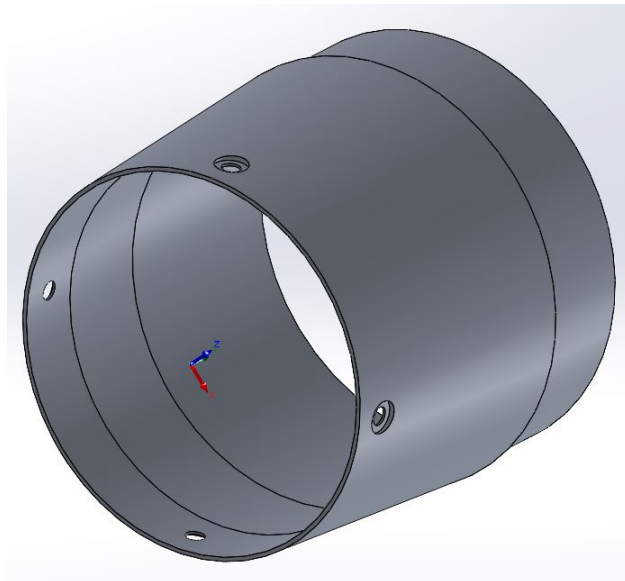


**Fig. 49 Boattail**

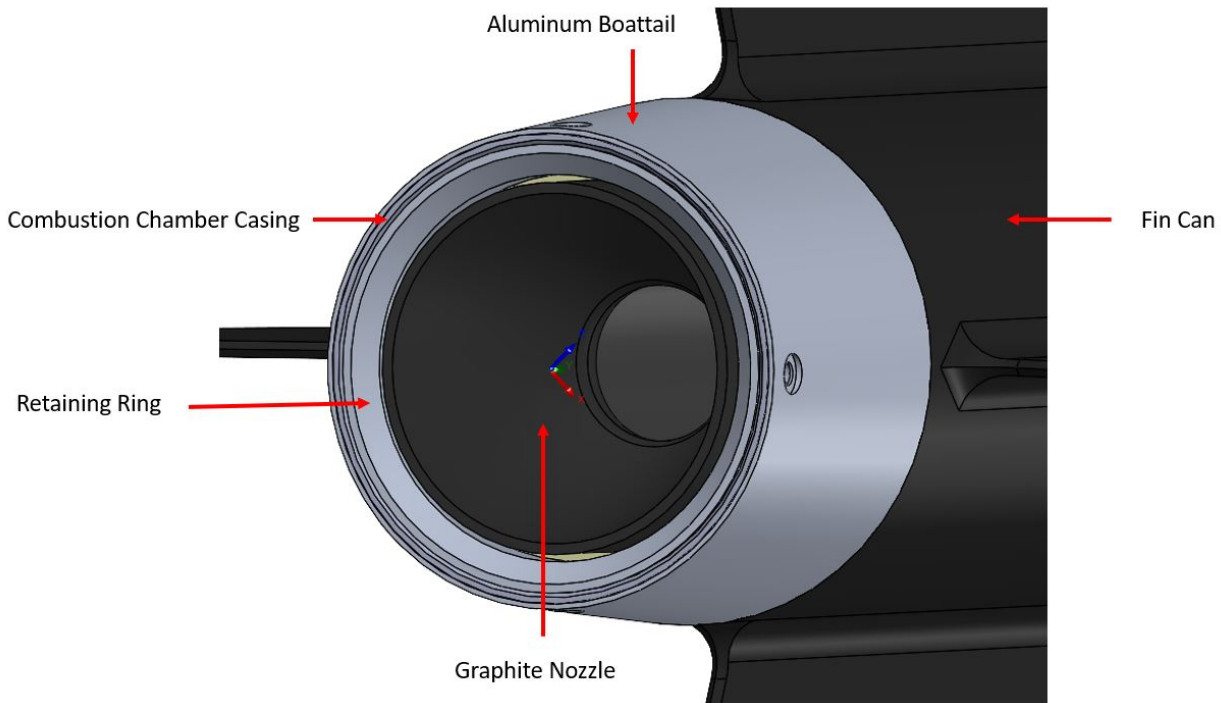


**Fig. 50 Boattail Assembly**

The boattail is machined out of aluminum and doubles as a heat sink to mitigate thermal loads on the combustion chamber. In previous years, the boattail was built to be a heatsink first with aerodynamics as an afterthought. At the time, the primary concern was that the combustion chamber was made of aluminum 6061 T-6 which can anneal and over-age if exposed to high temperatures, thus reducing its strength. With a new nozzle placement, heating of the combustion chamber has become less of a concern so the new boattail is an aerodynamic piece first and foremost. To this end, it is thinner, lighter and requires fewer bolts than the previous boattail.

### C. Recovery

The recovery system for LotS is a two-stage reefing parachute system that was largely developed for the KotS. Due to the system not being flown in 2022, the decision was made to keep the major structure of the system the same, but upgrading, replacing, and optimizing where possible. Some of the major changes include an optimized deployment system, an electro-mechanical solution for tangling, a new parachute, and an updated rigging setup. The newly sewn main parachute is sewn of black/yellow rip-stop nylon, is 3.25m in constructed diameter, with an elliptical canopy shape with a 0.707 eccentricity. All geometric characteristics are kept identical to the previous parachute, including the use of the same metal reefing rings on each gore seam. This was done to retain the ability to utilize a similar strategy of reefing-line sizing as KotS, to streamline reefing line sizing once fabrication is complete. It is folded into a custom parachute bag, and pulled out by a small SRAD pilot chute. Figure 51 shows the KotS's parachute packed in its bag,

which will be similar to LotS's.



**Fig. 51 Packed KotS parachute in old parachute bag**

The first deployment event is actuated using CO<sub>2</sub> canisters which pressurize the parachute bay, shearing the shear pins holding the nosecone on, thereby releasing the pilot parachute into the air-stream. After inflation, the pilot parachute pulls the reefed main out of the parachute bag. Reefed descent then occurs at a target speed of 115 ft/s until 1500 ft AGL. At this point, a pair of SRAD titanium pyrotechnic line cutters activate, severing the reefing line and allowing the parachute to disreef to its full size, slowing the rocket down to 28.5 ft/s. This is below 30 ft/s, as per the DTEG. There are no independently recovered items, all parts of the rocket are contained within this recovery scheme.

The recovery rigging is connected to the forged steel eye bolt that is screwed into the recovery bulkhead. The rigging begins with the 5000lbf Petzel gated swivel that connects directly to the eyebolt. Connected to this is the shock cord and two ring release system, that run in parallel. The newly-sized 25-ft long, 3/8" tubular kevlar shock cord purchased from OneBadHawk runs parallel to the long, control line that restricts the parachute's diameter. At the top of the shock

cord is the shroud line point of confluence (SLPOC), which is housed on a 5000lbf carabiner. The control line passes through SLPOC and continues parallel to one of the shroud lines, up and through the reefing rings. The uppermost part of the rigging is the 24" pilot parachute, which is sewn to the top of the the parachute through straps of high-strength webbing inside of the parachute vent. A diagram of the exact lengths used in the rigging and the concept of operations is shown in figures 52 and 53.

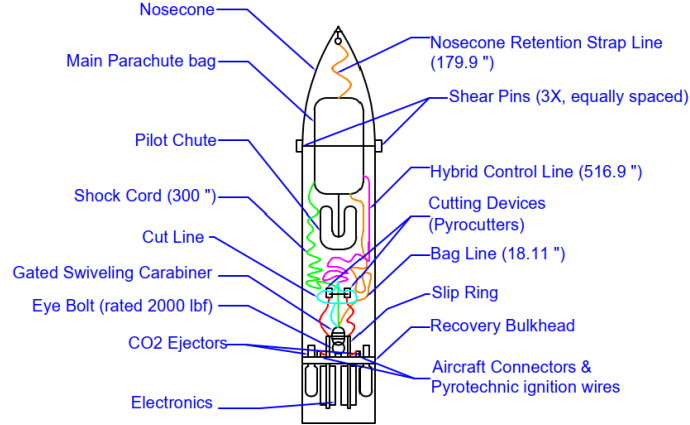


**Fig. 52 Diagram of packed recovery system**

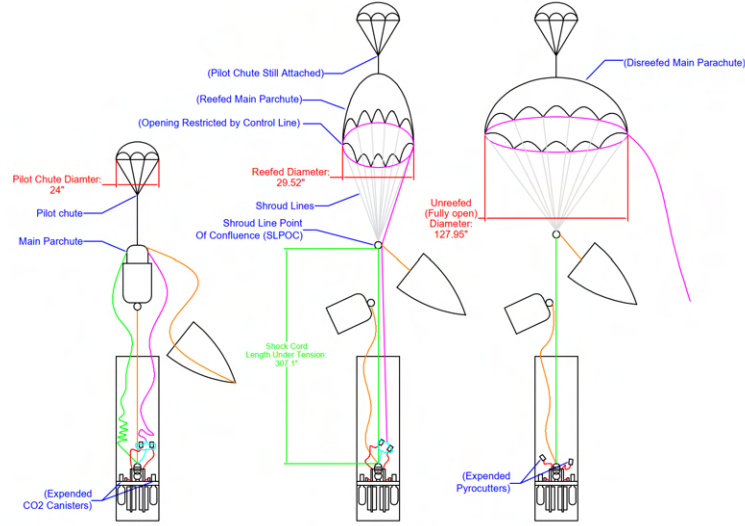


**Fig. 53 Diagram of recovery system concept of operations**

The recovery electronics, which includes the altimeters, arming boards and batteries, are located on the recovery electronics sleds attached underneath the recovery bulkhead. The recovery electronics sleds are 1/8" fibre reinforced plastic boards for radio transparency backed with a 3D printed stiffener to reduce vibrations. The recovery bulkhead uses

two hermetically sealed panel mount connectors to pass the CO<sub>2</sub> ejection and pyrocutter signal through the bulkhead. After passing through the bulkhead, the CO<sub>2</sub> ejection wires go to the CO<sub>2</sub> ejectors, which have been employed and used in the team for many years. Before reaching the pyrocutters, the signal first passes through a CENO 360 industrial sliring. The sliring is used to ensure the rotation of the pyrocutter wires, which are attached to the pyrocutters upstream of the swivel, stays consistent with the rotation of the parachute, thereby eliminating the chance that the pyrocutter wires wrap around the parachute lines, and rip out. A small, 3D printed cone is used to guide the wires around the rigging. Ground testing is currently being performed to ensure the reliability of this system. Other than that, the architecture and lengths of the system remains similar to that of last year's recovery system.

This year, time was spent optimizing the size of CO<sub>2</sub> cartridge needed. Previously, two large 38g canisters were used. This caused issues with our recovery electronics, as it had to work around these bulky canisters. Thus, it was decided that it was worthwhile to sacrifice some of the large safety overhead and optimize this canister down. The calculations behind the rapid pressurization of the parachute bay to detach the nose cone incorporate ideal gas law and pressure concepts. First, tensile testing performed on the nylon push-in rivets that anchor the nose cone determined that a force of approximately 960.8 Newtons fractures three of them. Before determining the exact forces required, the altitude at which the worst-case scenario for deployment needed to be determined. It is not guaranteed that LotS reaches the predicted apogee, but it still needs to be recovered successfully. Due to the appropriately sized vent hole, the pressure is assumed to have equalized both inside and outside in the parachute bay. Thus, the low-density, cold, atmospheric conditions for the predicted altitude of 30,000 feet result in the least favorable conditions, requiring more of the CO<sub>2</sub>'s energy being put into overcoming the reduced air density and temperature. After adding a factor of safety of 1.5, the result comes to just over 18 grams. Therefore, two (for redundancy) 20 gram canisters are used. Appendix IV.E shows these calculations in more detail.

The other new feature of this year's recovery system are custom-designed pyrotechnic line cutters. The rationale behind making a custom design was to have greater control over the cutting force of the cutter. Furthermore, the goal was to enable more reliable reuse and disassembly. A titanium housing was designed and machined. To ease loading, the design utilizes a 3D printed black powder casing, onto which the cutting pellet is superglued. The pellet is machined out of D2 tool steel, finished with 2000 grit sandpaper. It is subsequently hardened via a quenching process carried out with a handheld MAPP gas torch and brine solution. This design was successfully tested, and proved capable of cutting the cypress line that is used in the recovery system. More qualification testing is progress, and the design is flexible enough to accommodate black powder charges capable of cutting even stronger materials. A figure showing the successful test of the cutter is show in figure 54.

This year's new SRAD recovery bulkhead was inspired by last year's design, but with features to accommodate the sliring and updated component positioning. The team was also able to source a supply of 6" round Aluminum 7075-T6 stock, which the bulkhead was fabricated from. SOLIDWORKS Simulation was used to analyze the parts under both



**Fig. 54** Successful Test of the SRAD cutter

static and dynamic loading. Due to the rotating and stationary nature of parts within the recovery system, particular care was put into ensuring the deflection was low enough to keep parts from interfering even under worst-case loading. A modal time history analysis study was performed based on a rough approximation of Theodore Knacke's parachute opening forces diagram [7]. The studies were set up to apply the opening shock forces assuming the parachute deploys when the rocket is falling parallel to the ground. This forms a large bending moment on the eyebolt, which is the worst situation for interference on the slipring system. Figure ?? contains the results of the studies.

#### **D. Avionics and Electrical Ground Support Equipment**

Leviathan of the Sky's avionics system contains 3 main components: the RocketCAN bus, a pair of dissimilar COTS Altimeters, and an independent GPS tracking module from BigRedBee. The RocketCAN network consists of individual boards with single functionalities, which communicate through a Controller Area Network (CAN) bus. This system was initially introduced in 2019 on Shark of the Sky (SotS), but has undergone significant updates since then, including new revisions of every board based on lessons learned throughout the previous years. In addition, this year, new systems have been introduced and upgraded including a long-range live telemetry radio system, in-flight camera systems, and an on-the-pad charging system.

The Electrical Ground Support Systems (EGSE) has also had substantial upgrades this year. Both the Remote Launch Control System (RLCS) and Data Acquisition System (DAQ) have had notable changes to their boards and software. These changes provided not only better quality of life features for the equipment operators but also improved both reliability and repairability of the aforementioned systems. The most noteworthy change this year was the introduction of our Ground-Side Power Distribution system (GSPD) which provides a reliable power source for all ground systems and the rocket.

Both avionics and EGSE systems are summarized in Figure 55 below.

##### *1. RocketCAN*

The avionics modules on the rocket use a Controller Area Network (CAN) bus to communicate. The CAN protocol was primarily selected for its ruggedness; it has strong noise immunity and is suitable for safety-critical outdoor applications. Additionally, CAN is a democratized protocol. There is no bus 'master' or 'slave' and all boards have an equal opportunity to take control of the bus. This aids the fault tolerance of the system — any individual board can fail without affecting the rest of the bus. Each of the modules can send and receive messages independently using the bus. For example, the Live Telemetry Transmitter (LTT) board can send a message to the vent actuator board to open the vent valve. This modular approach maximizes reliability and robustness and reduces coupling between the different avionics systems. Additionally, if any individual board fails it can quickly and easily be replaced with an identical spare copy. Table 9 gives an overview of the different systems on the rocket

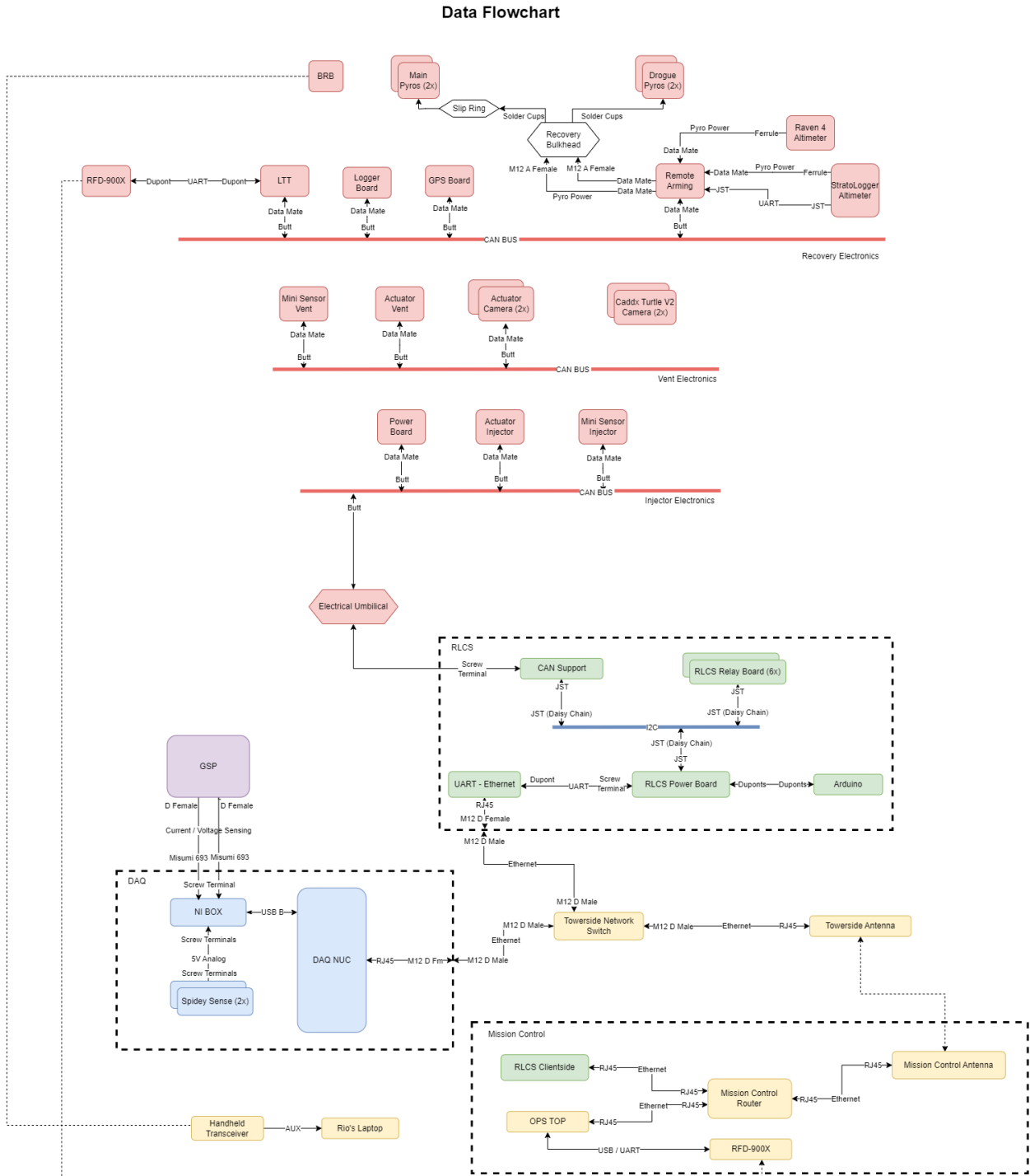


**Fig. 55** Block diagram of RocketCAN system and EGSE, showing the data flow between the various components

### Bus Topology and Harness Design

To allow all the RocketCAN systems to communicate there is a harness that runs the length of the rocket, connecting the boards in a tree topology. The bus can be separated into multiple sections for disassembly and transport via in-line

System Name	Location(s)	Description
Actuator Board	Injector Section, Vent Section (x3)	Used to control the pneumatic solenoids for actuating the SRAD injector and vent valves and power each flight camera.
GPS Board	Recovery Electronics Bay	Detects the GPS location of the rocket and relays it over the CAN bus.
Live Telemetry Transmitter	Recovery Electronics Bay	Sends and receives messages from the ground, relaying telemetry and commands to and from other systems on the CAN bus. It also controls and regulates power to the CAN bus, allowing the rest of the bus to be shut off to save energy.
Logger Board	Recovery Electronics Bay	Records all CAN messages to an SD card, including all telemetry and commands for post-flight analysis.
Mini Sensor	Injector Section, Vent Section	Capable of measuring from a pressure transducer and thermistor, as well as an IMU and barometer. Used to measure pressure in the combustion chamber, pneumatic lines, and oxidizer tank, as well as gather pressure and altitude data.
Caddx Turtle Camera	Vent Section (x2)	A COTS drone camera. Two cameras in the vent section are used with 180-degree lenses to capture pseudo-360 degree video of the rocket flight.
Remote Arming	Recovery Electronics Bay	Allows for the redundant COTS recovery altimeters to be armed remotely via the CAN bus, as well as gathering comprehensive telemetry data about the recovery system to ensure correct operation.
On-the-Pad Charging	Injector Section	Provides charging capabilities and status reporting for the rocket's LiPo battery. Prevents rocket battery drainage whilst on the pad and provides warnings concerning low rocket battery voltage levels.

**Table 9 Summary of RocketCAN systems and locations**

Harwin Gecko connectors, which are reconnected during final assembly.

Electrically, a CAN bus consists of a differential wire pair for communications connecting the modules together in a tree topology. Each end of the bus is terminated with a  $120\ \Omega$  resistor that ties the high and low lines together when they aren't driven. The RocketCAN implementation includes the CAN bus wire pair, a common ground line, and regulated



**Fig. 56 Male (G125-FC10605F1-0150L) and female (G125-MC10605M1-0150L) gecko cable assemblies**

+5VDC and unregulated +12VDC power lines.

The harness is connected to each system using Harwin Datamate connectors. These connectors, shown in the figure below, along with the Gecko in-line connectors above were selected as they are shock resistant and can survive the intense mechanical vibrations experienced during flight thanks to their screw-locking mechanism. This has been confirmed through testing, including post-flight analysis of the electrical systems on LotS's predecessor, Shark of the Sky, which had a high-g landing due to a failed main parachute.



**Fig. 57 Female Harwin Datamate connector assembly (M80-9410642) with a Male Harwin Datamate PCB mounted connector (M80-5400642) beside it**

Since the harness is subject to high loads and wide temperature ranges, particularly the section of the harness which connects the vent and injector sections and runs along the outside of the oxidizer tank, the use of high-quality wire is critical. As such the CAN bus harness is made primarily from 5 conductor shielded cable with Tefzel jacketing, conforming to MIL-C-27500. This is connected to the COTS pre-crimped contacts provided by Harwin, which also use durable, high-temperature PTFE insulation. All connections are made using suitable butt splices and clear heat shrink complying with the IREC DTEG safety-critical wiring guidelines.

### Common RocketCAN Hardware

Most RocketCAN boards are built around the PIC18F26K83 microcontroller (abbreviated as “PIC18”). The PIC18 is an 8-bit microcontroller running at 12 MHz selected for its low power draw, expansive I/O capabilities including



**Fig. 58 Tefzel jacketed cable used for rocket harnessing (M27500-22TG5T14)**

CAN support, low price and high availability throughout worldwide chip shortages. Most of the RocketCAN boards do not perform any complicated processing that would require a larger or more powerful processor, allowing cost savings and simpler embedded code. Some boards such as Logger Board that need to handle a large amount of data use a 16 bit microcontroller from the dsPIC33 series, selected for its higher clock speed and data bandwidth.

The PIC18 microcontrollers are wired up very similarly across all RocketCAN boards. The MCLR, ICSPDAT and ICSPCLK wires connect to the PICKit3 programmer used to load code onto the boards. OSC1 and OSC2 connect to an external 12 MHz crystal oscillator. CAN\_RX and CAN\_TX connect to a CAN transceiver such as the MCP2562. Lastly, a number of debugging LEDs are included which will often show board status or a heartbeat indicating the board is alive and well.

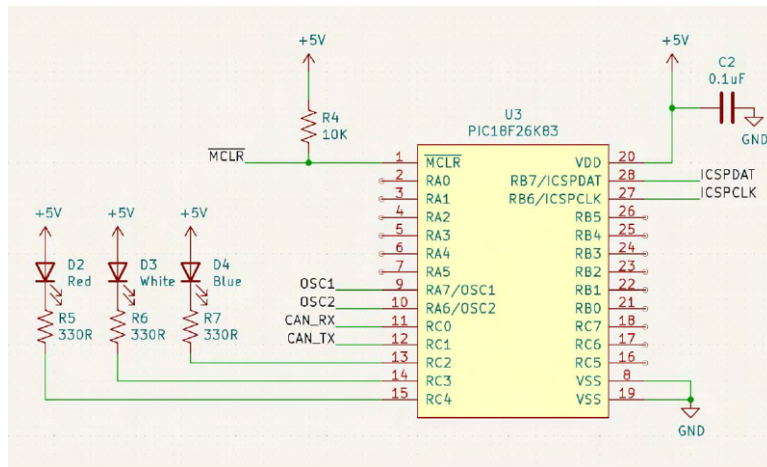


**Fig. 59 Schematic of standard PIC18F26K83 connections**

Another common fixture on RocketCAN boards is the CAN transceiver. This is a chip that is responsible for converting the differential CANH and CANL signals into digital CAN\_RX and CAN\_TX signals. The MCP2562 was selected for this purpose due to its ease of use and price. Additionally, drop-in replacements are available should availability become a concern due to ongoing shortages.

The boards are programmed using a PICKit3 which can also act as an in-circuit debugger. It requires three lines to be connected to the microcontroller: MCLR, ICSPDAT and ICSPCLK. These lines along with power and ground are broken out to a Dupont connector placed on each board for ease of programming.

The last feature common across all RocketCAN boards is the CAN connector and power circuitry. Each board is

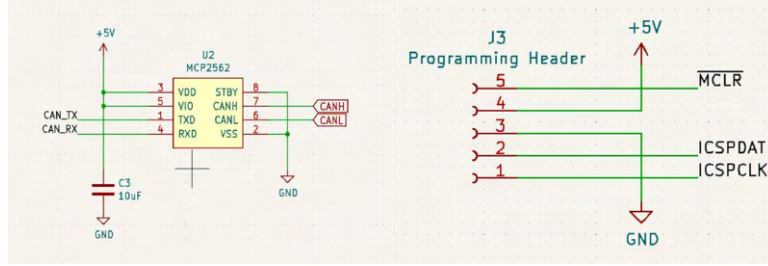


**Fig. 60 Schematic of the MCP2562 CAN transceiver and PICKit3 programming header schematic**

equipped with a current sensing resistor on the +5 V line which allows it to measure and report how much current it is drawing. The voltage drop across the resistor is amplified by an INA180 current-sense amplifier and measured by the microcontroller using its internal analog-to-digital converter. This in combination with a polyfuse allows boards to detect and appropriately react to an internal fault.

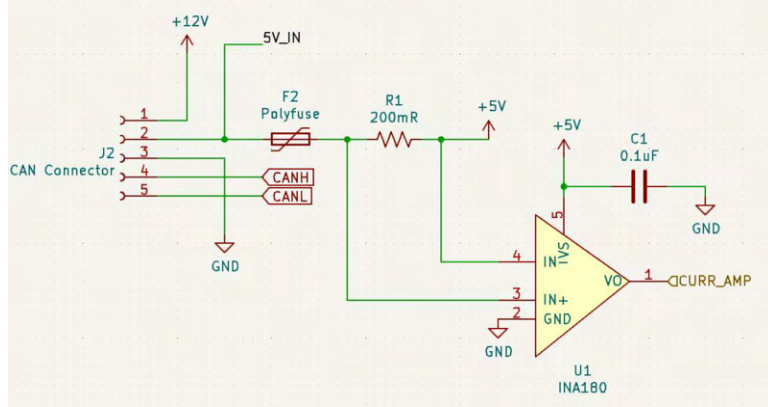


**Fig. 61 CAN connector and current sensing schematic**

### Common RocketCAN Software

To handle the intricacies of CAN and ensure a common set of message types, board IDs, and data field formats, all RocketCAN boards use a shared library known as “canlib” to interface with the CAN bus. Canlib provides functions to build and inspect the various CAN message types, ensuring the format of the data field is well-defined, and abstracts over the specific CAN hardware used which allows its use on the various microcontrollers in the system.

All boards on the CAN bus must fail safely, and the software is an important factor in this. Each board periodically produces a “nominal” status message to indicate that it is still online and functioning correctly. If any of the internal error checks on a board fails the status message will be replaced with an error message indicating the error detected, which will be relayed to the operator over the live telemetry system. Additionally, safety-critical boards will automatically go into an appropriate safe state if an error is detected. For example, if the vent actuator board detects a critically low battery voltage, it will send a low battery warning and open the vent valve in order to safe the rocket. The nature of the safe

mode depends on the function of each board, but it is generally a state which will minimize hazards to both the rocket and the human operators. The democratized nature of the CAN bus system means that if any of the boards suddenly stops functioning, the bus will remain online and the other boards on the bus can continue functioning normally.

## Message Format and Arbitration

RocketCAN uses the standard CAN 2.0A message format, on top of which the RocketCAN message system has been designed. An example of a standard CAN message is shown in the figure below.

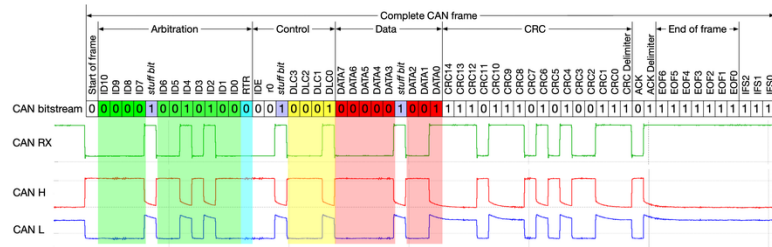


**Fig. 62** Example CAN message

The key fields in the CAN message are the Arbitration, Data, and CRC bits. The CRC, or Cyclic Redundancy Check, is built into the CAN hardware, and provides robust error detection for each message, ensuring no false data or commands are read, without the need for any software. The data field of a can message can be up to 8 bytes long and is what carries the information in each message. The 11 arbitration bits are used to determine the priority level of a message, with all zeros being the highest priority, and all ones being the lowest. RocketCAN splits these bits into two further fields, the board ID and message type. The first six bits are the message type, these are the more significant bits with respect to priority which ensures that higher priority messages (such as valve commands) are selected to be sent over lower priority ones. The lower 5 bits are used to determine which board is sending the message, this is a convenient place to store this information and has the added benefit of breaking message ties by prioritizing more important boards such as remote arming or actuator board.

## Telemetry Architecture

The primary method of communication between the rocket and mission control is the live telemetry system. Telemetry data sent on the RocketCAN (such as position from GPS board and acceleration from Mini Sensor) are serialized by the Live Telemetry Transmitter (LTT) board as a UART stream and sent to mission control through the RFD900x radio modem and SRAD antenna. In the other directions, LTT deserializes commands from mission control into CAN messages where they can be processed by all boards on the RocketCAN bus. The RFD900x modem was selected for its long range and ease of use as a transparent UART link over radio. It operates on the 900MHz band and has transmit power up to 1 watt.

An SRAD antenna is used on the rocket side of communication. It is made by routing long traces on a PCB as two orthogonal dipoles, with dimensions designed to fit into the body tube horizontally. This approach allows the antenna to lay flat inside the rocket, reducing the vertical space required. The two traces are connected to the RFD900x modem individually; the trace with the best received signal is automatically selected for communication. This eliminates blind spots in the radiation pattern, allowing radio communication from any direction regardless of the orientation. The antenna is shown in Figure 63.

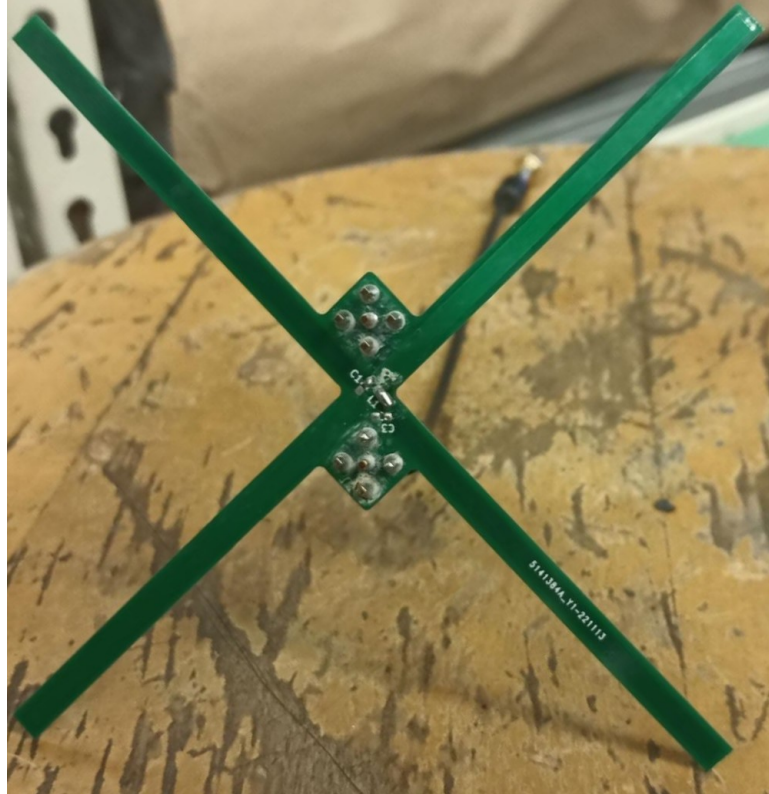


**Fig. 63 PCB Trace Antenna on Rocket Side**

On mission control side, two antennae are used. During flight, the communication is done through a SRAD helical antenna. This helical antenna is made from light-weight fibreglass, making it easy to move around by hand and aim. Furthermore, its circular polarization helps it maintain connection even when the rocket is spinning. When the rocket is on the pad or has landed, a high-gain COTS Yagi antenna is used in parallel to improve reliability.

The ground systems communicate with mission control via a pair of Ubiquiti Litebeam 5AC Gen2 antennas which provide a high-bandwidth Ethernet link. These antennas were validated at the 2022 SAC, and this year are installed on new, taller towers to further improve signal quality and reliability. DAQ and RLCS both connect to a router located at the tower which then forwards the data over the antenna link.

Additionally, while the rocket is on the pad the ground antennas act as a backup line of communication via the

electrical umbilical. The rocket's main CAN bus lines are routed through the umbilical to the DAQ system, which contains a board that can transmit and receive CAN messages over a USB connection. This data stream is then passed over the ground radio link along with the usual data from DAQ and RLCS. Because the electrical umbilical disconnects after liftoff this backup link is fully sufficient to launch the rocket in the event of a live telemetry failure.

## Power Architecture

The RocketCAN bus is powered by a single 3S 2200mAh lithium polymer battery. The battery is connected through the charging board, which controls power to the rest of the CAN bus in the form of both an always-on, fused but unregulated 12V line directly from the battery for higher power systems such as actuators, and a buck converter that steps down the battery voltage to a stable 5 V which is used to operate the microcontrollers and other digital electronics on the bus. The buck converter delivers up to 2 A of current and is equipped with overcurrent protection. Furthermore, every board on the RocketCAN bus is guarded by a polyfuse, which will automatically disconnect that board from the bus if it has a short circuit. This ensures that an electrical fault on any one of the boards will not affect the operation of the RocketCAN bus as a whole.

Additionally, a backup source of power is provided through the electrical umbilical from the Ground Side Power Distribution system. This system ensures the rocket's batteries will be fully charged until personnel leave the pad, and ideally until the moment of takeoff. However, all power budgets have been designed with a worst-case scenario of the electrical umbilical disconnecting immediately after personnel leave the pad for fill operations.

Since the rocket must be able to sit for multiple hours on the pad waiting for an opportunity to launch, a long battery life is critical. To allow this charging board can shut down the rest of the CAN bus and enter a hibernation mode to conserve battery power. In addition, the cameras, which draw the most power of any system, can be individually shut down to conserve power while the rest of RocketCAN is in operation. The below table shows the power consumption. All of the values have been found experimentally to ensure accuracy.

**Table 10 CAN Bus Power Consumption**

System	Quantity	Active Power Draw
Charging	1	300 mW
Live Telemetry	1	5260 mW
Actuator	2	530 mW
Remote Arming	1	950 mW
Camera	2	3000 mW
Mini Sensor	2	170 mW
Logger	1	180 mW
GPS	1	300 mW

Based on the power draw, the expected power schedule during operations is summarized in the below table. These

calculations were performed assuming the rated 24.42 Wh of the 3S lipo battery, and for the remote arming system (which is powered by a pair of 9V batteries) 4 Wh per battery. The expected battery life for RocketCAN as well as the other electrical systems on the rocket are shown.

**Table 11 CAN Bus Power Schedule**

Operational Phase	Duration	RocketCAN	Recovery Electronics	Big Red Bee
Final integration	3 hours	0.6 Wh	Off	Off
Waiting for launch	6 hours	-0.6 Wh (charging)	1.38 Wh	6 hours
Fill operations and flight	1 hour	8.95 Wh	0.95 Wh	1 hour
Total Usage		8.95 Wh	2.33 Wh	7 hours
Remaining Margin	15.47 Wh	1.77 Wh	3+ hours	

## Actuator Board

Actuator board is responsible for controlling two key actuators in the rocket: the injector valve and the vent valve. These are both pneumatically actuated valves which are controlled by 12 V solenoids. These solenoids are identical and each draw 33 mA, well within the current capabilities of the unregulated Li-Po battery connected to the 12 V line. Additionally, the board supports a pair of limit switches which are used to report the position of the controlled actuator over the CAN bus. The two copies of actuator board are identical, being differentiated only in software by their CAN board ID. This allows for easy hot-swaps if faults are detected with either of the primary copies.

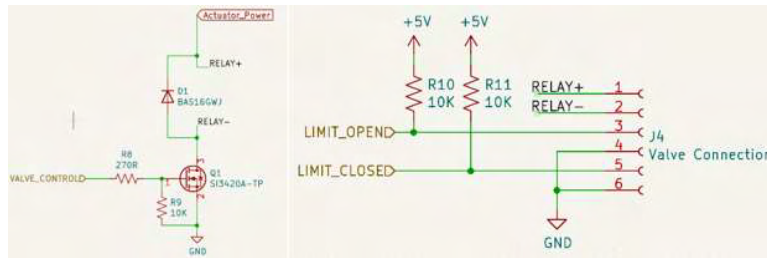


**Fig. 64 Schematics of the actuator control circuitry on Actuator board**

Actuator board is designed to fail open. This has the effect of opening the vent valve, where pneumatic pressure is required to close it, and preventing the injector valve from actuating prematurely due to an electrical failure. This is achieved through the use of an N-channel MOSFET in a low-side-switching configuration, which was chosen for simplicity and reliability. A flyback diode is included to prevent voltage spikes from the inductive load of the solenoid. Another of the same shock resistant Harwin Datamate connectors used on the CANBus is used to connect the wiring to the solenoid and limit switches.

Power for the actuator can be selected from the 5 V or 12 V lines, or a dedicated external battery. For the solenoids used in the rocket 12 volts is necessary, but the relatively low current requirements allow them to be effectively run off

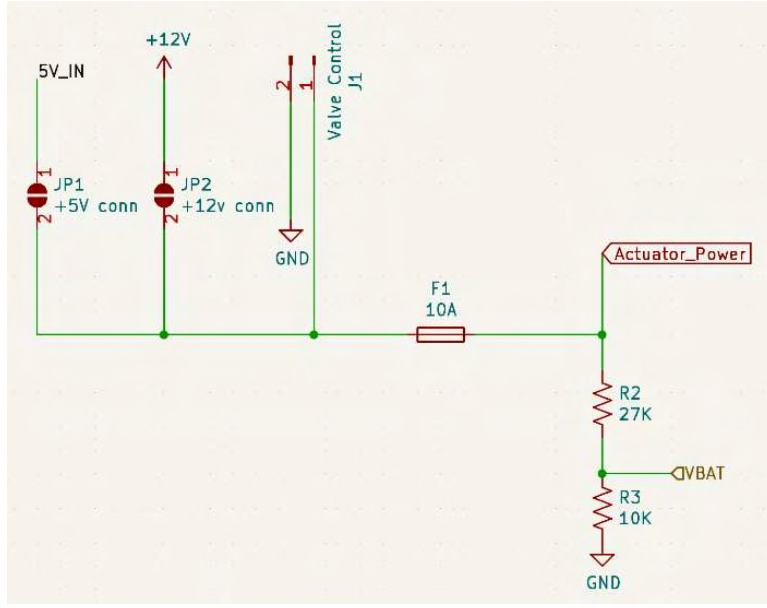


**Fig. 65 Power selection for the actuator power**

of the common 12 V line without requiring the additional mass of a dedicated battery. If future actuators require lower voltage or more current, the existing board design can be easily reused with an alternate power source. Voltage sensing of this line was also added so that it can be reported to operators over LTT when doing avionics readiness checks.

### Charging Board

The inception of the Charging Board project was in response to major issues that we faced at previous competitions. Having to sit on the pad for extended periods of time while we waited to launch, meant that our batteries would continuously drain until they were dead. This would then eliminate the possibility of our rocket from launching.

To combat this, we designed a charging board and an external quick-disconnect connector that provides 24V from two car batteries as well as redundant tethered CAN communication connection to the Remote Launch Control System. This redundant CAN connection was done so that we still have control over the rocket if our Live Telemetry system, which is responsible for arming the rocket, fails. The charging board converts the 24V from the car batteries or from an onboard 3s LiPo into a 13V and 5V rail that provides power to solenoids and other circuit boards, and keeps our batteries charged while the rocket is on the pad. As a result, we have increased our control over the rocket through a redundant tethered communication connection and have enabled the rocket to sit on the pad for long periods of time without the worry of flight-critical batteries dying.

### GPS Board

With the use of an M10578-A2 GPS receiver, the GPS board locates the rocket in space and transmits this data over the CAN bus. This data is transmitted through the live telemetry system to provide a secondary method of tracking the

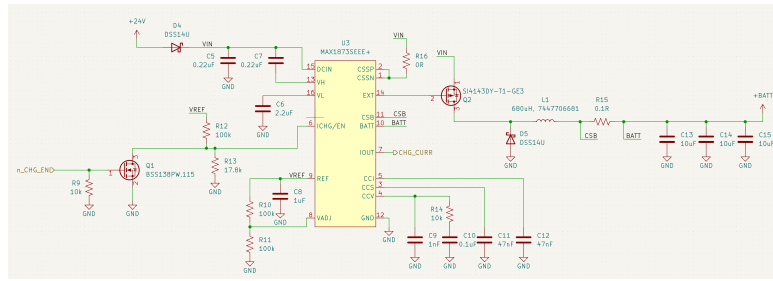


**Fig. 66** Battery Charger circuit responsible for keeping the rockets main battery charged

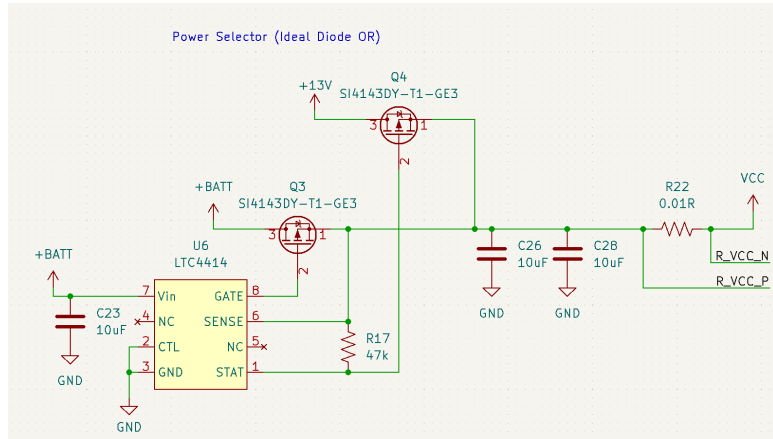


**Fig. 67** Power selector between 24V (from external car batteries) and 3s LiPo (from onboard battery)

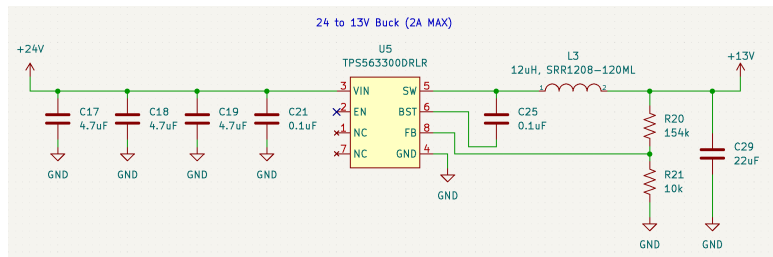


**Fig. 68** 13V Buck Converter to power flight-critical solenoids on the rocket

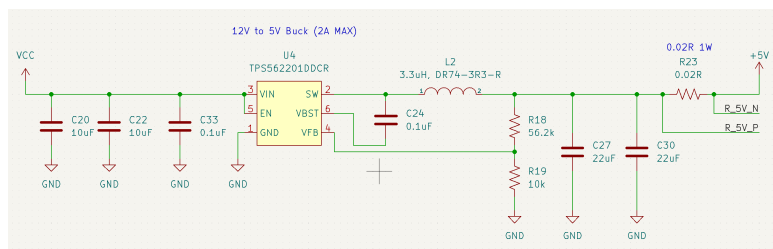


**Fig. 69** 5V Buck Converter to power other circuit boards on the rocket

rocket and is also stored by Logger Board to provide valuable flight data to be analyzed later. Because the GPS receives an RF signal, care was taken to match the impedance of the trace to the antenna. The maximum possible width and shortest allowable path was given, and all high-speed signals were kept away from the trace without compromising their own shortest possible path. The ground plane was also connected through vias to give as short a path as possible for the return path and to relieve any thermal concerns.

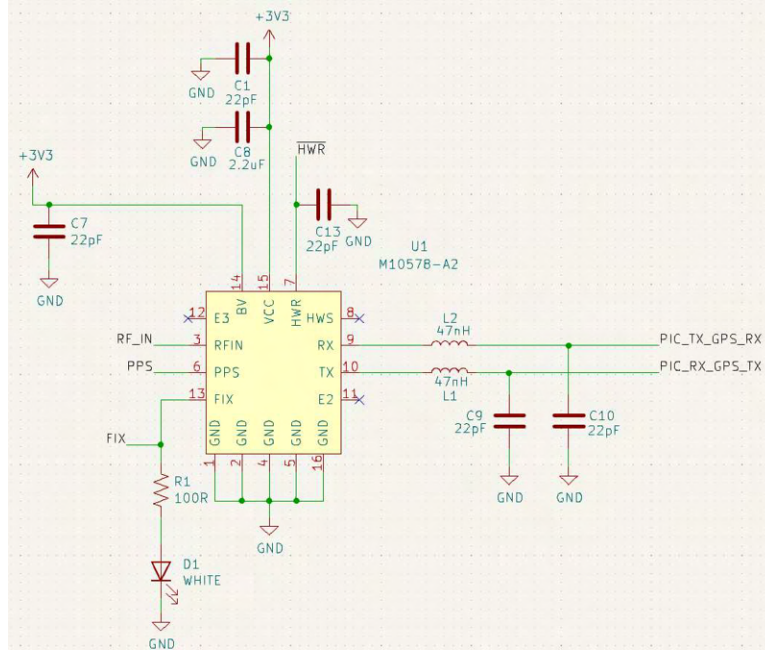


**Fig. 70 Schematic of the connections to the GPS module**

Because the GPS module can take up to 30 seconds to obtain a fix on its position when starting up from a cold state, the ability to power the GPS from an external battery was added to this board. Two diodes allow the module to be independently and redundantly powered from either the auxiliary battery or the CAN bus 5 V line. This allows the GPS module to be powered on before the rest of the RocketCAN bus to ensure a timely fix. In the event of a dead auxiliary battery both the battery voltage and GPS fix state are both reported over the CAN bus so operators can replace the battery or delay until a fix is achieved. However, in order to save on the mass of an auxiliary battery, it was decided that the longer start-up time to achieve a fix was acceptable and an additional battery will not be flown.

### Live Telemetry Transmitter

The purpose of the Live Telemetry Transmitter (LTT) is to act as a two-way CAN to UART converter between the RocketCAN bus and the radio modem as described in the Live Telemetry Architecture section. The board uses 12V as its power source. A DC-DC switching regulator steps 12V down to 5V to supply the radio modem, and a linear regulator produces 3.3V from 5V to supply the PIC18LF26K83 microcontroller. This way, LTT can remain powered up

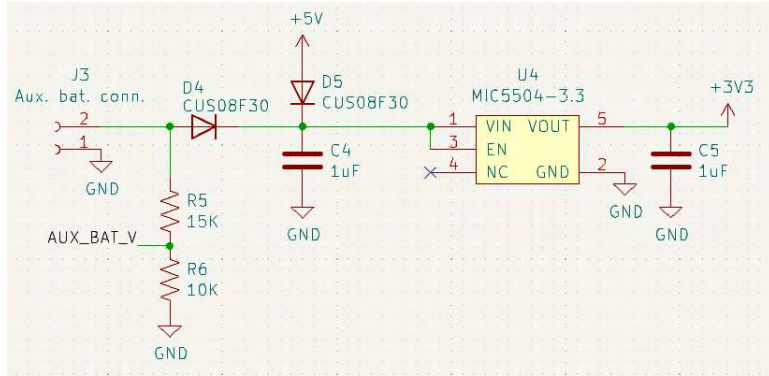


**Fig. 71 Schematic of the power supply for the GPS module**

and communicating with mission control while the 5V line on RocketCAN is turned off to conserve power. In addition, power to the radio module can be switched off or reset by the microcontroller, either manually through hard wired RLCS CAN connection or automatically through a timeout timer in the code.

The CAN messages are serialized into ASCII messages consists of hexadecimal digits and separators. Each serialized message has a CRC8 code attached to ensure the integrity of data. This can prevent cases such, as single bit error turning a "close injector" command into "open injector" and launch the rocket. While ASCII is not the most optimal format to transfer data in terms of bandwidth, a human readable format makes verifying the radio communication much easier using a FTDI cable and serial terminal. There is enough bandwidth over radio to accommodate for the overhead.

### Logger Board

Logger Board uses a DSPIC33EP512GP502 instead of a PIC18F26K83 as the main MCU due to its fast-processing speed for reliably saving data as it comes in. This MCU also runs on 3.3 V which interfaces with the 3.3 V microSD card. It is responsible for saving all the data sent over the CAN bus to a microSD card for postflight analysis. Of particular interest is the telemetry from the GPS and mini sensor systems which give data on the flight performance of the rocket. Because of the modular nature of our RocketCAN architecture, its function is simple but reliable, and any failure by one board will not result in a loss of information from other boards on the CAN bus. The microSD card is mounted in a vibration-resistant holder that was flight-proven during the launch and hard landing of our rocket Shark of the Sky in 2019. For further logging reliability all data will be transmitted in real-time to the ground through the Live Telemetry System, where it will also be recorded.

### Mini Sensor

The purpose of Mini Sensor is to measure various physical parameters during flight and report this data using the CAN bus. It carries a variety of on-board sensors including a magnetometer, accelerometer, a gyroscope, a barometer and an atmospheric temperature sensor. It also includes connection points for up to two external thermistors and two

pressure transducers. The board may also be configured to enable the use of a wheatstone bridge amplifier which can allow the board to acquire more accurate sensor readings, or readings from more sensitive devices, such as strain gauges. This functionality was not utilized in the current rocket but may prove useful in future design cycles. The data from all sensors is relayed over the CAN bus to be logged by Logger Board and relayed to the ground over the Live Telemetry System.

The on-board magnetometer indicates the strength and direction of magnetic fields, which is useful for determining the direction of flight (relative to Earth's magnetic field). The accelerometers measure the direction and intensity of inertial and gravitational forces experienced by the rocket, which is useful for characterizing engine performance and the load on the rocket throughout flight. The gyroscope measures the angular velocity of the rocket, which is useful for determining the amount of rotation experienced by the rocket during flight. The barometer measures atmospheric pressure, which is useful for inferring the altitude of the rocket. The data from the atmospheric temperature sensor is useful for characterizing the thermal conditions experienced by the rocket during flight. The external pressure and temperature sensors produce data that is useful for characterizing the performance of the engine during flight.

A PIC18LF26K83 microcontroller is responsible for operating all of these sensors and sending the appropriate CAN messages. The data from the accelerometers, magnetometer, barometer, atmospheric temperature sensor, and gyroscope are collected by commercial sensor chips and polled using an internal I2C interface. The readings from external devices produce raw analog signals which are polled directly by the microcontroller's built-in analog-to-digital converters.

### **Caddx Turtle Cameras**

There are two camera units in use, both of which are Caddx Turtle V2 micro FPV cameras. The camera module is split into two separate parts, the FPV camera itself and a digital video recorder (DVR) board. The camera is connected to the DVR board via a 20-pin wrapped ribbon cable. The camera is a 1/2.7", 2-megapixel CMOS sensor and a 1.8mm lens to record videos in Full HD (1920 x 1080p) at 60 frames per second. Additionally, there is a microphone to support audio recording. Each DVR board is powered on and off via an additional actuator board that is connected to the rocket's CAN network, allowing control of the camera's operating state from mission control. The camera is configured to start recording as soon as power is supplied to the DVR board and video files are automatically saved upon loss of power. As a result, manual control of the recording action is not required.

### **Remote Arming**

Remote arming main purpose is to eliminate the need for operators to climb a step ladder and use a magnet attached to a pole to arm the altimeters while standing directly under the rocket. In addition, it provides valuable instrumentation that allows for constant monitoring of the recovery system health before and during flight, allowing a comprehensive check of the system performance immediately prior to launch. The system communicates via RocketCAN, which in turn

receives commands from the operator via RLCS to arm or disarm the system. A block diagram of remote arming is shown in the figure below.

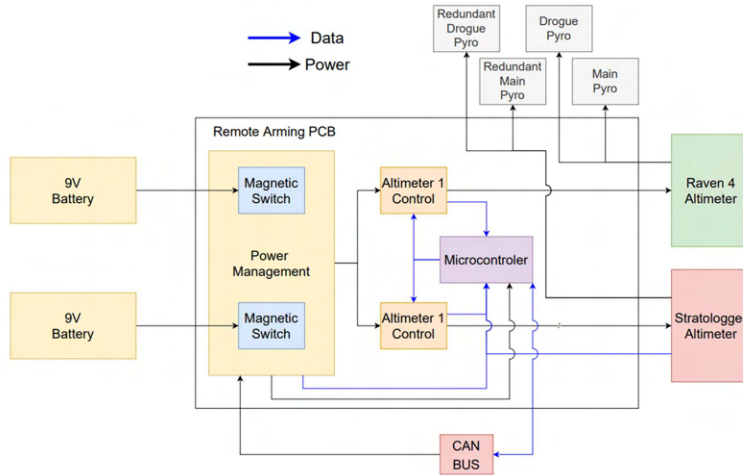


**Fig. 72 Remote arming block diagram**

Remote arming is a single SRAD PCB, which all the key components of the recovery system are attached to securely, either with screws or screw locking Harwin Datamate connectors. This significantly reduces the complexity of the recovery wiring, reducing the risk of mistakes or faults in the harness such as bad crimps. The complete system is shown below.

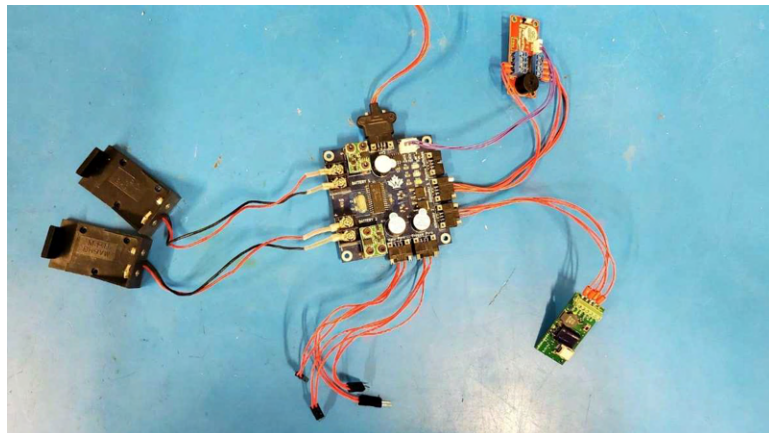


**Fig. 73 Complete Remote Arming System**

### *Failing Safely*

A key problem for remote arming is to create a system which always fails safe. Most systems on the rocket need to fail safe, however usually this has a well-defined, single meaning. For example, the vent valve should always fail open to ensure there is never an SRAD pressure vessel which cannot be vented. However, for remote arming, failing safely does

not always mean the same thing. While the rocket is on the ground, remote arming needs to fail in the disarmed state, as if it fails armed, the pyrotechnics could accidentally be triggered, and an operator could be injured. However, once the rocket launches, the altimeters must stay armed, or the recovery system will fail. As such once in flight the system must fail armed.

It is not possible to design a system which will always fail armed and will always fail disarmed, so a compromise was made. The system has been designed such that it will always fail armed. However, a pair of magnetic switches ensure that the recovery system can always be manually disarmed in the same way that the altimeters have been armed in previous years. In addition, buzzers which are continuously on whenever the altimeters are powered ensure that there is no possibility of personnel approaching the system without knowing it is armed.

Since both arming circuits are controlled by a single microcontroller, several measures have been taken to ensure that it does not cause a single point of failure:

- There is a pull up resistor which ensures that if the microcontroller fails or loses power, the circuit will keep the altimeter powered.
- The code on the microcontroller ensures that its default state on power up is armed, as such any temporary loss of power will not result in the altimeters disarming.
- A watchdog timer is used, such that if the main loop is ever hung up, the microcontroller will be reset.
- The microcontroller is powered both by the recovery batteries, and the Rocket's CAN bus, which adds redundancy and reduces the chances of a brown out.

### *Remote Arming ConOps*

Since the logic of remote arming is designed to default to armed, some care must be taken in setting up the system for launch. The procedure is as follows:

- Since the magnetic switch's default state is on, during assembly the 9V batteries should be installed first, the magnetic switches turned off, and then the e-matches should be attached. This is true regardless of remote arming.
- Once the rocket has been fully assembled, inspected, and loaded onto the launch rail, but before the rail is raised, the CAN bus should be powered up, remote arming should be commanded to disarm the altimeters, and then a magnet should be used to turn on the magnetic switches, checking the remote arming telemetry to ensure both switches are functioning correctly. The indicator buzzer will also play a repeating tone to indicate both batteries are functioning correctly.
- The CAN bus can then be powered down and remote arming will continue operating using recovery battery power.
- Once the rocket is vertical on the tower and ready for launch, remote arming will be commanded to arm. The telemetry will then be checked to ensure the system is ready for launch. This includes the following:
  - Both battery and magnetic switch voltages are good.

- Remote arming reports both altimeters armed.
- Current draw from the recovery batteries matches expected value for all systems armed.
- Drogue and main pyro voltages for each altimeter read as expected for the armed state.
- Altitude data is being received from the Stratologger altimeter.

### *Power Management*

Remote arming is powered by two 9V batteries, each with their own voltage sensing and magnetic switch, as shown in Figure 74. A SM74611 smart diode is used with each battery to ensure a difference in voltage between the two does not cause issues. These diodes are designed for solar power generation and have a nominal voltage drop of only a few mV thanks to an internal FET and charge pump circuit, ensuring there is minimal power loss through the diode.

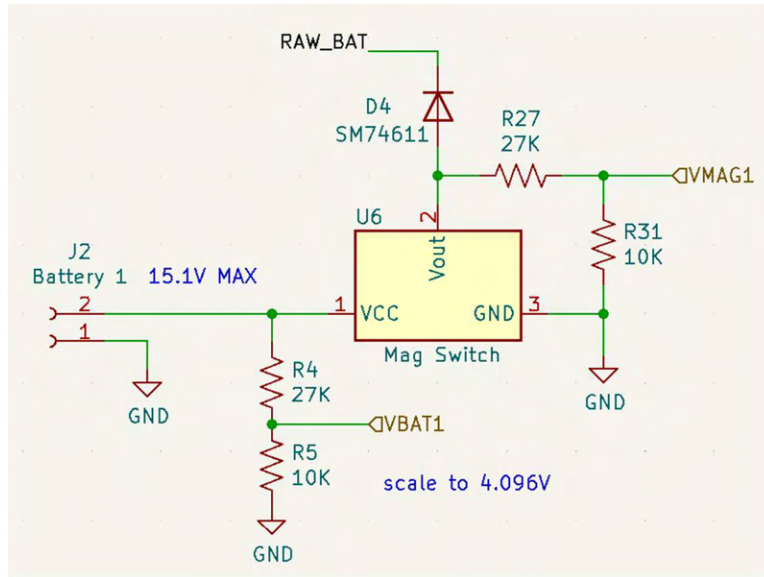


**Fig. 74 Remote arming power circuit for one of two batteries**

The microcontroller is powered by the CAN bus via the same PTC fuse and current sensing circuit as discussed in above, with the only difference being a CUS08F30 Schottky diode to prevent Remote Arming from powering the CANBus with its backup 5V regulator which draws power from the 9V batteries.

Current sensing from the 9V batteries is achieved using an INA180 amplifier as shown in Figure 61. Two shunt resistors are used in parallel to ensure single-fault tolerance. If one resistor is damaged, the current reading will be inaccurate, but the altimeters will still be powered.

### *Altimeter Control*

As seen in Figure 76, power to each altimeter is controlled by an AOD417 P-channel MOSFET, which is in turn controlled by a DMG2302UK N-channel MOSFET to allow the circuit to be controlled with the microcontroller's 5V

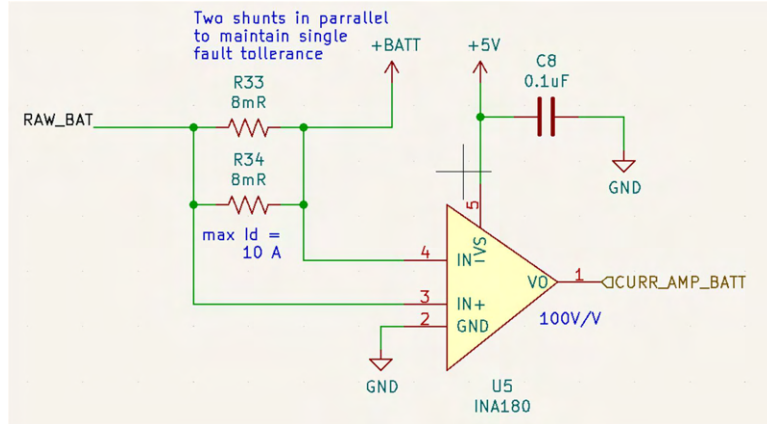


**Fig. 75 Recovery batteries current sensing circuit**

logic. This high side switching is slightly more complex than if low side switching was implemented with a single Nchannel MOSFET but ensuring that the altimeters and remote arming have a shared ground is needed for reading altitude data from the Stratologger. This MOSFET combination has already been flown as part of the injector valve control board for the rocket Shark of the Sky at SA Cup 2019 without issue and continued to function even after the rocket landed under drogue and experienced significant shock loading. The pull up solder jumpers are for use with the Raven 4 altimeter which does not have a dedicated positive pin for the drogue or main e-matches, and as such requires that they are externally connected to power. As mentioned previously, each power control circuit has a buzzer that is on whenever the altimeter is powered. Two different frequencies are used to make it possible to identify which altimeters are powered.

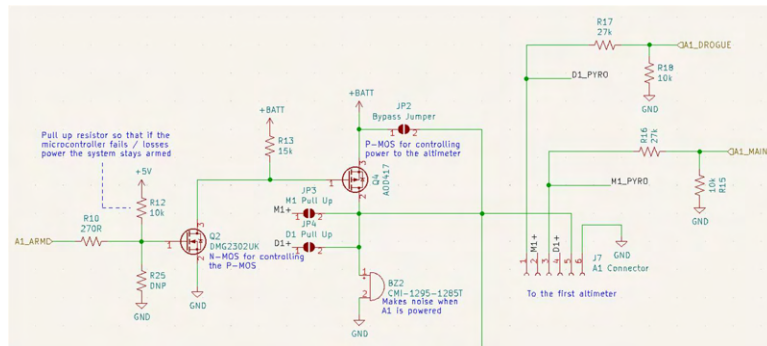


**Fig. 76 One of two altimeter arming circuits**

### Telemetry

Remote arming has a total of eleven different sources of telemetry, the telemetry channels are as follows:

- Battery 1 and battery 2 voltage
- Magnetic switch 1 and switch 2 output voltage

- Voltage reading for all four of the drogue and main e-matches. This voltage reads close to the battery voltage while the altimeters are powered, and the e-matches connected, and close to zero if not. As such it is easy to verify that the recovery system is entirely functional immediately prior to launch.
- Current draw from the 9V recovery batteries, this has a maximum value of 10A so that the current draw of the e-matches firing can be measured. As such the signal is very noisy and imprecise when reading the passive current draw of the microcontroller. This is mitigated via the use of software low pass filters which allow reasonably accurate measurements down to approximately 20mA.
- Current draw from the CAN bus using the same architecture used on all other RocketCAN boards.
- Remote arming parses the UART altitude stream from the Stratologger altimeter and transmits it over the CAN bus so that the altitude can be monitored live during flight. The level shifting circuit can be seen in the figure below.

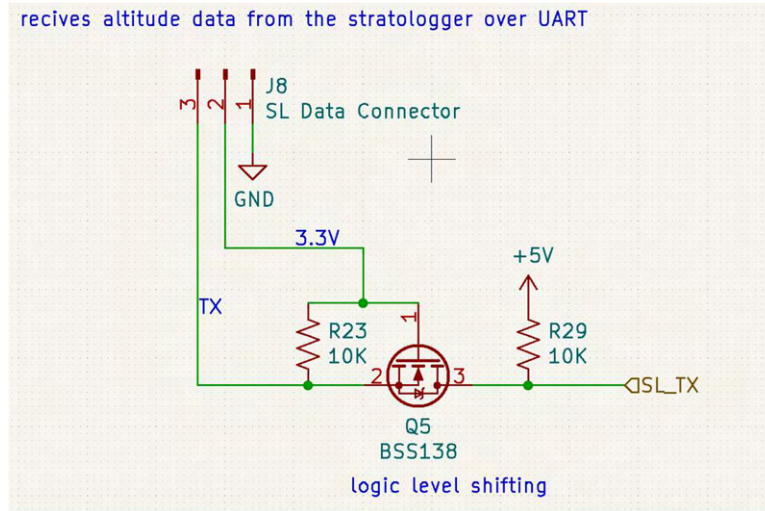


**Fig. 77 Stratologger telemetry level shifting circuit**

### Remote Arming Testing

As of present the remote arming system has undergone full system testing under benchtop conditions. It has also undergone a series of simulated flights where the complete recovery electronics system was put in a vacuum chamber. A partial vacuum was pulled to simulate an increasing altitude, then air was slowly introduced back in to simulate apogee and descent. Referencing an aircraft altimeter, it was confirmed that the drogue channel fired at “apogee”, and the main channel fired at a reading of 1500 ft, as well as that remote arming reported all the correct telemetry. Unfortunately, this test only works with the Stratologger altimeter since its altitude measurement is solely barometer based, while the Raven 4 uses an accelerometer along with the barometer. Both the Raven and Stratologger altimeters were tested with remote arming by connecting them to a computer and using their respective simulated flight tests.

The remote arming system uses a common power bus supplied by two redundant batteries. This single bus provides

power to both redundant altimeters. This provides an advantage over the past system which had two isolated redundant systems as it allows for a single battery failure as well as a single altimeter failure without a failure of the recovery system. This was deemed valuable as in 2019 both a battery failure and altimeter failure were experienced, and due to the isolated nature of the systems, this caused both recovery systems to fail. This situation is prevented with the use of a joined power bus. While a joined power bus was deemed valuable for added reliability, a new potential failure mode was identified. It is possible that a short-circuited e-match could cut power to both altimeters leading to a failure. To test this the main parachute pyro line was intentionally short circuited on one altimeter and that channel was fired while monitoring the status of the other altimeter. This test was then conducted with the two altimeters in opposite roles. This test confirmed that the brownout protection capacitors on each altimeter allow them to keep their state in the event of a drop of bus voltage due to a short-circuited e-match on the other altimeter. Therefore, this failure mode does not affect the operation of the other altimeter.

### COTS Recovery Electronics

Per the recommendations and requirements of the DTEG, LotS uses a pair of dissimilar COTS altimeters for recording the maximum altitude achieved and firing the recovery pyrotechnics to deploy the parachute. The first is a Perfectflite Stratologger CF. This barometer-based altimeter was selected due to its low cost and reliability. It has the added benefit of transmitting altitude data over UART throughout the flight. This data is received by remote arming and relayed down to the ground using RocketCAN, allowing for live altitude telemetry.

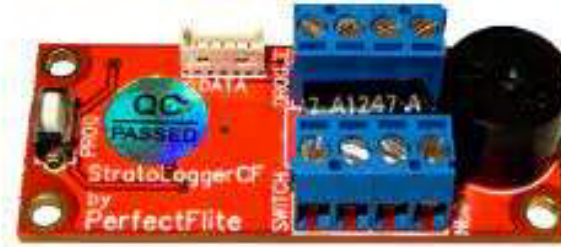


**Fig. 78 Stratologger CF altimeter**

The second altimeter used is a Featherweight Raven 4. This altimeter is significantly more advanced and uses a combination of an accelerometer and barometer for altitude estimation. As such, it gathers a large amount of data about the dynamic environment of the rocket throughout flight and provides a valuable redundant source of data for comparison against the data recorded by the SRAD avionics.

To ensure the two redundant recovery systems do not interfere, the Raven 4 is set to fire its charges after the Stratologger has fired. Immediately at apogee the Stratologger is set to fire the drogue pyrocutter to deploy the reefed main parachute by applying a current across the e-match for one second. Then two seconds after apogee, the Raven 4 is programmed to fire the redundant drogue pyrocutter in case of a failure of the Stratologger. When the rocket hits 1,500



**Fig. 79 Raven 4 altimeter**

ft above ground level, the Stratologger then fires the main pyrocutter to de-reef the parachute, followed by the Raven 4 firing the redundant main pyrocutter at 1,250 ft.

As part of the remote arming system, and for the COTS GPS tracking system, it is important to be able to power the systems on and off when the rocket is fully assembled. To allow this Featherweight magnetic switches are used. When a magnet is passed over the outside of the rocket it causes the switch to turn on, and when the magnet is passed over again, the switch turns off.

### COTS GPS Tracking

A BigRedBee tracks and transmits the location of the rocket to assist with discovering the rocket landing site during recovery. The BigRedBee has a built-in GPS receiver which tracks the location of the rocket. The BigRedBee transmits the location of the rocket every 30 seconds using the Automatic Packet Reporting System (APRS) on the 70 cm amateur radio band. The APRS transmitter is tuned to a frequency of 431.0 MHz, which lies within the recommended band plans for digital amateur radio transmissions in the US & Canada. Several team members possess an amateur radio license and are legally permitted to use this band. The APRS transmitter uses a 17 cm quarter-wave monopole antenna with a transmission power of 100 mW (20 dBm). The BigRedBee is powered by a rechargeable single-cell lithium-ion battery which has sufficient energy capacity to operate the BigRedBee for at least 10 hours. The BigRedBee is lightweight, which makes it suitable to be used in the avionics section of the rocket. It can be turned on and off via the use of a magswitch to allow its battery to be conserved.

The APRS packets are received by a Yaesu FT-65R handheld radio. This transceiver supports a wide range of VHF and UHF and features a 3.5 mm headphone jack. An audio cable connects the earphone output jack of the radio receiver to the microphone input jack of a field laptop. Thus, with the appropriate decoding software running on the laptop, the combination of the transceiver and laptop together can be used to receive APRS packets and pinpoint the location of the rocket landing site. The coordinates of the landing site are given to the ST PATS which is used to navigate toward the

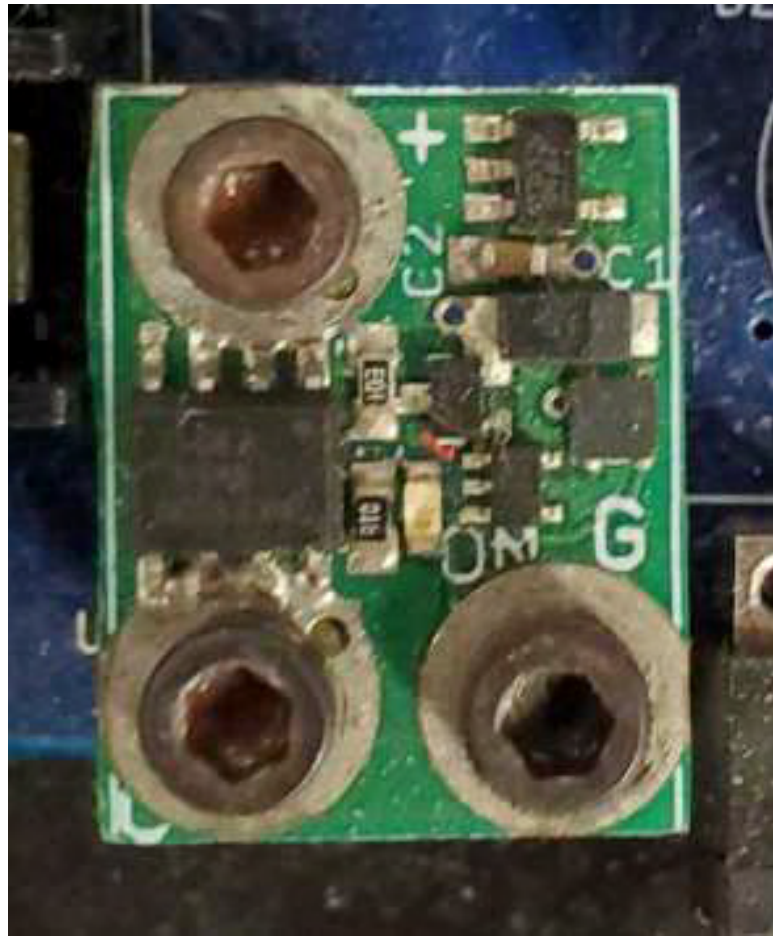


**Fig. 80** Featherweight magnetic switch

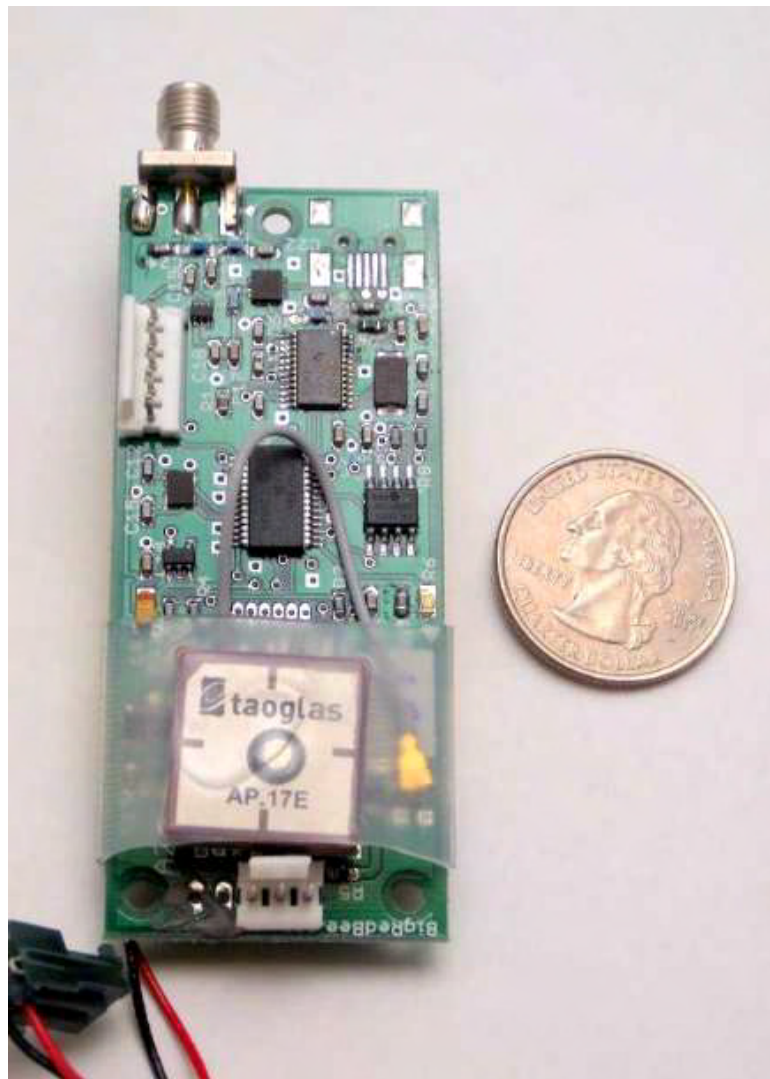


Fig. 81 BigRedBee APRS Transmitter

landing site.



**Fig. 82 Yaesu FT-65R radio transceiver**

## *2. Electrical Ground Support Equipment*

### **Ground Side Power Distribution**

Ground Side Power Distribution (GSPD) is a new SRAD system that supplies power to our ground side equipment (GSE). The intention of GSPD is to have a central hub in which all our GSE; DAQ, DAQ Laptop, RLCS, Ethernet Box and Antenna can be powered simultaneously using up to four car batteries or by generator. The system takes in 12V, from the car batteries or the ATX 430W power supply (which is used to convert the generator voltage to 12VDC) and filters it. The 12VDC is then fed through a 5V and 24V converter and filtered. The 5V, 12V, 24V and GND lines along with voltage, current and temperature sensing data are distributed to the GSE via an array of M12 connectors and cables. The components apart of GSPD are housed in a water and dust proof pelican case, modified for ease of usage and cooling.

Prior to GSPD, our power system consisted of an uninterruptible power supply (UPS), powered by a car battery through an inverter. Each GSE had its own AC block that plugged into the UPS. The downside of this system was the inability to simultaneously power on all of the GSE, the lack of ease switching between battery and generator power, the crudeness in voltage and current monitoring, the messiness of all the different cables for each piece of equipment and

the physical limitations of the UPS. At last year's competition, the UPS overheated and failed, playing a role in the scrub of our launch. GSPD is designed to solve the issues listed above and ensure we can safely power the GSE without worry of overheating.

### GSPD Boards

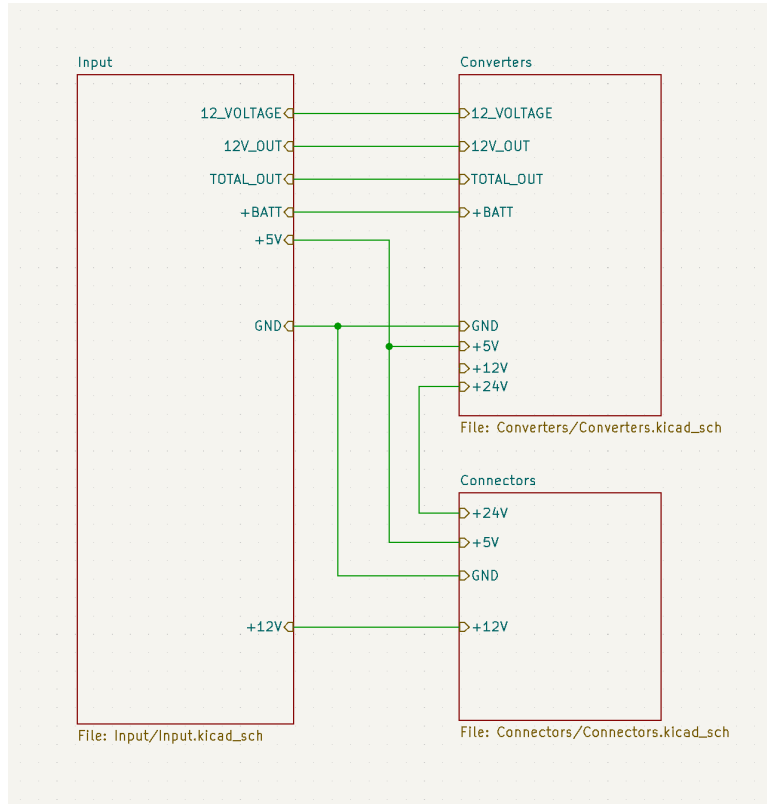


**Fig. 83 Connections between boards for GSPD**

The input board's primary purpose is to receive power from either the car batteries or ATX power supply. Looking at the input section of the schematic below, a three position switch is used to flip between battery power, generator power and off. The input incorporates several safety features including a fuse, inrush current limiter and reverse polarity protection. Originally, the input voltage was to be filtered using several 22mF caps. However, after testing, we realized the voltage line was clean enough without the 22mF caps and that the 100uF capacitor alone is able to handle sudden variations in voltage. This board also displays battery voltage on a digital voltmeter, uses a resistor divider so the voltage can be monitored by DAQ and incorporates two current sensors, one for 12V and the other for the entire system. We then pass both the raw 12V and filtered 12V line to the converter board.

Converter board takes the raw 12 volts from either the battery or power supply and converts the voltages to 5V and 24V using buck converters. The 5V converter used is the K7805-3AR3 with a max current of 3A and efficiency of 93%. This converter incorporates a 10uF capacitor at the input and 22uF capacitor at the output to help reduce ripples. The

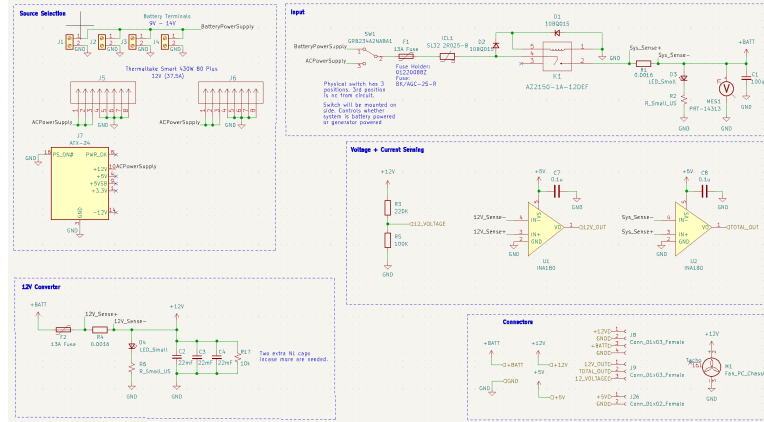


**Fig. 84 Schematic for Input Board**

24V converter used is the URB2424LD-20WR3 with a max current of 834mA and efficiency of 90%. This converter incorporates a 100uF capacitor at the input and output. High efficiency converters were selected to reduce heating and power losses. The 5V and 24V lines each have fuses rated under the maximum current the converters can handle along with a 10uF buck capacitors. This board is also home to the voltage and current sensing for the 5V and 24V lines along with a thermistor to measure the temperature of the surrounding air. The sensing data is directly fed to DAQ via an M12 connector/cable assembly.

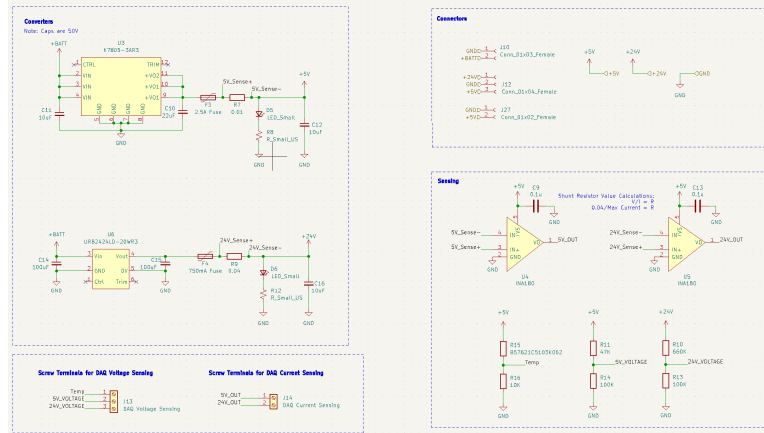


**Fig. 85 Schematic for Converter Board**

Connector board receives all the voltage lines and ground from the input and converter board and connects these lines to 9 4-pin screw terminals. Each screw terminal is partnered with an M12 connector, capable of providing power to any of the GSE. The team recently decided to standardize our connectors, with A type M12's being used for lower power demands, D type M12's used for data transmission to DAQ (voltage, current and temperature sensing) and T type M12's used to transmit power to equipment drawing a lot of current (such as the DAQ laptop). These connectors are mounted on the back of the GSPD case which is where we plug the cables connecting the equipment to GSPD.

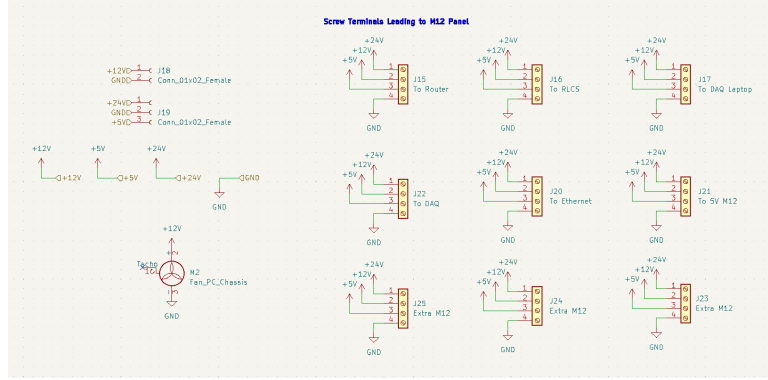


**Fig. 86 Schematic for Connector Board**

### GSPD Case

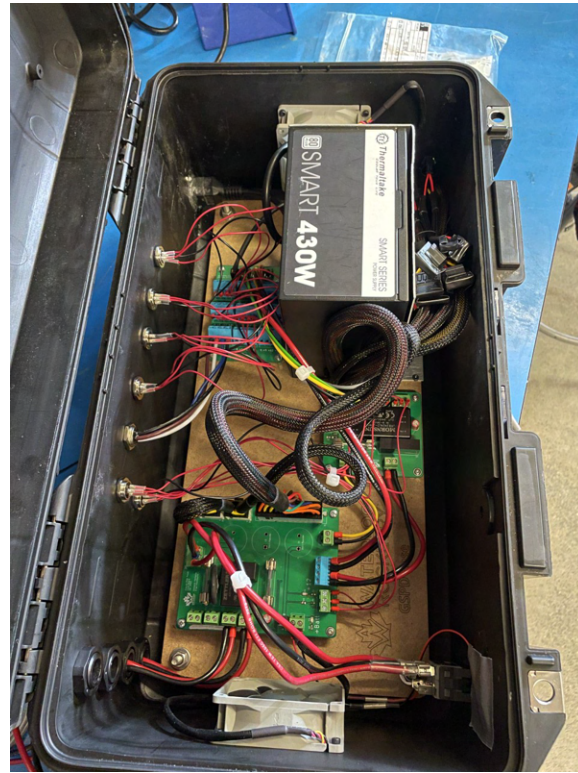


**Fig. 87 Inside the fully assembled GSPD case**

The pelican 1506 air case was selected, as it is light weight and large enough to fit all the components and PSU inside. The PCBs are all mounted to a laser cut wood board, which is securely fitted to the bottom of the case. Threaded holes on the back provide a water tight, firm hold on the M12 connectors. The connectors closest to the bottom of the photo are the data lines and lead to DAQ, the next one over is for DAQ laptop as it draws up to 6A of current and the remaining can handle current draw up to 4A. The PSU is mounted to the wood base using a bent aluminum sheet plate and a hole was drilled and caulked in the top left of the image for the PSU plug. In the bottom left of the image, there

four wire feeds for the four car batteries the system can support. In the bottom right a hole was carved for the switch and digital voltmeter and applied caulk for waterproofing. For board cooling, two 12V PC fans were added, one sucking air in and the other blowing out. To ensure no dust or water can get inside the case through the fan holes, these fans are covered with a water/dust proof mesh and 3D modelled a cover for the fans to protect them from rain.

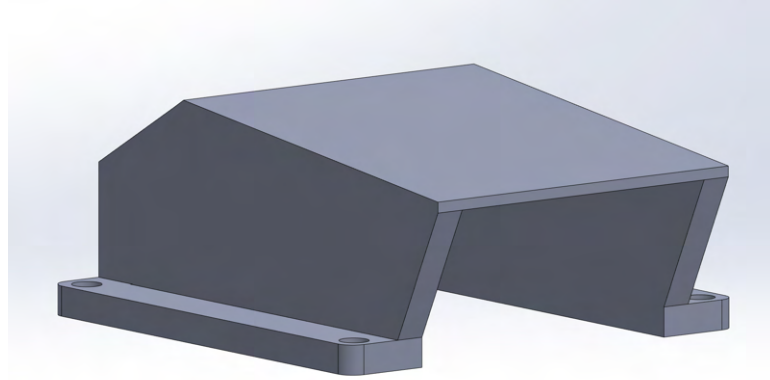


**Fig. 88 CAD for the fan cover**

### **Remote Launch Control System**

The Remote Launch Control System (RLCS) is the primary means of interfacing with the rocket and supporting fill plumbing during launch operations. The main objective of the system is to allow launching the rocket from up to 3,000 ft from the tower. Once the RLCS operator takes control of the launch process, no human intervention should be required at the launch site in any possible error state that requires a human to approach the system. In the event of total failure, the system must put all engine and fill systems into a known safe state so that personnel can approach the rocket without placing themselves in danger.

RLCS is made up of two halves, Clientside and Towerside, which communicate over a radio link formed by a pair of Litebeam 5ac gen2. Towerside is located beside the launch tower and handles actuating motorized valves and ignition. Clientside is located at mission control and houses switches that map to the various actuators and an LCD to display data to the operator. Both halves are built into weatherproof and robust Pelican cases to protect them from the elements.

#### *Clientside*

Clientside is used by the RLCS Control operator to control motorized valves and ignition. Clientside is a relatively simple system composed of an Arduino Mega, a LCD module several missile switches, and a custom PCB that regulates a 3S LiPo down to 5 V for power. Additionally, it exposes a USB port which allows it to send data to a computer for plotting and logging. Clientside contains a set of missile switch, each match to a motorized valve. There is also the ignition button paired with a arming missile switch for controlling current pass through nichrome ignition coil. The



**Fig. 89 RLCS Clientside**

LCD module displays the state of all motorized value(open, closed, and not connected), and it also display voltage of LiPo batteries and ignition coil current.



**Fig. 90 RLCS towerside**

#### *Towerside*

Towerside is more complicated because it needs to handle the high current draw of motorized valves. It is made up of a set of identical Relay boards connected over an I2C bus to a master Arduino Mega.

The various I2C boards in Towerside are connected over an I2C bus in a daisy-chain configuration. In addition to the two I2C wires SDA and SCL, there is a regulated 5 V line, an unregulated 12 V line, and a ground line. The 5 V line drives the various microcontrollers on the boards and the 12 V line is used to drive the relays on I2C Relay board. The I2C Relay boards additionally have a secondary daisy-chained power connection which uses low-gauge wire and is used exclusively to drive the actuators. This ensures that the high current draw of the actuators does not cause brownouts on the MCU power lines.

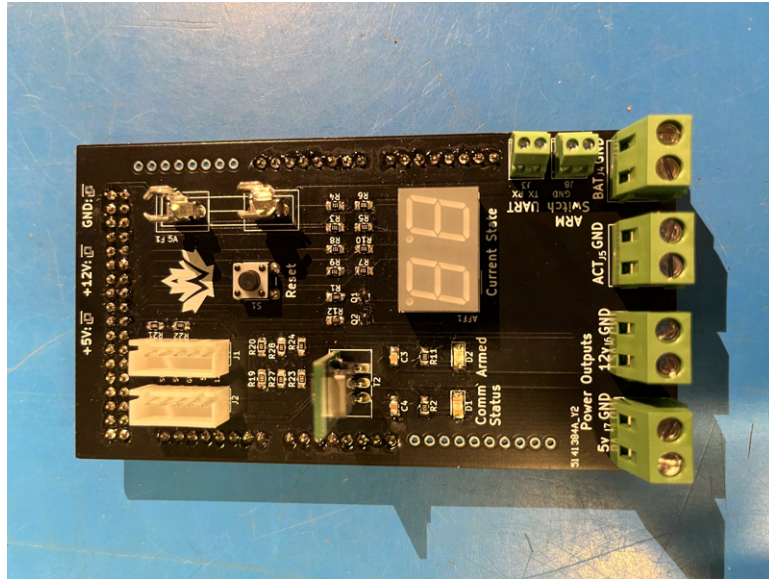


**Fig. 91 RLCS Towerside Power Board**

The main purpose of the Towerside Power Board is to supply 5V power to the Arduino, and provide power output, UART screw terminal for communication to Client-side, and keylock switch connector and JST I2C connector. The seven segment display on the board displays the current status of each motorized valve and ignition, with binary each bit represent a valve or ignition coil.

The main purpose of the RLCS Relay board is to operate the motorized valves that control the flow of oxidizer into the rocket during fill operations. Each Relay board is connected to one motorized valve. Relay board also detects the states of limit switches built into the valves, which are activated whenever the motor shaft arrives at a fully closed or fully open state. These limit switches indicate the current position of the motor shaft; this information is provided to human operators at mission control so that the operators are continually aware of the current position of every motorized valve in the system. Accurate tracking of the states of each of the launch control devices is critical for safety. In addition to operating motorized valves, the Relay board can also apply an electric current to an ignition coil to ignite the engine. The typical ignition current is approximately 5 A. The Relay board is equipped with a current-sense amplifier which continually measures the current sunk through whatever actuator or coil is connected. These measurements are reported to the human operators at mission control so that the operators are aware of the current flowing to the motors and ignition coils. Thus, if any of these electrical devices are malfunctioning, the human operators can easily identify the faulty component and take appropriate action.

Relay board uses a pair of relays to control actuation direction and power to the actuator independently. This requires two actions to be taken in order to actuate a valve or fire an ignition coil (where the coil is wired to the normally open contacts of the direction relay).

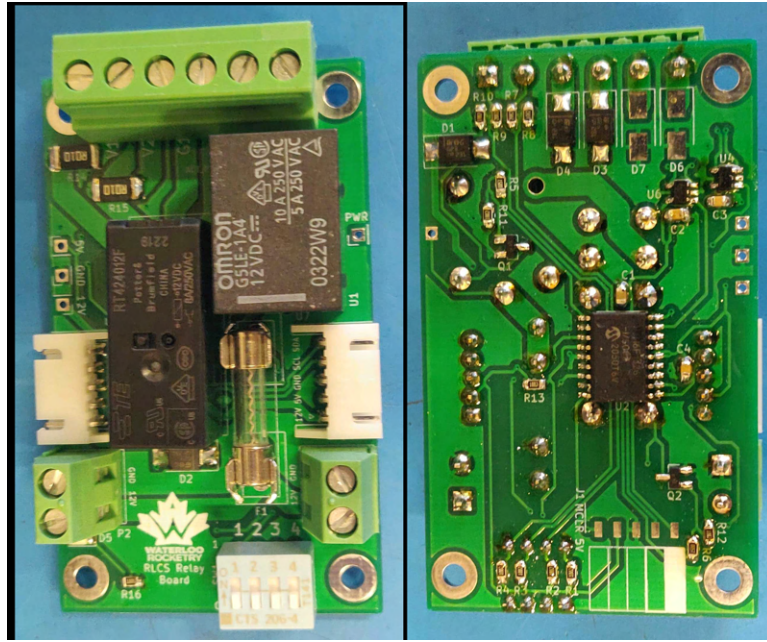


**Fig. 92 RLCS Relay Board**

### *System Safety*

The entire system is designed to prevent unintended actuation of valves and fail safely. Both Clientside and Towerside have keyed-alike arming and disarming switches respectively, both of which retain the key when turned. This means that whenever the tower is approached the key is removed from Client Side, disarming it, and then inserted into Towerside, also disarming it. In this configuration it is physically impossible to arm Clientside while personnel are at the tower since the key is also physically with them, and even if a fault caused either Clientside or Towerside to unintentionally arm the other half would still be disarmed.

Within Towerside, two relays are required to actuate in order to trigger any action. The relays are wired in series such that one provides power to the actuator and the second determines which direction the actuator should move in. The plumbing system is also set up such that if any individual actuator fails the system can still be safely vented.

Clientside and Towerside continually send command and sensor data messages to each other. This means that if either one unexpectedly fails, or the radio link between them drops, both can detect this by noticing silence on the line. If Towerside does not hear from Clientside for 10 seconds, it will automatically set all actuators to a predefined ‘safe state’ that is baked into its firmware. This means opening all vent valves and closing or de-energizing all others in order to make the system safely approachable by personnel. Clientside will also report any silence of at least 3 seconds to the operator, which could indicate a flakey radio connection or an issue with Towerside.

RLCS controls the following actuators necessary for fill and engine start:

- The Remote Fill Valve, which controls the entry of N<sub>2</sub>O into the fill system

- The Line Vent Valve, which opens the fill system to atmosphere in order to vent N<sub>2</sub>O
- The linear actuator that triggers the remote disconnect mechanism
- Two nichrome coils inside the engine ignition puck
- The Injector Valve, which controls the flow of N<sub>2</sub>O into the combustion chamber, via RocketCAN
- The Tank Vent Valve, which allows the oxidizer tank to be vented of N<sub>2</sub>O, via RocketCAN

Moreover, RLCS uses sensors to collect the following data, and report that data back to the operator:

- The current state of all valves (open/closed)
- The amount of current flowing through each nichrome coil inside the ignition puck
- Voltage of all LiPo batteries

### *Electrical Overview*

Changes to the RLCS this year includes a respin of the RLCS Towerside power board, which is for providing power to the Towerside Arduino Mega and breakout IO, this new revision of the board fixed many issues of the old revision of the board. The RLCS Towerside has also been modified to switch 24V power for rocket avionics.

### **Data Acquisition System**

The goal of the Data Acquisition (DAQ) system is to provide a more convenient and accurate method of obtaining ground sensor data during fill and launch operations. It will also allow data to be plotted and logged in real time on a computer in a more readable manner than the LCD on Clientside. These capabilities have been further enhanced this year due to the recent introduction of an on-board computer.

The DAQ system uses a pair of Ubiquiti Litebeam AC to communicate between mission control and itself. These antennas have been fully qualified at both cold flows and parachute tests. So far, no reliability or range issues have been observed, and preliminary range testing suggests that they will have more than the required 3000 ft of range required for competition. However, should this not be the case, RLCS is also fully capable of handling the entire required ground data acquisition on its own. Range verification will be conducted at the competition to determine which system will handle the ground sensor data; whichever proves more reliable will be used.

The heart of the DAQ system is a National Instruments USB-6218 Multifunction I/O Device (the “NI module”). It supports up to 32 analog input channels with a sensitivity down to 4.8 uV. This makes it suitable for both 0-5 V / 4- 20 mA sensors and mV/V strain gauges such as load cells with no external amplification. Sensors are wired into the NI module through a set of DIN rail terminal blocks for ease and reliability of configuration. Sensors with a 4-20 mA signal are supported by placing a 100-ohm resistor between the negative sensor wire and ground, and measuring the voltage drop across the resistor which will vary linearly with the current. Thermistors are also supported with the same internal resistor configuration forming a voltage divider with the external thermistor.

New this year is the on-board small-form-factor computer. Once the sensor voltages are collected by the NI module, they are passed over USB to the integrated Framework mainboard, a compact single-board computer running the necessary software to send the data over to mission control. At startup, the mainboard automatically runs the DAQ server in preparation to connect and send data to computers at mission control over the same Ubiquiti Litebeam 5AC antennas and radio link as RLCS uses.

At mission control, a custom robust laptop built around the framework mainboard is used to display and log all DAQ and telemetry data. It will be enclosed in a watertight aluminum case with three built-in monitors, along with standard laptop functionality such as a keyboard, trackpad, camera, microphone, speakers, and Wi-Fi.



**Fig. 93** Connector ports on DAQ system

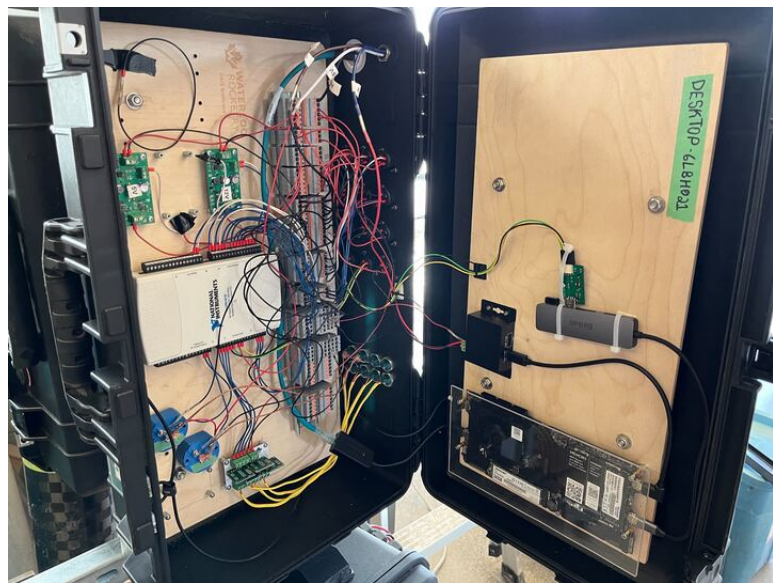


**Fig. 94** Internals of DAQ system

Once the sensor voltages are collected by the NI module, they are passed over USB to the local mainboard. This

computer then relays them in real time over an ethernet link to a computer at mission control, which plots and logs the data. Since ethernet cables have a maximum length of only 100 m, the Ubiquiti Litebeam AC antennas were selected to act as a transparent link that can span the distance between the launch tower and mission control.

Power to the sensors is delivered by a DAQ Power Board, a custom PCB designed for ultra-low output noise. This is achieved by a dual step-down design where a high-efficiency buck converter regulates the input voltage down to 2 V above the desired output voltage and the final regulation is achieved by a pair of less efficient but ultra-low-noise linear dropout regulators (LDOs). Three copies of this board power the +5 V, +10 V, and +12 V power rails within the DAQ system. The output noise of the board was too low to be measured accurately but is at most 10 uV peak to peak.

DAQ Power board was designed for 1 A output at a configurable voltage between 5 and 15 V. To achieve this a 1 A buck converter is followed by two 500 mA LDOs which share the output load. Additionally, pairing up the LDOs reduces the output noise by a factor of 1.4. To allow optimal efficiency of the LDOs, the feedback pin of the buck converter is actively controlled by one of the LDOs. This lets the LDO choose its own input voltage optimally and eliminates a secondary manual configuration of the boost converter.

Power to the integrated computer is delivered by a COTS USB-C PD DC-DC charger. This module is able to accept voltage from the +12 V power rail and convert it to the appropriate PD voltage required to operate the Framework mainboard. This charger was not only chosen due to its viability in providing power to the computer but also its considerably large input voltage tolerance between 9-36V - helpful in case of voltage noise - and in addition, has low voltage protection to protect both itself and the computer from damage due to high current draw from dangerously low voltage levels.



**Fig. 95 COTS DC-DC USB-C PD charger used for powering integrated computer**

## ST PATS

ST PATS is a tracking system that displays the location and direction of the rocket to facilitate its recovery. Physically, it is a small, handheld, battery powered device that can be used in cars or on foot during recovery operations. ST PATS

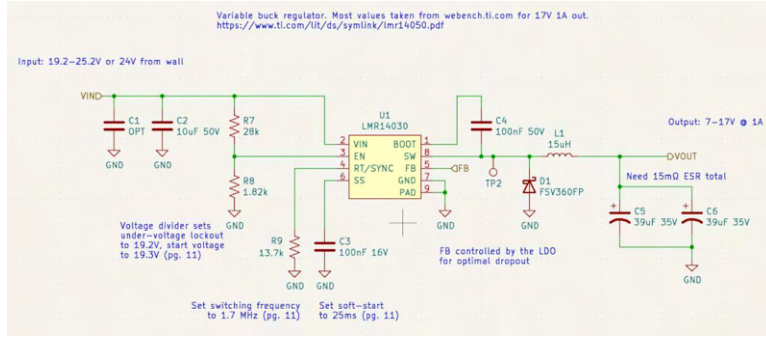


**Fig. 96 Schematic of the buck regulator on DAQ Power board**

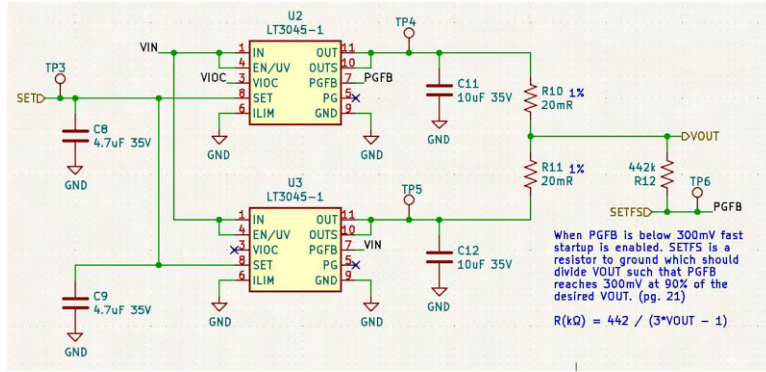


**Fig. 97 Schematic of the parallel LDOs on DAQ Power Board.**

can receive coordinates of the rocket from both live telemetry radio and USB serial. The serial connection allows it to receive decoded APRS coordinates from a laptop, providing redundancy alongside with live telemetry radio. The rocket's location is compared with its own GPS to calculate the direction to the rocket.

ST PATS uses the same RFD900X radio modem to receive live telemetry data over radio. The modem automatically filters radio packets by destination and decodes it into an ASCII stream, which gets parsed by Feather M0 to obtain the coordinates.

Locally, Adafruit Ultimate GPS breakout board is used as it was the easiest to get at the time of design. The board is configured to send GPS data twice a second to the Feather M0. In addition to the coordinates, the data also provides local magnetic variation and current time to the program. The magnetic variation is important for compass calibration and ensures the correctness of the calculated direction.

Adafruit LIS2MDL magnetometer is used as the compass, chosen again due to availability. It provides the device heading so an arrow can be shown on the display, pointing to the rocket. As the magnetic field is different depending on the location and environment, the program incorporates both min-max normalization and GPS magnetic variation data to calibrate the compass output.

For display, Adafruit SHARP 168x144 Display is used. It has advantages of low power, good resolution, and great visibility under the sun. Additionally, it has a much higher refresh rate compared to most e-ink displays. These

properties make it suitable for use in battery powered, outdoor use devices like ST PATS. The display can be seen in use in daylight in Figure 98.



**Fig. 98 ST PATS local GPS and compass test**

The microcontroller used in ST PATS is Adafruit Feather M0 Adalogger. It has great support for all the other Adafruit components used on board. Additionally, the board supports multiple hardware serial connections, making it easy to communicate with USB, GPS, and radio telemetry. For more, logs can be saved to an external storage via on-board SD card slot. The Adalogger has a built-in battery regulator and charger, providing a safe way to use and charge LiPo batteries. As known by most, Earth is not flat. Therefore, the direction of the rocket cannot be calculated with 2D Euclidean geometry directly. To overcome this, the program projects the rocket coordinates from latitude and longitude into polar coordinates using azimuthal projection, centered at the current location. The direction can then be calculated by subtracting the compass heading from the polar coordinate heading.

## E. Payload

The payload onboard LotS contains two distinct experiments. The first is a prototype avionics assembly designed to collect, process, and store real time flight dynamics data. The second is a biological experiment concerning the effects of microgravity on alcohol dehydrogenase activity in sourdough yeast cultures.

### 1. State Estimation

#### Motivation

As noted in the introduction, one key focus for LotS was improved simulation and modelling efforts, including the formation of the flight dynamics team. While the instrumentation for altitude measurement is extremely robust due to the nature of the competition and overall design requirements, the same cannot be said for other dynamical variables. In order to assess the performance and accuracy of flight dynamics simulations, it is necessary to collect accurate state information about the rocket throughout its actual flight. Specifically, our goal is to estimate the position, velocity,

acceleration and orientation of the rocket at all points during the flight.

Without any active controls, real-time sensor data serves no useful purpose - so long as records of the data exist, any useful insights (e.g. related to flight dynamics validation) can be derived from post-processing the data. Looking forward, however, there are two primary reasons to develop real-time state estimation capabilities on the team. The first is the potential to develop active guidance systems, insofar as they are permitted by IREC rules. The team's aerostructures manufacturing capabilities have been pushed to their limits during the development of LotS, and the design, test, and integration of active guidance controls for the rocket itself is a strictly long-term consideration. The more immediate purpose for state estimation is for a deployable payload experiment under development for the team's planned 2024 rocket.

Originally, the 2023 payload was to be an autonomous, deployable aircraft based on the "Rogallo wing" developed by NASA in the 1960s. Due to delays in testing and development of the full aircraft, it was decided that the 2023 payload would instead house a prototype of the avionics that would fly on such a deployable payload, with a focus on the state estimation software component. The existing, modular framework of RocketCAN was used as the basis for the payload avionics, with additional hardware to handle intensive computing tasks and power distribution.

## **Electrical Architecture**

Multiple RocketCAN boards were used to provide critical functions for the payload system. This extends the same benefits as described in the Avionics section to the payload. RocketCAN boards have already been developed, previously verified in flight, and can be easily swapped in and out from a common pool of spares shared between the payload and avionics teams. In addition to the boards ported from RocketCAN, an SRAD power and communications board (GrandPapa) and a Microchip DM320209 development board (Kalman board) were integrated into the payload bus. The payload electrical architecture is summarized in 99.

### **GrandPapa Board**

Power distribution for the entire payload is handled by GrandPapa board. It provides a 5V power supply to the other payload boards, which can be switched on and off using commands over RocketCAN. GrandPapa itself has two sources of power. When the rocket is on the pad and connected to EGSE, GrandPapa draws power from the RocketCAN 12V line to power the payload and charge an onboard 6200 mAh Li-Po battery. Once disconnected from EGSE, GrandPapa can disconnect from RocketCAN and power the payload from the battery. The DC-DC conversion and battery charge circuits are shown in 100 and 101, respectively.

In order to prevent excess traffic and potential latency on RocketCAN, the payload has its own independent CAN bus. Following the KotS payload architecture, GrandPapa acts as an intermediary between the rocket bus and payload bus, passing diagnostic messages and some state information back to Live Telemetry and forwarding any relevant messages

### Payload 23 Electronics System

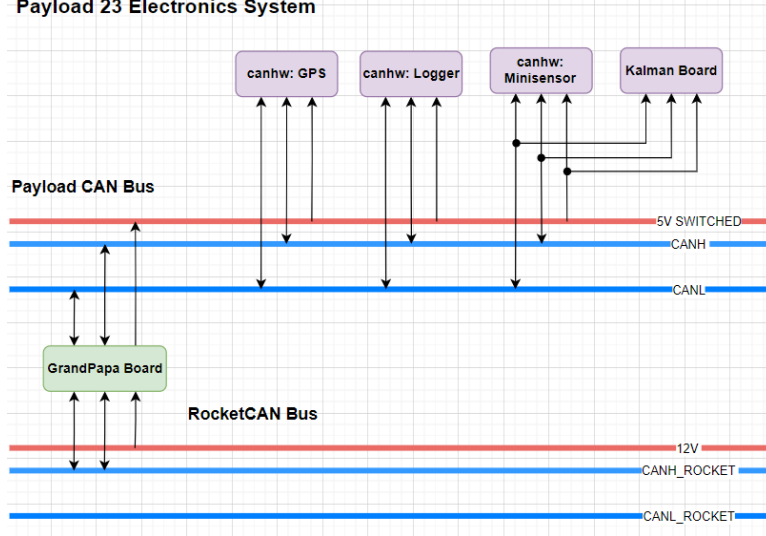


Fig. 99 Payload avionics

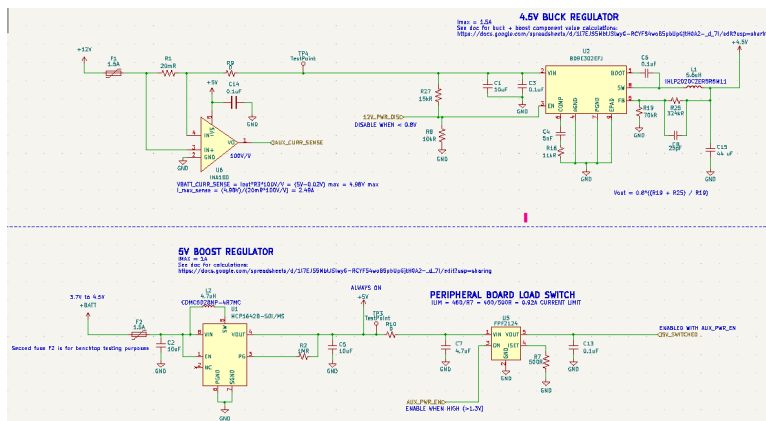


Fig. 100 GrandPapa board 4.5V buck and 5V boost converter circuitry

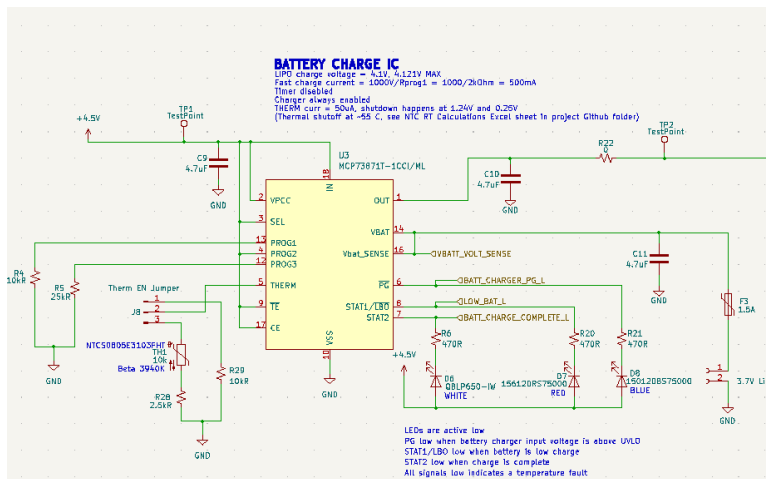


Fig. 101 GrandPapa board battery and charging circuitry

from the rocket to the payload. Otherwise, the payload bus is dedicated to sending data to and from Kalman board for state estimation purposes.

## Payload Concept of Operations

One of the capabilities of the Minisensor board is to collect live altitude, acceleration, orientation, and angular velocity data from an onboard inertial measurement unit (IMU). As with most IMUs, this data suffers from error. Sources of error can include physical imperfections in the measuring device, EMF interference, nonlinearity in sensor output, cross-axis sensitivity, and drift. Another important consideration for IMU data is that the sensor axes are fixed to the body coordinate frame of the rocket, which changes relative to the earth reference frame throughout flight.

The algorithm chosen to compensate for these inaccuracies in the payload is a linear Kalman filter. Kalman Filtering is a technique used to improve the accuracy of sensors using information about the physical system they are observing. The filter operates by making use of a dynamical model which predicts the future value of states based on linear combinations of the current states, at each time step. The filter then considers state observations produced by the sensors and combines these two to produce a new, more accurate, estimate of each state.

There are two main difficulties associated with using Kalman Filters for estimating the state of LotS. Firstly, the impact of the engine on flight dynamics needs to be modeled for the filter to be even remotely accurate. Super-sonic air resistance presents a similar problem. Secondly, the interplay between orientation and the other dynamic variables cannot be modeled linearly. We developed solutions to solve each of these issues.

To address the first, we made use of data produced by our Openrocket simulation to give us an estimate on our acceleration. These simulations factor in all of the aerodynamic effects we cannot model, so they should give us a rough estimate of the acceleration at any given time. We then use this estimate of acceleration to give us the change in acceleration, which we pass into the control input of the Kalman Filter. This allows us to use a constant-acceleration model, which is simple to implement.

To address the second, we applied Linear Approximation techniques at each time step of the filter and normalized the results obtained at each time step against the frame of reference of the rocket. However, computing each update step of the filter using Linear Approximation requires solving multiple matrix equations, and these computations must be performed many times each second. To achieve the necessary computing power, it was decided a more powerful, 32-bit microcontroller was necessary. Due to timeline constraints and the cost associated with developing a new board, a COTS development board housing a PIC32MZ2048EFM144 microcontroller was selected. A small adapter board was developed in order to connect a Harwin Datamate connector to the development board to adhere to the team standard for flight wiring. The full assembly is pictured in 103.

At the time of writing, the filter code has not undergone a complete integration test. The core mathematics of the filter have been verified on simulated data, and CAN message transmission to and from individual boards on the payload

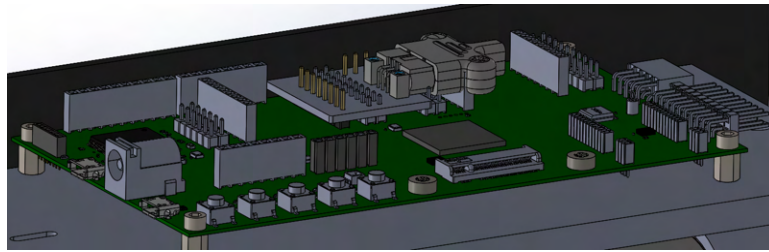


**Fig. 102 Kalman board and adapter board assembly**

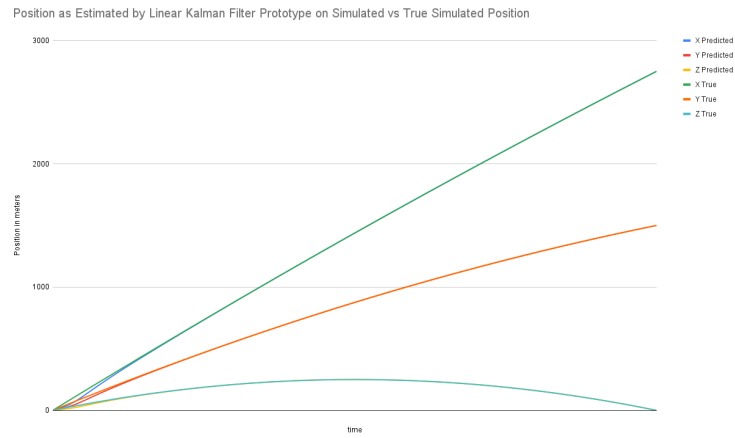


**Fig. 103 Position as Estimated by Linear Kalman Filter prototype on simulated data**

bus has also been validated. Complete testing would involve connecting all boards to the payload CAN harness and attempting to produce live state estimates based on data being provided by GPS and Minisensor over the bus.

Below is a depiction of the performance of our Linear Kalman Filter on Simulated data.

## 2. Live Yeast Culture

### Motivation

Mankind's relationship with the act of fermentation is extensive and broad; from traditional cuisines surrounding breads and yogurts to the synthesis of therapeutic proteins and antibiotics in the pharmaceutical industry, the connection between human society and symbiotic bacteria cultures runs deep, beyond what happens in the kitchen.

While it has went on to develop a certain nostalgic foothold in the Zeitgeist of pandemic related past time activities, sourdough starters remain an incredibly accessible peek into the world of microbiological enzyme production and bacterial interactions. *Saccharomyces cerevisiae*, the humble 'baker's yeast', has benefited from its fair share of scientific spotlight - having been the first eukaryote to undergo genomic sequencing and remaining a staple microbiological lab rat in experiments in elementary classrooms and universities alike, the applications of this single celled organism extend far past it's dough rising abilities. In recent years, the world of science has called it's familiar friend back to the table,

this time in the field of biopharmaceutical production. Preliminary studies have shown promise in the use of novel heterologous gene insertion into yeast cells for the purpose of vaccine, antibody, enzyme, opioid, cannabinoid, hormone, phenylpropanoid and blood product synthesis within the pharmaceutical sphere [8], introducing the possibility of a biomedical pharmaceutical industry centered around yeast powered medical product synthesis that could greatly benefit from the existence of therapies that encouraged increased yeast activity. The goal of LotS' payload team has been to pursue further experimentation in this field, specifically a hypergravity treatment for yeast samples.

The scientific exploration of hypergravity is not an entirely unexplored domain- with a study in 2021 suggesting a correlation between hypergravity exposure and increased total dehydrogenase activity within wheat seeds [9]. Alcohol dehydrogenase I activity, which exists by comparison as a functional cousin to the operations occurring within these space faring milt, plays a key roll in the reduction of acetaldehyde into ethanol during the fermentation of glucose [10], an integral part of the sourdough starter fermentation process. Should we determine the effects of hypergravity to in fact positively impact alcohol dehydrogenase I activity, it would suggest that biopharmaceutical production within genetically modified yeast cells, who original dehydrogenase pathways have been repurposed from the production of ethanol to that of medicinal compounds, would see increased production capabilities.

It is our hope that through comparison of ethanol levels within sourdough samples exposed to hypergravity conditions with those of the original mother sample acting as the control, we may be able to determine if alcohol dehydrogenase activity is in fact increased by hypergravity therapy. Should this be true, the door of scientific inquiry into the application of this fact in the world of optimized yeast powered biopharmaceutical production will be opened, with the potential to greatly enhance the speed and quantity of medicinal compound availability.

### *3. Cubesat*

The payload will be housed with an SRAD 3U CubeSat following the CubeSat Design Specification Rev. 14 [11]. The CubeSat will not be deployed during flight. The CubeSat design can be broken up into three major components as seen in 104: the structure, Systems Module, and Experiment Module.

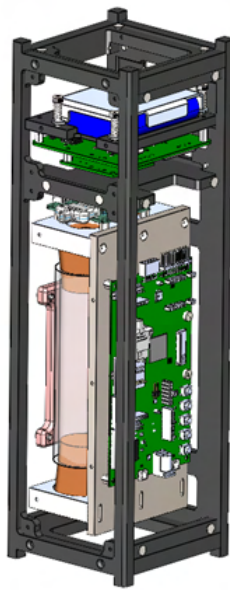


**Fig. 104** CubeSat Payload with cover panels and screws hidden. Note the structure in black as well as the Systems Module in the top third of the payload with the Experiment Module in the bottom two thirds of the payload.

The structure as shown in Figure B is the skeleton of the CubeSat and as a free-standing structure, the front and back faces along with the internal braces support the structure and do not require any of the modules to assemble. This allows for the internal modules to be easily slid out from the side of the structure when required.



**Fig. 105 Structure of the CubeSat with black pieces shown as structural members while yellow pieces represent cover panels**

The Systems Module as shown in Figure C houses the power electronics of the payload. On the top half of the Systems Module, all the power management PCBs for the payload are mounted to a base plate using standoffs. On the other side of the base plate, the single Li-Po battery is mounted using an aluminum sheet metal clamp.

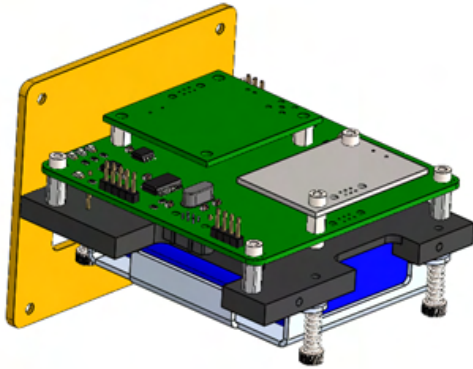


**Fig. 106 Systems Module of the payload with the power management PCBs mounted on top of the base plate of the module. The battery shown in blue is mounted to the bottom of the module.**

The Experiment Module as shown in Figure D carries both experiments on the payload. The Kalman filter board is mounted sideways to the base plate of the module. The biological sourdough experiment is housed within two 1.25 in ID clear food-safe PETG tubes that are sealed with corks and clamped down by aluminum end-pieces. A copy of Minisensor board is mounted to the top of the module, such that it is coaxial with the rocket body. Assembly drawings for these modules are included in Appendix G.

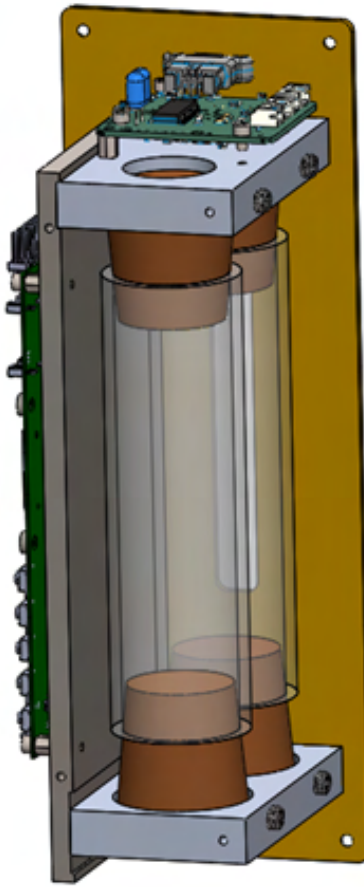


**Fig. 107** Systems Module of the payload with the power management PCBs mounted on top of the base plate of the module. The battery shown in blue is mounted to the bottom of the module.

As the design of the structure of this payload has only altered minorly compared to last year's payload, additional ANSYS FEA was not conducted on this design. Using a maximum acceleration during boost of 7.1G from the OpenRocket sims previously conducted as well as accelerometer data gathered during the flight of UXO recording 10G, a maximum axial acceleration of 15G was estimated for the worst-case condition of the payload. Using these values, the previous static structural and model FEA simulation of the CubeSat structure was employed for the similar design used in this year's payload. The first three modal frequencies were assumed to be near 718 Hz, 833 Hz, and 834 Hz. These frequencies will contribute negligibly to the dynamic behaviour of the system due to their perceived low ratios of effective mass to the total mass of the structure. Furthermore, as these modes have frequencies significantly greater than 100 Hz, the structure is predicted to be dynamically sound.

## F. Mechanical Ground Support Equipment

### 1. Ground Support Equipment (GSE) Architecture

The ground support equipment consists of all components which support the successful launch of LotS including the launch tower and ground-side plumbing. Significant improvements have been made for the 2023 competition year to increase the safety and decrease the setup time of ground support equipment. A layout of the ground support equipment at the pad is shown in Figure 108.

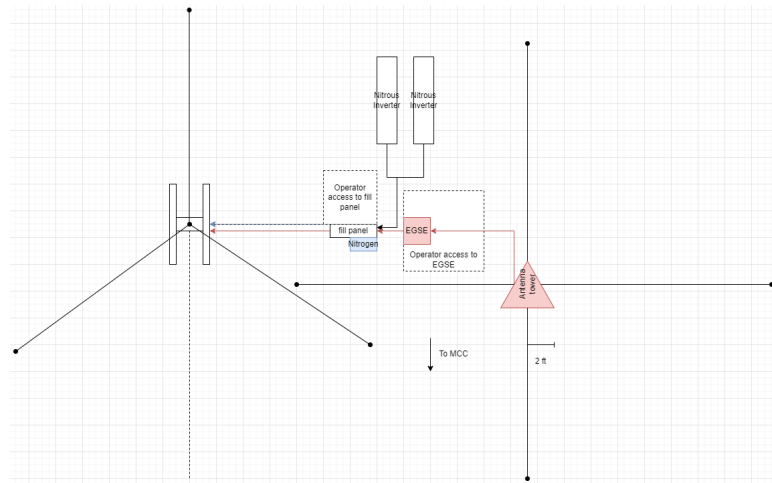


**Fig. 108 Launch Site GSE setup**

In addition to improvements in the physical GSE systems, improvements were made to the testing and setup procedures. This included writing procedures that explicitly detail which steps can be completed in parallel, and the addition of a launchpad setup test to practice and review the complete assembly and layout of the launchpad before competition.

### 2. Launch Tower

The launch tower used by the team is a comprised of five segments of steel lattice, connected to an 18" x 18" plate. This entire assembly is connected to a larger base frame via a hinge, allowing the base to be secured to the ground before the tower is raised. When raised, the tower is angled 5° from vertical as per IREC regulations, and secured by a series of three guy wires as shown previously in Figure 108. A 32' launch rail made up of 1.5" square aluminum T-slotted extrusion segments is mounted onto the tower, interfacing with the two launch lugs on the rocket which slide into the slot of the rail. A load cell is mounted at the base of the tower such that the rocket rests on it, allowing the mass of the rocket to be remotely monitored during propellant filling. General improvements made to the launch tower this year include a full inspection and repair of the entire tower structure, sourcing new guy wires and fasteners that conform to a single standard, and removing rust from all components. Additional legs were added to the base as shown in Figure

109 to ensure stability based on the results of improved wind-loading analysis.

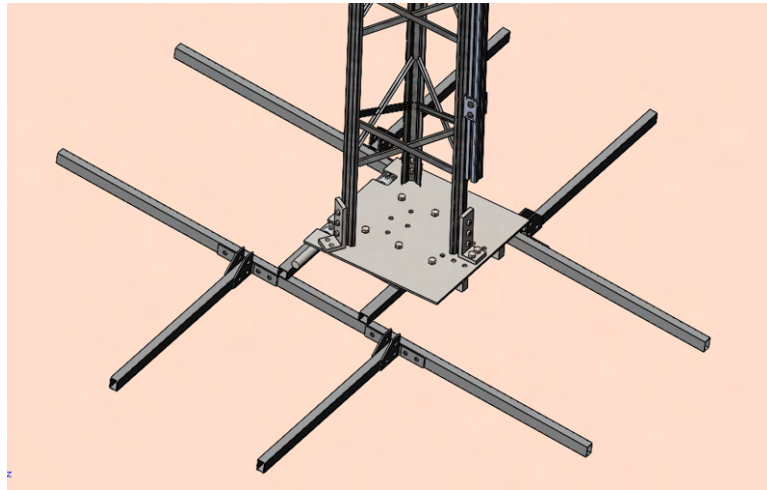


**Fig. 109 Expanded Launch Tower Base**

### Raising Improvements

The launch tower is raised using a gin pole and hand-drill operated winch. In 2022, it was discovered that the previous connection between the gin pole and the launch tower base had deteriorated, causing it to fail and requiring the tower to be raised manually. For 2023, a new connection between the gin pole and tower baseplate was designed and manufactured in-house and connected to the baseplate with six bolts. This new mount is shown in Figure 110 and is designed to withstand the bending loads exerted on the gin pole during tower raising with a proper FOS.

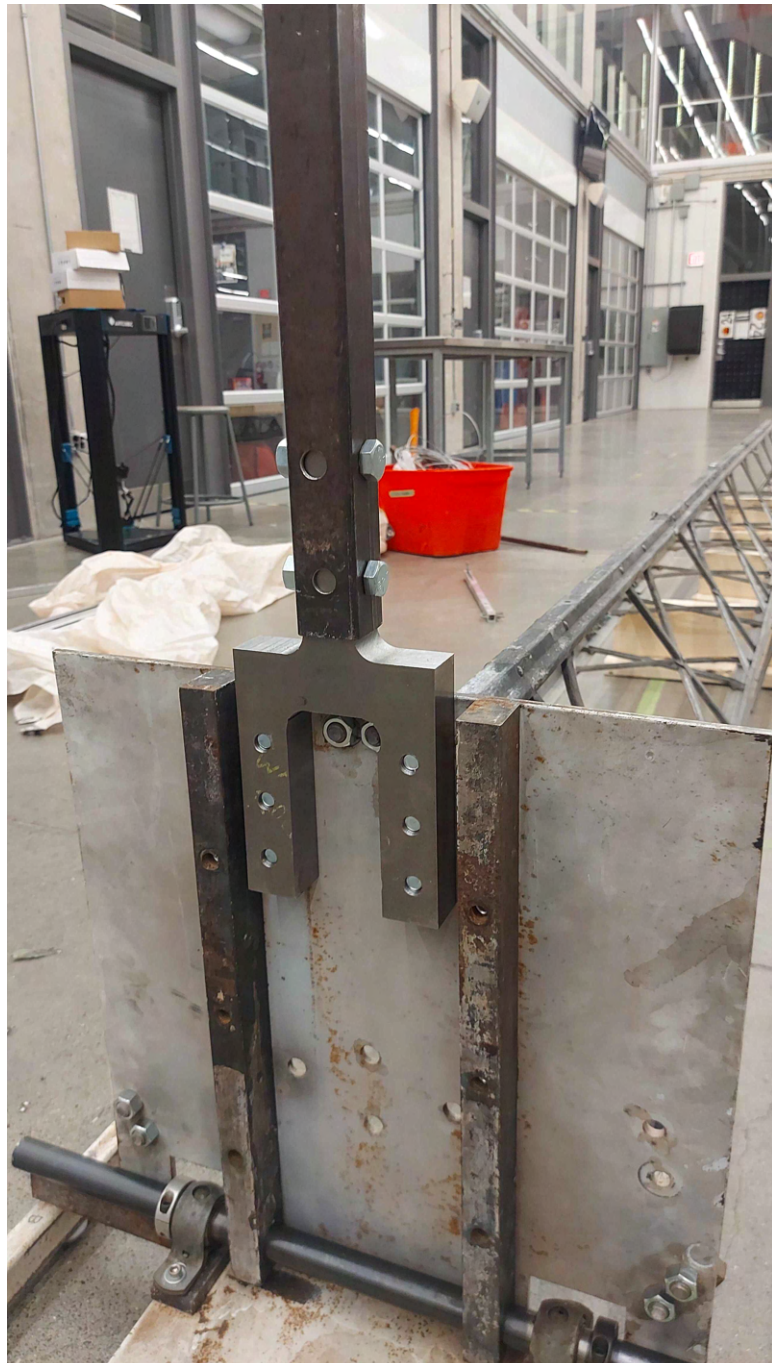


**Fig. 110 SRAD Gin Pole Mount**

The procedure for assembling and raising the tower was also updated this year to reduce setup time. This procedure outlines how the base, launch tower, and guy wires may be assembled in parallel, resulting in a much more efficient setup process. A procedure to control the fleet angle of the cable using a metal rod was added based on issues where the cable would layer unevenly and occasionally fall off the winch drum that were observed in previous tests.

## Rail Mounting Improvements

Improvements have also been made on the mounting and aligning of the launch rail, which is comprised of 5 segments of t-slotted aluminum extrusion. The previous mounting solution for these rails was a series of small square plate inserts that slid into the t-slot and were connected to the tower using a single bolt each, with a spacer between the rail and tower lattice. The rails were slid on one at a time, and secured by tightening the bolts from below. Given that each mounting plate had only one bolt, and the holes drilled into the tower lattice for these bolts were clearance holes, this caused frequent misalignment and binding as the rails were being slid into place. This year, a new clamping system was designed to improve ease of assembly and alignment. These new clamps consist of a U-shaped body that can be bolted onto the tower before final assembly with two mounting holes on both sides. Bolts passed through these holes thread into longer plates that slot into the aluminum extrusion, as shown in Figure 111. Adding a second connection point and using longer inserts means the rail no longer binds when being slid through the clamp. To secure the rail, the bolts on the sides, which are much more accessible, are tightened. Spacers placed between the clamp body and the rail keep the rail centered, and prevent the walls of the clamp body from bending inwards as was observed during initial trials.



**Fig. 111 Rail Mounting Clamp**

Additionally, rail alignment was simplified by the addition of alignment pins. These pins are threaded on one end and have a shank slightly smaller than the central hole of the T-slotted extrusion. Each rail segment has threads tapped into this central hole on one end. During installation, the rail is installed so the threaded hole is facing the top of the tower. The alignment pin is then threaded into this hole and the next rail segment is installed in the same orientation so

it slides onto the pin. This effectively fixes the rails in two axes, meaning rails only need to be rotated relative to each other in order to create the desired seamless transition between rail segments.

LotS' load cell mount is an integral part of our pre flight nitrous oxide fill process, and permits for accurate weight measurement of the amount of fuel being loaded into our rocket. With the use of a load cell and a set of adaptive structures that allow for integration of this device into our systems, a main focus of our mechanical GSE's team this year has been the optimization of this critical process. Precision is of particular important in this domain- should the tank be under-filled, we fail to reach max engine efficiency, and should it be overfilled, we risk spillage, excess weight and potential mechanical issues or chemical concerns within the propulsion system.

Previous iterations of our load cell mount, particularly in last year's KotS launch tower structure, presented a few significant concerns. Our use of a button style load cell required the concentration of the weight of our rocket onto an incredibly small footprint, causing significant issues with torsional binding of our load cell mount on the rail system, resulting in inaccurate measurements. Another cause for concern was the weight to which the load cell was rated; designed to bear up to 2000 pounds, the sensitivity of our measured results for an under two hundred pound rocket were subpar.

To circumvent these complications, this year's GSE team ensured the implementation of a new, beam style based load cell design. By directly bolting the mount to the load cell itself, we managed to eliminate the torsion and jamming on the launch rail we saw in previous iterations of this system, and the purchase of a load cell rated up to two hundred pounds permitted for much higher sensitivity readings, allowing for more accurate real time perception of our rocket's changing weight during propellant fill.



**Fig. 112 Load Cell Mount**

### *3. Antenna Towers*

At previous competitions, the antenna at the launch site was mounted on the launch tower, and the antenna at mission control was affixed to a shovel or vertical piece of wood. This created issues when connecting the antennas, as the towerside antenna needed to be rotated independent of the launch tower in two axes - horizontally to point towards base camp and vertically as the antennas were at different elevations. The low elevation of the basecamp antenna also presented connectivity issues as signals were blocked by surrounding vegetation or the terrain.

This year, two identical towers with metal extendable bases and telescoping carbon fiber masts were sourced so that the antennas can be mounted independently and at a high enough elevation to be clear of any obstructions. The towers can be raised to a maximum height of 33ft, and the height can be adjusted as desired by extending some or all the telescoping mast segments to properly align the antennas vertically. The towers are secured by three guy wires similar to the launch tower. To secure the mast in place once the individual segments have been telescoped out and locked, three

bolts are threaded through the base and tightened against the mast. In early tests, it was observed these bolts did not fully constrain the mast from rotating, and scratched the carbon fiber. To solve this, 3D printed clamps were made that go between the base and the mast, as seen in Figure 113. Similar clamps are also placed at regular intervals up the tower to secure power and Ethernet cables running up to the antenna. An additional side effect of the mast being free to rotate when the base bolts are not fully tightened is that the horizontal alignment of the antennas can be done from the ground by rotating the entire mast, simplifying the setup procedure and removing the need for more complicated antenna mounting solutions.

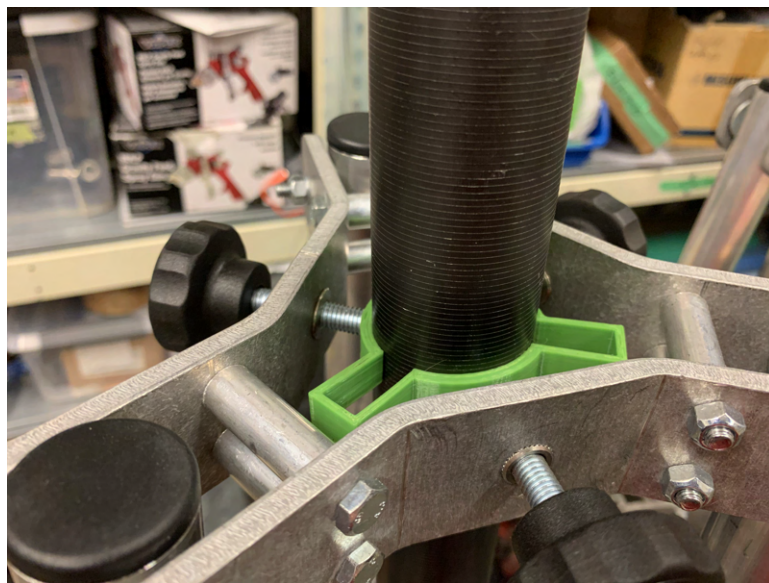


**Fig. 113 3D Printed Antenna Tower Mast Protector**

#### *4. Fill Plumbing*

Historically, setup times for static fires and launches have been a significant issue for the team. After being unable to launch last year, partially due to pad setup difficulties, a solution was needed to be able to quickly assemble the required ground equipment to support a launch or a static fire. The “containerized GSE” project was conceived with this goal in mind, being split into electrical and fluid gse systems.

The fluid GSE system is required to remotely load nitrous oxide into the rocket in a timely manner. Safety was a critical consideration during the design, since there will be nitrous oxide in the plumbing while operators are nearby. Additionally, the goal of the system was to avoid having to disassemble and sanitize the plumbing after every use, with the eventual goal to allow an accelerated testing cadence.

The panel includes many features to make operations easier and safer. Remote valves, a thermocouple and a pressure transducer allow for the system to be monitored and operated at a distance. The panel is designed so that at no point there can be pressure trapped without a way to vent it from a distance. The panel also includes manual backups for

both remote valves, a pressure gauge, as well as a pressure relief valve set to 1000 psi for safety. To allow the panel to be used without full sanitation after each use, a swappable filter element is included at the inlet of the panel to catch debris. Additionally, an inlet for a nitrogen purge is included to remove remaining nitrous oxide vapor after use. Quick disconnects interface from hoses to the panel, for quick assembly in the field. A complete P&ID for the panel is shown in figure 114.

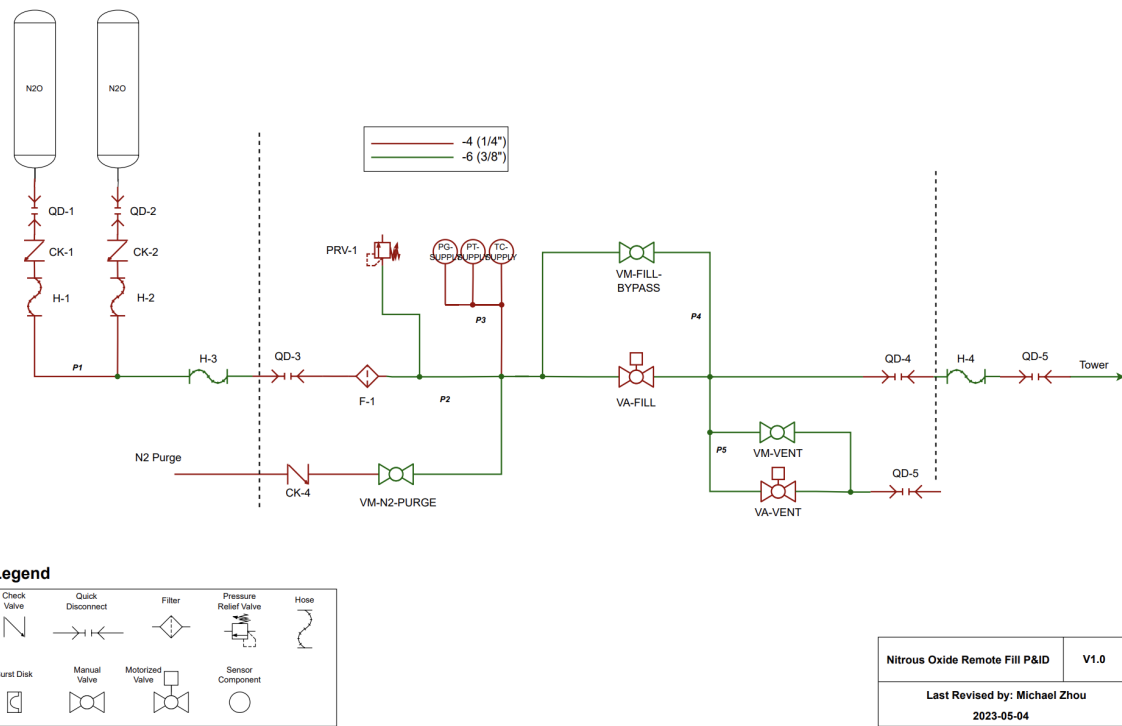


**Fig. 114 Nitrous Oxide Panel P&ID**

To ensure that the panel would be able to fill the tank in a timely manner, the required tubing size was determined using both Bernoulli's equation with losses and an equivalent Cv calculation. It was determined that 3/8" tubing with 1/4" NPT fittings was the most cost effective size that would meet the required fill time of 10 minutes maximum. In testing, the fill time was found to be approximately 4 minutes. Tubing was used for as much of the panel as possible to allow for easy assembly without the major clocking issues caused by NPT. Additionally, it will be easy to modify the tubing in the future if changes are required. Both JIC flared connections and Swagelok are used on the panel to connect tubing and interface with NPT components. The fully assembled panel is shown in figure 115.

To save costs, certain components on the panel were manufactured in house. The tube clamps were made based on the dimensions given in the Swagelok catalog, by water jetting the metal plates and 3d printing the tube support pieces. A tube clamp in use on the panel is pictured in figure 116.

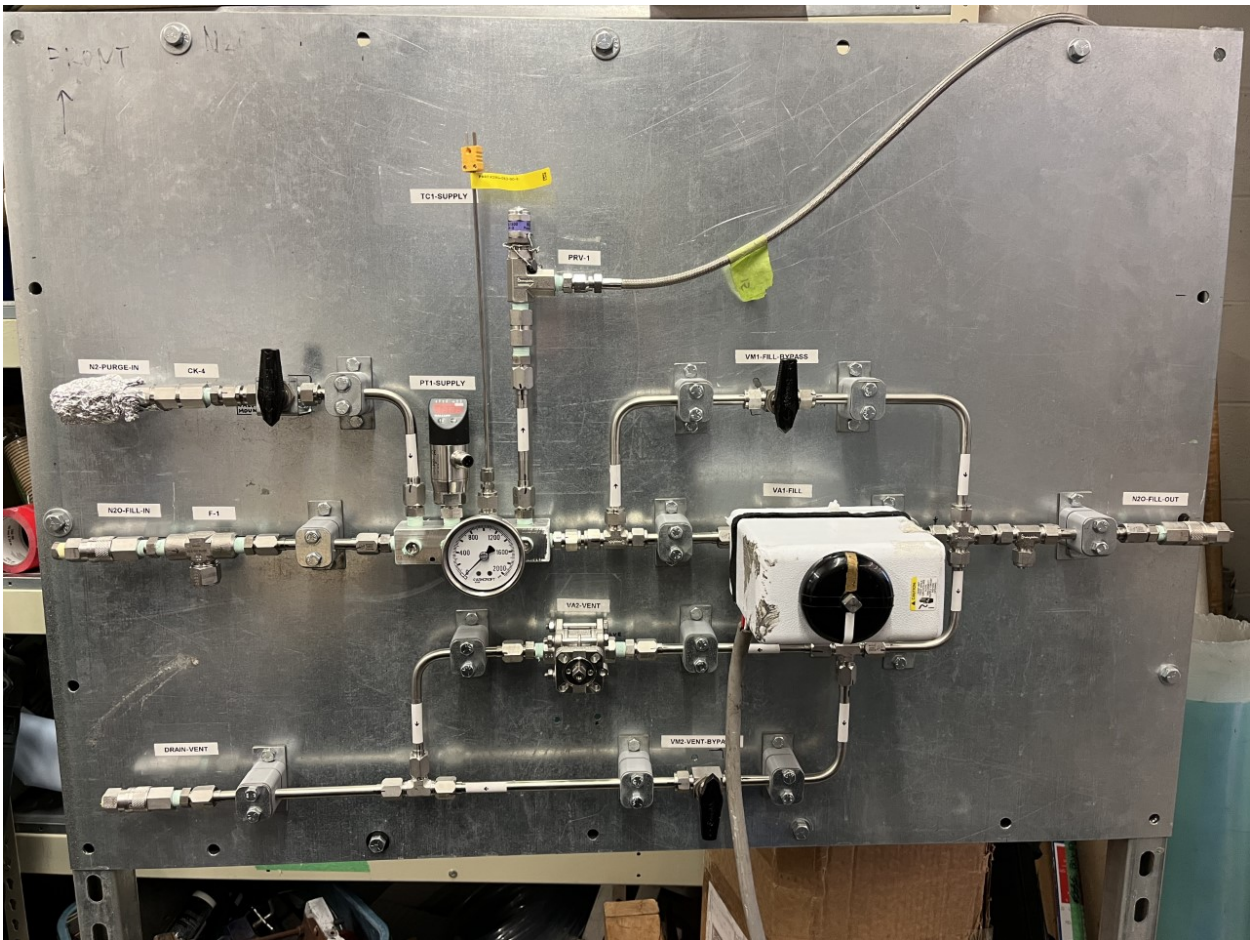


**Fig. 115 Assembled Nitrous Oxide Panel**



**Fig. 116 Student Manufactured Tube Clamp**

Additionally, a custom manifold block was made, due to the high costs of commercial manifold blocks, which is also pictured below in figure 117.

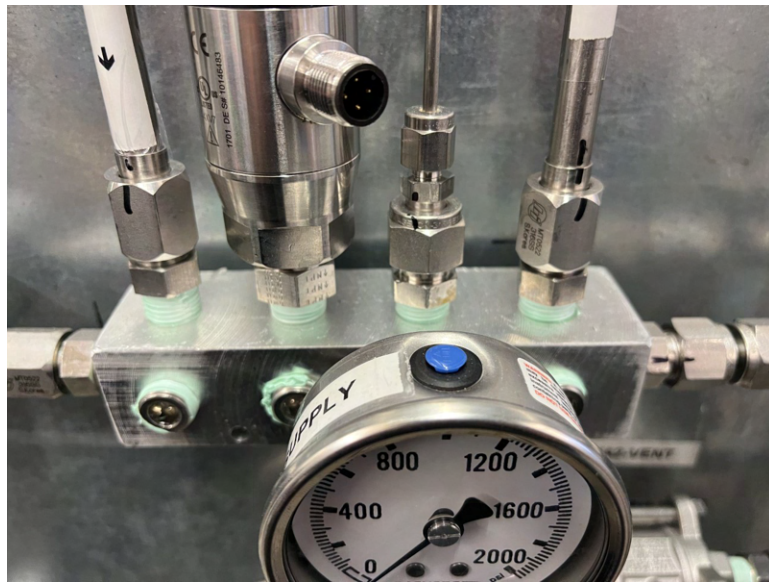


**Fig. 117 SRAD Manifold Block**

The assembled panel successfully passed a hydrostatic test at 1.5 times maximum expected operating pressure (1500 psi). The panel also supported the final static fire this year, and made plumbing assembly at the test site significantly easier.

##### *5. Fill Disconnect*

The launch tower additionally provides mounting features for the remote-disconnect mechanism. Due to the nature of hybrid fill operations, it is necessary that a mechanism exists to disconnect the fill line from the engine prior to launch. In addition, the rocket uses pneumatics to actuate the vent and injector valve. The rocket has sufficient compressed air storage onboard for the expected operations, however pneumatic systems are prone to small leaks, so to ensure sufficient air pressure during long delays on the pad, the compressed air supply is disconnected using the same mechanism right before launch. Disconnect is accomplished using a spring-loaded system secured with quick connect fittings. The female quick connect fittings, attached to the end of the fill hose, is mounted to an aluminum arm that pivots around a bracket mounted to the tower; the other end of this arm is connected to two tension springs. During fill, the female fitting is connected to the male quick connect fitting on the rocket. The release mechanism consists of a linear actuator controlled by RLCS, a bracket inserted between the male and female quick connect fittings, and a mounting structure to secure the linear actuator to the arm. Once fill has concluded, the linear actuator retracts to pull the bracket, which also pulls the collar on the female fittings, allowing the fittings to disconnect. Pulled by the tension springs, the fill arm pivots away from the rocket and pulls the fill hoses from the fill ports.

## *6. Electrical Disconnect*

Having charged batteries and a reliable communications line leading up to launch was a significant issue that was encountered in previous years. To address this issue, an umbilical electrical connector and disconnection system was developed. The mechanism used brass pogo pins attached to groundside that magnetically attached to flat brass contacts embedded in a terminal on the rocket. The pins and contacts were soldered to 14-gauge cables that supply the electrical and communications lines. As the rocket travels upwards, the shearing force disconnects the groundside terminal from the rocket.

Maintaining a flush surface finish of the rocketside port with the fairing was a key design attribute, thus flat contacts were embedded into rounded housing on this side of the mechanism and the entire terminal was sanded flush to the fairing. Each side of the electrical disconnect was contained within 3D-printed housing. FDM printing was used on the groundside terminal as the thermoplastic filament was lightweight enough such that the risk of damage caused by the housing making contact with the fins as it falls would be minimized. On the rocketside terminal it was established in prototyping that FDM did not have the required resolution to produce the rounded edge of the housing, therefore an SLA-printed housing was used in the final design.

The groundside terminal featured two separate 3D-printed components: a pin holder for the pogo pins and an outer casing.

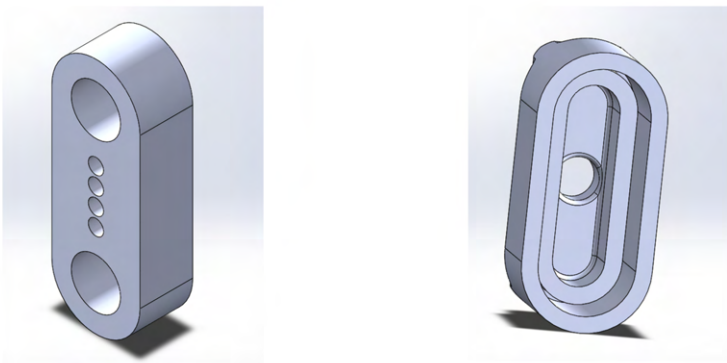


**Fig. 118 Electrical Disconnect Towerside**

The rocketside terminal also involved two components: a variation of the groundside pin holder that would house the flat contacts and round neodymium magnets screwed into a bracket that was fixed to the inside of the fairing.

All pins were epoxied into stepped holes that helped align the pins to the correct depth. This was important to ensure the pogo pins would compress completely when connected and the flat contacts would sit flush. Strain relief was implemented on both sides of the terminal to prevent shearing forces from acting directly on the cables.

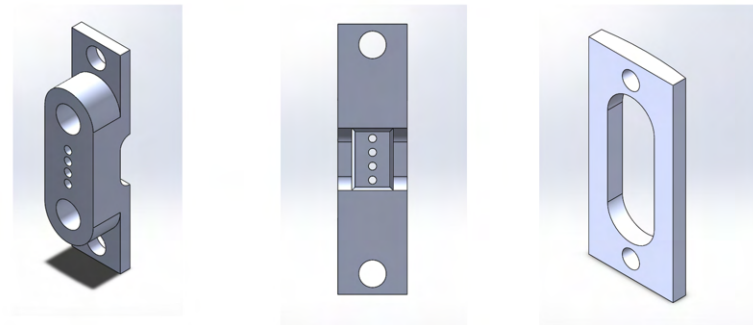


**Fig. 119 Electrical Disconnect Rocketside**



**Fig. 120 Assembled Electrical Disconnect Mechanism**

### III. Mission Concept of Operations Overview

The following section outlines the mission concept of operations for Leviathan of the Sky, including the flight plan and simulated flight dynamics.

#### A. Flight Plan

The Leviathan of the Sky flight plan is divided into 9 steps, beginning with pre-launch operations and ending with vehicle recovery. An overview of the ConOps is shown in figure 121

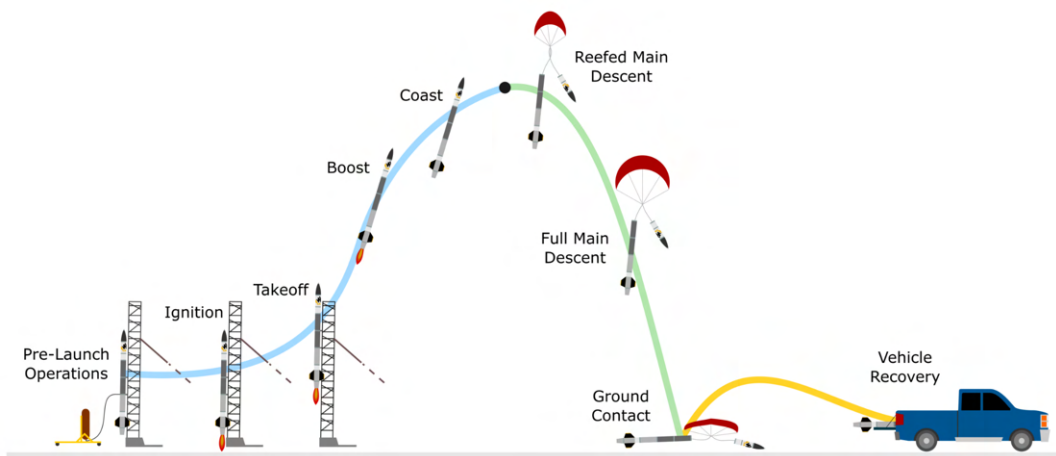


**Fig. 121 LotS Flight Plan**

## *1. Pre-Launch Operations*

**Start:** *T-15 minutes.* Launch setup is complete and the rocket is in position on the launch tower.

**End:** *T-30 seconds.* Flight director receives clearance to begin ignition.

Pre-launch operations begin once launch setup is complete, and the launch pad director has reviewed and signed off on all completed setup procedures. This includes the completed setup of all ground support equipment, as well as the railing of the rocket and raising of the launch tower. All team members depart the launch site and return to mission control, with the exception of the primary and secondary fill operators who don the required personal protective equipment. The operators perform final system verification checks, hook up the nitrous supply to the fill panel, and retreat to the minimum safe distance. The rocket is switched to internal power.

Remote fill is performed through the Remote Launch Control System (RLCS), and rocket data is monitored by the data acquisition and live telemetry operators. Once required launch conditions have been met, the fill line is disconnected remotely. The flight director then requests authorization to begin ignition. The pre-launch operations phase ends when authorization has been received.

## *2. Ignition*

**Start:** *T-8 seconds.* Signal sent to ignition puck.

**End:** *T-0 seconds.* Launch vehicle begins to accelerate.

After the signal is sent from the remote launch control system to the ignition puck, and a drop in current indicating successful ignition is received at mission control, the injector valve is opened and combustion begins, accelerating the rocket.

## *3. Takeoff*

**Start:** *T+0 seconds.* Launch vehicle accelerates up the launch rail.

**End:** *T+0.3 seconds.* Launch vehicle departs the launch rail.

During the takeoff phase LotS accelerates up the launch rail, departing with an off-rail velocity of 149 ft/s and static stability margin of 1.77 cal.

## *4. Boost*

**Start:** *T+0.3 seconds.* Launch vehicle has departed the launch rail.

**End:** *T+14.8 seconds.* Engine burnout.

After departing the launch rail, the Kismet engine will continue to burn for 14.5 seconds. At 6.6s and 6480 ft the rocket reaches a maximum velocity of 1543 ft/s, or Mach 1.41.

## *5. Coast*

**Start:**  $T+14.8$  seconds. Engine burnout.

**End:**  $T+40.9$  seconds. Launch vehicle achieves apogee.

After engine burnout, the rocket continues to coast for 26.1 seconds until it reaches an apogee of 29554 ft. At the time of burnout, the static stability margin is 2.5 calibers. The maximum stability margin reached during ascent is 5.1 calibers.

## *6. Reefed Main Descent*

**Start:**  $T+40.9$  seconds. Altimeters detect apogee.

**End:**  $T+160$  seconds. Altimeters detect 1,500 ft above ground level.

When LotS reaches apogee, the altimeters will detect a decrease in altitude and trigger deployment of the main parachute, which opens initially in a reefed state. This will slow descent of the rocket to a constant velocity of 205.7 ft/s, until it reaches 1,500 ft AGL.

## *7. Full Main Descent*

**Start:**  $T+160$  seconds. Main parachute disreefs.

**End:**  $T+219$  seconds. Launch vehicle comes in contact with ground.

When the altimeters detect 1,500 ft AGL a message is relayed over the CANbus to the recovery electronics, which automatically trigger the pyrocutters and disreef the main parachute. Once the parachute is fully deployed, the rocket will slow to a descent velocity of 22.4 ft/s. The on-board GPS will continue to track the location of the rocket as it descends, which is relayed to the telemetry operator at mission control.

## *8. Ground Contact*

**Start:**  $T+219$  seconds. Launch vehicle comes to rest on ground.

**End:** End of OPS. All sensors read baseline values unless suspected faulty.

After ground contact, the geographical location of the rocket is noted by the operations director for vehicle recovery.

At the launch site, the fill system is vented through the remote launch control system. The data acquisition operator confirms all sensors are reading baseline values, and launch operators approach the test site for final system checks before the launch procedure is declared complete.

## *9. Vehicle Recovery*

**Start:** End of OPS. Launch vehicle location is determined.

**End:** Launch vehicle is recovered.

After the launch site has been safed and the range returns to green, the operations director organizes the vehicle

recovery team and relays the launch vehicle's location. Once granted authorization to proceed, the recovery team heads to the GPS location to recover the rocket. A primary inspection is performed on site, to determine the risk level of approaching and transporting LotS. If the inspection signifies there is no potential risk to personnel the rocket is transported back to mission control for a full post-flight inspection, at which point the mission is declared complete.

## B. Flight Dynamics

### 1. OpenRocket Simulations

OpenRocket is used to simulate flight for the rocket. The rocket is initially split into 5 different sections to make modeling the rocket accurately easier. This is also done to keep CAD files organized and used as a general integration tool. Each individual component within the sections have their masses and Center of Gravity's (CG's) tracked by using their respective 3D models. Mass data has an expected number, as well as a maximum and minimum number to allow for manufacturing variations in simulations. Once parts are created, masses can be measured directly instead. The data is compiled into a spreadsheet that will return a CG for each section that can be used as a section CG override in OpenRocket. Key outputs of the program include max velocity, which is used for fin flutter calculations, as well as apogee and stability.

### 2. RSE Files

RSE files contain engine data and are required for OpenRocket to run a simulation. Thrust, engine mass, and engine CG data in relation to time is taken from static fire testing and used to create an RSE file. This allows OpenRocket to track the changing CG and mass during the flight of the rocket, as well as the thrust produced.

### 3. Other Flight Simulation Software

OpenRocket has generally been the standard for the team, but other programs were explored this year to see if better simulation accuracy could be achieved. RASAero and RocketPy were selected as possible alternatives to OpenRocket, but initial research showed that RocketPy was generally less user-friendly and required an understanding of Python in order to use the program, leading to RocketPy being eliminated from consideration. RASAero was used to model KotS and the simulation was compared to OpenRocket's. Although they yielded similar numbers for some key outputs such as velocity and apogee, RASAero made assumptions about engine location that resulted in it's simulation stability data being drastically different. This is due to RASAero being designed to work with solid rocket engines. The assumption results in the non-accurate CG location of the engine, so RASAero could not be used for accurate modeling of stability. Due to this OpenRocket is continued as the sole simulation software used by the team.

**Table 12 Example Simulation Results in OpenRocket**

Variable	Value
Apogee	29556 ft
Minimum Stability	1.77 calibers
Maximum Stability	5.09 calibers
Apogee Stability	2.48 calibers
Maximum Velocity	1561 ft/s
Off-Rail Velocity	149.78 ft/s

#### *4. Improvement in Accuracy of Simulations*

In order to improve the consistency and accuracy of simulations, changes were made to the integration process. Data for components and sections were gathered in cycles, allowing data to be updated consistently and in a structured way. Having up-to-date and accurate numbers allows for better simulations results, and increases the confidence in rocket design. Changes to the rocket can also be made in-between cycles if simulations reveal that certain sections may result in negative outcomes.

Through this system of cycles it was noted that changes in surface finish resulted in widely varying apogee results. OpenRocket offers different finishes ranging from rough paint to mirror surface. Although it was initially assumed that LotS would use the regular paint finish for simulation purposes, increasing the smoothness level to smooth paint greatly increased the rocket apogee. Based on this result, a project is currently ongoing to accurately measure the surface finish of previous team rockets and paint samples. This will then be used to determine the optimal painting method for LotS and further improve the accuracy of the simulations.

Additionally, in order to eliminate statistical errors from hand-running a limited amount of different test scenarios, the Monte Carlo method has been employed to factor in random variables that may affect the rocket's performance. A software plugin is written in-house and used on top of OpenRocket in order to allow repeated randomized sampling on input data such as Wind Speed and Wind Direction at launch time to account for the unpredictability of the launch conditions. By running a large number of tests we were able to affirm the results obtained from the hand-ran results. We were also able to gain new insights on the absolute worst-case scenarios and the conditions of which they occur in. The data and methodology of which are detailed in Appendix A - Monte Carlo.

## **IV. Conclusions and Lessons Learned**

### **A. Technical Lessons Learned**

#### *1. The Importance of Well-Defined Testing*

There were many lessons taken away from the team's failure to launch at competition in 2022, one of the most prominent being the importance of representative, well-constrained testing with properly documented methods and

results. It is an experienced truth on this team that there are almost always issues that you won't catch until you try something new. Because of this, it is best to avoid doing anything new with your systems in moments where failure is critical, such as leading up to a launch attempt. This means testing as much as possible, in as many ways as are reasonable, prior to competition. Tests should aim to reproduce a potential failure mode that may be experienced during use, or to otherwise characterize the system.

In order to ensure that testing achieves its purpose, it is important to first determine the potential conditions and constraints involved in system use. Then, a procedure is developed. Any deviations from the procedure are recorded, including reasoning for those deviations and their potential effect on the test results. Although testing should strive to include quantitative results wherever possible, the importance of qualitative results should not be ignored.

## *2. The Relation Between Good Design and an Understanding of Fabrication Processes*

The path to optimization often includes complex topology, as evidenced by several new parts on the rocket this year, including but not limited to the team's new aluminium 3D printed fill bulkhead. While this offers a number of practical advantages, most noticeably in the areas of mass optimization and simplification of assembly, it also requires more advanced machining techniques. Although we pride ourselves on making as many parts as possible in-house, this year Waterloo Rocketry has also partnered with external sources, such as the Multi-Scale Additive Manufacturing lab, in order to fabricate parts that are not possible to create in a student machine shop. The wide range of machining skill sets now available to the rocketry team, ranging from new students making their first parts to seasoned experts of metal 3D printing, means that a greater emphasis must be placed on the skills of the fabricator available to make the part. This boils down to a simple principle, which we have found to be useful in aspects of life beyond the team: a good designer understands how their part can be made.

## **B. Operational and Managerial Lessons Learned**

### *1. Process Control*

Sometimes, it is necessary for work to be completed under adverse conditions. Doing critical work while being hot and tired in the desert, or sleep-deprived at the test site after a long day, is a good way to make mistakes. The best prevention against these mistakes is a proper procedure. Over the last year, the team has put a lot of work into improving our process control. Procedures are written, reviewed, and tested before their critical use case, and are organized and tracked at a team-wide level. This has led to a noticeable increase in reliability on the team, especially during high-pressure times like static fires. It also helps with future knowledge transfer, in case any in-person training or discussion has managed to slip through the cracks.

## *2. Architectures and High-Level Tracking*

There is a critical threshold in project management where proper structure becomes not only recommended, but entirely necessary. Over the last year or two, Waterloo Rocketry has reached that point. This year, the team has put a big focus on tracking and utilizing architectures and numbering systems in order to maintain information and control during design, fabrication, assembly, and integration of projects. For the most part this takes the form of spreadsheets, such as fabrication trackers, procedure registries, and other such documents. These have made overall management of the team much more efficient, as it is easy to reference and understand the state of things at a moment's notice. There is much less need to ask people for updates, or dig through the team Slack in order to find what information you're looking for. There is a balance to how much overhead should be implemented. It is certainly possible to go too far in the other direction and implement levels of red tape that become obstacles to engineering, but for now the team is not near that point.

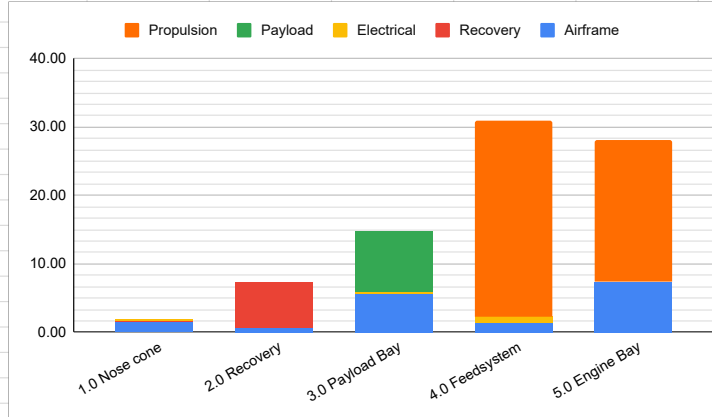
## **Appendix A: System Weights, Measures and Performance Data**

THIS PAGE INTENTIONALLY LEFT BLANK

Section / Component	Mass [Lb]	Mass [Kg]
<b>1.0 Nose cone</b>		
Nosecone Harness	0.03	0.01
Nosecone Tip	0.31	0.14
BigRedBee	0.10	0.05
Nosecone	1.00	0.45
Shear Pin Coupler	0.30	0.14
BigRedBee Mount	0.20	0.09
<b>Overall:</b>	<b>1.94</b>	<b>0.88</b>
<b>2.0 Recovery</b>		
Parachute	2.73	1.24
Rigging	1.07	0.49
Bulkhead + eyebolt	1.40	0.64
Recovery Electrical Sled	1.37	0.62
Parachute bay bodytube	0.49	0.22
Bulkhead Upper Coupler	0.21	0.10
Shear Pin Coupling Ring	0.07	0.03
<b>Overall:</b>	<b>7.34</b>	<b>3.33</b>
<b>3.0 Payload Bay</b>		
Payload Bay Harness	0.11	0.05
Cubesat Payload	8.82	4.00
Cameras	0.23	0.10
Upper Bodytube	4.80	2.18
Payload Adaptor	0.56	0.26
Bulkhead Lower Coupler	0.28	0.13
Bottom Doubling Ring	0.08	0.04
<b>Overall:</b>	<b>14.88</b>	<b>6.75</b>
<b>4.0 Feedsystem</b>		
Feedsystem Harness	0.35	0.16
Vent Bulkhead	1.09	0.49
Vent Valve	0.31	0.14
Vent Section Pneumatics	0.30	0.14
Vent Section Electronics	0.19	0.09
Oxidizer Vent Plumbing	1.18	0.53
Oxidizer Tank Casing	20.58	9.33
Fill Bulkhead	3.02	1.37
High Pressure Plumbing	0.49	0.22
Injector Valve	1.13	0.51
Injector Section Pneumat	0.12	0.05
Injector Section Electroni	0.52	0.24
CC Instrumentation	0.38	0.17
Electrical Disconnect	0.03	0.01
Fill Disconnect Hatch	0.40	0.18
Longerons	0.38	0.17
Fairings	0.49	0.22
<b>Overall:</b>	<b>30.95</b>	<b>14.04</b>
<b>5.0 Engine Bay</b>		
Injector Bulkhead	1.85	0.84
CC Casing	6.16	2.79
CC Contents	9.07	4.12
Nozzle Components	3.62	1.64
Fin Can Body	6.47	2.93
Fin Can Coupler	0.20	0.09
Boattail	0.68	0.31
<b>Overall:</b>	<b>28.05</b>	<b>12.73</b>
<b>Dry Mass (Entire Rocket)</b>		
<b>Overall</b>	<b>83.16</b>	<b>37.72</b>
<b>Wet Mass (Entire Rocket)</b>		
Oxidizer	37.30	16.92
Fuel	5.55	2.52
<b>Overall:</b>	<b>126.01</b>	<b>57.16</b>

Section	Sec. Length [in]	Top plane distance [in]
<b>Nosecone</b>	<b>25</b>	<b>0</b>
<b>Recovery</b>	<b>7.25</b>	<b>25</b>
<b>Payload Bay</b>	<b>34.14</b>	<b>32.25</b>
Recelec	13	-
Payload Adaptor	13.79	-
Vent System	7.35	-
<b>Feedsystem</b>	<b>71.72</b>	<b>66.39</b>
Ox tank	61.92	-
OTAS	9.8	-
<b>Engine Bay</b>	<b>37.8125</b>	<b>138.11</b>
CC	37.8125	-
<b>TOTAL</b>		<b>175.92</b>

Rocket Sections	Airframe	Recovery	Electrical	Payload	Propulsion	Propellant	Rocket Total			
<b>1.0 Nose cone</b>	1.62	0.19	0.13	0.00	0.00		<b>1.94</b>			
<b>2.0 Recovery</b>	0.77	6.57	0.00	0.00	0.00		<b>7.340536</b>			
<b>3.0 Payload Bay</b>	5.72	0.00	0.34	8.82	0.00		<b>14.87806</b>			
<b>4.0 Feedsystem</b>	1.42	0.00	0.94	0.00	28.58	37.30	<b>68.24846031</b>			
<b>5.0 Engine Bay</b>	7.35	0.00	0.00	0.00	20.71	5.55	<b>33.60697</b>			
<b>Total (Lb)</b>	<b>16.88</b>	<b>6.76</b>	<b>1.41</b>	<b>8.82</b>	<b>49.29</b>	<b>42.85</b>	<b>126.0140263</b>			
% of Dry	20.30%	8.13%	1.70%	10.61%	59.27%					
Dry Mass	83.16 Lb									
Dead Mass	74.34 Lb									
Prop. Mass Frac.	34.01 %									
<b>Airframe</b>	<b>Mass (Lb)</b>	<b>% Total System</b>	<b>% Total Dry</b>							
Upper Composites	6.29	37.25%	7.56%							
Lower Composites	8.04	47.63%	9.67%							
Couplers	1.14	6.73%	1.37%							
Tip	0.12	0.71%	0.14%							
Longerons	0.38	2.28%	0.46%							
General Mounts	0.35	2.07%	0.42%							
Payload Adaptor	0.56	3.33%	0.68%							
Total	16.88	100.00%	20.30%							
<b>Propulsion</b>	<b>Mass (Lb)</b>	<b>% Total System</b>	<b>% Total Dry</b>							
OTAS Plumbing	4.75	9.64%	5.71%							
Vent Plumbing	2.88	5.83%	3.46%							
OX Structure	20.58	41.75%	24.75%							
CC Structure	0.00	0.00%	0.00%							
CC Bulkhead	2.23	4.53%	2.68%							
CC Contents	15.23	30.90%	18.32%							
Nozzle Parts	3.62	7.35%	4.36%							
Total	49.29	100.00%	59.27%							
<b>Recovery</b>	<b>Mass (Lb)</b>	<b>% Total System</b>	<b>% Total Dry</b>							
Metallic	0.19	2.81%	0.23%							
Parachute	3.80	56.21%	4.57%							
Electronics Sled	1.37	20.27%	1.65%							
BH Components	1.40	20.71%	1.68%							
Total	6.76	100.00%	8.13%							
<b>Electrical</b>	<b>Mass (Lb)</b>	<b>% Total System</b>	<b>% Total Dry</b>							
Harness	0.52	7.67%	0.62%							
Boards	0.17	2.51%	0.20%							
Camera/Battery	0.23	3.40%	0.28%							
Total	0.92	100.00%	1.10%							



			Apogee (ft)	Lowest Stability prior to apogee OR when it hits 2 stability if constant decrease towards stability at apogee	Stability at Apogee	Highest stability	Max velocity(ft/s)	Avg Apogee for all of shape		
Shape four fins tail stabilizer shape	1. Expected mass and length cycle 3.0	a) expected wind and pressure	29556	1.77	2.48	5.09	1561	30059.25	Cases B and C are run with 70F and 1000 mbar	
		B) 15mph wind with 85th worse percentile pressure and temp for stability	29369	1.5 (launch)	2.92	5.09	1559			
		C) 0mph wind with 85th worse percentile pressure and temp for stability	29961	2 @ 2.25s before apogee	0.34	5.11	1560		Cases A, B, C are run with regular paint finish	
		D) Improved Surface Finish with Expected pressure and temp	31635	2.01 (launch)	2.75	5.08	1592			Case D is run with smooth paint finish
	2. Max mass cycle 3.0	a) expected wind and pressure	28914	2.2 (launch)	2.86	5.28	1518			
		B) 15mph wind with 85th worse percentile pressure and temp for stability	28627	1.24 (launch)	3.92	5.33	1515			
		C) 0mph wind with 85th worse percentile pressure and temp for stability	29282	1.98 @ 1.95s before apogee	0.71	5.33	1517			
		D) Improved Surface Finish with Expected pressure and temp	30897	2.32 (launch)	2.8	5.33	1547			
	3. Min mass cycle 3.0	a) expected wind and pressure	29997	2.01 (launch)	2.06	4.89	1588			
		B) 15mph wind with 85th worse percentile pressure and temp for stability	29792	1.34 (launch)	2.22	4.88	1585			
		C) 0mph wind with 85th worse percentile pressure and temp for stability	30362	2.02 @ 2.6s before apogee	0.025	4.89	1587			
		D) Improved Surface Finish with Expected pressure and temp	32153	2.13 (launch)	2.37	4.89	1621			
4. Min mass Nosecone/ Recovery/Payload , max mass feed/engine	4. Min mass Nosecone/ Recovery/Payload , max mass feed/engine	a) expected wind and pressure	29550	1.87 (launch)	2	4.83	1557			
		B) 15mph wind with 85th worse percentile pressure and temp for stability	29353	1.25 (launch)	2.91	4.87	1555			
		C) 0mph wind with 85th worse percentile pressure and temp for stability	29905	1.99 @ 2.6s before apogee	0	4.88	1556			
		D) Improved Surface Finish with Expected pressure and temp	31595	2.06 (launch)	2.6	4.85	1587			

			Average Apogee (ft)	Max velocity(ft/s)	AVG Apogee for all of shape		
Monte Carlo Simulation Results	1. Expected mass and length cycle 3.0	a) Averaged wind and pressure	29560.37598	1557.742782	30510.06312		Methodology: Monte Carlo Approach eliminates uncertainties from the launch condition by approximating environment variables by repeated random sampling.
		D) Improved Surface Finish with Expected pressure and temp	31643.57972	1587.69685			In our implementation, we randomized the Temperature, Pressure and Wind (Speed and Direction) by applying Gaussian Distributions based off of local historical data to approximate the actual values.
		a) Averaged wind and pressure	28918.98524	1515.006234			We reran each of the different rocket models for each cases 100 times with randomly generated environment values each (from their respective Gaussian Distributions).
		D) Improved Surface Finish with Expected pressure and temp	30823.47736	1543.298885			We generate input from the Gaussian Distributions in our in-house Python plugin and use each instance as input to each OpenRocket run. We then collect the full run log from OpenRocket and conduct post-processing to gain insights.
		a) Averaged wind and pressure	29943.91043	1584.908793			For each of the averaged data, we simply take the mean across all runs of the same case and display them in the sheet. This gives us a good expected value as an aggregated across all different possible scenarios.
	2. Max mass cycle 3.0	D) Improved Surface Finish with Expected pressure and temp	32111.62369	1617.66601			For maximum/minimum cases, we want to gain insights on the specific conditions at which the worst/best case occurs in. We take the maximum/minimum value from the best/worst run. Further insights and analyses can then be conducted.
		a) Averaged wind and pressure	29548.45046	1553.907152			Launch Environment Data Randomization:
	4. Min mass Nosecone/Recovered/Payload, max mass feed/engine	D) Improved Surface Finish with Expected pressure and temp	31530.10203	1583.190617			The data below are weather data collected at Truth and Consequences, NM at valid launch times over the past 6 years on the same days as the launch window of IREC 2023. We use them to generate the Gaussian Distributions.
							6AM to 5PM      Temperature(F)      PRESSURE(mbar)      Windspeed(mph) MEAN      88.2344444      1008.05376      8.448888889 STDDEV      10.51093975      3.938207212      4.45098329

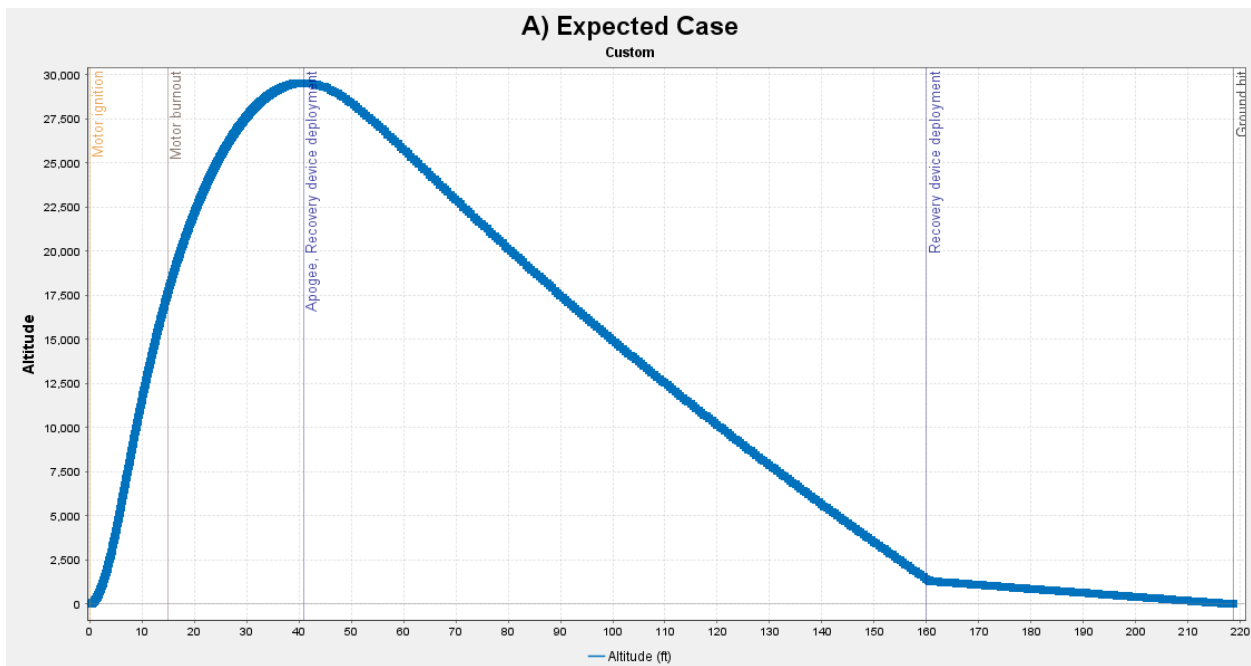


**Fig. 122** Altitude vs. Time

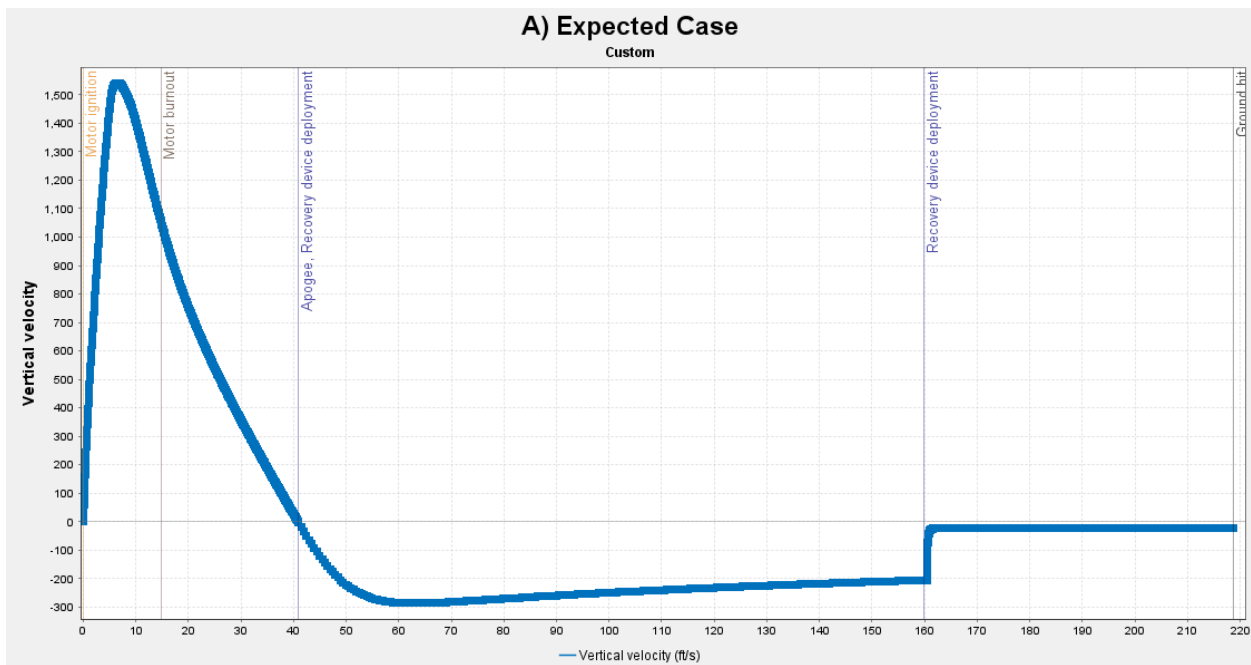


**Fig. 123** Vertical Velocity vs. Time

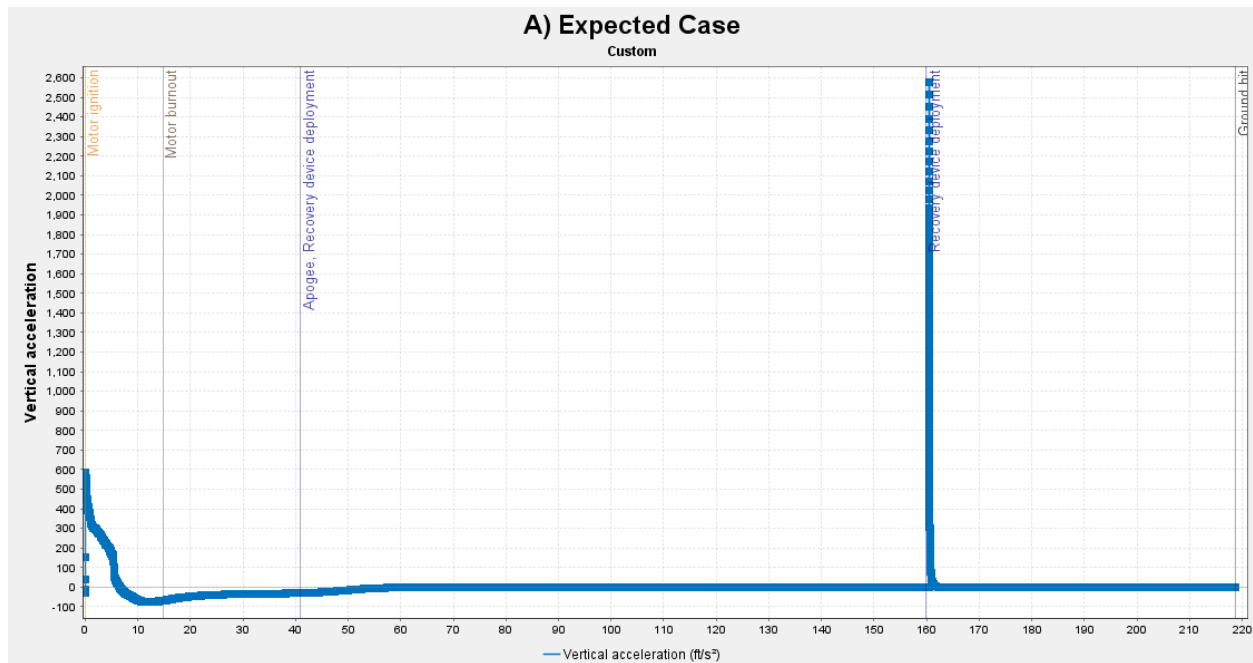


**Fig. 124** Vertical Acceleration vs. Time

## Appendix B: Calculations

### C. Loads Analysis Inputs

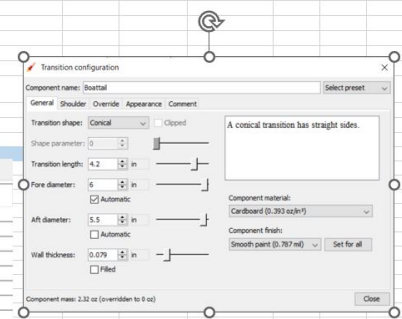
The following are images of the parameters that were input into the BENDIT7 spreadsheet in order to calculate the loads on the rocket.

Loadcases	Unit	CONVERT TO	notes	BENDIT FORMATTED, copy/paste these rows into the spreadsheet paste values only
Bendit inputs, unformatted				
Takeoff	MaxQ			
Altitude, ft AGL	0.30083	5925.8 ft		
Launch Altitude, ft	4848	4848 ft		
Launcher Length, ft	260	260 in	Rt	
Mach Number	0.021088	1.5223		
Flight Speed, fps	18.379	1688.3 fps		
q, Dynamic pressure, lb/ft <sup>2</sup>	0.381807314	2761.894817	lb/ft <sup>2</sup>	
Sref, Aerodynamic Reference area,	28.274	28.274 in <sup>2</sup>	Rt <sup>2</sup>	
Reference Length, Max Body Diameter, in	6	6 in		
Pr (no failure)	0.99	629.98		
Axial Acceleration, ft/sec <sup>2</sup>	629.98	38.331 ft/sec <sup>2</sup>		
Thrust, lbf	2457.386557	467.962796	lb	
3 w/ G, Lateral Offset	0.07	0.07 in	Rt	
3 w/ G, Longitudinal alignment angle, rad	0.07	0.07 deg	rad	
Body Station of Nozzle Throat, in	172.567	172.567	in	
Element where the thrust is applied	12	12		
Analysis Condition Right after Ignition?	TRUE	FALSE		
Element moment of inertia, in <sup>2</sup>	0.140800615	0.140800615 in ft <sup>2</sup>		
C. Nose Shell Modulus of Elasticity, psi	250416356.5	250416356.5		
Element to use as base for nose aerelastic effect	2	2		
Nose Steric Aerelastic Effect?	FALSE	FALSE		
No. nodes per panel	4	4		
1g gust amplitude, fps	29.3314	45.56722076		** In the AoA bypass, this effectively is "what is the wind gust at the simulation case"
Gust longitudinal autocorrelation Length, h	1000	1000		
Other inputs that are used in formulas to compute bendit inputs				
Parameter	value	unit		
Distance, nozzle throat to end of rock	3.353	in		
takeoff wind speed	20	mph		
max wind speed	50	kmh		

Fig. 125 Flight Data Input

Cycle 2 input format *** NOTE THIS IS NOT 100% CORRECT, NOT FINLESS, EXTERNAL RADIUS TO BE DOUBLE CHECKED***					Formatting for Results Graphs
Structural Sections	Top station	Section Mass - Finless	Prop mass	Prop Mass	
	Section Length (STA)		Takeoff	MaxQ	Part Aft Position
Nosecone	25	0	2.071		Nosecone 25 0
Recovery	7.25	25	9.1		Recovery 32.25 0
Releas	13	32.25	3.050896309		Vent System 66.59 0
Payload Adaptor	13.79	45.25	10.73448155		Ox tank 5 128.31 0
Vent System	7.35	59.04	4.330022144		OTAS 138.11 0
Ox tank 1	12	66.39	6.025499122	6.44746	Fin Root (CC3), 169.92 0
Ox tank 2	12	78.39	4.075499122	7.22697	Boattail (CC4) 175.92 0
Ox tank 3	12	90.39	4.075499122	7.22697	
Ox tank 4	12	102.39	4.075499122	7.22697	
Ox tank 5	13.92	114.39	4.728003513	8.38329 4.07661	
OTAS	9.8	128.31	10.0933		
CC 1	12	138.11	7.533110993	2.745 0.555	
CC 2	7.8125	150.11	3.529798823	2.745 0.555	
Fin Root (CC3), finless	12	157.92	7.2217155		
Boattail (CC4)	6	169.92	8.73		
<b>TOTAL</b>	<b>175.92375</b>	<b>175.92</b>	<b>89.975</b>		
OPENROCKET ROCKET ANALYSIS DATA					
Stability	Drag characteristics	Roll dynamics			
Component	CG / in	Mass / oz	CP / in	$C_{No}$	
1.0 Nosecone	15.25	33.8	10.938	2	
2.0 Recovery	29.81	127	28.625	0	
3.0 Payload Bay	51.5	197	48.32	0	
4.0 Feedsystem	101	469	100	0	
5.0 Engine Bay	158	367	153	0	
Trapezoidal fin set	165	50	163	7.42	
Boattail	84.86	0	172	-0.319	
<b>Total</b>	<b>103</b>	<b>1918</b>	<b>129</b>	<b>9.1</b>	

Fig. 126 Body Profile Data Input(1)



BENDIT7 Input Format, note: input element CN, body radius, nosecone Xcp manually into these charts							MAXQ CASE						
TAKEOFF CASE							MAXQ CASE						
Element Counter	Element Contents	xi, Element aft face body station, inches from nose tip	Ri, Element body external radius at body station xi, in	wi, Element weight (finless), lb	Element CNoi (finless), per radian	Element Xcp, (finless) from element front, in	Element Counter	Element Contents	xi, Element aft face body station, inches from nose tip	Ri, Element body external radius at body station xi, in	wi, Element weight (finless), lb	Element CNoi (finless), per radian	Element Xcp, (finless) from element front, in
0	0	0	0				0	0	0				
1	Nosecone	25	3	2.671	2	10.938	1	Nosecone	25	3	2.671	2	10.938
2	Recovery	32.25	3	9.1	0	3.625	2	Recovery	32.25	3	9.1	0	3.625
3	Reelec	45.25	3	3.0509	0	6.5	3	Reelec	45.25	3	3.0509	0	6.5
4	Payload Adaptor	59.04	3	10.7345	0	6.895	4	Payload Adaptor	59.04	3	10.7345	0	6.895
5	Vent System	66.39	3	4.33002	0	3.675	5	Vent System	66.39	3	4.33002	0	3.675
6	Ox tank 1	78.39	3	12.473	0	6	6	Ox tank 1	78.39	3	6.0255	0	6
7	Ox tank 2	90.39	3	11.3025	0	6	7	Ox tank 2	90.39	3	4.0755	0	6
8	Ox tank 3	102.39	3	11.3025	0	6	8	Ox tank 3	102.39	3	4.0755	0	6
9	Ox tank 4	114.39	3	11.3025	0	6	9	Ox tank 4	114.39	3	4.0755	0	6
10	Ox tank 5	128.31	3	13.1113	0	6.96	10	Ox tank 5	128.31	3	8.80461	0	6.96
11	OTAS	138.11	3	10.0933	0	4.9	11	OTAS	138.11	3	10.0933	0	4.9
12	CC 1	150.11	3	10.2781	0	6	12	CC 1	150.11	3	8.08811	0	6
13	CC 2	157.9225	3	6.2748	0	3.90625	13	CC 2	157.9225	3	4.0848	0	3.90625
14	Fin Root (CC3), finless	169.92	3	7.22172	0	6	14	Fin Root (CC3), finless	169.92	3	7.22172	0	6
15	Boattail (CC4)	175.92	2.75	8.73	-0.319	2	15	Boattail (CC4)	175.92	2.75	8.73	-0.319	2

Fig. 127 Body Profile Data Input (2)

The screenshot shows the BENDIT7 software interface. On the left, there is a configuration panel for a 'Trapezoidal fin set' with various input fields for fin parameters like rotation, cant, chord, height, sweep length, and position relative to the parent component. It also shows the component mass as 49.9 oz. On the right, there is a detailed data table for 'First Stage Fin Data' and other related calculations. The data table includes columns for Fin spar attachment element, C<sub>r</sub> root chord, C<sub>r</sub> tip chord, B exposed semispans, r<sub>LE</sub> sweep, 1<sub>r</sub> δ (fin), and Number of elements along the fin span. Below the table, there are notes about inputs from a Supersonic Barrowman spreadsheet and design log notes. At the bottom, there is a stability and drag characteristics table for the vehicle components.

First Stage Fin Data						
Fin spar attachment element	C <sub>r</sub> root chord, in	C <sub>r</sub> tip chord, in	B exposed semispans, in	r <sub>LE</sub> sweep, deg	1 <sub>r</sub> δ (fin), rad	Number of elements along the fin span
14	12	5.25	5.37	60.5	0.001745329	50
Fin panel weight, lb	Root Chord LE Body Station, in, xF	Fin α and δ Center of Pressure Body Station, in	Fin Alone Airfoil C <sub>No</sub> , per rad	Single Panel C <sub>No</sub> , rad <sup>-1</sup>	Total Tail Assembly C <sub>No</sub> (with Vortex Interference (only 2 stage)), rad <sup>-1</sup>	Fin ass'y Xcp, from the root chord LE, in
0.78	156.67	162.8394	14.6176	3.4158	7.42	
Tail Assembly α and δ Center of Pressure, in	Single Panel C <sub>No</sub> , rad <sup>-1</sup>	Wing Alone C <sub>No</sub> (based on Swing), rad <sup>-1</sup>	N/r, Fin Center of Pressure, Fraction of Root Chord, off Fin Apex, Eq. (14)	Body-Fin LIR Interference, Eq. (14)	Naked (single panel) Fin Ass'y C <sub>No</sub> (based on Sref), rad <sup>-1</sup>	
17	162.8394	3.4158	2.230867765	0.527573575	1.3086	14.6176

Fig. 128 Fin Data Input

## D. Aerostructures Calculations

Please note that some of the values are not accurate based on the numbers given in these calculations and the given formulas. This is because the value inputted are rounded from the true values so using values contained in these tables to calculate other values will result in the propagation of roundoff error.

### 1. Bodytube Safety Factor

This section contains a sample calculation for safety factor calculation for body station 32.3 (32.3 inches aft of the nosecone tip), which is in the parachute bay, at MaxQ. Many calculations were performed to analyze bodytube safety factors at key points on the bodytube, and at both takeoff and MaxQ, however all the calculations follow the same steps with minimal variations so only one is shown here to demonstrate the methodology. One global conservative assumption used in all calculations is that there are no vent holes in any bodytube. For the calculations, this implies that all the bodytubes are now pressure vessels where the gauge pressure inside the bodytubes is assumed to be equal to the difference between ground level and 30,000 feet. The input parameters are given in Table 13, and the safety factor is calculated in Table 14.

**Table 13 Bodytube Load Parameters at STA 32.3**

Parameter	Value	Unit	Source
Outer Radius ( $r_o$ )	3	in	
Inner Radius ( $r_i$ )	2.946	in	
Compressive Strength	12328.2 (85)	psi (MPa)	see Figure 32
Spaceport America Elevation	4595	ft	[12]
MaxQ Axial Loads at STA 32.3 ( $F_{axial}$ )	-56	lbf	Loads Analysis
MaxQ Shear Loads at STA 32.3 ( $F_{shear}$ )	25.7	lbf	Loads Analysis
MaxQ Bending Loads at STA 32.3 ( $F_{bend}$ )	608.1	lb-in	Loads Analysis

**Table 14 STA 32.3 Bodytube Analysis**

Parameter	Value	Unit	Equation
Area (A)	1.0087	in <sup>2</sup>	$\pi * r_o^2 * r_i^2$
Second Moment of Area (I)	4.458	in <sup>4</sup>	$\frac{\pi * r_o^4 * r_i^4}{4}$
Axial Stress ( $\sigma_{axial}$ )	-55.5	psi	$\frac{F_{axial}}{A}$
Shear Stress ( $\sigma_{shear}$ )	51.0	psi	$\frac{2F_{shear}}{A}$
Bending Stress ( $\sigma_{bend}$ )	409.2	psi	$\frac{F_{bend} * r_o}{I}$
Total Normal Stress ( $\sigma_{normal}^{total}$ )	353.68	psi	$-\sigma_{axial} + \sigma_{bend}$
Pressure at Ground Level	12.414 (85593)	psi (Pa)	$101325 * ((1 - (2.25577 * (10^{-5})) * AltitudeASL)^{5.25588})$ [13]
Pressure at 30,000 ft above ground level	3.525 (24305.4)	psi (Pa)	$101325 * ((1 - (2.25577 * (10^{-5})) * AltitudeASL)^{5.25588})$ [13]
Gauge Pressure at 30,000 ft	8.889	psi	Pressure at 30,000 ft - Pressure at ground
Hoop Stress ( $\sigma_{hoop}$ )	493.8	psi	$\frac{Gauge\ Pressure * r_o}{r_o - r_i}$
Longitudinal Stress ( $\sigma_{long}$ )	246.9	psi	$\frac{\sigma_{hoop}}{2}$
Sigma 1	600.6	psi	$\sigma_{normal}^{total} + \sigma_{long}$
Sigma 2	493.8	psi	$\sigma_{hoop}$
Tau	51.0	psi	$\sigma_{shear}$
Von Mises Stress	561.95	psi	$\sqrt{\frac{(\sigma_1 - \sigma_2) + (\sigma_2 - \sigma_3) + (\sigma_3 - \sigma_1) + 6(\tau_{12}^2 + \tau_{23}^2 + \tau_{13}^2)}{2}}$
Safety Factor	21.9		$\frac{\sigma_{compressivestrength}}{\sigma_{VonMises}}$

## 2. Payload Bay

### Bolt Failure

The clamping plate uses 4 x 6-32 bolts to prevent the payload from moving upward during descent. Table 15 below shows the properties of the specific 6-32 bolt used in the payload bay. Note that the shear stress is calculated from the tensile stress by dividing by  $\sqrt{3}$  as per the Von Mises criterion.

**Table 15 Payload Bay Bolt Parameters**

Parameter	Value	Unit	Source
Major Diameter	0.138	in	[14]
Minor Diameter	0.104	in	[14]
Threads Per Inch (TPI)	32		
Length	0.75	in	
Tensile Strength	170,000	psi	[4]
Shear Strength	98150	psi	$\frac{\text{TensileStrength}}{\sqrt{3}}$

The next table 16 details how the loads on the clamping plate, and thus the bolts, were calculated. The clamping plate is located at bodytube station 45.3 which corresponds to 45.3 inches from the nosecone tip. The MaxQ shear loads were added on top to give a more conservative answer.

**Table 16 Payload Bay Bolt Loads**

Parameter	Value	Unit	Source
CubeSat Mass	8.8	lbm	Payload Team
Acceleration	20	g's	Loads Analysis
Tensile Force from CubeSat	176	lbf	$F = ma$
Shear Force at STA 45.3 (MaxQ)	24.2	lbf	Loads Analysis

The safety factors for bolt failure were based on the calculation of the Von Mises stress in a rod. The bolt was approximated as a rod with a diameter equal to its minor diameter. One conservative assumption made during the calculations is that the full load, without bending, is taken up by a single screw. If a single screw will not fail, then 4 screws will not fail.

**Table 17 Payload Bay Bolt Failure Calculations**

Parameter	Value	Unit	Equation
Area	0.0085	in <sup>2</sup>	$\frac{\pi}{4} * d_{major}^2$
Tensile Stress	20769	psi	$\frac{F_{tensile}^{CubeSat}}{Area}$
Shear Stress	3798	psi	$\frac{4*(F_{shear}^{CubeSat})}{3*Area}$
Von Mises Stress	21786	psi	$\sqrt{\frac{(\sigma_{XX}-\sigma_{YY})+(\sigma_{YY}-\sigma_{ZZ})+(\sigma_{ZZ}-\sigma_{XX})+6(\tau_{XY}^2+\tau_{YZ}^2+\tau_{XZ}^2)}{2}}$
Safety Factor (Tension)	8.1		$\frac{\sigma_{tensile}^{bolt}}{\sigma_{tensile}}$
Safety Factor (Shear)	25.8		$\frac{\sigma_{shear}^{bolt}}{\sigma_{shear}}$
Safety Factor (Von Mises)	7.8		$\frac{\sigma_{tensile}^{bolt}}{\sigma_{VM}}$

### Shear Ring Failure

The shear ring uses West Systems 105 epoxy resin and 206 hardener to bond it to the outer airframe. It also contains the camera holes, which cause a stress concentration in the material.

**Table 18 Shear Ring Parameters**

Parameter	Value	Unit	Source
Tensile Strength	7300	psi	[15]
Shear Strength	4215	psi	$\frac{TensileStrength}{\sqrt{3}}$
Outer Diameter (OD)	5.9	in	
Height	2.625	in	
Payload Bay Total Mass	3.6 lbm		
Payload Mass	8.8	lbm	Payload Team
Total Mass	12.2	lbm	
Acceleration	20	g's	Loads Analysis
Stress Concentration Factor for Holes	3		[16]

When calculating the safety factor, it was conservatively assumed that the entire mass of the payload bay and payload were acting on the shear ring. Failure occurs when the epoxy bonding the shear ring to the bodytube fails. The results are shown in Table 19 below.

**Table 19 Shear Ring Failure Calculations**

Parameter	Value	Unit	Equation
Epoxy Contact Area	48.7	in <sup>2</sup>	$\pi * OD * Height$
Shear Force on Shear Ring	244	lbf	$F_{shear} = m_{total} * a_{rocket}$
Shear Stress	30.1	psi	$(\frac{2(F_{shear})}{Area}) * StressConcentrationFactor$
Safety Factor	137.6		$\frac{\sigma_{shearStrength}}{F_{shear}}$

### Internal Thread Shear

Internal thread shear occurs when the threads tapped into the grip material fail in shear. The analysis for internal thread shear is found in [17]. In this case, the threads of the tapped hole are made of aluminum 6061-T6.[5] The bolt is the same 6-32 used in Table 15.

**Table 20 Internal Thread Shear**

Parameter	Value	Unit	Equation
Thread Engagement Length ( $L_e$ )	0.125	in	
Internal Pitch Diameter ( $d_{p,int}$ )	0.1177	in	$d_{major} * 0.64951905/TPI$
Internal Thread Shear Area ( $A_{int,ts}$ )	0.0347	in <sup>2</sup>	$0.75 * \pi * d_{p,int} * L_e$
Tensile Force	176	psi	see Table 16
Shear Stress	5089	psi	$\frac{TensileForce}{A_{int,ts}}$
Tensile Strength of Plate	40000	psi	
Estimates Shear Strength of Plate	23094	psi	$\frac{TensileStrength}{\sqrt{3}}$
Safety Factor	4.5		$\frac{\sigma_{ShearStrength}}{\sigma_{ShearStress}}$

### Bolt Tear-Out

Bolt tear-out occurs when the bolt tears through the material between it and the edge of the part. The shear force on the plate used in the calculations is the shear at body station 45.3 (45.3 inches aft of the nosecone tip) at MaxQ since this is the highest shear force seen by the plate during flight. The plate is made of aluminum 6061-T6. [5]

**Table 21 Bolt Tear Out**

Parameter	Value	Unit	Equation
Plate Thickness (t)	0.25	in	
Length of Material Between Hole and Edge (l)	0.1	in	
Shear Out Area ( $A_{ShearOut}$ )	0.025	$in^2$	$t * l$
Shear Force on Plate ( $F_{Shear}$ )	24.2	lbf	
Shear Stress	968	psi	$\frac{F_{Shear}}{A_{ShearOut}}$
Shear Strength of Plate	30000	psi	
Safety Factor	30.9		$\frac{\sigma_{ShearStrength}}{\sigma_{ShearStress}}$

### Minimum Thread Engagement

To find the minimum thickness of plate that was needed for the clamping bolt holes, the minimum thread engagement length was calculated. Bolt parameters can be found in Table 15 and [4], and the plate material is aluminum 6061-T6. [5].

**Table 22 Minimum Thread Engagement**

Parameter	Value	Unit	Equation
Tensile Stress Area ( $A_t$ )	0.009	$in^2$	$\frac{\pi}{4}(d_{major} - \frac{0.9743}{TPI})^2$
Thread Pitch (P)	0.03125	in/thread	$\frac{1}{TPI}$
Minimum Thread Engagement Length ( $L_e$ )	0.098	in	$\frac{2A_t}{0.5*\pi*(d_{major} - 0.64952*P)}$
Thread Engagement Ratio (J)	4.5		$\frac{BoltTensileStrength}{PlateTensileStrength}$
Thread Engagement Length ( $L_{e2}$ )	0.418	in	$J * L_e$

### 3. Oxidizer Tank Aft Skirt

This section provides a summary of the failure modes which were analyzed for the oxidizer tank aft skirt and their respective factors of safety. A brief overview of the methods used to reach these values is also included. A summary of the load parameters for the the oxidizer tank aft skirt, STA 128.3, are presented in Table 23.

**Table 23 STA 128.3 Load Parameters**

Flight Regime	Axial Load (lbf)	Bending Load (lb-in)	Shear Load (lbf)	Source
Takeoff	-3261.8	12.9	0.2	Loads Analysis
Max Q	-271.1	1317.9	20.9	Loads Analysis
Main Deploy	349.4	Negligible *	Negligible *	Loads Analysis

The cross section chosen was a capped I beam shape. This was chosen for a high ratio of radius of gyration to cross-sectional area which gives good buckling resistance. The geometrical parameters of this cross section are provided in Table 24. A picture of the cross section is shown in Figure 129.

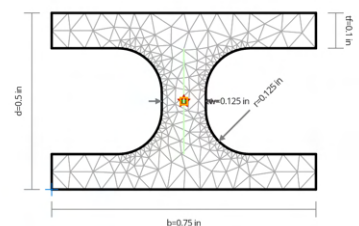
**Table 24 STA 128.3 Calculation Parameters**

Symbol	Value	Description	Units
$\alpha$	$23.6 * 10^{-6}$	Coefficient of thermal expansion for 7075	$\frac{1}{^{\circ}C}$
$A$	0.201	Cross-sectional area of a longeron	in
$A_1$	0.019	Cross-sectional area of a #10-32 bolt	in
$D$	0.19	Major diameter of a #10-32 bolt	in
$G$	3,900,000	Shear modulus of elasticity of 7075	psi
$J$	0.001305	Torsional constant	$in^4$
$k_3$	0.181	Least radius of gyration of a longeron	in
$l$	6.3	Length of a longeron	in
$L_1$	3	Number of longerons	N/A
$L_2$	0.1875	Longeron threaded length	in
$M_1$	12.9	Moment applied at the OTAS at takeoff	in-lb
$M_2$	0.00661	Moment of inertia about x axis (tangent to fairing)	$in^4$
$M_3$	0.00720	Moment of inertia about y axis (passes through rocket center)	$in^4$

\*Note this is an assumption made by considering that the rocket will be almost entirely vertical during main deploy due to the reefed parachute straightening the rocket during the majority of the decent.

$P_1$	1087.3	Axial load at takeoff per longeron	lb
$P_8$	349.4	Tensile load at recovery total	lb
$R$	2.7189	Radial distance from rocket center to longeron centroid	in
$S$	73,000	Yield strength of 7075	psi
$T$	58	Anticipated temperature drop in the feedsystem	°C
$U$	0.000218	Warping constant	$in^6$
$V$	1	Column end condition. 1 signifies pinned ends	
$Y$	10,400,000	Young's Modulus for 7075	psi

⊕ Origin ● Centroid — 11-Axis ⚪ Shear Centre □ Plastic Cent.



> Cross-Section Type	I-Section
> Depth	$d = 0.5$ in
> Breadth	$b = 0.75$ in
> Flange Thickness	$t_f = 0.1$ in
> Web Thickness	$t_w = 0.125$ in
> Inner Radius	$r = 0.125$ in

**Fig. 129 Longeron cross section**

Table 25 includes all of the calculated values at takeoff. The same analysis was completed at Max Q. Takeoff was found to be the limiting case.

**Table 25 STA 128.3 Analysis**

Parameter	Value	Unit	Equation
Compressive Load due to Bending	3.16	lbf	$P_2 = \frac{2M_1}{RL_1}$
Compressive Load due to Feedsystem Thermal Contraction	1655.8	lbf	$\frac{P_3 l}{3AY} = \alpha Tl - \frac{P_3}{k_5}$
Total Axial Load	2744.64	lbf	$P_4 = P_1 + P_2 + P_3$
Limiting Slenderness Ratio	53.0		$\frac{l}{k_3} = \sqrt{\frac{2\pi^2 VY}{S}}$
Slenderness Ratio	34.8		$\frac{l}{k_3} = 34.8$
Johnson Buckling Load	57275.5	lbf	$\sigma_1 = S - \left(\frac{IS}{2\pi k_3}\right)^2 \frac{1}{VY}$
Eccentric Euler Buckling Load	5615.71	lbf	$\sigma_{max} = \frac{P_6}{A} \left(1 + \sec\left(\sqrt{\frac{P_6}{YA}} \frac{l}{2k_3}\right)\right)$
Torsional Buckling Stress	374061	psi	$F_4 = \frac{GJ + \frac{\pi^2 YU}{l^2}}{M_2 + M_3}$
Max Tensile Stress	1738.31	psi	$\sigma_2 = \frac{P_8}{A}$
Max Compressive Stress	13654.93	psi	$\sigma_3 = \frac{P_4}{A}$
Shear Stress for Longeron Thread Shear Out	521.21	psi	$\sigma_2 = \frac{\frac{P_8}{6}}{\pi D L_2}$

As a result of these values, the FOS for each method of failure can be calculated. These are summarized in Table 26.

**Table 26 STA 128.3 FOS**

Parameter	FOS
Johnson Buckling	20.87
Eccentric Euler Buckling	2.05
Torsional Buckling	27.39
Tensile Failure	41.99
Compressive Failure	5.35
Thread Shear Out	57.56
Buckling Simulation	1.72

## E. CO<sub>2</sub> Pressurization

The pressurization calculations are performed using the ideal gas law and pressure formula. Table 27 presents the required parameters determined using known variables. The ideal gas law is used under the assumption that air and

carbon dioxide are the only gases present.

**Table 27 CO<sub>2</sub> Pressurization**

Parameter	Value	Unit	Equation
Target Pressure Difference (T)	79008	Pa	$\frac{F}{Area}$
CO <sub>2</sub> Mass (m)	18.5432	g	$\frac{P*V*M}{R*T}$

## **Appendix C: Project Test Reports**

THIS PAGE INTENTIONALLY LEFT BLANK

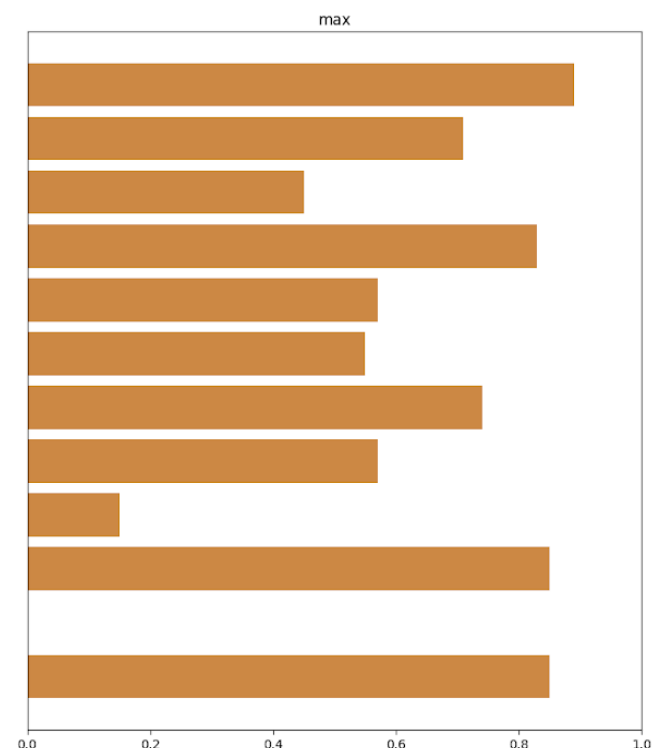
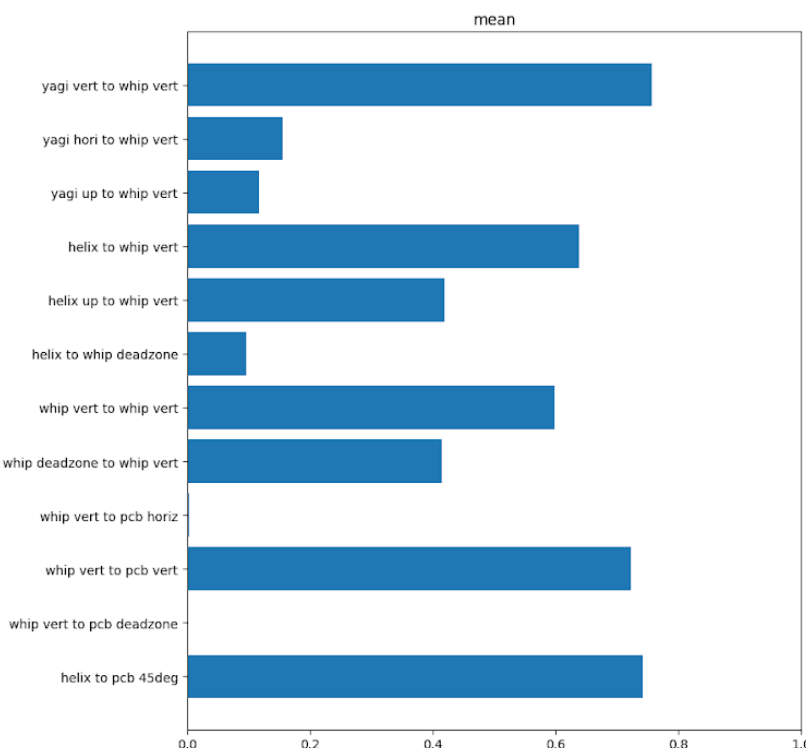
<b>Test</b>	Radio Antennae Test
<b>Project</b>	Live Telemetry / Radio Redesign
<b>System</b>	Electrical
<b>Location</b>	Laurel Creek Reserve
<b>Date</b>	2023-02-05
<b>Description</b>	Record and compare the received signal strength of different antenna orientations and combinations.
<b>Purpose</b>	Decide on which set of antenna will be used during comp
<b>Personnel</b>	<ul style="list-style-type: none"> <li>• Rio Liu</li> <li>• Jack Christensen</li> <li>• Davis Liu</li> </ul>

<b>Requirements</b>	Outdoor weather, no approval required
<b>Materials and Equipment</b>	Live telemetry transmitter, laptops, FTDI cables, coax cables, helical antenna, yaggi antenna, whip antenna, PCB antenna
<b>PPE Required</b>	Clothing suitable for staying outdoors
<b>Procedure</b>	<a href="https://docs.google.com/document/d/1GBqLUC8O-0OCZx5nKChhHoYIWZTQdyskBkcopFUsf8/edit?usp=sharing">https://docs.google.com/document/d/1GBqLUC8O-0OCZx5nKChhHoYIWZTQdyskBkcopFUsf8/edit?usp=sharing</a>
<b>Deviations</b>	<ul style="list-style-type: none"> <li>• Patch antenna was skipped due to incompatible connector</li> <li>• PCB - Helix configuration were tested additionally</li> <li>• We kinda went with whatever orientations we could think of during testing, and did not follow test plan exactly on this part</li> </ul>
<b>Results</b>	<ul style="list-style-type: none"> <li>• Yagi is the best for directional antenna</li> <li>• PCB (surprisingly) is the best for unidirectional antenna           <ul style="list-style-type: none"> <li>◦ But it is the most sensitive to polarization and deadzone</li> </ul> </li> <li>• Aligned helical antenna is similar to whip           <ul style="list-style-type: none"> <li>◦ But helical antenna works for both polarizations</li> </ul> </li> <li>• Somehow whip antenna is OK in deadzone and mismatched polarization</li> </ul>
<b>Conclusions</b>	



## TEST REPORT - Antennae Test

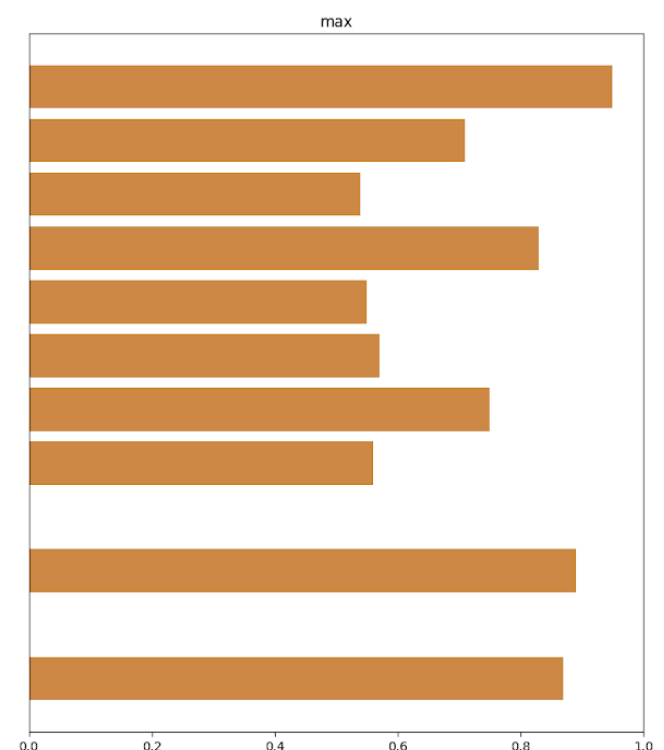
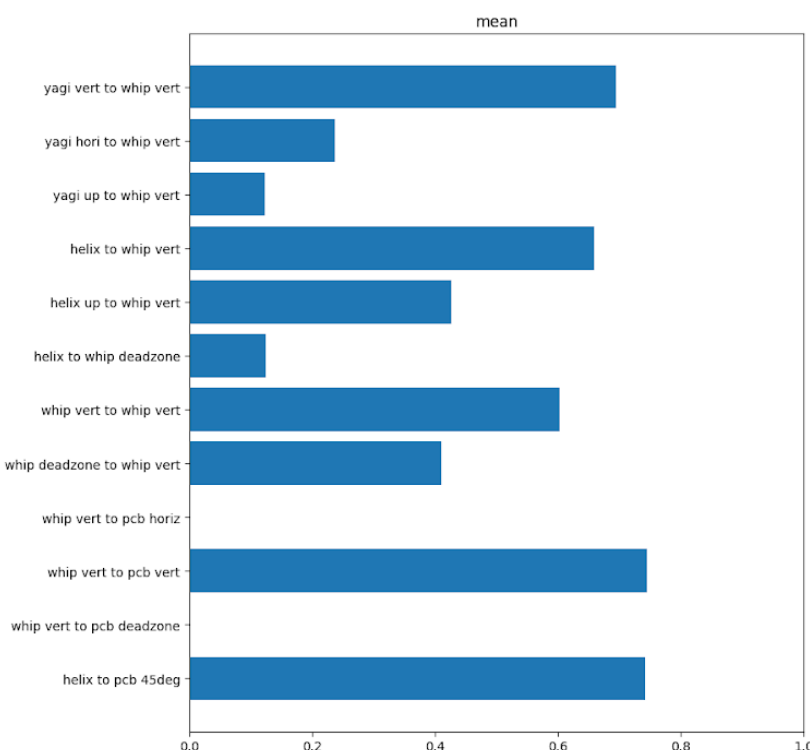
Local 1 RSSI





## TEST REPORT - Antennae Test

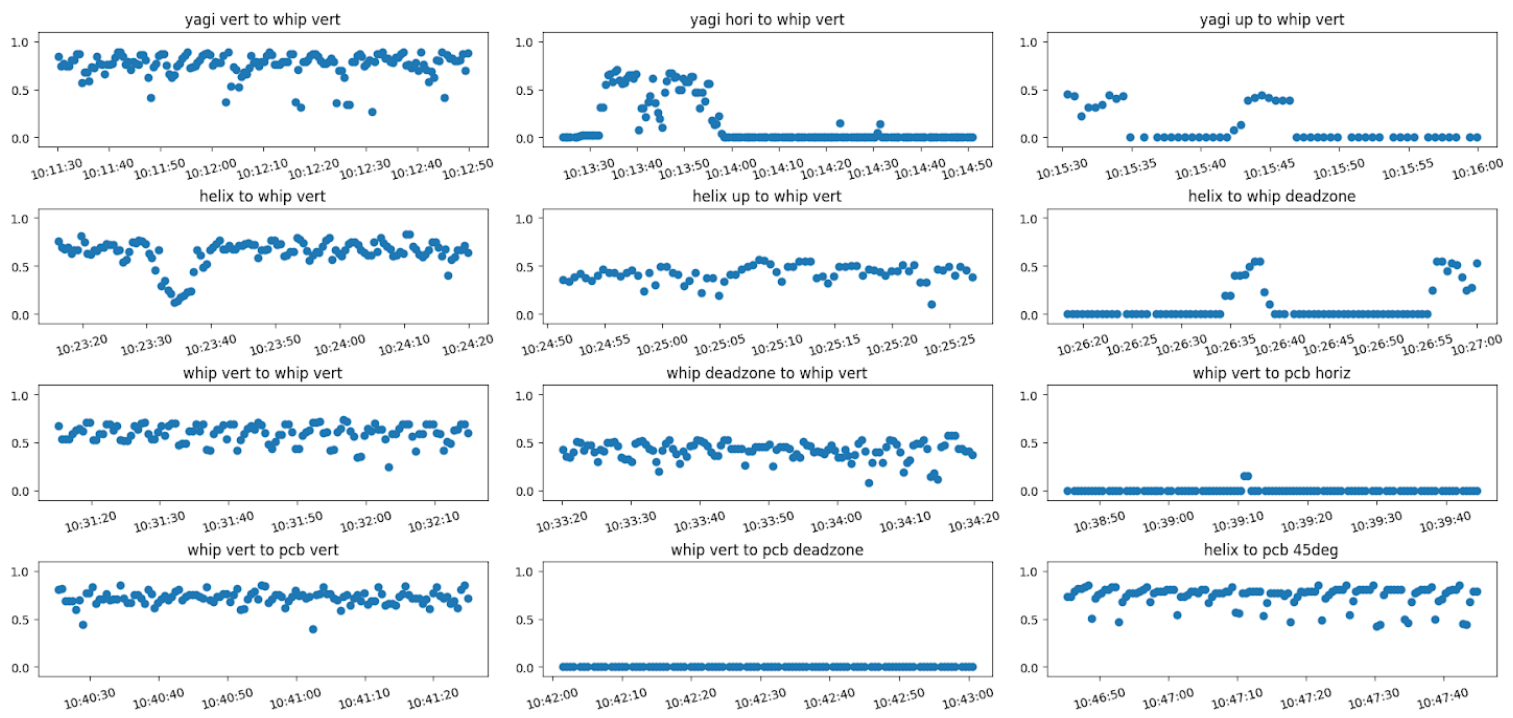
Remote 1 RSSI





## TEST REPORT - Antennae Test

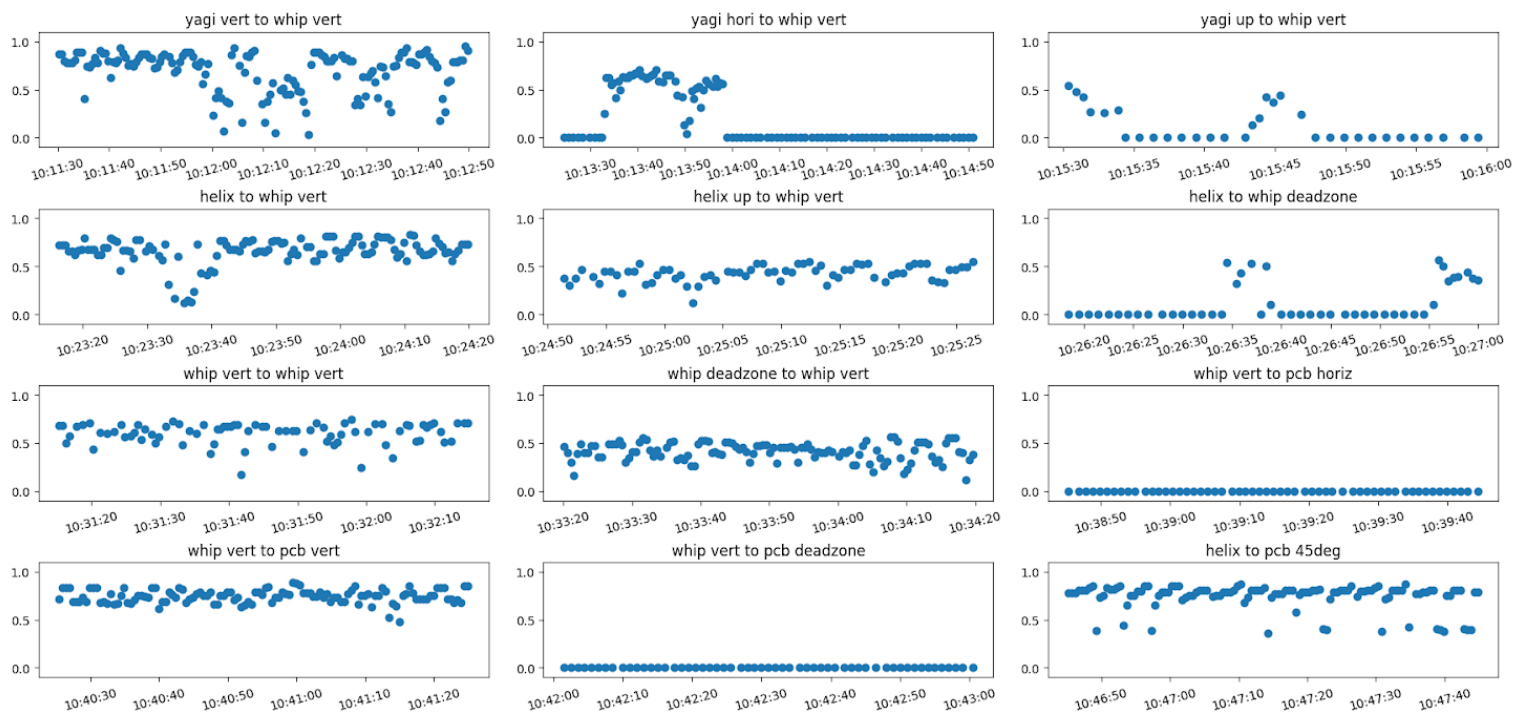
Local 1 time data





## TEST REPORT - Antennae Test

Remote 1 time data



<b>Test</b>	Static Fire 7
<b>Project</b>	Kismet Engine
<b>System</b>	Propulsion
<b>Location</b>	Texas Test Site
<b>Date</b>	2023-01
<b>Description</b>	See "Static Fire Setup and System Checks"
<b>Purpose</b>	Fire ground config of engine to validate new changes to feedsystem and combustion chamber
<b>Personnel</b>	See "Static Fire Setup and System Checks"

<b>Requirements</b>	See "Static Fire Setup and System Checks"
<b>Materials and Equipment</b>	See "Static Fire Setup and System Checks"
<b>PPE Required</b>	See "Static Fire Setup and System Checks"
<b>Procedure</b>	See "Static Fire 8 Operations Procedures"
<b>Deviations</b>	No recorded deviations.
<b>Results</b>	<ul style="list-style-type: none"> <li>• Successfully validated implemented changes to engine</li> <li>• For further details, see "Static Fire 7 Test Results"</li> </ul>
<b>Conclusions</b>	<ul style="list-style-type: none"> <li>• Ready to proceed with flight engine development</li> </ul>

<b>Test</b>	Wet Dress Rehearsal
<b>Project</b>	Kismet Engine
<b>System</b>	Propulsion
<b>Location</b>	Test area outside E5
<b>Date</b>	2023-05-14
<b>Description</b>	Final engine integration testing, as well as validation of onloading/offloading procedures for the flight engine
<b>Purpose</b>	<ul style="list-style-type: none"> <li>• Validate feedsystem configuration</li> <li>• Test avionics integration into engine</li> <li>• Time onloading and offloading procedures</li> </ul>
<b>Personnel</b>	<ul style="list-style-type: none"> <li>• Delaney Dyment - Operations Director</li> <li>• Jack Christensen - Control</li> <li>• Rio Liu - Telemetry</li> <li>• Thomas Fairhead - Primary</li> <li>• ABM Hussien/Aaron Leszkowiat - Secondary</li> </ul>

<b>Requirements</b>	<ul style="list-style-type: none"> <li>• No required approvals</li> </ul>
<b>Materials and Equipment</b>	<ul style="list-style-type: none"> <li>• See 2023-GSE-01 through 2023-GSE-05</li> </ul>
<b>PPE Required</b>	<ul style="list-style-type: none"> <li>• See 2023-GSE-01 through 2023-GSE-05</li> </ul>
<b>Procedure</b>	<ul style="list-style-type: none"> <li>• See LotS 2023 Operations Procedures</li> </ul>
<b>Deviations</b>	<ul style="list-style-type: none"> <li>• Pneumatic line freezing inducing leak</li> <li>• Issues with rocketside check valves</li> <li>• Change to procedure due to only having one cylinder in final test</li> <li>• Vent valve thermistor showed no obvious temperature drop</li> <li>• FOD discovered in feedsystem</li> </ul>
<b>Results</b>	<ul style="list-style-type: none"> <li>• Validated feedsystem config</li> <li>• Validated avionics integration</li> </ul>

	<ul style="list-style-type: none"><li>• Launch time to fill validated, time to vent deemed not realistic due to setup changes</li></ul>
Conclusions	<ul style="list-style-type: none"><li>• Further testing of vent valve thermistor required</li><li>• Begin immediate investigation into methods to reduce FOD in system from supply cylinders during testing</li><li>• Investigate pneumatic line freezing</li></ul>

## Static Fire 8 Data

### Raw Data

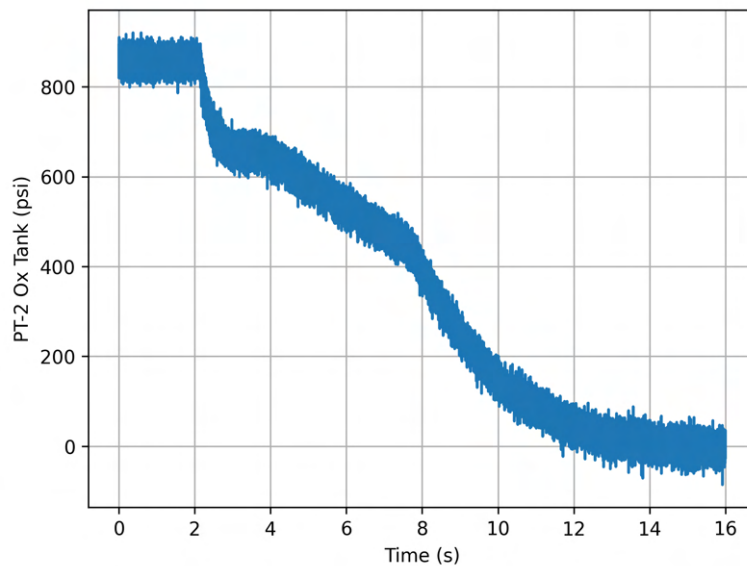


**Fig. 130** Oxidizer Tank Pressure vs Time (Raw)

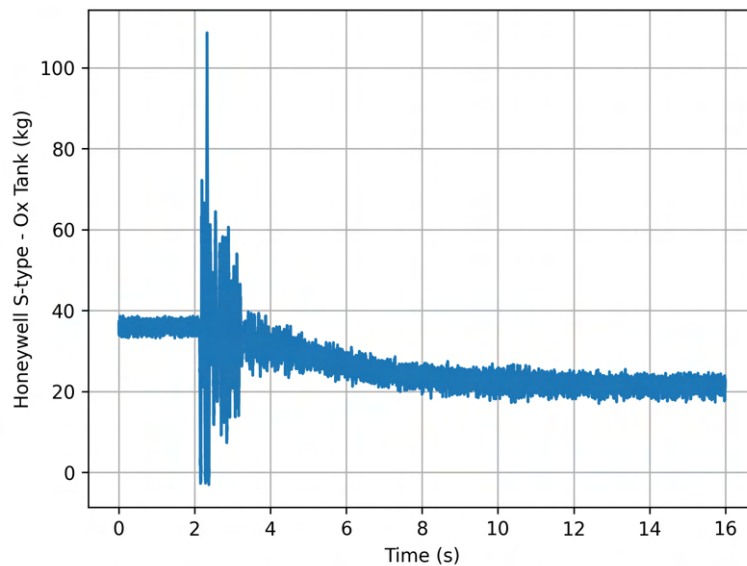


**Fig. 131** Oxidizer Tank Mass vs Time (Raw)

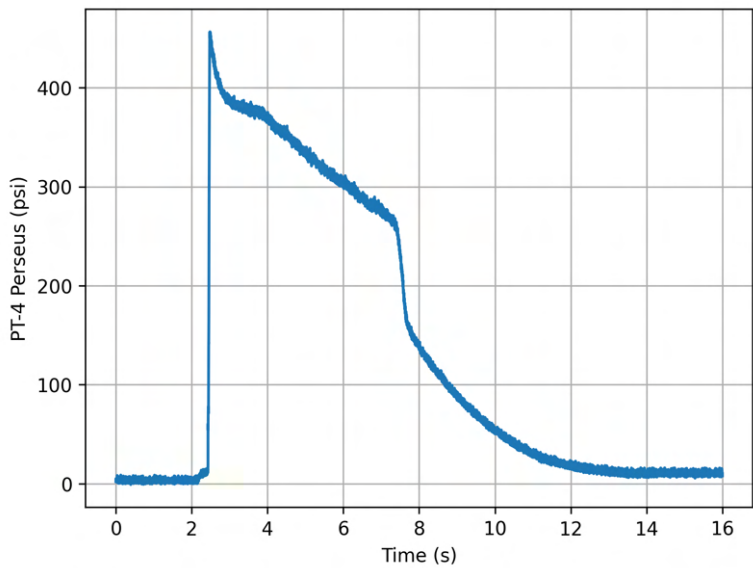


**Fig. 132 CC Pressure vs Time (Raw)**

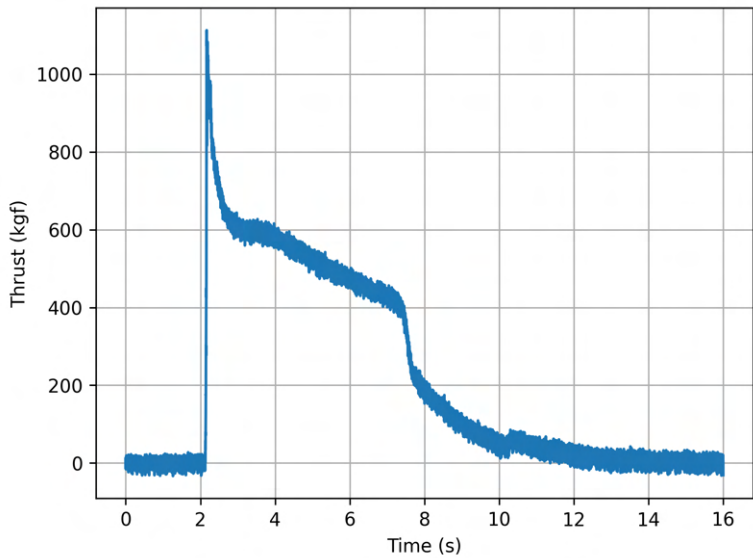


**Fig. 133 Thrust vs Time (Raw)**

### **Smoothed Data**

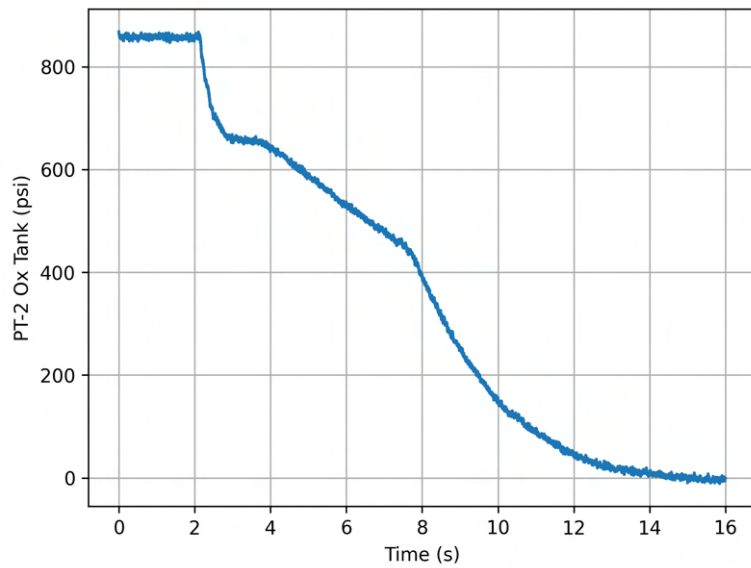


**Fig. 134 Oxidizer Tank Pressure vs Time (Smooth)**

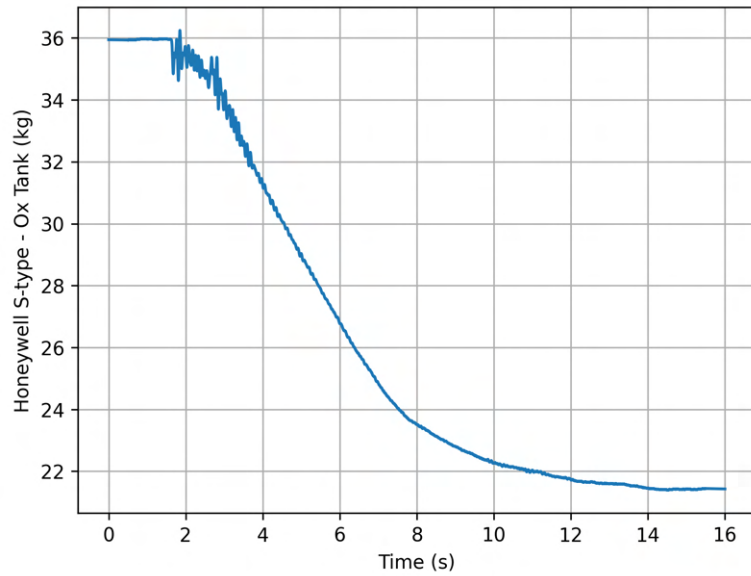


**Fig. 135 Oxidizer Tank Mass vs Time (Smooth)**

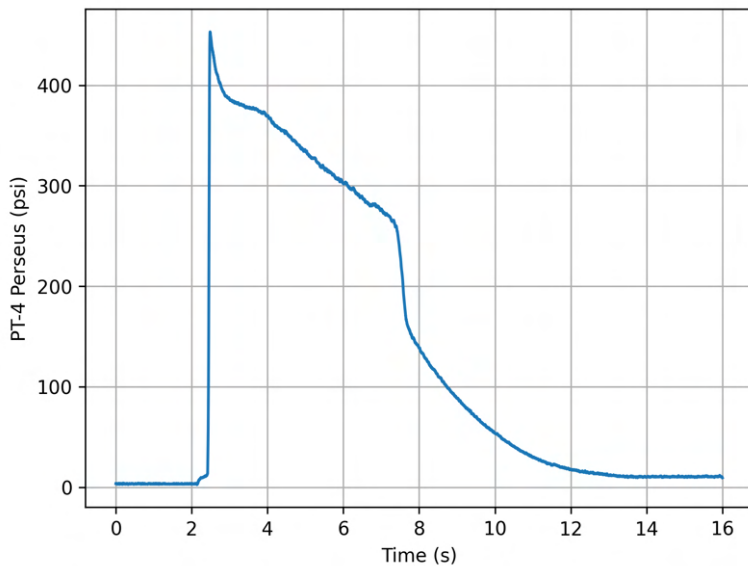


**Fig. 136 CC Pressure vs Time (Smooth)**

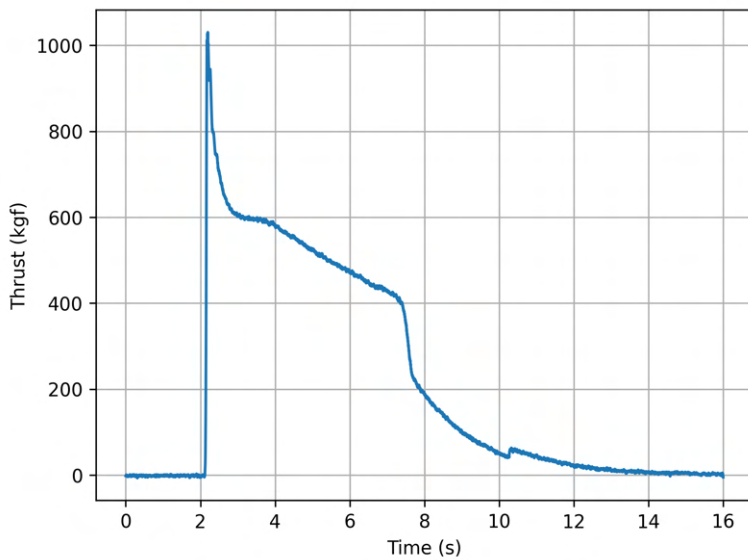


**Fig. 137 Thrust vs Time (Smooth)**

## Static Fire 8 Analysis

### Obtaining $\dot{m}_{ox}$

The first step in the analysis of the engine is to obtain the oxidizer mass flow from the load cell data. This can be quite challenging due to the noise in the load cell data. A Python tool has been developed to perform this fitting process.

The raw load cell data is first split into the liquid and vapour phases of the burn. The load cell has a lot of noise at the start of the burn because the oxidizer tank exhibits significant motion during the startup transient of the engine. This region of the data is overwritten with a straight line fit from the data point immediately before the injector valve is opened, to a region after the tank reading has stabilized.

Then, a quadratic polynomial is fitted to the liquid phase data, while a quartic polynomial is fitted to the vapour phase data. The mass flow rate can then be obtained by taking the derivative of the polynomials. The degree of the fitted polynomials must be carefully selected to ensure the resulting fit is accurate. Anywhere from degree 3-5 has been shown to work with the vapour phase data, but for the liquid phase data only a quadratic polynomial produces good results.

Finally, the transient between the liquid and vapour phases of the resulting  $\dot{m}$  curve is smoothed with a Savitzky-Golay filter.

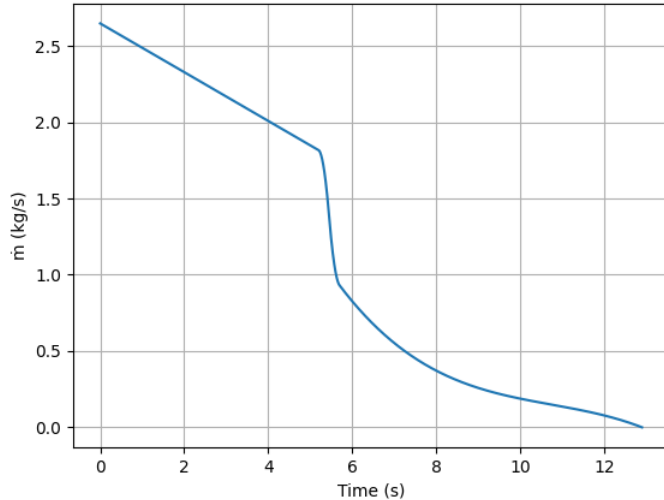


**Fig. 138**  $\dot{m}_{ox}$  vs Time

### $I_{sp}$ Bands

Using this  $\dot{m}_{ox}$  data, it is possible to obtain a rough idea of the  $I_{sp}$  of the engine during the burn.

$$\tau = I_{sp} \dot{m} g_0$$

$$I_{sp} = \frac{\tau}{\dot{m}g_0}$$

$$I_{sp} = \frac{\tau}{\dot{m}_{ox}(1 + OF^{-1})g_0}$$

During the liquid phase of the burn, it is known that the OF ratio is within 7 and 9. Thus, a plot can be created with  $OF = 7$  as the lower band and  $OF = 9$  as the higher band.

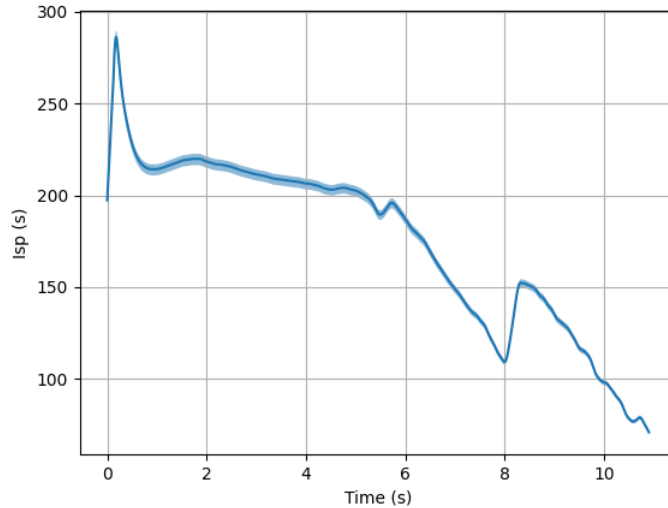


**Fig. 139**  $I_{sp}$  vs Time

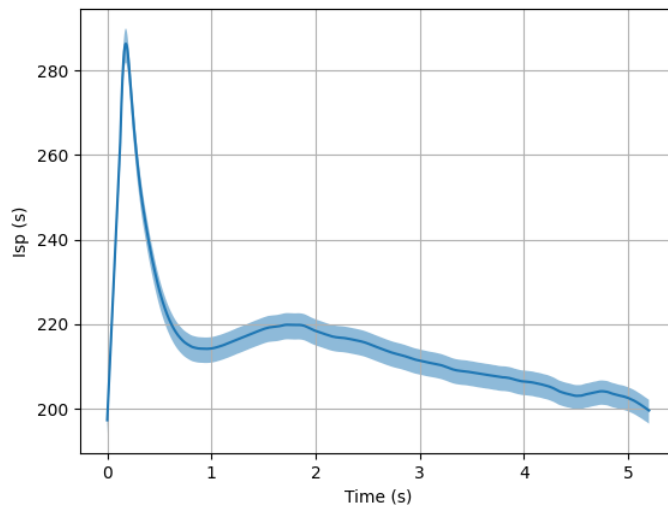


**Fig. 140**  $I_{sp}$  vs Time (Liquid Phase)

If a constant  $OF = 8$  is assumed for the liquid phase, the  $I_{sp}$  is 216.4s. This is partly due to the thrust spike at the start of the burn; the thrust force produced is very high compared to the flow rate out of the injector so the specific

impulse in that spike is extremely high. Around  $t = 5.5s$  there is a small sinusoid pattern in the  $I_{sp}$  graph. This is not physical, but caused because the  $\dot{m}_{ox}$  tool does not create a perfect curve of the mass flow during the liquid-vapour transition point. The spike at  $t = 8s$  is of unknown origin. The source of the spike is present in the measured thrust data.

The  $OF \in [7, 9]$  assumption is not accurate for the vapour phase. The actual OF will shift considerably lower, so the efficiency in the vapour phase will be considerably lower than the bands shown. However, the vapour phase performance is not of large importance in the engine design. The liquid phase performance is much more important as it is the source of the majority of the impulse.

## Regression Analysis

### *Theory*

In order to achieve maximum performance, the OF ratio of the hybrid engine should be as close to stoichiometric for the propellant combination (around 8 for HTPB/ $N_2O$ ) as possible. Thus, a regression rate study must be performed to predict the OF ratio during the burn.

The naive approach is simply to measure the expended oxidizer (from the load cell data) and the expended fuel (weighing the fuel grain before and after the burn) to determine the burn average OF. During Static Fire 8, 14.5 kg of oxidizer and 2.06 kg of fuel was consumed for an OF ratio of 7.04.

However, the naive approach does not consider OF shift during burn. OF shift is a major concern during hybrid engine development. Fuel grain regression is generally approximated by the following empirical model:

$$\dot{r} = aG_{ox}^n$$

We use the convention that  $G_{ox}$  is in units of  $g/cm^2s$  and the model produces an  $\dot{r}$  in  $mm/s$  for the chosen  $a$  and  $n$ . This relatively simple model has been shown to work well across a wide range of engines, though the constants  $a$  and  $n$  tend to vary significantly engine to engine.

This relation has some important consequences. The value of  $n$  typically lies between 0.5-0.8 which implies that large drops in oxidizer flux are met with disproportionately smaller losses in regression rate. This results in the vapour phase of the burn typically having a low OF ratio and consuming larger amounts of fuel than expected.

To better quantify the effects of this relation, a simulation is developed to quantify the change in OF over the course of the burn. For a circular port (such as the one used in the Kismet engine), the fuel mass flow rate can be determined:

$$\Delta m_f = \pi((r + \dot{r}\Delta t)^2 - r^2)l\rho_f$$

$$\Delta m_f = \pi((\dot{r}\Delta t)^2 + 2r\dot{r}\Delta t)l\rho_f$$

$$\frac{\Delta m_f}{\Delta t} = \pi(\dot{r}^2 \Delta t + 2r\dot{r})l\rho_f$$

$$\dot{m}_f = 2\pi r\dot{r}l\rho_f$$

Where  $r$  is the port radius,  $l$  is the fuel grain length and  $\rho_f$  is the fuel grain density. Uneven regression was observed during SF8, so the port radius is discretized into an array of radii at each point along the length of the grain. There is a corresponding array with scaling factors  $k$  on the value of  $a$ , where:

$$k(x) := \frac{\text{final port radius at } x}{\text{max port radius}}$$

and  $x$  is the distance down the grain. This allows to the regression rate to vary at different points along the fuel grain, which provides a more accurate flux result. The simulation numerically integrates the contribution at each point down the grain to determine the overall mass flux.

With the fuel mass flow rate computed, the OF ratio can be determined:

$$OF := \frac{\dot{m}_{ox}}{\dot{m}_f}$$

The combustion temperature, molecular weight and heat ratio are determined by a Cantera equilibrium calculation. This calculation only requires the OF ratio and the chamber pressure. The calculation tends to overestimate the heat ratio, so a correction factor is applied based on results from the Rocket Propulsion Analysis software.

The heat ratio and nozzle dimensions can be used to solve for the exit mach number:

$$\frac{A_e}{A^*} = \left(\frac{\gamma+1}{2}\right)^{-\frac{\gamma+1}{2(\gamma-1)}} \frac{\left(1 + \frac{\gamma-1}{2}M_e^2\right)^{\frac{\gamma+1}{2(\gamma-1)}}}{M_e}$$

This equation is solved numerically to determine  $M_e$ . Then the exit pressure can be solved:

$$P_e = P_{cc} \left(1 + \frac{\gamma-1}{2}M_e^2\right)^{-\frac{\gamma}{\gamma-1}}$$

Which can be used to solve for the theoretical specific impulse for this chamber pressure, exit pressure and OF ratio:

$$I_{sp} = \frac{1}{g_0} \sqrt{2T_{cc} \frac{R}{M} \frac{\gamma}{\gamma-1} \left[1 - \left(\frac{P_e}{P_{cc}}\right)^{\frac{\gamma-1}{\gamma}}\right]}$$

Now the thrust can be computed. A parameter  $\eta$  is introduced to account for mixing efficiency and some other small losses in the nozzle.

$$\tau = g_0 I_{sp} (\dot{m}_{ox} + \dot{m}_f) \eta + (P_e - P_a) A_e$$

This system can be numerically integrated across the length of the burn to determine  $OF(t)$ . The general procedure for fitting  $a$ ,  $n$  and  $\eta$  are as follows. Firstly, pick a value for  $n$ . Then, tune  $a$  until the total mass of fuel regressed agrees with the measured value from SF8. Then, tune  $\eta$  so that the liquid phase thrust curve matches the real curve. The choice of  $n$  affects the slope of the curve, so there is an optimal value.

There are some caveats with this method. The exit pressure plot is not accurate during the vapour phase, because the nozzle flow equations assume full expansion in the bell nozzle. As the mass flux decreases, at some point the flow will detach from the nozzle walls and the equations no longer apply. Generally, the liquid phase results should be accurate, though.

### *Results*

The optimal values for the constants were determined to be  $a = 0.228$ ,  $n = 0.675$ ,  $\eta = 0.94$ . This produces the following results:

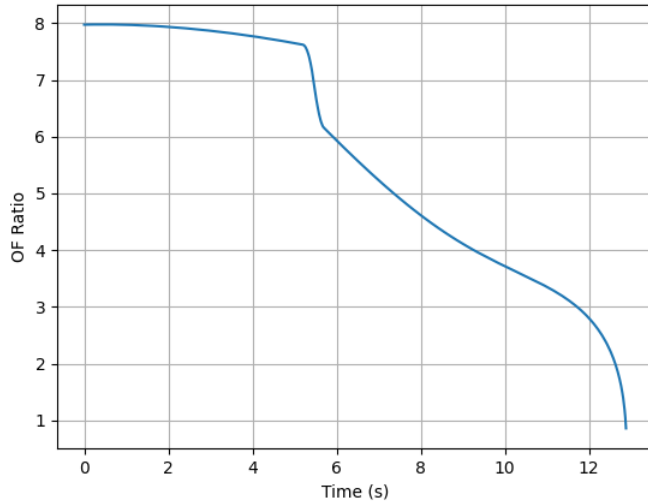


**Fig. 141 OF vs Time (Simulated)**

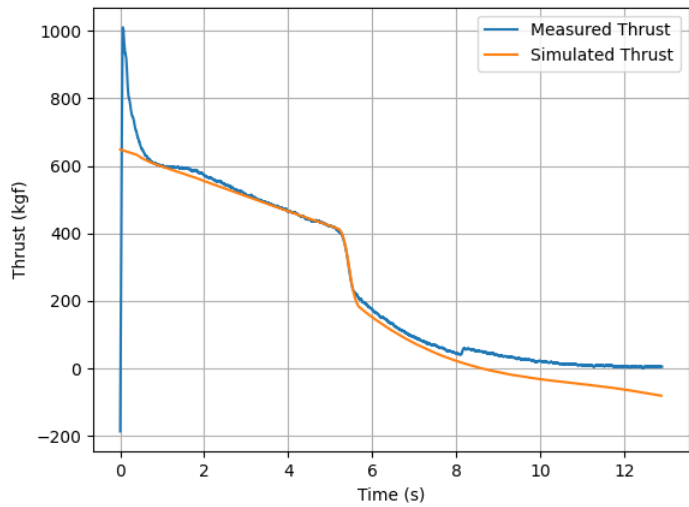


**Fig. 142** Thrust vs Time

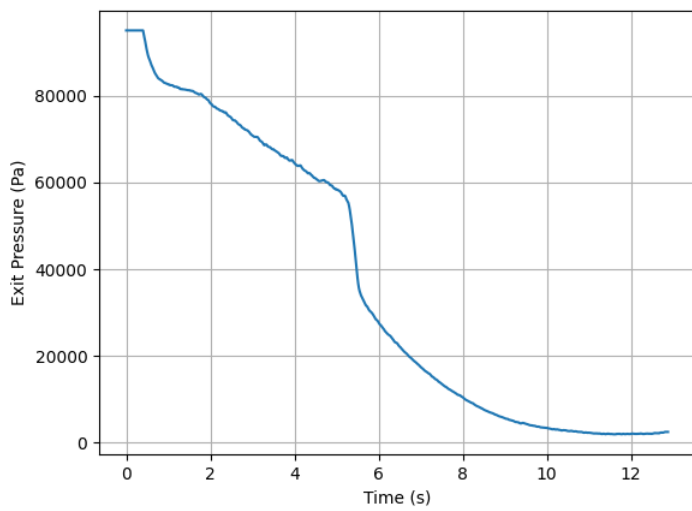


**Fig. 143**  $P_e$  vs Time (Simulated)

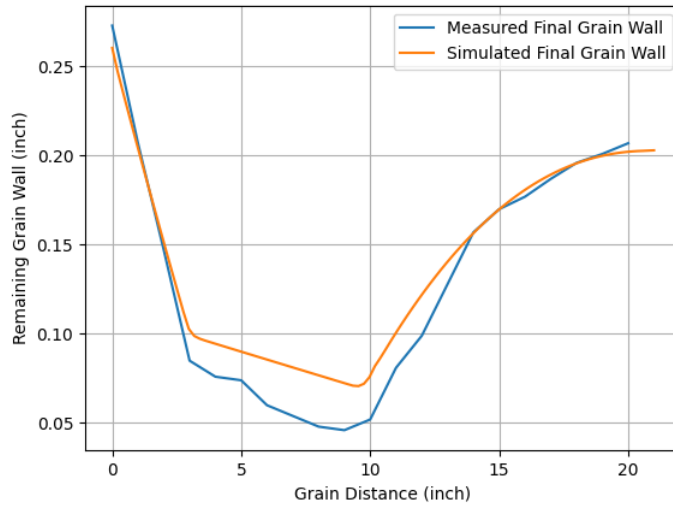


**Fig. 144 Remaining Grain Thickness vs Position**

The simulated thrust becomes negative at the end of the burn because the isentropic flow equations predict the exit pressure to be effectively zero, meanwhile the engine is barely producing any thrust. This is not correct, but as mentioned it is not expected that the vapour phase thrust curve will be accurate. The discrepancy in final wall thickness at the point of oxidizer jet impingement is thought to be due to an oversimplification of the regression model. The jets likely cause a significantly higher local regression rate boost compared to the modelled amount. However, the total burnt fuel with these constants is 4.535 lbs, which is acceptably close to the 4.54 lbs measured value. Finally, it has been found that the parameter  $\eta$  is not particularly sensitive to the input parameters. I.e for a reasonable choice of  $a$  and  $n$ , the value of  $\eta$  typically falls in the range of  $\eta \in [0.9, 0.95]$ .

## CFD Combustion Analysis

### Introduction and Motivation

When designing hybrid rocket engines, it is difficult to predict the performance of the engine without physically testing it. While there is a comprehensive set of theory and research available to aid in the design of the hybrid rocket engine (isentropic flow equations, regression rate laws, etc.) it can still be very challenging or impossible to evaluate and optimize many areas of the engine.

For example, it can be quite challenging to predict the flow patterns and mixing behaviour of the engine. The complex combustion processes occurring inside the engine cannot be modelled through the basic theory alone. Hence, modern Computation Fluid Dynamics technology was leveraged to simulate the complex reacting flow in the engine. A 3D steady-state, reacting flow simulation was developed using Ansys FLUENT to provide insight into the performance and flow structures in the combustion chamber.

### Computational Models

#### *Solver Setup*

This simulation is steady-state and performed using the pressure-based solver. The PRESTO! scheme was selected for the pressure discretization and second order upwind schemes were employed for all other variables. The simulation is performed with an oxidizer mass flow rate of 2.22 kg/s (mean during the liquid phase of the SF8 burn). The fuel mass flow rate is set so that the overall OF ratio is 8. The fuel is modelled to regress evenly across the entire exposed grain surface. For this simulation, no 2D simplification was performed; the entire combustion chamber was modelled. The chamber walls are assumed to be adiabatic. The fuel grain is modelled as being 50% regressed. The  $k - \omega$  SST turbulence model was used with curvature, corner flow and compressibility corrections enabled. No multiphase modelling is done for the nitrous oxide; it is simulated purely in the vapour phase.

#### *Reacting Flow*

To model the reacting flow within the combustion chamber, the Eddy Dissipation Concept (EDC) model was chosen. This model considers both chemical kinetics and turbulent mixing. It is an extension of the Eddy Dissipation Model (EDM) which postulates that combustion is limited by the turbulent mixing of the flow (and hence, does not compute the chemical reaction rates). That is, the reaction rates of the combustion species are much faster than the mixing rate of the species ( $D_a \gg 1$ ). While this assumption may be accurate in some cases, it is difficult to apply the Eddy Dissipation Model directly to the  $N_2O$ -HTPB reaction in our engine. This is because the eddy dissipation model does not consider chemical kinetics at all, and hence cannot effectively model multistep reactions. In an engine with  $N_2O$  as the oxidizer, the nitrous oxide must first dissociate before it can combust with the fuel. This means the reaction  $N_2O \rightarrow \text{products}$  must be modelled, which cannot work using EDM as any turbulence in the oxidizer stream will cause

it to dissociate. This is in contrast to the EDC model, which generally performs well across a wide range of  $D_a$  with the default constants.

However, the downside to the EDC model is that it is significantly more computationally expensive than EDM or most other reacting flow models. A detailed chemical kinetics mechanism must be solved at each time-step (most mechanisms are large) and the problem is considered ‘stiff’ because the reaction timescales tend to be much smaller than the flow timescales. Furthermore, it can be difficult to obtain a good mechanism for the combustion process at hand.

In this study, the widely validated GRI-Mech 3.0 mechanism is used. It is primarily designed for methane-oxygen combustion, but it was found to perform acceptably well for the purposes of this study. The HTPB pyrolysis products are modelled as a 0.49:0.49:0.02 mixture of acetylene ( $C_2H_2$ ), ethylene ( $C_2H_4$ ) and hydroxide ( $OH^-$ ). The approach of using a 1:1 ratio of acetylene and ethylene has been used in several prior studies [18]. The decomposition of 1,3-butadiene (the primary component of HTPB) has been shown to occur through the pathway  $C_4H_6 \rightarrow C_2H_2 + C_2H_4$ , so this approach should yield valid results. 1,3-butadiene cannot be used directly because the GRI-Mech 3.0 mechanism does not contain this species and mechanisms which consider species with more carbon atoms tend to be unfeasibly large. The hydroxide was added as our nozzle design software (Rocket Propulsion Analysis or ‘RPA’) has chemical formulas of HTPB which contain a small percentage of oxygen. The enthalpies of formation of the pyrolysis products have been corrected based on the enthalpy of formation of HTPB from the RPA software ( $-2.08 \cdot 10^6 J/kg$ ).

#### Mesh

A polyhedral mesh consisting of 1310720 cells, 6704979 faces and 4532285 nodes was selected for the problem. Sections of the mesh can be seen in figures xx and xx. The first section slices a pair of mixer spokes in half, while the second section is perpendicular to the spokes. Within the mesh, the postcombustor area is given extra refinement compared to the rest of the flow domain as we are primarily interested in characterizing the mixing behaviour of the engine. Three inflation layers are added to ensure  $y+ < 250$  for proper turbulence modelling.

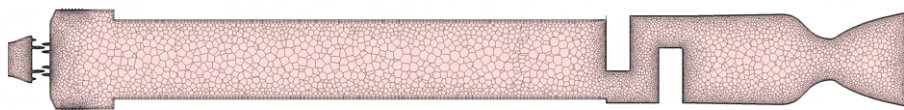


**Fig. 145 CFD Mesh (1st Section)**

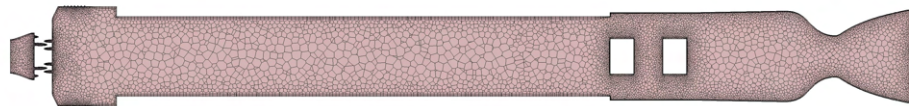
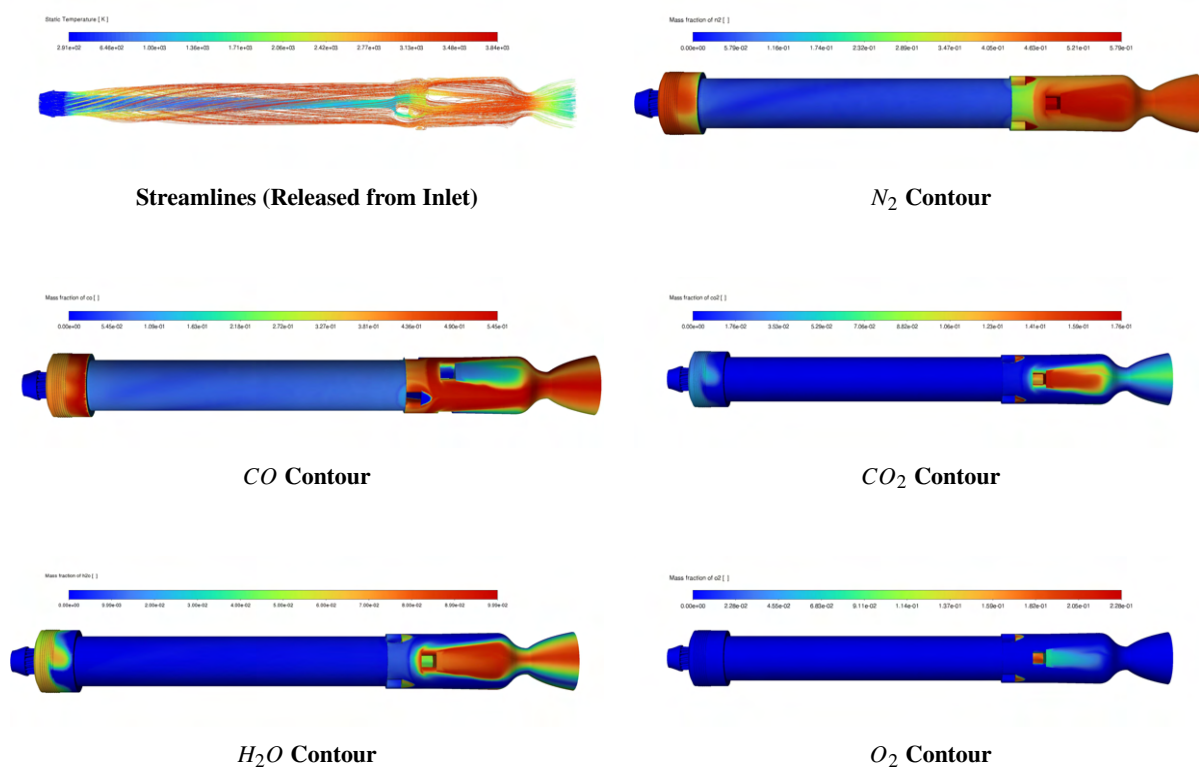


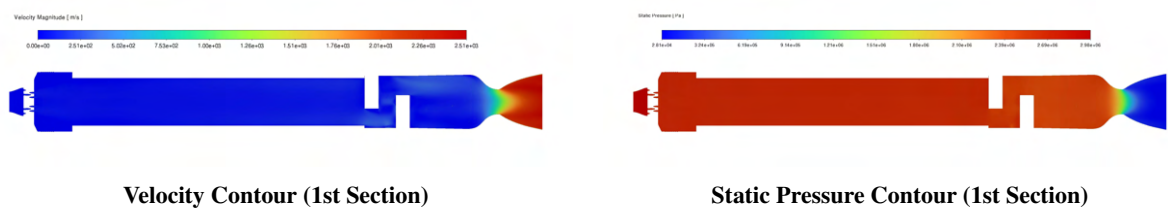
**Fig. 146 CFD Mesh (2nd Section)**

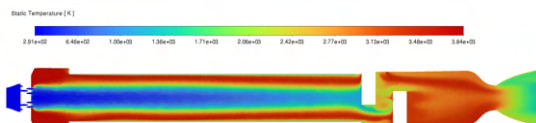
## Results

### *Unsectioned*

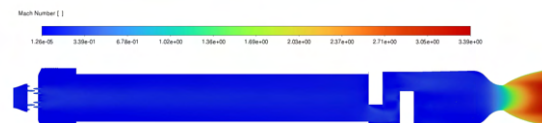


### *Section 1*

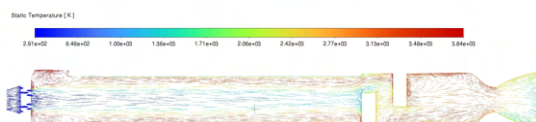




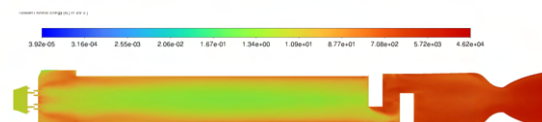
**Static Temperature Contour (1st Section)**



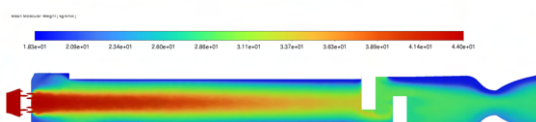
**Mach Number Contour (1st Section)**



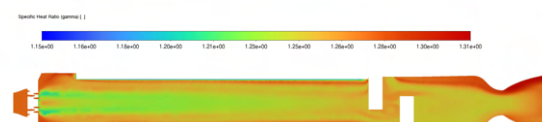
**Streamlines (1st Section)**



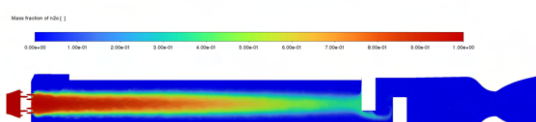
**Turbulent Kinetic Energy Contour (1st Section)**



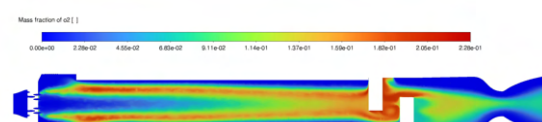
**Mean Molecular Weight Contour (1st Section)**



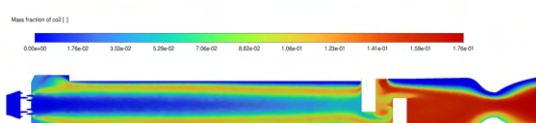
**Heat Ratio Contour (1st Section)**



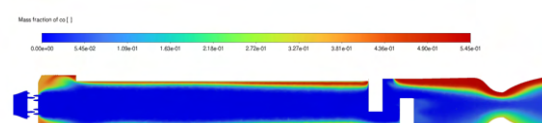
**$\text{N}_2\text{O}$  Contour (1st Section)**



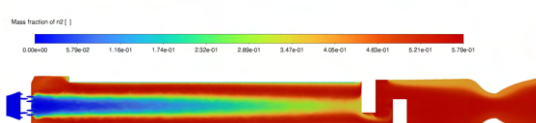
**$\text{O}_2$  (1st Section)**



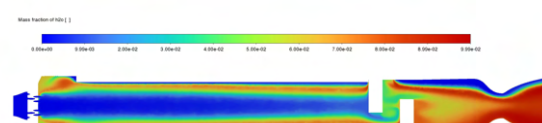
**$\text{CO}_2$  Contour (1st Section)**



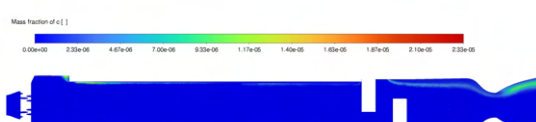
**$\text{CO}$  Contour (1st Section)**



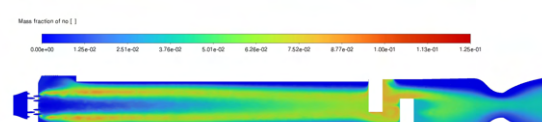
**$\text{N}_2$  Contour (1st Section)**



**$\text{H}_2\text{O}$  Contour (1st Section)**

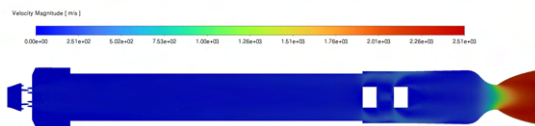


**C Contour (1st Section)**



**NO Contour (1st Section)**

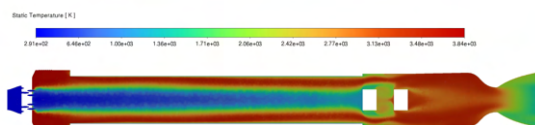
## Section 2



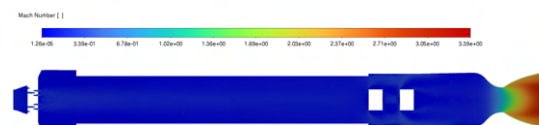
Velocity Contour (2nd Section)



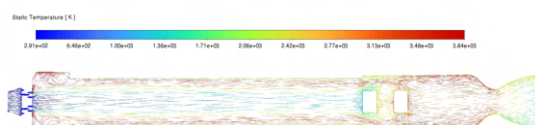
Static Pressure Contour (2nd Section)



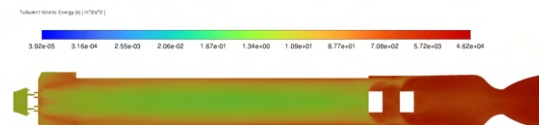
Static Temperature Contour (2nd Section)



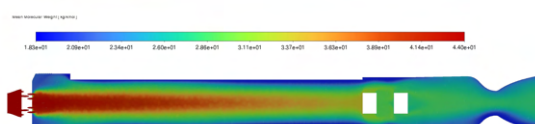
Mach Number Contour (2nd Section)



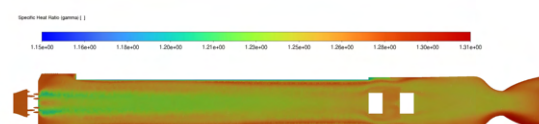
Streamlines (2nd Section)



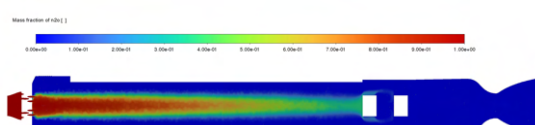
Turbulent Kinetic Energy Contour (2nd Section)



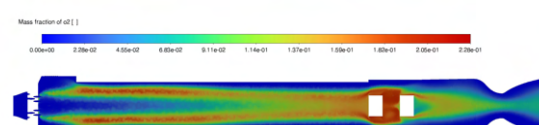
Mean Molecular Weight Contour (2nd Section)



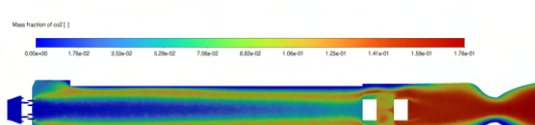
Heat Ratio Contour (2nd Section)



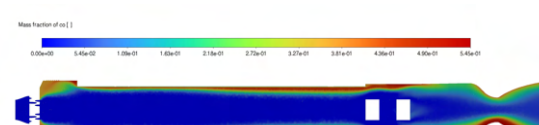
N<sub>2</sub>O Contour (2nd Section)



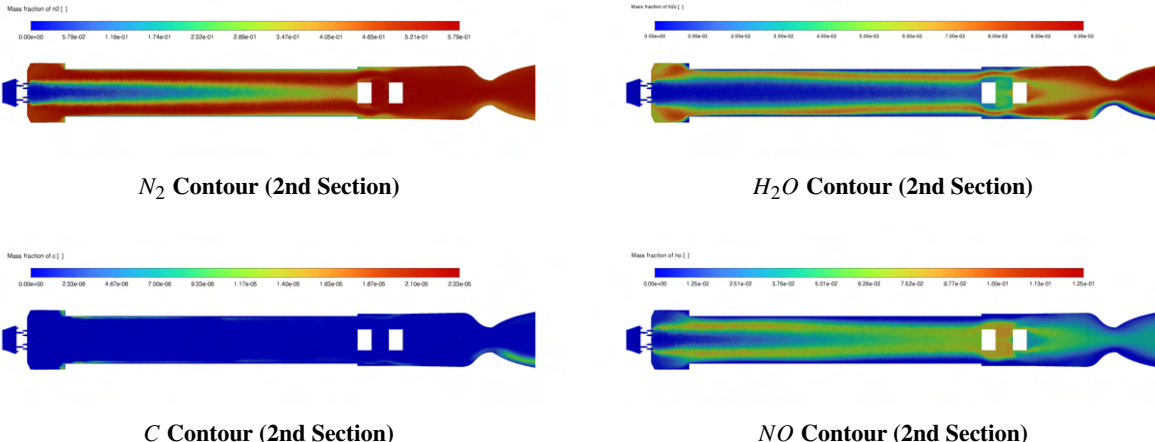
O<sub>2</sub> (2nd Section)



CO<sub>2</sub> Contour (2nd Section)



CO Contour (2nd Section)



### Discussion

The simulation predicts a mass-averaged exit velocity of 2328 m/s and an exit pressure of 80.9 kPa. This corresponds to a thrust of 609.8 kgf, which is 14% larger than the measured thrust force at the same flow rate in Static Fire 8 (534 kgf). The chamber pressure is also over predicted by 8.5%, with the simulation suggesting 384 psi compared to the measured value of 354 psi. This can likely be traced to the high flame temperature: the predicted max flame temperature of 3840K is considerably higher than the typical maximum for nitrous oxide and HTPB (the RPA software predicts 3300K). The source of this error is currently unknown but is thought to be caused by incorrect enthalpies of formation of the propellants. The six largest exhaust products are shown in Table xx. These products constitute about 98% of the exhaust mass. The simulation predicts a very high amount of carbon monoxide formation as opposed to carbon dioxide, which suggests the combustion is not very complete. There is also a small percentage of unreacted O<sub>2</sub> in the exhaust. Furthermore, a moment of 0.57 Nm is predicted to be generated by the engine, but no measurement is available to verify the accuracy of this prediction.

Interestingly, the simulation predicts an uneven regression phenomenon similar to that observed in the fuel grain after SF8. In the mass fraction plots, it can be seen that the diffusion flame between the regression products and the core oxidizer stream gets very close to the grain surface just before the halfway point of the fuel grain. The exact cause of this pattern is currently unknown.

In future simulations, the refinement in the fuel grain area will also be increased as some ‘checkerboarding’ was observed in the grain area. However, increasing the refinement of the mesh is met with a significant computational cost. It currently takes more than 2 days to converge this model on a dual EPYC 7B12 machine due to the severe computational complexity of the chemical kinetics in the EDC model.

**Table 28 Exhaust Mass Fractions**

Species	Exit Mass Fraction
$N_2$	0.5145
$CO$	0.2180
$CO_2$	0.1205
$H_2O$	0.0833
$O_2$	0.0264
$NO$	0.0197

## Appendix D: Hazard Analysis

Hazard	Possible Causes	Likelihood and Ratio-nale	Mitigation Strategy	Risk After Mitigation
Unintended gunpowder ignition	Gunpowder comes in contact with spark or heat source	Medium Risk; Gunpowder must be used during the final assembly of the recovery pyrotechnics, which include electronics	Gunpowder is kept in the original container inside a sealed ammunition box at all times except for during final assembly, at which point only the two recovery technicians are present, wearing appropriate PPE. Batteries are not plugged in when gunpowder is exposed	Low Risk
Recovery CO2 canister bursting	CO2 canister is inadvertently punctured	Low Risk; Canisters are used during the final assembly of the recovery pyrotechnics and contain very high pressure CO2	CO2 canisters are stored in a sealed ammunition box except for during final assembly, at which point only the two recovery technicians are present, wearing appropriate PPE	Minimal Risk
Lithium polymer (LiPo) battery fire	Battery is overcharged, short circuited, or punctured	Medium Risk; Multiple LiPo batteries used across systems and in close contact with technicians	All LiPo batteries are stored in a sealed ammunition box, and securely mounted in all systems when in use. Only correct 3S LiPo chargers are used for charging. All systems are appropriately fused directly after the battery in case of shorts	Low Risk

Accidental ignition puck ignition	Substantial electrical charge or heat source applied to ignition puck	Low Risk: The ignition puck stores a very large amount of chemical energy and cannot be extinguished, but requires a substantial activation energy to ignite	Pucks are stored in a sealed ammunition box until final engine assembly, after which electrical leads are covered at all times. Engine is kept away from any significant heat source	Minimal Risk
Accidental e-match ignition	Exposure to electrical charge or heat source	Medium Risk: E-matches store a small amount of chemical energy that could cause burns, and require relatively small charges to ignite	E-matches are securely stored until final assembly, at which point only the two recovery technicians are present, wearing appropriate PPE. Leads are kept shorted until final assembly to prevent discharged through the body of the e-match	Low Risk
Electric shock	Exposure to high voltage sources or creation of low impedance paths and exposure to medium voltages	Medium Risk: Electric shock can cause a serious risk of injury or death, but high voltage systems are avoided and all SRAD systems use voltages of 24V or less	All high voltage systems are COTS and CSA approved. Electronics are never handled with wet hands, and batteries are disconnected before work is done on electrical circuits	Minimal Risk
Launch tower falling on personnel	Tower is raised or secured incorrectly	High Risk: If the launch tower where to fall it would pose a serious risk of injury or death due to its large height and weight	Tower raising procedure is tightly controlled and followed, no personnel are ever under the tower during raising, all personnel wear hard hats during operations	Low Risk

Contact or inhalation of toxic composite materials	Large variety of harmful dust and vapors formed during many airframe manufacturing activities	High Risk: Most of the byproducts generated are some combination of irritants, toxins, and carcinogens, often with acute long term effects	All Chemical MSDS are carefully tracked, and reviewed before use. Standard operating procedures are followed, and appropriate PPE is used	Low Risk
Nitrous Oxide decomposition	Given sufficient catalyst or activation energy, nitrous can explosively decompose	High Risk: In the unlikely event that decomposition occurs, it would likely cause a substantial explosion that could cause huge amounts of harm	Only nitrous compatible materials are used for any system that may come in contact with nitrous. Careful sanitation and inspection procedures are followed for all plumbing. Procedures are designed to minimize time spent by operators near nitrous, and only COTS parts are used in systems that are pressurized during operator presence	Minimal Risk
Contact with Nitrous Oxide	Leaky fittings, incorrect plumbing usage	Very High Risk: Nitrous oxide is an asphyxiant, stored under very high pressures, and due to phase change during expansion, can reach very low temperatures. All of which pose a significant hazard to operators	Procedures for working with nitrous are very clearly written, reviewed, and practiced. All functions related to nitrous are done remotely if possible. Operators wear appropriate PPE including safety glasses, face shields, shop coats, and thermal gloves. A secondary operator is present whose role is to keep the primary operator safe in the event of an anomaly	Low Risk

Injury due to compressed nitrogen gas; direct or accelerated debris	Leaky fittings, incorrect plumbing usage	Medium Risk: High velocity compressed nitrogen, or particles accelerated by it can easily cause injury, particularly to eyesight	All personnel in the area where compressed nitrogen is being used must wear safety glasses and be aware of the pressurized system. In addition, proper ventilation must be in place to prevent asphyxiation. Systems must be carefully operated according to procedures	Low Risk
Injury due to misuse of power tools or other machine shop equipment	Incorrect use of tools or bad process	High Risk: Almost all rocket components are manufactured by students. Most machines and power tools used have the capability to prevent serious harm if misused	General machine shop training plus specific machine training required to use machines. Standard operating procedures required for any new tools or processes. Full time staff available to advise on best usage and safety	Low Risk
Pinching or abrasions during rocket assembly	Careless or rushed assembly, sharp edges and points	Medium Risk: There are many tight interfaces and parts that must fit together during assembly of the rocket. Many of which could have sharp edges, pinch points, and other sources of injury	All parts should be sufficiently de-burred to prevent sharp edges. Assembly procedures written for each system and practiced. Great care taken during flight hardware assembly	Low Risk

Dehydration	The desert is very hot, and team members are working long strenuous days at competition	Very High Risk: Members are working hard and sweating a lot, staying properly hydrated requires a larger amount of water than is intuitive	Ensure large stockpiles of available water, ensure team members follow a strict hydration schedule and that each team member is consuming sufficient water. Instruct team members on signs of dehydration, and tell them to watch for signs in themselves and each other	Medium Risk
Sunburn	Members are spending large amounts of time in direct sunlight for multiple days	Very High Risk: Direct sunlight in the middle of the desert in the summer can very quickly cause sunburn, and members may not realize until badly burnt	Ensure large stockpiles of available sunscreen for members, and enforce strict application schedules. Encourage members to wear fully covering clothing when possible	Medium Risk

## **Appendix E: Risk Assessment**

The following section details the risks to personnel, the launch vehicle, and associated equipment that may occur during the mission of operations of Leviathan of the Sky. The following table provides a rating for probability of occurrence, severity, and detectability. For each risk, the ratings are multiplied to give a risk priority number (RPN). An RPN of under 30 is considered acceptable.

**Table 30 Risk Assessment Matrix**

<b>Rating</b>	<b>Occurrence (OCC)</b>	<b>Detectability (DET)</b>	<b>Severity (SEV)</b>
5	Highly likely to occur	Hazardous without warning	Undetectable with training
4	Moderately likely to occur	Hazardous with warning	Moderately detectable with training
3	May or may not occur	Major loss of functionality	Easily detectable with training
2	Moderately unlikely to occur	Minor loss of functionality	Moderately detectable without training
1	Highly unlikely to occur	Little to no effect on function	Easily detectable without training

Failure Mode	Possible Effects	Potential Cause	Mitigation Strategies	O C C	D E T	S E V	RPN
<i>Pre-Launch Operations</i>							
Rocket ignites during preparations	Injury to surrounding personnel	Premature activation of ignition circuit	Ignition circuit requires arming locked out system, manual depression of ignition button for several seconds, and independent activation of injector valve.	1	3	3	9
	Cannot complete launch, primary mission goal failure		Oxidizer is not present in fill system during initial preparations.				
			Ignition circuit is not armed until immediately prior to fill.				
Rocket falls from launch rail during launch preparations	Injury to surrounding personnel	Stopping mechanism fails to support the weight of the rocket	Tower is raised with the rocket on top, with the tower structure and gin pole supporting the rocket during erection	2	2	4	16
	Damage to rocket	Rail buttons rip out of bulkhead	Launch rail is kept level to avoid stress on rail buttons				
			All personnel involved in launch tower erection wear hard hats				
Nitrous oxide escapes from the supply plumbing during fill procedure	Freezing of body parts, unconsciousness, or other bodily harm	Leaks in valves, fittings, or hoses	Plumbing components have been tested without failure and have adequate factors of safety	2	3	2	12
		Premature activation of remote	Check valve is rated to well over				
		Failure of oxidizer tank check valve	All plumbing components are visually inspected during assembly				
		Fill line does not adequately depressurize upon disconnect	Remote disconnect system requires power supply connection and activation of arming switch				
			During remote fill procedure, all personnel are to remain well away from supply plumbing				
			Personnel are to remain well away from fill line following disconnect prior to launch				
Explosion of oxidizer tank during fill procedure	Blast or flying debris causing injury	Overpressurization due to clogging of the vent	Pressure relief valve is installed for overpressurization	1	3	2	6
	Cannot complete launch, primary mission goal failure		Burst disk is installed for overpressurization				
	Oxidizer tank fails to hold normal operating pressure	All open ends of plumbing are covered during assembly, only uncovered before launch					
		Oxidizer tank is designed to rupture laterally instead of radially, minimizing flying debris					
		Oxidizer tank is pressure tested to 1.5x expected maximum operating pressure					
Rocket ignites during fill procedure	Injury to nearby personnel	Premature activation of ignition circuit	All personnel are to remain well away from the rocket during fill procedure	1	3	3	9
	Cannot complete launch,		Ignition circuit requires activation of a key switch and an emergency stop button prior to arming				

	primary mission goal failure		Ignition circuit is not armed until launch personnel receive confirmation from range safety personnel			
Operators are no longer able to control the valves onboard the rocket	Loss of injector control	Radio contact loss between RLCS operator and rocket	All connections are terminated properly to avoid potential intermittent shorts	2	2	8
		CAN module failure on radio or valve boards	The bus is off for most of the day, minimizing quiescent current draw			
		Microcontroller failure on radio/valve boards	Vent valve is designed to open if unable to re-establish radio contact			
	Loss of vent control	Main battery runs out and bus goes down	Injector valve is designed to remain in current state upon radio contact loss	2	2	8
			If microcontroller goes down, vent valve board is hardwired to open the valve			
	Loss of primary venting method	Solenoid valve fails closed	Loss communication to valve causes it to fail open	2	2	4
			If launch abort is required, open injector valve very slightly. If this fails, allow oxidizer tank to overpressurize and rupture burst disk.			
			The vent board continuously measures its battery voltage and is programmed to open the valve if the battery is low.			
Feedback from fill sensing system is lost	Unable to confirm fill level of tank	CAN module failure on fill sensing board	Full scale test of system is performed prior to flight	3	2	12
			Pressure sensors, load cell data, and thermistor located at vent valve will provide enough data to determine fill level of rocket			
<i><b>Ignition Phase</b></i>						
Engine does not ignite when command is given ("hang fire"), but does ignite when team approaches to troubleshoot	Injury to personnel	Primary igniter is activated, but gives no visual or electrical confirmation	Ignition relies on continuous delivery of current over several seconds, activated when operator holds down ignition button.	2	1	8
	Cannot complete launch, primary mission goal failure		Primary igniter produces a great deal of dark smoke for visual confirmation of successful ignition			
	Electrical ignition signal is delayed	Display on RLCS indicates that ignition circuit is active, personnel do not approach during this time.				
		All ignition control systems are to be disarmed prior to approach by personnel				
		Personnel are not to approach the rocket if the oxidizer tank contains NOS				
<i><b>Takeoff Phase</b></i>						
Rocket deviates from	Contact with personnel causing severe injury, death	Failure of launch tower components	Off the rail velocity and stability are simulated prior to launch and deemed acceptable			

## Coast Phase

Rocket deviates from nominal flight path	Contact with personnel at high speeds causing severe injury, death	Unexpectedly high wind gusts	Rocket flight is simulated with high winds and does not experience significant deviation	2   1   3   6
	Cannot complete launch, primary mission goal failure		Tail fins are designed to maintain a static stability margin of between 1.5 and 6.0 cal throughout flight Tail fins are unobstructed during ascent on tower All participants are aware of launch and can take cover if necessary A maximum allowed wind speed is set for launch	

#### *Reefed Main Descent*

Parachute fails to deploy, rocket comes in contact with personnel	Severe injury to personnel, death	Failure of altimeters	Altimeters are commercial components	2   2   3   12	
		Insufficient pressure in the recovery bay to break shear bolts	Two altimeters are used for redundancy		
		Pilot chute fails to pull out main parachute			
	Cannot complete launch, primary mission goal failure	Line tangles due to incorrect packing	All decoupling systems are ground tested prior to launch		
			Recovery system is tested in a wind tunnel prior to launch		

Parachute disreefs at or near apogee, rocket drifts into unexpected area	Cannot recover vehicle	Parachute disreefs early	2-ring system is rated to well above expected stress	2   3   2   12
	Contact with personnel or equipment causing injury or damage	2-ring system breaks under load when reefed parachute is deployed	All decoupling systems are ground tested prior to launch	
			Rings are checked for signs of wear prior to launch	

#### *Full Main Descent*

Parachute fails to disreef	Contact with personnel or equipment causing injury or damage	Pyrocutters fail to cut line	Avionics and disreefing mechanism are tested prior to launch	3   2   2   12
		Disreefing line becomes tangled and keeps parachute from fully deploying	All decoupling systems are ground tested prior to launch	
Rocket airframe separates into multiple assemblies	Injury to personnel due to high speed contact with falling component	Failure of recovery lines, resulting in component freefall not slowed by parachute	All recovery lines in system are designed for use with parachutes	2   1   4   8
			All participants are aware of launch and can take cover if necessary	

## **Appendix F: Assembly, Preflight, Launch and Recovery Checklists**

THIS PAGE INTENTIONALLY LEFT BLANK



---

# Leviathan of the Sky Hybrid Rocket

## 2023 IREC

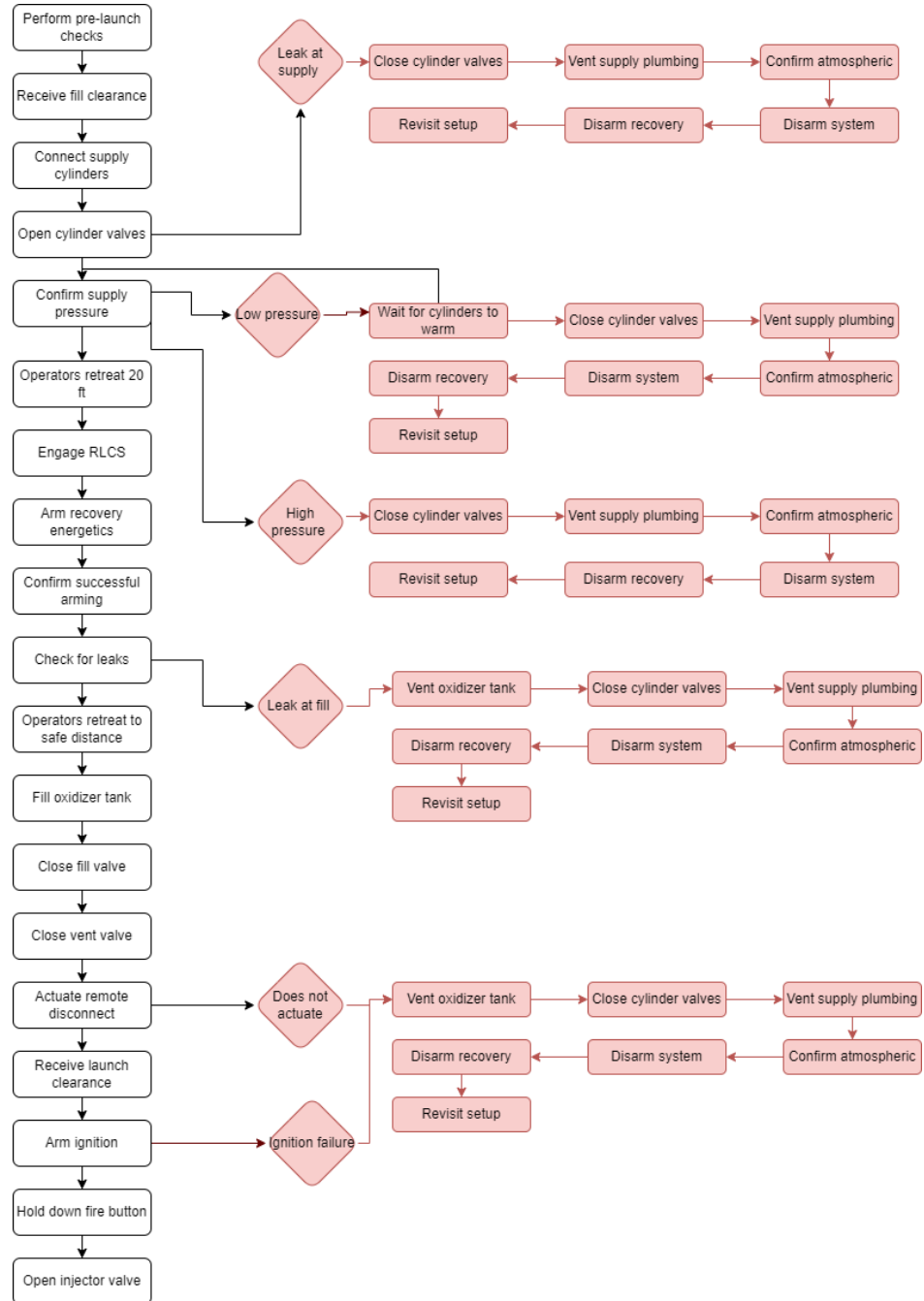
Launch Operations Procedures

Compiled on 2023-02-14

## Background and Reference

## Flow Chart

The following flow chart depicts a high-level overview of the launch operations procedures.



## Contents

---

This document contains two nominal procedures:

- **N1**, *Final Setup and Pre-Launch Checks*, comprises the final checks and tests performed on the Remote Launch Control System (RLCS) prior to rocket launch, as well as avionics systems arming.
- **N2**, *Fill and Launch Operations*, comprises steps for oxidizer fill and rocket launch.

Additionally, this document contains five abort procedures:

- **A1**, *Abort Procedure - Leak At Supply Plumbing*, is used if a plumbing leak is detected when the supply cylinder is initially opened.
- **A2**, *Abort Procedure - Low Supply Pressure*, is used if the oxidizer pressure is below the acceptable limit for launch.
- **A3**, *Abort Procedure - High Supply Pressure*, is used if the oxidizer pressure is above the acceptable limit for launch.
- **A4**, *Abort Procedure - Leak At Fill Plumbing*, is used if a plumbing leak is detected during manual fill leak checks.
- **A5**, *Abort Procedure - Remote Disconnect or Ignition Failure*, is used if the remote disconnect or ignition systems fail, necessitating a full vent of the oxidizer tank.
- **A6**, *Abort Procedure - RLCS Failure*, is used if the remote launch control system fails, necessitating a full vent of the oxidizer tank.
- **A $\gamma$** , *Abort Procedure - Voice Contact Loss*, is used if the operators at the launch site lose the ability to communicate with the operators at launch control.

## Personnel Required

---

The launch operations team consists of four personnel:

- 1     The **Operations Director [OPS]** is stationed at Launch Control. **OPS** directs operations procedures and communicates with the other launch personnel.
- 2     The **Control System Operator [CONTROL]** is stationed at Launch Control and is responsible for operation of RLCS, including remote fill, disconnect, and ignition.
- 3     The **Primary Fill Operator [PRIMARY]** is initially stationed at the Launch Tower and carries out all tasks occurring at the Launch Tower. **PRIMARY** engages the remote disconnect system, connects the ignition wires to the rocket, and operates all manual valves during the manual portion of fill.
- 4     The **Secondary Fill Operator [SECONDARY]** is the backup for **PRIMARY**, and communicates with **OPS**. If **PRIMARY** becomes incapacitated, **SECONDARY** is responsible for removing them from danger.
- 5     The **Data Acquisitions Operator [DAQ]** is stationed at Launch Control and is responsible for monitoring the fill data acquisition system.
- 6     The **Live Telemetry Operator [TELEMETRY]** is stationed at Launch Control. **TELEMETRY** is responsible for monitoring the on-board avionics and live telemetry.

## Sign-Off

---

*To be completed by all test personnel after reading and familiarization with procedures*

- |   |   |       |       |
|---|---|-------|-------|
| 1 | <input type="checkbox"/> <b>Operations Director [OPS]</b>           | _____ | _____ |
| 2 | <input type="checkbox"/> <b>Control System Operator [CONTROL]</b>   | _____ | _____ |
| 3 | <input type="checkbox"/> <b>Primary Fill Operator [PRIMARY]</b>     | _____ | _____ |
| 4 | <input type="checkbox"/> <b>Secondary Fill Operator [SECONDARY]</b> | _____ | _____ |
| 5 | <input type="checkbox"/> <b>Data Acquisitions Operator [DAQ]</b>    | _____ | _____ |
| 6 | <input type="checkbox"/> <b>Live Telemetry Operator [TELEMETRY]</b> | _____ | _____ |

## [N1] Final Setup and Pre-Launch Checks

---

### Prior to Start

- 1     Ensure that the following procedures are complete:
  - 2         LIST ALL ASSEMBLY PROCEDURES HERE DELANEY
- 3     Ensure that all personnel as defined above are available and have completed the sign-off.
- 4     Ensure that the following personnel have walkie-talkies and communication is functional:
  - 5         **OPS**
  - 6         **CONTROL**
  - 7         **PRIMARY**
  - 8         **SECONDARY**
  - 9         **DAQ**
  - 10       **TELEMETRY**
- 11      Ensure that **OPS** is in possession of the system control key.
- 12      Ensure that the injector valve is closed.
- 13      Ensure that fill disconnect is connected.
- 14      Ensure all caps are removed from vent lines.
- 15      Ensure that **SECONDARY** is in possession of a multimeter.
- 16      Ensure that the air compressor is on.
- 17      Ensure that the inverters are flipped.
- 18      Ensure that the locations of Launch Control, Launch Tower, and the Minimum Safe Distance are clearly defined.

Launch Control	Launch Tower	Minimum Safe Distance

### Nominal Procedure

- 1     **PRIMARY**: Confirm that the following valves are initially closed:
  - 2         First Cylinder Valve [SC-1]
  - 3         Second Cylinder Valve [SC-2]
  - 4         Remote Fill Valve [MV-1]
  - 5         Series Fill Valve [BA-2]
  - 6         Parallel Fill Valve [BA-1]

- 7        Line Vent Valve [MV-2]  
 8        Parallel Vent Valve [BA-3]
- 9        **PRIMARY**: Confirm that the ignition connectors are disconnected from the rocket.  
 10       **SECONDARY**: Confirm that the voltage across the ignition connectors is 0 V.  
 11       **OPS**: Give the system control key to **CONTROL**.  
 12       **CONTROL**: Confirm that all actuators are in the off/closed state:  
 13        Remote Fill Valve [MV-1]  
 14        Line Vent Valve [MV-2]  
 15        Remote Disconnect  
 16        Primary Ignition  
 17        Secondary Ignition  
 18        Injector Valve [IJ-1]  
 19        Rocket Vent Valve [RV-1]
- 20       **CONTROL**: Engage the key switch and enable actuators.  
 21       **CONTROL** and **SECONDARY**: Confirm that all actuators actuate as intended:  
 22        Remote Fill Valve [MV-1]  
 23        Line Vent Valve [MV-2]  
 24        Remote Disconnect
- 25       **CONTROL** and **SECONDARY**: Confirm that the ignition voltage is between 9 V and 13 V when the ignition button is fired:  
 26        Primary Ignition  
 27        Secondary Ignition
- 28       **DAQ**: Confirm that all DAQ readings are displaying appropriately.  
 29       **TELEMETRY**: Confirm that all avionics readings are displaying appropriately.  
 30       **OPS**: Record the resting DAQ values:
- | [M] Dry Mass (lbs) | [P1] Supply Pressure (psi) | [P2] Fill Line Pressure (psi) | [P3] Oxidizer Tank Pressure (psi) |
|--------------------|----------------------------|-------------------------------|-----------------------------------|
|                    |                            |                               |                                   |
- 31       **CONTROL**: Disarm the system and give the control key to **OPS**.  
 32       **PRIMARY**: Arm remote disconnect by connecting the springs and fill adapter.  
 33       **PRIMARY**: Turn the regulator on the air compressor to maximum.  
 34       **PRIMARY**: Confirm that the air compressor pressure is above 90 psi.  
 35       **DAQ**: Confirm that the pneumatic pressure transducer [P4] is in agreement.  
 36       **PRIMARY**: Connect the ignition connectors to the rocket.  
 37       **SECONDARY**: Inside the towerside box, confirm that the resistance across the ignition coils is less than 20  $\Omega$ .

## [N2] Fill and Launch Operations

---

### Prior to Start

- 1     Ensure that the following procedure is complete:
  - 2         **N1, Final Setup and Pre-Launch Checks**
- 3     Ensure that the following personnel have walkie-talkies and communication is functional:
  - 4         **OPS**
  - 5         **CONTROL**
  - 6         **PRIMARY**
  - 7         **SECONDARY**
  - 8         **DAQ**
  - 9         **TELEMETRY**
- 10     Ensure that **PRIMARY** and **SECONDARY** are wearing face shields and have no exposed skin.
- 11     Ensure that **PRIMARY** is wearing thermal gloves.
- 12     Ensure that **OPS** is in possession of the system control key.
- 13     Ensure that key is inserted in towerside and box is disarmed.

### Nominal Procedure

- 1     **SECONDARY**: Confirm that no personnel other than **PRIMARY** and **SECONDARY** are within the Minimum Safe Distance.
- 2     **OPS**: Confirm that the actuator key switch is disabled and that only **OPS** is in possession of the system control key.
- 3     **OPS**: Confirm that the Range Safety Officer and Launch Control Officer have given clearance to proceed with fill procedures.
- 4     **DAQ**: Confirm that all DAQ readings are nominal.
- 5     **TELEMETRY**: Confirm that all avionics readings are nominal.
- 6     **PRIMARY**: Confirm that the following valves are initially closed:
  - 7         First Cylinder Valve [SC-1]
  - 8         Second Cylinder Valve [SC-2]
  - 9         Remote Fill Valve [MV-1]
  - 10       Series Fill Valve [BA-2]
  - 11       Parallel Fill Valve [BA-1]
  - 12       Line Vent Valve [MV-2]
  - 13       Parallel Vent Valve [BA-3]
- 14     **PRIMARY**: Open the cap and connect the fill line to the first supply cylinder.
- 15     **PRIMARY**: Open the cap and connect the fill line to the second supply cylinder.
- 16     **PRIMARY**: Slowly open the First Cylinder Valve (SC-1) through  $\frac{3}{4}$  of a turn.

- If leaks are observed:
    - OPS**: Proceed to procedure **A1** - Leak At Supply Plumbing.
- 17       **PRIMARY**: Slowly open the Second Cylinder Valve (SC-2) through  $\frac{3}{4}$  of a turn.
- If leaks are observed:
    - OPS**: Proceed to procedure **A1** - Leak At Supply Plumbing.
- 19       **PRIMARY**: Communicate the supply line pressure as visible on the Pressure Gauge.
- If the supply line pressure is below 800 psi:
    - OPS**: Proceed to procedure **A2** - Low Supply Pressure.
  - If the supply line pressure exceeds 1200 psi:
    - OPS**: Proceed to procedure **A3** - High Supply Pressure.
- 23       **DAQ**: Confirm that the supply line pressure as read by **PRIMARY** agrees with the supply line pressure transducer [P1].
- 24       **OPS**: Record the resting rocket dry mass and supply pressure:

[M] Dry Mass (lbs)	[P1] Supply Pressure (psi)

- 25       **PRIMARY**: Open the Series Fill Valve [BA-2].
- 26       **PRIMARY**: Remove the key from the towerside box.
- 27       **PRIMARY** and **SECONDARY**: Retreat to 20 ft.
- 28       **OPS**: Give the key to control.
- 29       **CONTROL**: Confirm that the following valves are closed:
  - Remote fill valve [MV-1]
  - Line vent valve [MV-2]
- 32       **CONTROL**: Insert the key and engage the system.
- 33       **CONTROL**: Arm recovery energetics.
- 34       **TELEMETRY**: Confirm that remote telemetry indicates successful arming.
- 35       **PRIMARY**: Confirm that you can hear the beeping from the recovery electronics.
- 36       **PRIMARY** and **SECONDARY**: Retreat 100 ft from the fill system.
- 37       **CONTROL**: Open the Remote Fill Valve [MV-1].
- 38       **DAQ**: Confirm the following pressures are increasing:
  - [P2] Fill line pressure
  - [P3] Oxidizer tank pressure
- 41       **CONTROL**: Close the Remote Fill Valve [MV-1].

- 42     **CONTROL:** Close the Rocket Vent Valve [RV-1].
- 43     **DAQ:** Confirm the following pressures are stable:
- 44         [P2] Fill line pressure
- 45         [P3] Oxidizer tank pressure
- 46        • If the pressures are decreasing:  
46             **OPS:** Proceed to procedure A4 - Leak At Fill Plumbing.
- 47     **PRIMARY** and **SECONDARY**: Retreat to the Minimum Safe Distance.
- 48     **SECONDARY**: Confirm that **PRIMARY** and **SECONDARY** are at the Minimum Safe Distance.
- 49     **PAUSE POINT**
- 50     **CONTROL:** Open the Rocket Vent Valve [RV-1].
- 51     **CONTROL:** Open the Remote Fill Valve [MV-1].
- 52     **DAQ:** Monitor the display for rocket mass and oxidizer tank pressure.
- 53     **OPS:** Proceed only when the following is true:
- 54         Vent valve thermistor [T1] shows steep temperature decrease.
- 55         Rocket mass [M] plateaus
- 56         Oxidizer tank pressure [P3] is under 1000 psi.
- 57     **CONTROL:** Close the Remote Fill Valve [MV-2].
- 58     **CONTROL:** Close the Rocket Vent Valve [RV-1].
- 59     **CONTROL:** Open the Line Vent Valve.
- 60     **DAQ:** Confirm that the fill line pressure [P2] is atmospheric.
- 61     **CONTROL:** Actuate Remote Disconnect.  
61        • If Remote Disconnect fails to actuate:  
62             **OPS:** Proceed to procedure A5 - Remote Disconnect or Ignition Failure.
- 63     **PAUSE POINT**
- 64     **OPS:** Perform pre-launch checks:
- 65         Request clearance for launch from the Launch Control Officer.
- 66         Confirm that all surrounding personnel are aware of launch.
- 67     **CONTROL:** Perform engine startup procedure:  
68         Arm the Primary Ignition switch.  
69         Hold down the Fire button until the Primary current reading drops to 0 A.  
69        • In the event of a failed ignition (current drop not observed within 1 minute):  
70             **CONTROL:** Disarm the Primary Ignition switch.  
71             **CONTROL:** Arm the Secondary Ignition switch.  
72             **CONTROL:** Hold down the Fire button until the Secondary current reading drops to 0 A.  
73        • In the event of a second failed ignition (current drop not observed within 1 minute):  
73             **CONTROL:** Disarm the Secondary Ignition switch.

- 74            **OPS**: Proceed to procedure **A5**.
- 75            **CONTROL**: Start the engine by opening the Injector Valve in 5, 4, 3, 2, 1.
- 76            **ALL**: Observe the rocket during takeoff, ascent, and recovery:
- 77             First vehicle motion
- 78             Launch rail departure
- 79             Engine burnout
- 80             Reefed parachute deployment
- 81             Parachute disreefing
- 82             Approximate recovery area/direction
- 83            **DAQ**: Call out altitude every 1,000 ft, and apogee.
- 84            **CONTROL**: Disarm RLCS and give the system control key to **OPS**.
- 85            **OPS**: Confirm that RLCS is disarmed and **OPS** is in possession of the system control key.
- 86            **OPS**: Proceed only when clearance is received from the Launch Control Officer to approach the Launch Tower.
- 87            **PRIMARY** and **SECONDARY**: Approach the Launch Tower and insert the towerside key.
- 88            **PRIMARY**: Close the First Cylinder Valve [SC-1].
- 89            **PRIMARY**: Close the Second Cylinder Valve [SC-2].
- 90            **PRIMARY** and **SECONDARY**: Remove the towerside key and retreat 20 ft from the fill system.
- 91            **OPS**: Give the master key to **CONTROL**
- 92            **CONTROL**: Engage the key switch and enable actuators.
- 93            **CONTROL**: Open the Remote Fill Valve [MV-1].
- 94            **DAQ**: Confirm that the supply line pressure [P1] is atmospheric.
- 95            **PRIMARY**: Open the Parallel Vent Valve [BA-3].
- 96            **PRIMARY**: Open the Parallel Fill Valve [BA-1].
- 97            **PRIMARY**: Disconnect the supply lines from the supply cylinders.
- 98            **PRIMARY**: Close the caps on the supply cylinders.
- 99            **OPS**: Proceed with teardown and disassembly.

## Abort Procedures

---

### [A1] Abort Procedure - Leak At Supply Plumbing

---

- 1     **PRIMARY**: Close the First Cylinder Valve [SC-1].
- 2     **PRIMARY**: Close the Second Cylinder Valve [SC-2].
- 3     **PRIMARY**: Slowly open the Parallel Vent Valve [BA-3].
- 4     **PRIMARY**: Slowly open the Parallel Fill Valve [BA-1].
- 5     **DAQ**: Confirm the following pressures are atmospheric:
  - 6     [P1] Supply pressure
  - 7     [P2] Fill line pressure
- 8     **PRIMARY**: Disarm the system:
  - 9     Disconnect the ignition leads from the rocket.
  - 10     Detach the torsion springs from the disconnect mechanism.
  - 11     Disconnect the fill lines from the supply cylinders.
  - 12     Close the caps on the supply cylinders.
- 13     **PRIMARY** and **SECONDARY**: Retreat 20 ft.
- 14     **OPS**: Give the master key to control.
- 15     **CONTROL**: Ensure all actuators are in the "off" position.
- 16     **CONTROL**: Engage the control box.
- 17     **CONTROL**: Disarm the recovery energetics.
- 18     **CONTROL**: Disengage the control box.
- 19     **OPS**: Regain possession of the master key.
- 20     **OPS**: Revisit plumbing setup.

### [A2] Abort Procedure - Low Supply Pressure

---

- 1     **PRIMARY**: Close the First Cylinder Valve [SC-1].
- 2     **PRIMARY**: Close the Second Cylinder Valve [SC-2].
- 3     **PRIMARY**: Slowly open the Parallel Vent Valve [BA-3].
- 4     **PRIMARY**: Slowly open the Parallel Fill Valve [BA-1].
- 5     **DAQ**: Confirm the following pressures are atmospheric:
  - 6     [P1] Supply pressure
  - 7     [P2] Fill line pressure
- 8     **PRIMARY**: Allow the supply cylinders to warm up.
- 9     **OPS**: Revisit N2.

- 10     If the cylinders do not warm up:
- 11       **PRIMARY**: Disarm the system:  
12         Disconnect the ignition leads from the rocket.  
13         Detach the torsion springs from the disconnect mechanism.  
14         Disconnect the fill lines from the supply cylinders.  
15         Close the caps on the supply cylinders.
- 16       **PRIMARY** and **SECONDARY**: Retreat 20 ft.
- 17       **OPS**: Give the master key to control.
- 18       **CONTROL**: Ensure all actuators are in the "off" position.
- 19       **CONTROL**: Engage the control box.
- 20       **CONTROL**: Disarm the recovery energetics.
- 21       **CONTROL**: Disengage the control box.
- 22       **OPS**: Regain possession of the master key.
- 23       **OPS**: Revisit tank setup setup.

### [A3] Abort Procedure - High Supply Pressure

---

- 1       **PRIMARY**: Close the First Cylinder Valve [SC-1].
- 2       **PRIMARY**: Close the Second Cylinder Valve [SC-2].
- 3       **PRIMARY**: Slowly open the Parallel Vent Valve [BA-3].
- 4       **PRIMARY**: Slowly open the Parallel Fill Valve [BA-1].
- 5       **DAQ**: Confirm the following pressures are atmospheric:  
6         [P1] Supply pressure  
7         [P2] Fill line pressure
- 8       **PRIMARY**: Disarm the system:  
9         Disconnect the ignition leads from the rocket.  
10        Detach the torsion springs from the disconnect mechanism.  
11        Disconnect the fill lines from the supply cylinders.  
12        close the caps on the supply cylinders.
- 13       **OPS**: Give the master key to control.
- 14       **CONTROL**: Ensure all actuators are in the "off" position.
- 15       **CONTROL**: Engage the control box.
- 16       **CONTROL**: Disarm the recovery energetics.
- 17       **CONTROL**: Disengage the control box.
- 18       **OPS**: Revisit cylinder cooling methods.

#### [A4] Abort Procedure - Leak At Fill Plumbing

---

- 1     **CONTROL:** Insert the key and engage control.
- 2     **CONTROL:** Close the Remote Fill Valve [MV-1].
- 3     **CONTROL:** Open the Line Vent Valve [MV-2].
- 4     **DAQ:** Confirm the following pressures are atmospheric:
  - 5        P2: Fill line pressure
  - 6        P3: Rocket Tank pressure
- 7     **CONTROL:** Disengage the control system.
- 8     **PRIMARY** and **SECONDARY**: Return to plumbing setup
- 9     **PRIMARY**: Close the First Cylinder Valve [SC-1].
- 10     **PRIMARY**: Close the Second Cylinder Valve [SC-2].
- 11     **PRIMARY**: Slowly open the Parallel Vent Valve [BA-3].
- 12     **PRIMARY**: Slowly open the Parallel Fill Valve [BA-1].
- 13     **DAQ:** Confirm the following pressures are atmospheric:
  - 14        [P1] Supply pressure
  - 15        [P2] Fill line pressure
- 16     **PRIMARY**: Disarm the system:
  - 17        Disconnect the ignition leads from the rocket.
  - 18        Detach the torsion springs from the disconnect mechanism.
  - 19        Disconnect the fill lines from the supply cylinders.
  - 20        Replace the caps on the supply cylinders.
- 21     **PRIMARY** and **SECONDARY**: Retreat 20 ft.
- 22     **OPS**: Give the master key to control.
- 23     **CONTROL:** Ensure all actuators are in the "off" position.
- 24     **CONTROL:** Engage the control box.
- 25     **CONTROL:** Disarm the recovery energetics.
- 26     **CONTROL:** Disengage the control box.

#### [A5] Abort Procedure - Remote Disconnect or Ignition Failure

---

- 1     **CONTROL:** Open the Rocket Vent Valve.
- 2     **CONTROL:** Disengage control.
- 3     **DAQ:** Monitor the DAQ display for rocket mass and oxidizer tank pressure as the oxidizer tank vents.
- 4     **OPS:** Proceed only when the following is true:
  - 5        Rocket mass is equal to the pre-launch recorded mass
  - 6        Oxidizer tank pressure [P3] is atmospheric

- 7         The Launch Control Officer has given clearance to approach the Launch Tower.
- 8         **PRIMARY** and **SECONDARY**: Approach the Launch Tower.
- 9         **PRIMARY**: Close the First Cylinder Valve [SC-1].
- 10       **PRIMARY**: Close the Second Cylinder Valve [SC-2].
- 11       **PRIMARY**: Open the Parallel Vent Valve [BA-3].
- 12       **PRIMARY**: Slowly open the Parallel Fill Valve [BA-1].
- 13       **DAQ**: Confirm the following pressures are atmospheric:
- 14         [P1] Supply pressure
- 15         [P2] Fill line pressure
- 16       **PRIMARY**: Disarm the system:
- 17         Disconnect the ignition leads from the rocket.
- 18         Detach the torsion springs from the disconnect mechanism.
- 19         Disconnect the fill lines from the supply cylinders.
- 20         Close the caps on the nitrous oxide supply cylinders.
- 21       **OPS**: Give the master key to control.
- 22       **CONTROL**: Ensure all actuators are in the "off" position.
- 23       **CONTROL**: Engage the control box.
- 24       **CONTROL**: Disarm the recovery energetics.
- 25       **CONTROL**: Disengage the control box.
- 26       **OPS**: Proceed with teardown and disassembly.

#### [Aγ] Abort Procedure - Voice Contact Loss - For Launch Control Operators

- 1         **CONTROL**: Remove the system control key from the client side box.
- 2         **OPS**: Attempt to regain communication with the operators at the pad:
- 3         Send "**OPS** to **SECONDARY**, **OPS** to **SECONDARY**, **SECONDARY** please come in".
- 4             If contact is restored:
- 5               Return to normal operations.
- 6               Check batteries in radio.
- 7               Check that radio is set to the proper channel.
- 8               Check that radio volume is high enough.
- 9               Wait 30 seconds, then send message again.
- 10             If contact is restored:
- 11               Return to normal operations.
- 12       **OPS**: Wait 30 seconds.
- 13       **OPS**: Send "**OPS** to **SECONDARY**, **OPS** to **SECONDARY**, going to full abort. I say again, going to full abort."
- 14       **OPS**: Inform the ESRA official that launch operations will be aborted.
- 15       **OPS**: Wait for operators to return from pad.
- 16       **OPS**: Proceed with teardown and disassembly.

## [A7] Abort Procedure - Voice Contact Loss - For Launch Pad Operators

---

- 1     **SECONDARY**: Attempt to regain communication with the operators at launch control:
- 2        Send “**SECONDARY** to **OPS**, **SECONDARY** to **OPS**, **OPS** please acknowledge”.
  - If contact is restored:
    - 3        Return to normal operations.
- 4        Check batteries in radio.
- 5        Check that radio is set to the proper channel.
- 6        Check that radio volume is high enough.
- 7        Wait 30 seconds, then send message again.
  - If contact is restored:
    - 8        Return to normal operations.
- 9     **SECONDARY** and **PRIMARY**: Approach the rocket, listening for hisses coming from fill system.
- 10     **PRIMARY**: Insert the key into the towerside box.
- 11     **PRIMARY**: Close the First Cylinder Valve [SC-1].
- 12     **PRIMARY**: Close the Second Cylinder Valve [SC-2].
- 13     **PRIMARY**: Slowly open the Parallel Vent Valve [BA-3].
- 14     **PRIMARY**: Slowly open the Parallel Fill Valve [BA-1].
- 15     **SECONDARY** and **PRIMARY**: Remove the key from towerside and return to launch control.

## [Aδ] Abort Procedure - Delay On The Pad

---

- 1     **DAQ**: Monitor the ox tank pressure [P3].
  - If the ox tank pressure rises above 850 psi:
    - 2     **CONTROL**: Open the Rocket Vent Valve [RV-1].
    - 3     **DAQ**: Confirm when the pressure has reached 800 psi.
    - 4     **CONTROL**: Close the Rocket Vent Valve [RV-1].
    - 5     **OPS**: Repeat as needed.
  - If a full abort is required:
    - 6     **OPS**: Proceed to procedure **A5**.

## [Aε] Abort Procedure - RLCS Contact Loss

---

- 1     **DAQ**: Monitor the DAQ display for rocket mass and oxidizer tank pressure as the oxidizer tank vents.
- 2     **OPS**: Proceed only when the following is true:
  - 3     Rocket mass is equal to the pre-launch recorded mass.
  - 4     Oxidizer tank pressure [P3] is atmospheric.
  - 5     The Launch Control Officer has given clearance to approach the Launch Tower.
- 6     **PRIMARY** and **SECONDARY**: Approach the Launch Tower.
- 7     **PRIMARY**: Close the First Cylinder Valve [SC-1].
- 8     **PRIMARY**: Close the Second Cylinder Valve [SC-2].
- 9     **PRIMARY**: Open the Parallel Vent Valve [BA-3].
- 10     **PRIMARY**: Slowly open the Parallel Fill Valve [BA-1].
- 11     **DAQ**: Confirm the following pressures are atmospheric:
  - 12     [P1] Supply pressure
  - 13     [P2] Fill line pressure
- 14     **PRIMARY**: Disarm the system:
  - 15     Disconnect the ignition leads from the rocket.
  - 16     Detach the torsion springs from the disconnect mechanism.
  - 17     Disconnect the fill lines from the supply cylinders.
  - 18     Close the caps on the nitrous oxide supply cylinders.
  - 19     Use the magnetic arming poll to disarm recovery electronics.
- 20     **OPS**: Proceed with teardown and disassembly.

## **Appendix G: Engineering Drawings**

THIS PAGE INTENTIONALLY LEFT BLANK

### **Acknowledgments**

There are a great number of people without whom this rocket, and this team, would not be where they are today. We give sincere thanks to our advisors, who have offered sound advice and support over the past year and for many prior. Specifically, we would like to thank Dr. Andrew Milne, Dr. Jean-Pierre Hickey, Andy Phillips, and Dan Steinhaur for their significant contributions to our team. We would also like to acknowledge the contributions of all our sponsors. Without their support, we would not be able to continue providing valuable learning opportunities for our team members and community. In particular, Stein Industries has made and continues to make significant investments in our team's success. Stein Industries and Dan Steinhaur deserve special acknowledgment for the many years of support that they have provided to our team. In addition, we thank the Sedra Student Design Center for their continued support. To the management, the machine shop staff, and the building operations and cleaning staff, thank you for the many hours of work that go into creating a space for our students to learn and work safely and comfortably. To the friends and family of our team members, thank you for your support and understanding of the commitment and dedication of the people on this team. To our alumni, thank you for the time and effort you put in that paved the way for the current generation of Waterloo Rocketry. We would not be where we are without your dedication and advice, and we thank you for everything that you have taught us. Finally, to our team members: you are the heart and soul of this team, and we hope that your efforts in building this rocket have given you something valuable. We are proud of you, and we thank you for the late

nights, early mornings, and seemingly endless dedication that you have given to get us to this point. You have made this team something special.

## References

- [1] Kim, J., and Lee, C., “Transition of combustion instability in hybrid rocket by swirl injection,” *Acta Astronautica*, Vol. 158, 2019, pp. 323–333. <https://doi.org/10.1016/j.actaastro.2018.07.036>.
- [2] Newlands, R., *The science and design of the hybrid rocket engine*, 2017.
- [3] Edge, E., “Minimum Thread Engagement Equations and Calculator ISO,” 2000-2023. URL [https://www.engineersedge.com/thread\\_strength/thread\\_minimum\\_length\\_engagement.htm](https://www.engineersedge.com/thread_strength/thread_minimum_length_engagement.htm).
- [4] McMaster-Carr, “Black-Oxide Alloy Steel Socket Head Screw 6-32 Thread Size, 3/4" Long,” ???? URL <https://www.mcmaster.com/91251A151/>.
- [5] Inc., A. A. S. M., “Aluminum 6061-T6; 6061-T651,” ???? URL <https://asm.matweb.com/search/SpecificMaterial.asp?bassnum=ma6061t6>.
- [6] Howard, Z., “How To Calculate Fin Flutter Speed,” *Peak of Flight*, Vol. 291, 2011, pp. 2, 6.
- [7] Knacke, T. W., “Parachute Recovery Systems Design Manual,” 1992.
- [8] Kulagina, N., Besseau, S., Godon, C., Goldman, G. H., Papon, N., and Courdavault, V., “Yeasts as Biopharmaceutical Production Platforms,” *Frontiers in Fungal Biology*, Vol. 2, 2021.
- [9] Swamy, H. R. S. M. e. a., B.K., “Novel hypergravity treatment enhances root phenotype and positively influences physio-biochemical parameters in bread wheat (*Triticum aestivum L.*),” *Scientific Reports*, Vol. 11, 2021.
- [10] Raj, S. B., Ramaswamy, S., and Plapp, B. V., “Yeast Alcohol Dehydrogenase Structure and Catalysis,” *Biochemistry*, Vol. 53, 2014, pp. 5791–5803.
- [11] Johnstone, A., “"CubeSat Design Specification Rev. 14,” 2020. URL <https://static1.squarespace.com/static/5418c831e4b0fa4ecac1bacd/t/5f24997b6deea10cc52bb016/1596234122437/CDS+REV14+2020-07-31+DRAFT.pdf>.
- [12] “Spaceport America,” 2023. URL [https://en.wikipedia.org/wiki/Spaceport\\_America](https://en.wikipedia.org/wiki/Spaceport_America).
- [13] Toolbox, E., “Atmospheric Pressure vs. Elevation Above Sea Level,” 2003. URL [https://www.engineeringtoolbox.com/air-altitude-pressure-d\\_462.html](https://www.engineeringtoolbox.com/air-altitude-pressure-d_462.html).
- [14] Edge, E., “AISI Internal Screw Threads Size and Tolerances Table Chart,” 2001. URL [https://www.engineersedge.com/thread\\_strength/internal\\_screw\\_threads\\_chart.htm](https://www.engineersedge.com/thread_strength/internal_screw_threads_chart.htm).
- [15] Systems, W., “105 Epoxy Resin/206 Slow Hardener,” 2014. URL <https://www.westsystem.com/wp-content/uploads/105-206-Epoxy-Resin-1.pdf>.

- [16] Brachman, R., and Krushelnitzky, R., “Yeast Alcohol Dehydrogenase Structure and Catalysis,” *Geosynthetics International*, Vol. 9, 2015, pp. 189–213. <https://doi.org/10.1680/gein.9.0215>, URL <https://www.icevirtuallibrary.com/doi/abs/10.1680/gein.9.0215>.
- [17] MechaniCalc, “Bolted Joint Analysis,” 2014-2023. URL <https://mechanicalc.com/reference/bolted-joint-analysis>.
- [18] Nardozzo, P., Connell, T., Boyer, J., Yetter, R., and Young, G., “Diffusion flame studies of solid fuels with nitrous oxide,” *International Journal of Energetic Materials and Chemical Propulsion*, Vol. 19, 2020, pp. 73–93. <https://doi.org/10.1615/IntJEnergeticMaterialsChemProp.2020028356>.